NATIONAL AND KAPODISTRIAN UNIVERSITY OF ATHENS

SCHOOL OF SCIENCE

FACULTY OF BIOLOGY

# Study of pathogenetic mechanisms of Parkinson's disease in neuronal cellular models

**Athanasia Antoniou, MSc**

**Biologist**

DOCTORAL THESIS

Athens 2022

ΕΘΝΙΚΟ ΚΑΙ ΚΑΠΟΔΙΣΤΡΙΑΚΟ ΠΑΝΕΠΙΣΤΗΜΙΟ ΑΘΗΝΩΝ

ΣΧΟΛΗ ΘΕΤΙΚΩΝ ΕΠΙΣΤΗΜΩΝ

ΤΜΗΜΑ ΒΙΟΛΟΓΙΑΣ

# Μελέτη παθογενετικών μηχανισμών της νόσου Πάρκινσον σε κυτταρικά μοντέλα νευρώνων

**Αθανασία Αντωνίου, MSc**

**Βιολόγος**

ΔΙΔΑΚΤΟΡΙΚΗ ΔΙΑΤΡΙΒΗ

Αθήνα 2022

«Η έγκριση της Διδακτορικής Διατριβής από το Τμήμα Βιολογίας της Σχολής Θετικών Επιστημών του ΕΚΠΑ δεν υποδηλώνει αποδοχή των απόψεων του συγγραφέα (ν. 5343/1932, άρθρο 202)»

«Το κείμενο της Διδακτορικής Διατριβής δεν αποτελεί προϊόν λογοκλοπής.»

**ADVISORY COMMITTEE:**

1. ASSOCIATE PROFESSOR PAPAZAFIRI PANAGIOTA (SUPERVISOR)

2. RESEARCH DIRECTOR REBECCA MATSAS

3. PROFESSOR SPIROS EFTHIMIOPOULOS

**EXAMINATION COMMITTEE:**

1. ASSOCIATE PROFESSOR PAPAZAFIRI PANAGIOTA, FACULTY OF BIOLOGY

2. RESEARCH DIRECTOR REBECCA MATSAS, HELLENIC PASTEUR INSTITUTE

3. PROFESSOR SPIROS EFTHIMIOPOULOS, FACULTY OF BIOLOGY

4. ASSOCIATE PROFESSOR DIDO VASSILACOPOULOU, FACULTY OF BIOLOGY

5. PROFESSOR LEONIDAS STEFANIS, FACULTY OF MEDICINE

6. RESEARCH DIRECTOR REGIS GRAILHE, INSTITUTE PASTEUR KOREA

7. RESEARCH DIRECTOR GEORGE PANAGIOTOU, BSRC FLEMING

**ACKNOWLEDGEMENTS**

Completing this thesis, a product of several years' work, I feel deeply indebted to many people who have greatly inspired and supported me during my studies and contributed to the writing of this thesis. I feel extremely lucky that I had the chance to meet and work with all these great people.

In particular, I would like to express my gratitude to:

**Dr Rebecca Matsas,** the supervisor of my thesis, for giving me the opportunity to become a part of the stem cell research group at Hellenic Pasteur Institute and for her support and scientific guidance all these years. Moreover,I thank her for all of the opportunities I was given to further my research and brought my work to a higher level.

**Associate Prof. Panagiota Papazafeiri**, and **Prof. Spyros Efthimiopoulos**, my co-supervisors for their support, guidance, valuable comments and feedback that helped me greatly to complete this work.

**Prof. Leonidas Stefanis**, **Dr. George Panayotou** and **Associate Prof. Dido Vassilacopoulou** for being members in my examination committee.

**Dr. Regis Grailhe**, for welcoming me in his lab and introducing me to the high-throughput world. His guidance and supervision was essential during this work. While working in his lab, I had the chance to meet many wonderful people and of course to explore the very interesting Korean culture.

**Prof.Piotr Bregestovski**, for introducing me to the electrophysiology world. His love and enthusiasm for research played a crucial role in my personal development. And I would also like to thank him for introducing me to the world of yoga- a priceless gift!

**Dr Era Taoufik** for her invaluable guidance, encouragement, academic stimulus and generous help. Her insight in this project helped me keep perspective on where my research fits on to the bigger picture, especially during times that motivation was running low.

**Dr Florentia Papastefanaki,** for being always willing to help with image and data analysis, answering all questions I had and for the nice scientific discussions and comments. And of course for giving me a new nutritional perspective!

**Dr. Nelly Prodromidou**, for her valuable insight into the proteomics data analysis. I want also to thank her for the discussions, for helping with the experiments and being patient with me during some tough times!

**Dr. Geogia Kouroupi**, for passing on her knowledge in the induced pluripotent stem cells. I also thank her for the help, support and the very nice and smooth collaboration we had all these years in the different projects.

**Dr. Rania Zygogianni**, my lab-mate, for being a great collaborator and friend. Her precious support and friendship made this journey easier and more pleasant even during the most difficult times. Rania, you had to wait alone in the "Dr side" for quite some time but I am coming soon!

I also want to thank the other members of Dr. Matsa's lab, **Dr. Katerina Seglia**, **Dr. Kostis Tsioras**, **Nikos Kokorakis** for providing a pleasant and fun environment in the lab during the last (several!) years!

I am also grateful to **Dr. Thomaidou** and the members of her lab, **Dr. Elsa Papadimitriou**, **Irini Thanou**, **Mairy Margariti**, **Dr. Pari Koutsoudaki** and **Dr. Katerina Aravantinou**. I really appreciate the help, their good ideas and humour!

I would also like to thank **Dr. Evaggelia Xingi** for her support on light microscopy and **Dr. Dafni Chroni** for her help on electrophysiology experiments.

I cannot forget to thank **Dr. Martina Samiotaki** for her help in conducting the proteomics experiments and analysis.

Moreover, I would like to thank **Ioanna Boumpoureka**, **Dr. Maria Xilouri** and **Dr. Ismini Kloukina** for their contribution to this work.

It is also important to thank my friends for their emotional support, fun and care all these years. Special thanks to my sister, **Marianthy**, for being there,listening and supporting. I would also like to thank my partner, **Nikos**, for his patience and love.

Finally and most importantly, I want to express my deepest gratitude to my parents, **Lampros** and **Dora**, for their endless love and support.

*To my family*

**CONTENTS**

**ABBREVIATIONS**

**AA** Ascorbic Acid

**AD** Alzheimer's Disease

**ACh** Acetylcholine

**ALS** Amyotrophic Lateral Sclerosis

**AMPA** a-amino-3-hydroxy-5-methylisoxazole propionic acid

**APs** autophagosomes

**αSyn** alpha synuclein

**BDNF** Brain-Derived Neurotrophic Factor

**BMP** Bone Morphogenic Proetin

**cAMP** dibutyryl cyclic adenosine monophosphate

**CMA** Chaperone-Mediated Autophagy

**CMV** Cytomegalovirus

**CNS** Central Nervous System

**COX** – 2 cyclo-oxygenase-2

**CSF** Cerebrospinal Fluid

**DA** Dopamine

**DAergic** Dopaminergic

**ER** Endoplasmic Reticulum

**GABA** Gamma Amino Butyric Acid

**GBA1** β-Glucocerebrosidase gene

**GCase** β-Glucocerebrosidase

**GDNF** Gial-Derived Neurotrophic Factor

**GFP** Green Fluorescent Protein

**GPi** internal globus pallidus

**GWASs** Genome Wide Association Studies

**HSP** Heat Shock Proteins

**iPSC** induced Pluripotent Stem Cell

**LBs** Lewy Bodies

**LC3** Microtubule-associated protein 1 light chain 3

**L-DOPA** Levedopa

**LRRK2** Leucine Rich Repeat Kinase 2

**MA** Macroautophagy

**MAM** Mitochondria-Associated Membrane

**MAO-B** Monoamine Oxidase- B

**MAP2** Microtubule-Associated Protein 2

**MEA** Multi-Electrode Array

**mTORC1** mechanistic target of rapamycin complex 1

**MPTP 1-**Methyl-4-Phenyl-1,2,3,6-Tetrahydropyridine

**MPP+ 1**-Methyl-4-Phenylpyridinium

**MSA** Multiple System Atrophy

**NAC** Non-Amyloid-β Component

**nbM** nucleus basalis of Meynert

**NMDA** N-Methyl-D-Aspartate

**PD** Parkinson's Disease

**PRS** Polygenic Risk Score

**REM** Rapid Eye Movement

**ROS** Reactive Oxygen Species

**PrP** Prion Protein

**SMA** Spinal Muscular Atrophy

**SN** Substantia Nigra

**SNARE** SNAP Receptor

**SNpc** Substantia Nigra pars compacta

**STR** Striatum

**TH** Tyrosine Hydroxylase

**TNT** Tunneling Nanotubes

**TUJ1** Tubulin beta III

**UPS** Ubiquitin-Proteasome System

**VMAT2** Vesicular Monoamine Transporter 2

**VTA** Ventral Tegmental Area

**5-HT** Serotonin

## 1. INTRODUCTION

### 1.1 Parkinson's disease

#### 1.1.1 General

Parkinson's is a condition known since ancient times. In the ancient Indian medical system of Ayurveda,it is mentoned under the name Kampavata (where "kampa" means tremor in Sanskrit). In Western medical literature it was described as "shaking palsy" by Galen, the physician from Pergamum (2nd century A.D.), at AD 175. However, it was not until 1817 that a detailed medical essay on the subject was published by the London physician James Parkinson. The publication was entitled "An Essay on the Shaking Palsy" [1]. However, a French neurologist named Jean Martin Charcot was the first to truly recognize the importance of Parkinson's work 65 years later and name the disease after him [2].

Parkinson's disease (PD) is the second most common neurodegenerative disease in the elderly population, after Alzheimer's disease (AD), with a higher prevalence in men, regardless of race or social class; it affects approximately 1.5 to 2.0% of the elderly population over 60 years and 4% for those over 80 years of age [3].

Neuronal loss in the substantia nigra, causing striatal dopamine deficiency, and intracellular inclusions containing protein aggregates of α-synuclein are the classical neuropathological hallmarks of Parkinson disease. Several other cell types throughout the central and peripheral autonomic nervous system are also affected, probably early in the disease [4].

Clinically, PD is characterized by tremor at rest, rigidity, akinesia and postural instability [5]. Beyond the perception of PD as a movement disorder, a variety of non- motor features, such as cognitive impairment,dementia, autonomic dysfunction, sleep disturbances, and hyposmia (impaired sense of smell), have been shown to be part of the disease and contribute significantly to the overall burden [6].Psychiatric symptoms, such as depression, anxiety, hallucination, delusion, apathy and anhedonia, impulsive and compulsive behaviors, may also manifest in most patients with PD [7].

In any case, PD remains a progressive disorder that eventually leads to severe disability. Therefore, modifying the course of the disease and delaying disability are the major unmet needs that must be addressed by current and future research efforts. A great potential for the future lies in the development of methods to identify at-risk individuals and early manifestations that precede the onset of defining motor symptoms.

### 1.1.2 Clinical features of PD

#### 1.1.2.1 Motor symptoms

From a motor point of view, PD is characterized by a clinical syndrome commonly known as parkinsonism, which includes four main features: Tremor at rest, Rigidity, Akinesia (or bradykinesia) and postural instability. These four features are not always observed in every patient, at least not in a specific time frame [8].

*Tremor at rest* is a rhythmic, oscillatory, involuntary movement that occurs when the affected body part is relaxed and supported by a surface, thereby cancelling the effect of gravitational forces [9-11]. It disappears during active movement, and can typically reappear after a few seconds if the arms are kept extended (reemergent tremor).

*Rigidity* refers to increased muscle tone that can be felt on examination by passive movement of the affected segment (limb or neck), and involves both flexor and extensor muscle groups [12, 13].

*Akinesia (or bradykinesia)* refers to the slowing of movements with a progressive loss of amplitude or speed during attempted rapid alternating movements of body segments [12-14].

*Postural instability*. Parkinson's disease patients tend to adopt a stooped posture due to loss of postural reflexes, which is a major contributor to falls [12, 15].

#### 1.1.2.2 Non-motor symptoms

Non-motor symptoms are a common feature of PD [12]. These include autonomic dysfunction, cognitive/neurobehavioral dysfunction, and sensory and sleep abnormalities [16].

Autonomic failure may be the presenting feature of PD, although it is typically associated with multiple system atrophy (MSA). Features include orthostatic hypotension, sweating disorders, sphincter dysfunction and erectile dysfunction [17-19].

Neuropsychiatric symptoms can be as disabling as motor symptoms. The Sydney Multicenter Study of PD found that 84% of patients studied had cognitive decline and that 48% met diagnostic criteria for dementia after 15 years of follow-up [20]. PD associated dementia is also correlated with a number of other neuropsychiatric comorbidities. Among these patients, depression (58%), apathy (54%), anxiety (49%) and hallucinations (44%) were commonly reported [21]. In addition to cognitive and affective disorders, many patients with PD exhibit features of obsessive–compulsive behaviors, such as cravings (especially for sweets) [22], binge eating, compulsive foraging, hypersexuality, pathological gambling, compulsive shopping and punding, which is characterized by an intense fascination with repeatedly

touching, examining, sorting and arranging objects [23]. These behavioral symptoms, sometimes referred to as “hedonistic homeostatic dysregulation”, have been attributed to dopamine dysregulation syndrome which is associated with the use of dopaminergic medications, particularly dopamine agonists, but the mechanism of these aberrant behaviours is not well understood [24].

Although sleep disturbances (e.g., excessive sleepiness, sleep attacks) were once largely attributed to pharmacological treatment of PD [25], some clinicians now believe that these features are an integral part of the disease [26]. This is supported by the observation that rapid eye movement sleep behavior disorder, which occurs in about one-third of patients with PD, is a major risk factor for the development of PD [27-30]. Insomnia is also common (>50% prevalence), but the occurrence varies widely among patients [31, 32]. The sleep disturbances observed in patients with PD may be related to a 50% loss of hypocretin (orexin) neurons [33, 34]. Although excessive daytime sleepiness may contribute to fatigue, this common symptom is also observed independently of sleepiness [35].

Sensory symptoms such as olfactory dysfunction, pain, paresthesia, akathisia, oral pain and genital pain are common but are often not recognized as PD symptoms [36-42]. Olfactory dysfunction (hyposmia) may be an early marker of PD and it has been postulated to be related either to neuronal loss in the corticomedial amygdala or to a decrease in dopaminergic neurons in the olfactory bulb [43].

### 1.1.3. PD as a system-level disorder

The basal ganglia circuit is functionally located between the cortex and the thalamus. The main function of the circuit is to process signals coming from the cortex, to produce an output signal that returns to the cortex, via thalamus, to modulate the execution of movements. The basal ganglia are located in the basal telencephalon and consist of five interconnected nuclei: the caudate, the nucleus, the putamen, the globus pallidus, the substantia nigra (SN) and the subthalamic nucleus. Although the caudate nucleus and the putamen are partly separated by the internal capsule, several cellular bridges connect the two nuclei, which are similar in their anatomical and functional characteristics. Therefore, the two structures together are commonly referred to as corpus striatum or striatum [44]. The SN is divided into two parts: the pars reticulata (SNpr) and the pars compacta (SNpc), which lies medial to the pars reticulate. The pars compacta serves mainly as a projection to the basal ganglia circuit, supplying the striatum with dopamine. The pars reticulata conveys signals from the basal ganglia to numerous other brain structures [45].

The functional architecture of the basal ganglia has led to the formulation of a model of basal ganglia function that has become very popular [46, 47]. According to this model, the striatum - the main

input nucleus of the circuit- transmits the flow of information received from the cortex to the output nuclei of the basal ganglia, substantia nigra pars reticulata and medial globus pallidus, via a direct and an indirect pathway. The two pathways originate from different subsets of striatal neurons and, in this model, remain functionally segregated. In the direct pathway, striatal GABAergic neurons, containing dynorphin -the dynorphin family of neuropeptides comprises six peptides of different lengths formed from the precursor prodynorphin that activate κ-opioid receptors in the peripheral and central nervous systems [48]- as a co-transmitter and expressing D1 dopamine receptors, project monosynaptically to the substantia nigra pars reticulata and medial globus pallidus. In the indirect pathway, striatal output reaches target nuclei via a more complicated route. In fact, another subset of GABAergic neurons - containing enkephaline and expressing D2 receptors - projects to the lateral globus pallidus, which sends GABAergic projections to the subthalamic nucleus. The subthalamic nucleus, in turn, sends its glutamatergic efferents to the output nuclei and to the lateral globus pallidus. From the output nuclei, inhibitory, GABAergic projections reach the ventral lateral and ventral anterior nuclei of the motor thalamus. Thalamic nuclei then send glutamatergic projections to the motor cortex, thus closing the loop [44](Figure 1).

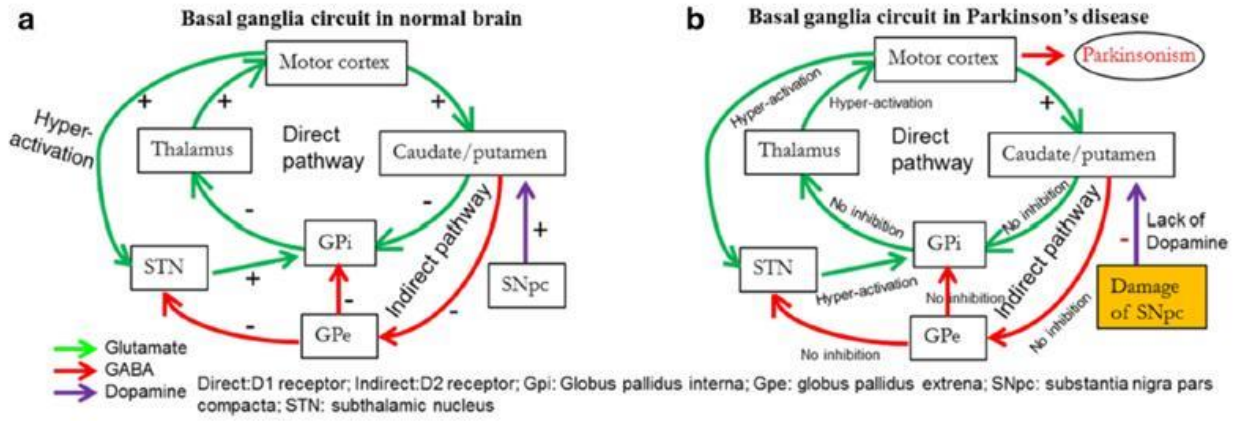


***Figure 1 :*** *Neuronal circuits and neurotransmission mechanisms in the brains of healthy individuals and those with Parkinson's disease. a: Neuronal circuit in basal ganglia in the physiological brain. b: Degeneration of substantia nigra pars compacta (SNpc) impairs the cortico-striatal circuit in PD brain. Decrease in DA levels in the SNpc and striatum causes loss of control of striatal neuronal firing, leading to withdrawal of inhibitory effects on globus pallidus as well as thalamus, therefore, the thalamus becomes over-excitable, which activates the motor cortex excessively. This ultimately leads to impairment of motor coordination and causes Parkinsonism.(PD: Parkinson's disease, DA: dopamine, SNpc: substantia nigra pars compacta ) (adopted from [49])*

Although, the basal ganglia have traditionally been considered the major brain region involved in PD since the disease is characterized by the loss of dopaminergic neurons in the substantia nigra pars

compacta., this theory ignores the influence of altered interactions between the basal ganglia and other cerebral components on Parkinsonian symptoms and may result in a restricted clinical picture and limit the therapeutic approaches.

The basal ganglia work closely with the cortex and cerebellum to form basic circuits involved in motor and cognitive tasks of varying complexity, from sensorimotor mapping to reasoning [50-53]. There is strong evidence that the cerebellum and the basal ganglia receive input from, and send output to, the cortex via multisynaptic anatomically segregated loops that perform distinct functional operations [54, 55]. Moreover, recent evidence suggests that there is an anatomical substrate for bidirectional communication between the cerebellum and the basal ganglia. In this respect, studies on rats [56] and monkeys [57] have demonstrated that cerebellum has a strong disynaptic projection to striatum via the thalamus. Recent studies in cebus monkeys have also shown that the subthalamic nucleus (STN) has a disynaptic projection to the cerebellar cortex via the pontine nuclei (PN). Similar data have recently been found in humans, using diffusion tensor imaging (DTI) [58, 59]. This broader perspective may allow us to understand the dopamine-related causes of PD symptoms as linked to the circular dynamic relations involving the meso-level multiple circuits within basal ganglia, cerebellum and cortex and their reciprocal interactions at the whole system level [60](Figure 2).

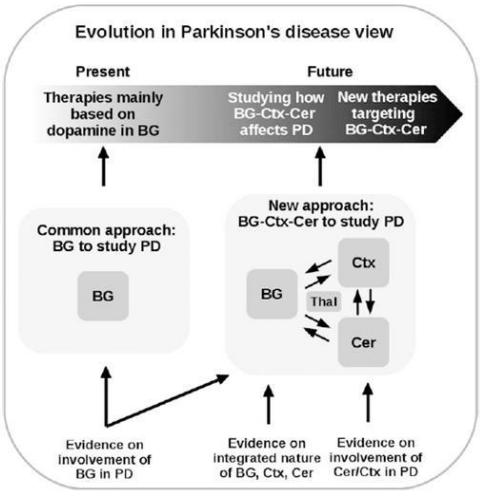


***Figure 2:*** *Graphical summary of the systems-level view to the study of PD proposed in this article. Pivoting on evidence supporting the integrated nature of BG, Ctx, and Cer, largely interacting through Thal, and the involvement of Cer and Ctx in PD, the view urges studying PD by focusing on the BG–Ctx–Cer system rather than on BG in isolation. Studying how such system affects PD is a crucial step to draw a more articulated clinical picture of the disease and to devise innovative therapeutic approaches. BG, basal ganglia; Thal, thalamus, Cer, cerebellum; Ctx, cortex; PD, Parkinson's disease. (adopted from [60])*

### 1.1.4 Neurotransmitter systems in PD

#### 1.1.4.1 Role of dopamine

The main brain area affected by PD is the substantia nigra, pars compacta (SNpc), a vital part of the basal ganglia [61]. This area is predominantly composed of neurons which secrete dopamine (DA), an essential brain monoamine, which functions primarily as an inhibitory neurotransmitter. In healthy brain, DA regulates the excitability of striatal neurons, which are involved in controlling the balance of body movement. In PD, DA-neurons of SNpc degenerate, and DA levels are diminished [61, 62]. Inadequate DA levels cause less inhibition of the activity of striatal neurons, allowing them to fire excessively. This makes it difficult for PD patients to control their movements, leading to tremor, rigidity, and bradykinesia, the hallmarks of PD-associated motor symptoms [63](Figure 1).

#### 1.1.4.2 Role of glutamate

Glutamate is the most abundant excitatory neurotransmitter in the central nervous system (CNS). It exerts its physiological effects on several classes of predominately post-synaptic ionotropic receptors such as a-amino-3-hydroxy-5-methylisoxazole propionic acid (AMPA) and kainic acid receptors, which are mainly permeable to sodium and potassium ions, and N-methyl-D-aspartate (NMDA) receptors, which are mainly permeable to calcium ions [64]. Synaptic transmission can also be mediated via metabotropic glutamate receptors, of which there are eight subtypes, coupled to either phospholipase C (subtypes 1 and 5) or adenylate cyclase (subtypes 2–4 and 6–8) which pre-synaptically modulate the release of GABA and glutamate [64, 65]. Glutamate is associated with both the direct and the indirect pathways of the basal ganglia, via metabotropic receptors [65, 66]. The receptors are highly expressed throughout the basal ganglia. It is hypothesized that the loss of dopamine neurons leads to an increase in glutamatergic activity in the basal ganglia. Pre-clinical studies with NMDA and AMPA antagonists have shown improvements in various motor symptoms of PD [67]. These results suggest that selective inhibition of glutamatergic hyperactivity may be an effective strategy for the treatment of some PD symptoms, particularly those that do not respond to L-dopa therapy [68]. Both clinical and pre-clinical data suggest that modulation of glutamate via AMPA receptor potentiation is therapeutically effective in the treatment of cognitive impairement and depression in PD and other CNS disorders [69].

#### 1.1.4.3 Role of GABA/$Ca^{2+}$ system

Gamma amino butyric acid (GABA) is an inhibitory neurotransmitter, which controls calcium ion ($Ca^{2+}$) influx directly via GABAergic receptors and, indirectly, via astrocytes [70]. The $Ca^{2+}$ /GABA

mechanism stabilizes neuronal activity both at the cellular and systemic levels. In the case of PD, due to mitochondrial damage, the $Ca^{2+}$ -buffering system become impair, which causes $Ca^{2+}$ -excitotoxicity leading to neuronal loss in the SNpc [71]. It has been observed that ~80% of newly diagnosed PD patients have abnormal olfaction, which is due to damage of the DA-neurons in the olfactory bulbs [72]. The function of DA neurons, in the midbrain and in the olfactory system are controlled by glial cell-derived neurotrophic factor (GDNF), which is also regulated by the $Ca^{2+}$ /GABA system. Moreover, GDNF function as a chemo-attractant for GABAergic cells and for axons of DA neurons. The neuroprotective effects of GDNF were observed in PD animal models when administered in GABAergic neurons in the striatum, but not in the SNpc [73], which suggests that the collapse of the GABA/ $Ca^{2+}$ system is involved in DA-neuronal death in PD [74].

#### 1.1.4.4 Role of serotonin

Serotonin (5-HT) also plays an important role in PD development, especially in several motor and non-motor symptoms, including tremor, cognition, depression, and psychosis, as well as levedopa (L-DOPA)-induced dyskinesia [75]. There is ~25% loss of serotonergic receptor (HT1A) at the median raphe nucleus in PD patients, and this is correlated with the severity of resting tremor [76], which suggests that loss of 5-HT projections in midbrain is more relevant for initiation of PD tremor than loss of nigrostriatal DA-projections. Although, a strong relation between decline of 5-HT and depression have been found by several investigators in PD [77], the importance of 5-HT and it relationship with the progression of PD needs to be further investigated.

#### 1.1.4.5 Role of acetylcholine

Acetylcholine (ACh), which plays significant role in cognition, is downregulated in several neurological diseases, including PD and AD [78]. Within the basal forebrain subventicular region, there is a broad band of cell clusters, known as nucleus basalis of Meynert (nbM), which are mainly cholinergic. Different patterns of neuronal loss have been observed in the nbM of patients with PD and other forms of dementia, which supports the idea of an involvement of the cholinergic system in PD [78, 79].

### 1.1.5 Neuropathological features

Macroscopically, the main characteristic morphological change in the PD brain is observed in cross-sections of the brainstem, where in almost all cases there is a loss of the dark pigmented area in the substantia nigra pars compacta (SNpc) and locus coeruleus. This loss of pigment correlates directly with

the death of dopaminergic (DA) neuromelanin-containing neurons in the SNpc and noradrenergic neurons in the locus coeruleus [80]. Cell death in the SNpc is mostly restricted to a specific group of neuromelanin-containing dopaminergic neurons, namely A9 neurons, whereas other neuronal and glial cell types are largely spared (Figure 2). Quantitative morphometric studies of postmortem PD brains have estimated a loss of approximately 30% of DA neurons in the SNpc by the onset of motor symptoms, taking the age of the individual into account [81-85]. After the onset of motor symptoms, the loss of nigral DA neurons increases to 60% or more and correlates strongly with the severity of motor features and disease progression [84-86].

Microscopically, the pathological hallmark of PD is the presence of abnormal cytoplasmic deposits within the neuronal cell bodies that are immunoreactive for the protein α-synuclein. These pathological protein aggregates are called Lewy bodies (LBs) and are often accompanied by dystrophic neurites (Lewy neurites), that are usally axonal [87].

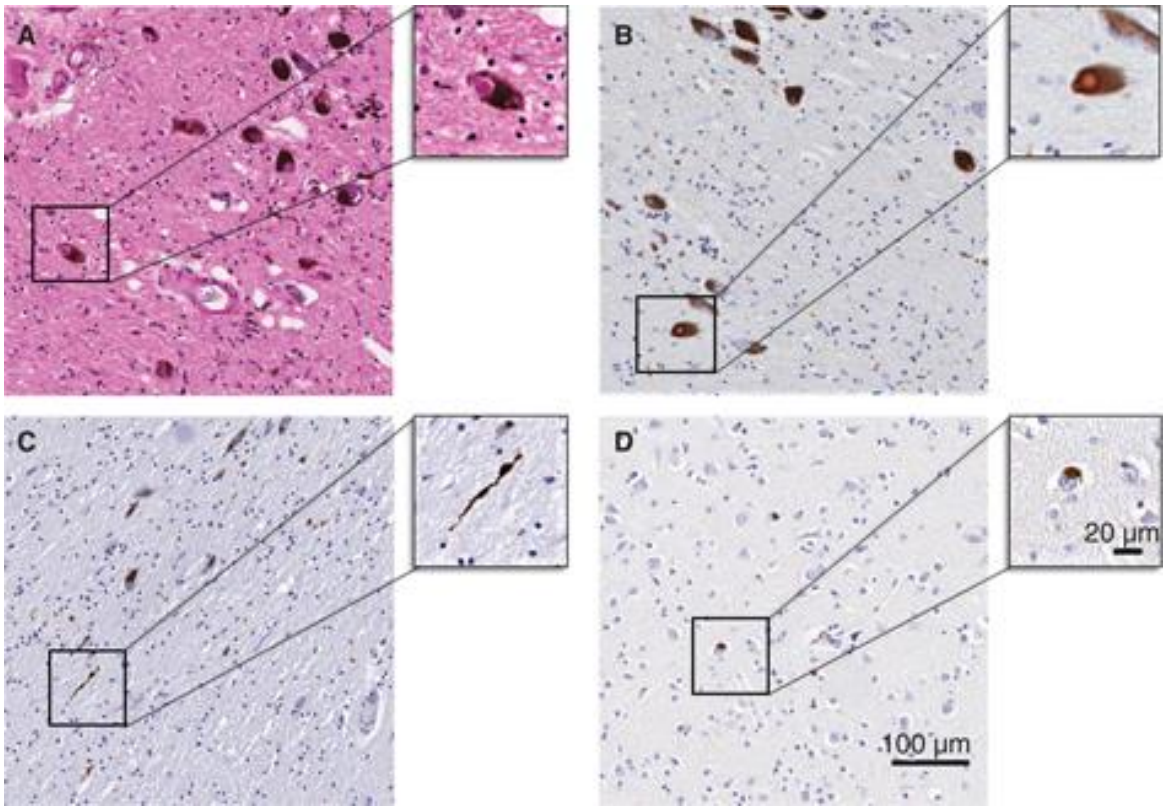


***Figure 2 :*** *Examples of Lewy-pathology in the substantia nigra pars compacta( SNpc) (A–C) and the prefrontal cortex (D) in coronal sections of a post-mortem PD brain. (A) Typical brainstem Lewy body inside a neuromelanin-containing DA neuron in routine hematoxylin and eosin histological staining. Lewy neurites are not visible in this type of*

*histological preparation. (B) Typical brainstem Lewy body with the characteristic halo, visualized by α-synuclein immunohistochemistry, a much more sensitive method that can also reveal dystrophic Lewy neurites as seen in (C). (D) Cortical Lewy body, less well defined and without a halo.(adopted from [88])*

***Lewy body pathology***. Lewy Bodies (LBs) are intracytoplasmic inclusions that are composed of a granular and fibrillar core with a surrounding halo (Figure 2A and 2B). The size of a LB can vary from 5 to 30 μm in diameter, and more than one LB can be found within a single neuron [89]. Two types of LB have been described in the literature: classic brainstem and cortical LBs (Figure 2B and 2D). Regarding their morphology, the main difference is that cortical LBs have less distinct outlines, are typically smaller, and lack the halo. The primary structural component of LBs is filamentous α-synuclein [87], a protein that is ubiquitously expressed in the brain. In PD and other synucleinopathies, it adopts an amyloid-like filamentous structure and develops into an abnormally phosphorylated and aggregated form. The halo of a LB is composed mainly of α-synuclein [90]. LBs also include a number of proteins, such as ubiquitin, parkin, tau, cytoskeletal proteins (such as neurofilaments, MAPs, and tubulin),heat shock proteins (HSPs), oxidized/nitrated proteins, proteasomal and lysosomal elements, and others [91].

***Braak staging.*** The main staging system in PD pathology was introduced by Braak and colleagues in 2003. This was based on semiquantitative assessment of LB distribution, at postmortem, in a large autopsy series [92]. In Braak stages 1 and 2, LB lesions are observed mainly in the dorsal motor nucleus (IX /X), reticular formation, and anterior olfactory nucleus. At these stages, patients are considered asymptomatic or presymptomatic, although they may have some early nonmotor features, especially autonomic (e.g., constipation), olfactory, and sleep-related dysfunction [93, 94]. As the disease progresses (stage 3), the SNpc becomes involved, with LB pathology and neuronal loss observed in melanated neurons. At this stage, the pathology also extends to the locus coeruleus and amygdala, eventually reaching the temporal limbic cortex (transentorhinal area) in stage 4. During stages 3 and 4, the typical clinical motor features begin to manifest. Finally, during stages 5 and 6, the main feature is the involvement of the entire neocortex and high-order areas, including the prefrontal cortex and primary sensory and motor areas [92, 95]. Clinically, this is translated to severe PD with significant gait disturbances and dementia. The Braak hypothesis was later revised to suggest that α-synuclein-associated pathology may actually be initiated in nasal and intestinal mucosal areas, particularly in the olfactory bulb and enteric cell complexes ("dual-hit hypothesis") [96].

Since its introduction in 2003, the Braak staging system has been a subject of controversy. Subsequent studies have shown that a proportion of PD brains do not appear to conform to this pattern [97, 98], while attempts to correlate Braak staging with clinical dysfunction have also been unsuccessful [99]. Another criticism of the Braak system is that it is not based on neuronal loss but on the distribution of Lewy-related pathology [100].

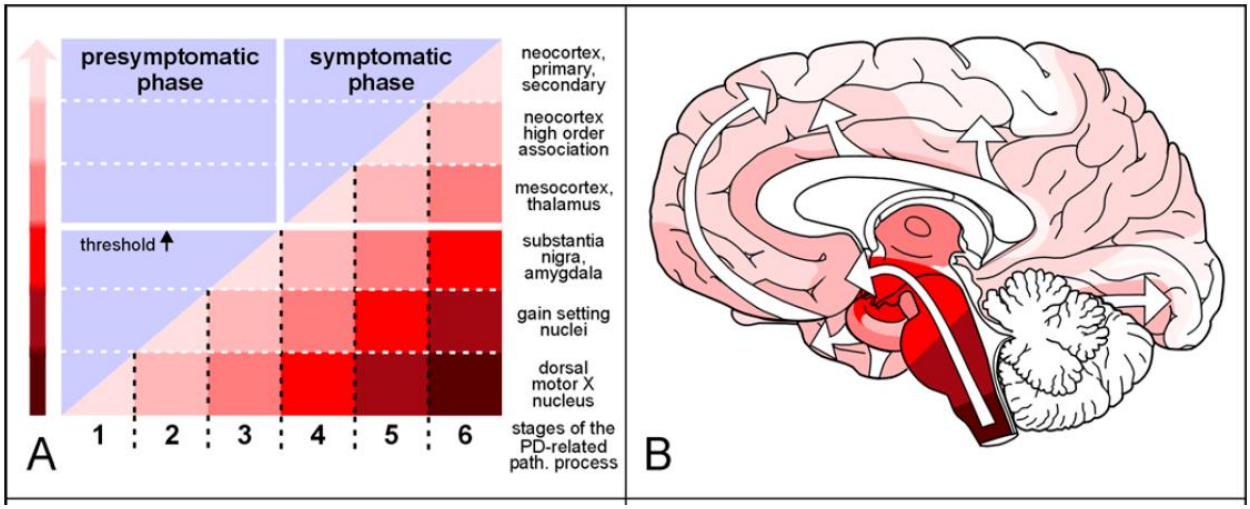


***Figure 3 :*** *PD presymptomatic and symptomatic phases according to Braak hypothesis. A. The presymptomatic phase is marked by the appearance of Lewy neurites/ bodies in the brains of asymptomatic individuals. In the symptomatic phase, the individual neuropathological threshold is exceeded (black arrow). The increasing slope and intensity of the colored areas below the diagonal indicate the growing severity of the pathology in vulnerable brain regions (right). The severity of the pathology is indicated by darker degrees of shading in the colored arrow (left). B Diagram showing the ascending pathological process (white arrows). The shading intensity of the colored areas corresponds to that in A (adopted. by [101]).*

### 1.1.6 Etiology of PD

PD is a multifactorial disease in which both genetic and environmental factors play a role. Age is the major risk factor for PD, with the median age of onset being 60 years [102]. The incidence of the disease increases with age to 93.1 (per 100,000 person-years) in age groups between 70 and 79 years [103, 104]. In addition, there are cross-cultural differences, with higher prevalence reported in Europe, North America and South America compared to African, Asian and Arab countries [105].

#### 1.1.6.1 Environmental factors

***Cigarette Smoking.*** Cigarette smoking has been extensively studied in relation to PD, with mostly consistent results. Most epidemiological reports are case-control studies showing reduced risk of

developing PD, with larger cohort studies also concurring [106]. The reasons for this reduced risk are not fully understood. Activation of nicotinic acetylcholine receptors on dopaminergic neurons by nicotine or selective agonists has been shown to be neuroprotective in experimental models of PD [107, 108]. Nicotine can also stimulate the release of dopamine, which is involved in reward mechanisms; therefore, it is difficult to confirm whether smoking prevents PD or whether PD helps prevent habitual cigarette use. As a result of a reduction in dopamine in patients with PD, patients may be less prone to addictive behaviors and thus less likely to smoke. This hypothesis is supported by the fact that patients with prodromal PD and PD were able to quit smoking much more easily than control subjects [109].

***Caffeine*.** A number of studies have examined the effect of caffeine on the development of PD and reported a reduced risk of developing PD in coffee drinkers [110]. Caffeine is an adenosine A2A receptor antagonist that is thought to be protective in PD [111]. It has been reported that the risk of developing PD is reduced by 25% in coffee drinkers [112]. Regular tea drinkers have also been found to have a lower risk of developing PD [113]. As with smoking, the causative role of caffeine in the prevention of PD is not yet clear. In addition, there were differences between studies in terms of gender. Because estrogen competitively inhibits caffeine metabolism, interactions between estrogen and caffeine may partly explain why the risk for PD in postmenopausal women is dependent on hormone replacement therapy [114, 115].

***Pesticides, herbicides, and heavy metals.*** In 1983, the association between 1-methyl-4-phenyl-1,2,3,6-tetrahydropyridine (MPTP) and nigrostriatal degeneration was first discovered when several individuals developed typical PD signs after injecting themselves with a drug contaminated with MPTP [116]. MPTP is metabolized to the neurotoxin MPP+ (1-methyl-4-phenylpyridinium), which is a mitochondrial complex I inhibitor that selectively damages dopaminergic cells in the substantia nigra [115, 117]. The identification of MPTP as a cause of nigral degeneration led to the idea that PD might be caused by an environmental toxin. Paraquat (a herbicide structurally similar to MPP+) [118] and rotenone (a pesticide) are also selective complex I inhibitors and induce dopaminergic depletion [119]. The association between exposure to these chemicals and the risk of developing PD has been investigated in other epidemiological studies [120].

1.1.6.2 Genetic factors

It is estimated that genetic variation contribute approximately 25% to the overall risk of developing PD [121-123]. Genetic variants associated with PD vary in frequency and risk of PD. On the one

hand, genome wide association studies (GWAS) have identified a large number of common genetic variants that individually contribute only modestly to the risk of developing PD. On the other hand, there are a number of variants in single genes that are sufficient to cause disease (i.e., are pathogenic). These monogenic causes of PD have been identified predominantly by linkage analysis of affected families.

1.1.6.2.1 Sporadic PD-GWAS data

The genetics of sporadic PD has progressed primarily through case-control GWAS of common genetic variants. GWAS are powerful techniques for identifying genetic loci that have a small but additive effect on the trait of interest and can identify biological pathways relevant to that trait. The combined effect of multiple common genetic variants contributes to the risk of developing sporadic PD. While twin studies show greatest PD heritability when onset is below 50 years of age, GWAS heritability is greatest in those with PD onset over 50 years, demonstrating that common variants have the greatest genetic contribution to the risk of late-onset PD [121, 122]. Most GWAS related to idiopathic PD have focused on variants associated with the risk of developing PD. Only a minority have examined possible associations with other characteristics such as age of PD onset, progression of disease or response to medications. In addition, most studies have used European cohorts, limiting the applicability of results to worldwide populations. Information from these GWAS can be utilized in two main ways: first, the biological functions captured by associated variants can identify underlying disease mechanisms; second, the combined information from all associated variants can produce a 'polygenic risk score' to quantify an individual's genetic risk of developing a trait. GWAS have identified new genes relevant to the risk of developing PD. However, it can be challenging to determine the actual functional impact of the variants associated with the trait. Furthermore, significant variants tag a genomic region with which that variant is in linkage disequilibrium and most common variants are found in non-coding regions of the genome. Therefore, post-GWAS analyses are critical in assigning biological function to GWAS variants. Examples of post-GWAS analyses include pathway analysis (where groups of variants are analysed together to determine the relevance of sets of gene to the trait] and expression quantitative trait loci (eQTL) analysis (where variants associated with gene expression are identified,thus identifying a regulatory element) [124]. In PD, robust associations from multiple GWAS and subsequent post-GWAS analyses have been identified for SNCA, RAB29, MAPT, BST1, GAK, LRRK2 and HLA-DRB5 amongst others [123, 125]. GAK plays a role in synaptic endocytosis,thus linking this pathway in sporadic PD and the rare forms of DNAJC6 and SYNJ1 monogenic PD. Interestingly, some of these genes harbour common variants that increase risk to sporadic disease as well as rare variants that cause monogenic PD, indicating shared biological pathways (e.g., SNCA). A

polygenic risk score (PRS) allows quatification of the combined effect of GWAS variants in an individual. In addition, the PD risk PRS has been consistently shown to correlate with age of onset in multiple ethnicities, although PD GWAS on age of onset have found very few significant variants [126-129].A recent study used a novel approach to assess association between the PRS of genes within pre-specified functional pathways and the risk of PD and identified 46 significantly associated pathways, including 6 that did not involve any of the previously identified GWAS loci [130, 131]

1.1.6.2.2 Monogenic PD

Although PD is generally an idiopathic disorder, there is a minority of cases (5-10%) that have a family history, and approximately 5% have a Mendelian inheritance [132]. In addition, individual risk for PD is in part the product of as yet poorly defined polygenic risk factors. The genes that have been identified as potential causative genes of PD are referred to as "PARK" in the order of their identification. To date, 23 PARK genes have been associated with PD [133]. Mutations in the PARK genes show either autosomal dominant (e.g. SCNA, LRRK2 and VPS32) or autosomal recessive inheritance (e.g. PRKN, PINK1 and DJ1) and are summarized in Table 1. The involvement of some of these genes has not been clearly confirmed (PARK5, PARK11, PARK13, PARK18, PARK21, and PARK23), whereas others are considered risk factors (PARK3, PARK10, PARK12, PARK16, and PARK22) [134].

*Autosomal dominant PD*

Autosomal dominant forms of PD occur with an earlier onset than classic PD.The first type of familial PD, caused by a point mutation in the α-synuclein gene (SNCA), was discovered in 1997 [135]. A53T is a missense point mutation, which means that one amino acid is changed: the 53rd amino acid is changed from alanine to threonine. This mutation is the result of a change from guanine to adenine at position 209 of the SNCA gene (G209A). The A53T mutation was first documented in families of Greek and Italian ancestry and is associated with autosomal dominant, early-onset PD [135]. It has also been detected in a Korean family [136]. The A53T mutation results in an earlier age of onset and shorter disease duration [135]. Moreover,the A53T mutation has been shown to have faster kinetics of fibrilization than the wild-type protein [137]. Four other point mutations, as well as gene duplication or triplication, have since been associated with autosomal dominant PD [138-143]. Four other point mutations, as well as gene duplication or triplication of the locus, have since been associated with autosomal dominant PD [138-143].Autosomal dominant monogenic PD is also caused by mutations in the gene encoding leucine-rich repeat kinase 2 (LRRK2). Six LRRK2 mutations have been confirmed as pathogenic [144], the most common

of which is p.G2019S, estimated to be responsible for 1% of sporadic and 4% of familial PD worldwide [144].Recent genetic studies have led to the discovery of additional mutations in other genes responsible for autosomal dominant PD, including VPS35 (Table 1).

*Autosomal recessive PD*

Autosomal recessive forms also occur with an earlier onset than classic PD. Three of the PARK -genes causing autosomal recessive PD have been linked to mitochondrial homeostasis (PRKN, PINK1 and DJ -1). Specifically, the proteins PINK1 and Parkin (encoded by the PRKN gene) have both been implicated in the same mitochondrial quality control pathway, with PINK1 recruiting Parkin to dysfunctional mitochondria and initiating mitophagy [145]. Mutations in PRKN are the most common cause of autosomal recessive familial PD, occurring in up to 50% of all cases with early onset [134]. Finally, several autosomal recessive genes have been associated with atypical parkinsonism with variable features (Table 1), including ATP13A2 (PARK9), PLA2G6 (PARK14), FBX07(PARK17), and SYNJ1 (PARK20) [146-149].

***Table 1****: PARK- genes involved in familial Parkinson's disease [88].*

| **PARK** | **Gene** | **Inheritance** | **Description** | **Clinical features** | **Reference** |
|---|---|---|---|---|---|
| PARK1 | SNCA | AD | α-synuclein | Ranging from classical PD to early-onset cases with dementia, autonomic dysfunction, and rapid progression | [135, 142, 150] |
| PARK4 | | | | | |
| PARK2 | PRKN | AR | parkin RBR E3 ubiquitin protein ligase | Early-onset PD, slow progression, often features of dystonia | [151] |
| PARK5 | UCHL1 | AD | ubiquitin C-terminal hydrolase L1 | Classical PD—only one family, findings not since replicated | [152] |
| PARK6 | PINK1 | AR | PTEN-induced putative kinase 1 | Early-onset PD, slow progression | [153] |
| PARK7 | DJ-1 | AR | Parkinsonism-associated deglycase | Early-onset PD, slow progression | [154] |
| PARK8 | LRRK2 | AD | Leucine-rich repeat kinase 2 | Classical PD with less frequent dementia and slower progression | [155] |

| | | | | | |
|---|---|---|---|---|---|
| PARK9 | ATP13A2 | AR | Cation-transporting ATPase 13A2 | Early-onset (adolescence), atypical parkinsonism with dementia, spasticity and supranuclear palsy (Kufor–Rakeb syndrome) | [149, 156] |
| PARK11 | GIGYF2 | AD | GRB10 interacting GYF protein 2 | Classical PD | [157] |
| PARK12 | HTRA2 | AR | HtrA serine peptidase 2 | Classical PD | [158] |
| PARK14 | PLA2G6 | AR | Calcium-independent phospholipase A2 enzyme | Early onset with atypical features (dystonia parkinsonism) | [148] |
| PARK15 | FBX07 | AR | F-box protein 7 | Early onset with atypical features (pallido-pyramidal syndrome) | [146] |
| PARK17 | VPS35 | AD | Vacuolar protein sorting-associated protein 35 | Classical PD | [159] |
| PARK18 | EIF4G1 | AD | Eukaryotic translation initiation factor 4 gamma 1 | Classical PD | [160] |
| PARK19 | DNAJC6 | AR | HSP40 Auxilin | Early-onset PD, slow progression | [147] |
| PARK20 | SYNJ1 | AR | Synaptojanin 1 | Parkinsonism with dystonia and cognitive decline | [161] |
| PARK21 | DNAJC13 | AD | Receptor-mediated endocytosis 8 (RME-8) | Classical PD | [162] |
| PARK23 | VPS13C | AR | Vacuolar protein sorting-associated protein 13C | Early-onset PD, rapid progression | [163] |

### 1.1.7 Mechanisms involved in PD pathogenesis and spread

A number of mechanisms have been implicated in PD pathogenesis, with aggregation of misfolded proteins playing a central role in the development of the disease [164]. Several other processes are thought to be involved, with several studies suggesting that gene mutations, environmental toxins, mitochondrial dysfunction, oxidative stress, excitotoxicity, neuroinflammation and abnormal proteostasis play a role in the development and progression of PD [5, 165, 166] (Figure 4).

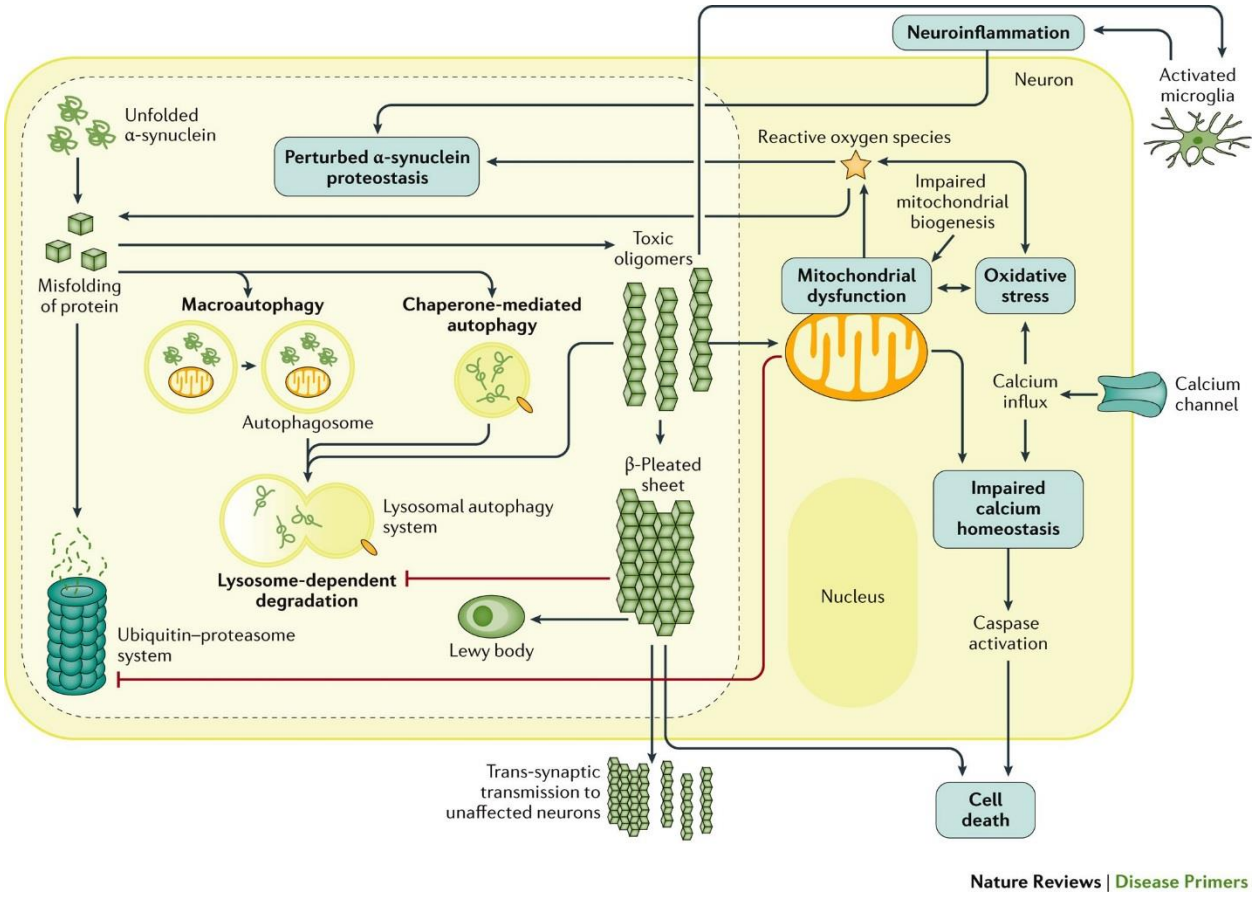


***Figure 4 :*** *Mechanisms involved in Parkinson's disease (PD) pathogenesis. Accumulation of misfolded proteins like α-synuclein, defects in mitochondrial function, oxidative stress, neuroinflammation, calcium dysregulation and axonal transport are implicated in PD pathogenesis. (adopted from [4])*

#### 1.1.7.1 Aggregation and spread of misfolded proteins

***Alpha-synuclein (aSyn).*** One of the characteristic pathologies of PD is the intracellular accumulation of LB in DA neurons of SNpc, which contain misfolded aggregates of aSyn and other associated proteins [165, 167]. Converging evidence from various in vitro and in vivo studies suggested

that αSyn misfolding and aggregation is a major pathogenic event in PD. This process involves the formation of non-fibrillar off-pathway and soluble transient pre-fibrillar intermediate species termed as "oligomers', which eventually convert into insoluble fibrillar aggregates with distinct cross β-sheet conformation [168](Figure 5).

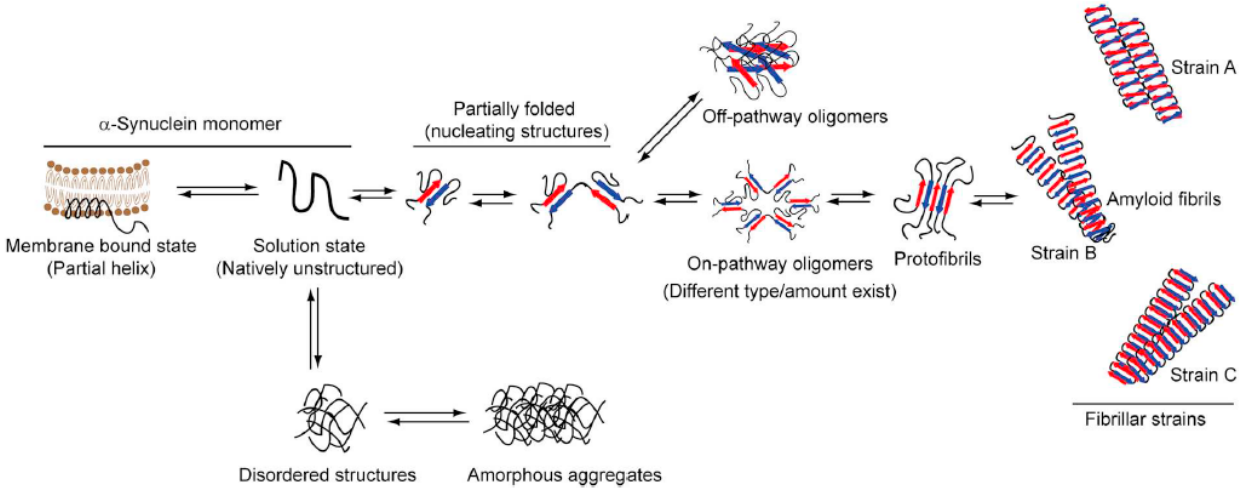


***Figure 5 :*** *Conformational states of α-Syn. α-Syn monomer exists in two states, i.e., solution (natively unstructured) and membrane-bound state (partially helical conformation). Upon incubation, the natively unstructured monomer converts into oligomers (on-pathway or off-pathway) via partially folded nucleating structures. The on-pathway oligomers eventually convert into highly ordered cross-β-sheet amyloid fibrils whereas the fate of off-pathway oligomers is unclear. Natively unstructured protein can also form disordered structures, which results in the formation of amorphous aggregates. Under different assembly/solution conditions, native protein can form different types of amyloid fibrils, i.e., fibrillar strains. (adopted from [168])*

Direct evidence for the involvement of αSyn in disease pathogenesis came with the discovery of the autosomal dominant PD mutations and multiplication of gene encoding αSyn. Since then, the effects of these familial PD mutations on the structure and aggregation properties of αSyn has been extensively studied [169-171]. *In vitro* studies have found that the familial PD mutations A53T, E46K, and H50Q accelerate αSyn fibrillation [172-174], whereas A30P, A53E, and G51D delay the aggregation rate *in vitro* [141, 175, 176]. The recently discovered mutation A53V, which is associated with late-onset PD [177], also accelerates αSyn aggregation and promotes early oligomerization similarly to the A53T mutation [178]. Despite several studies, the basis for the differences in the fibrillation/ oligomerization properties of wild-type (WT) α-Syn and its mutants remains elusive. Moreover, how the disease-associated point mutations alter the disease phenotype is also not clear. Dysregulation of cellular processes and toxic gain or loss of

function are among the major molecular mechanisms that may be responsible for the neurotoxicity associated with αSyn aggregation. Previously, αSyn amyloid fibrils were thought to be the toxic species responsible for the pathogenesis of PD. However, recent studies indicate that the oligomers formed during αSyn aggregation are the most potent neurotoxic species responsible for the pathogenesis of PD [179, 180]. It has been hypothesized that permeabilization of dopaminergic vesicles by αSyn oligomers and subsequent generation of reactive oxygen species in dopaminergic neurons is the cause of associated neurotoxicity and neurodegeneration in case of PD [181, 182]. Moreover, the familial mutations also affect the early oligomerization of αSyn and alter the associated pathogenicity. The study of the primary events of αSyn aggregation, which include oligomerization, is very important to understand the etiology of PD. However, these oligomeric species are highly metastable and transient. Therefore, characterizing and quantifying the relative abundance and nature of each of these oligomeric species is challenging. Although α-Syn oligomers are the toxic species and contribute to the disease pathogenesis, αSyn fibrils play a crucial role in disease spread and progression [183-185].

Previously it has been reported that αSyn fibrils are infectious similar to prions. The "prion hypothesis" states that aSyn spreads throughout the CNS in a manner similar to "prion proteins", infecting neighboring new, healthy neurons, and that this cycle continues until most of the CNS neurons are infected. Therefore, "prion-like infection" of aSyn may be responsible for disease progression and neurodegeneration in some types of PD [186]. According to Braak's hypothesis, aSyn, bacteria or viruses can travel through the olfactory tract and into the Vagus nerve to the medala and spread throughout the CNS, which may be responsible for triggering sporadic PD [187]. Recently, Chandra and colleagues discovered that enteroendocrine cells (EECs) in the gastrointestinal tract have many neuron-like properties and that aSyn is expressed in both EEC lines and native EECs of the mouse and human gut. These cells are directly connected to aSyn -containing nerves and form a neural circuit between the gut and the nervous system (gut-brain interaction hypothesis) [188]. Moreover, numerous clinical and pathological evidences have localized misfolded aSyn in EECs before it occurs in the brain. These phenomena suggest that PD pathogenesis originates in the gut and spreads to the CNS via cell-to-cell "prion-like propagation" [188]. Although the "prion hypothesis" provides useful insights into the progression of PD, the presence of aSyn is not always necessary for the occurrence of PD pathology or parkinsonism. Therefore, the "prion hypothesis" of PD remains controversial, although aSyn can infect healthy cells like a prion [189].

Other mechanisms have been implicated in the transmission of aSyn. Exosomes are ~50–150-nm vesicular structures that contain a variety of cellular material, including protein, and are released by

numerous cell types, presumably as a means of intercellular transport of cargo [190]. A well-established and growing literature indicates that exosomes are involved in the release of aSyn and other proteins involved in the pathogenesis of PD [191, 192]. Several laboratories have demonstrated the secretion of αSyn by exosomes in cell-based assays, in which it is readily taken up by recipient cells and causes toxicity [193, 194]. Recently, it was shown that exosome-associated αSyn purified from the cerebrospinal fluid (CSF) of patients with Alzheimer's Disease (AD) and dementia with Lewy bodies (DLB) can be taken up by endocytosis and induce αSyn aggregation when injected into wild-type mouse brain [195]. Although contact-independent transfer between cells in the brain is likely responsible for much of the transmission of protein aggregates, there is emerging evidence that mechanisms involving direct contact between cells may also play a role. Tunneling nanotubes (TNTs) are thin (∼50– 200-nm), transiently lived membranous connections between cells that can span distances up to ∼100 μm and facilitate the transfer of a variety of macromolecules and cellular structures, including nucleic acids, proteins, mitochondria, the endoplasmic reticulum, the Golgi apparatus, and endosomes. TNTs were originally described in PC-12 neuroendocrine cells, but have also been described in multiple mammalian cell types, including neurons [196-198]. TNTs have been reported to mediate the neuron-to-neuron and astrocyte-to-astrocyte transmission of αSyn fibrils [199, 200] as well as intercellular transfer of Aβ and tau aggregates [201, 202].

***Other misfolded proteins.*** A number of molecular, genetic and biochemical studies have shown that a mixture of multiple misfolded protein aggregates, such as p-tau and Aβ, is also commonly seen in human post-mortem brains of patients diagnosed as mixed dementia with Lewy bodies (DLB) and PD with dementia (PDD) [72]. Examination of brains of several PD patients by Gomperts and colleagues showed mixed amyloid deposition in their brains associated with cognitive declines without dementia, indicating that amyloid contributes to cognitive, but not motor decline over time [203]. In the same way, Hepp and colleagues found that the burden and extent of Aβ pathology contributed to cognitive impairment in PDD and LBD [204] Hyperphosphorylation of tau (p-tau) can lead to an accumulation of paired helical filaments of tau, known as neurofibrillary tangles (NFT), a characteristic pathology of different neurodegenerative diseases, including Alzheimer's Disease (AD), frontotemporal dementia with parkinsonism (FTDP), and progressive supra-nuclear palsy (PSP) [205]. The p-tau can also colocalize with LB, which is often associated with the development of sporadic PD [206]. Similarly, in FTDP, mutation of the gene encoding microtubule associated protein (MAPT) leads to increased accumulation of p-tau [206]. The p-tau has also been associated with mutations of the LRRK2 gene [133]. Although NFTs are associated most closely with AD, they can co-localize with aSyn in LB and play an important role in destabilizing the DA-neuronal architecture, ultimately leading to rapid degeneration and death of DA neurons [204, 205, 207].

#### 1.1.7.2 Mitochondrial damage and oxidative stress

The theory of oxidative stress is one of the most promising theories in the research of PD and other age-related neurodegenerative diseases [208]. This theory postulates that mitochondria are the "hotspot" for degenerative processes. In PD, abnormal activity of complex-I in mitochondria has been observed to directly affect cellular ATP production and lead to cell death [209]. Brain monoamines, such as DA and 5- HT, generally act as antioxidants [210]. However, degradation of DA by monoamine oxidase-B (MAO -B) in conjunction with ground state $O_2$ leads to the formation of reactive oxygen species (ROS) [211]. Researchers have found increased markers of oxidative stress and related changes (including free radical damage to DNA, proteins, and lipids) in PD patients [211].

#### 1.1.7.3 Excitotoxicity

DA is an inhibitory neurotransmitter that normally maintains the excitatory state of subthalamic nuclei (STN) at basal levels. However, in the case of PD, the STN is overactivated due to a lack of DA neurons, resulting in excessive production of the neurotransmitter glutamate [68]. Excess glutamate binds to its ionotropic receptors (NMDA or AMPA) and opens the voltage-gated calcium ($Ca^{2+}$) channels (VGCC), causing $Ca^{2+}$ excitotoxicity. Excessive $Ca^{2+}$ exposure can damage mitochondria and produce ROS, leading to oxidative stress [212, 213]. In addition, environmental toxins can cause increased production of glutamate, leading to $Ca^{2+}$ excitotoxicity, which makes DA neurons vulnerable to neurodegeneration [212, 214-216].

#### 1.1.7.4 Neuroinflammation

A cascade of events is involved in neuroinflammatory processes in PD, including activation of microglia and increased secretion of cytokines [217]. For example, researchers have found strong links between proinflammatory cytokines and degeneration of DA neurons after subchronic administration of MPTP in animals [218]. Several studies have shown that levels of inflammatory enzymes, such as cyclo-oxygenase-2 (COX - 2), are increased several-fold in DA neurons of the postmortem PD brain and in a mouse model of PD [219].

#### 1.1.7.5 Impairment of proteostasis

***Ubiquitin-Proteasome System (UPS) and heat shock proteins (HSP).*** UPS is the most efficient disposal system of the cell and is mainly responsible for the degradation of short polypeptides into small intracellular and plasma membrane proteins in cells [220]. It is also responsible for the degradation of

misfolded or damaged proteins in the cytosol, nucleus or endoplasmic reticulum [221]. Impairment or failure of this system has been observed in the pathogenesis of PD, leading to aggregation of misfolded amyloid proteins, such as LB, resulting in neurodegeneration in SNpc [222, 223]. In the case of PD, several other proteins, such as Parkin and UCH-L1, are involved in the degradation of misfolded aSyn in addition to UPS. Experimental evidence suggests that UCHL1 is involved in the production of ubiquitin that is found to colocalize with LB [224]. Inactivation of ubiquitin hydrolases with ubiquitin aldehyde produces toxic effects in primary neuronal cultures. Low-level proteasome inhibition (100 nM MG115) in human neuroblastoma cells (SH -SY5Y) over several weeks showed mitochondrial degeneration, increased protein oxidation and aggregates resembling sporadic PD [225, 226]. Inactivation of UCHL-1 in mice leads to axonal dystrophy syndrome or motor ataxia [227]. Parkin mutations in Drosophila show selective DA -neuronal death as well as deficits in locomotion similar to those of PD –patients [228, 229].

Molecular chaperones or heat shock proteins, comprise one of the most efficient, highly conserved cellular defense mechanisms involved in protein folding, refolding of partially misfolded proteins, and protein degradation [230, 231]. The major HSPs involved in PD are HSP 26, 40, 60, 70, 90, and 100. Some of the HSPs are localized in synapses and axons, and their levels are downregulated in both PD [232] and other neurodegenerative diseases [231]. HSPs can bind to aggregated aSyn or tau oligomers or prefibrillar structures and interfere by forming low MW soluble oligomers or higher order insoluble structures, which reduces their toxicity[233, 234].. HSPs also play a central role in the regulation and precise functioning of the ubiquitin-proteasome and autophagy-lysosomal signaling pathways [231, 234, 235].

***Autophagy and protein synthesis..***Large protein debris which are too large to fit through the narrow proteasome tube,, such as oligomers and fibrils of aSyn, cannot be degraded via UPS [236, 237]. Autophagy is the specialized mechanism present as alternative protein clearance machinery in each cell to degrade such conformations. [236, 238, 239].On the basis of the method of delivery of cargo to the lysosome, autophagy can be categorized into three classes: chaperone-mediated autophagy (CMA), macroautophagy (MA), and microautophagy [240].

CMA is more specific and exerts its activity through interaction with the heatshock cognate protein (HSC70), which specifically binds to small soluble proteins to be degraded via a specific pentapeptide targeting motif (KFERQ) [241]. HSC70 docks the proteins to be degraded to the lysosomal membrane receptor, lysosome-associated membrane protein 2 (LAMP2A), and then transports them to the lysosomes where they are degraded by lysozymes [242]. Experimental evidence suggests that downregulation of autophagy-related genes, Atg5 or Atg7, in the CNS leads to aggregation of poly-

ubiquitinated protein debris in neurodegenerated tissues in mice [243, 244]. aSyn has been shown to be selectively translocated to lysosomes for degradation by the CMA [236]. Therefore, dysfunction of the CMA decreases the efficiency of aSyn degradation, leading to excessive accumulation of this protein, which significantly impairs neuronal activity. In addition, decreased levels of LAMP1, LAMP2A and HSC70 were observed in SN of PD patients, suggesting dysregulation of CMA [245, 246].

Macroautophagy (MA) is a preserved intracellular degradation pathway that involves directing substrates like damaged or superfluous organelles (mitochondria, peroxisomes), aggregated proteins, aggregation-prone proteins, etc. toward the lysosome via double-membrane vesicles known as autophagosomes (APs). The phagophore, a cup-shaped double-membrane vesicle, is the perceivable herald of APs. Edges of phagophores extend and fuse with each other and lead to the formation of APs. The mechanism of MA has been divided into different stages: initiation, elongation, and maturation of APs. Noteworthy progress has been made on the identification of proteins that control the biogenesis of APs, although how APs are built up and what could be the source of the AP membrane are prime questions in this area. Many studies advocate a relationship between the endoplasmic reticulum (ER) and autophagy structures and put forth the hypothesis that AP membranes are derived from the ER[247].However, ER is not the only source; mitochondria, ER−mitochondrial contact sites, Golgi apparatus, plasma membrane, and the ER−Golgi intermediate compartment are also involved in the biogenesis of APs, as they supply lipids to the growing isolation membrane [248], but the underlying molecular mechanism is still unclear. There are many genes as well as proteins involved in the biogenesis of APs, most of which are conserved from yeast to human. Atg1 is the autophagy-related gene-1, also known as ULK1 in mammals, which is reported to form complexes in combination with Atg13 and FIP200. The activity of ULK1 kinase is essential for recruitment of VPS34 (vacuolar protein sorting 34) to the phagophore [249]. VPS34 is a class-III phosphatidylinositol- 3-kinase catalytic subunit-3 (PI3KC3) complex which is required for the formation of the phagophore. After completion of the initiation process, it further leads to elongation of AP, which is mainly controlled by the ubiquitin-like conjugation system. This system consists of Atg7 [ubiquitin-activating-enzyme (E1)-like] and Atg10 [ubiquitin-conjugating enzyme (E2)-like], which both assist in the conjugation of Atg12 with Atg5 and form a complex which ultimately forms another complex, Atg12-Atg5, with Atg16L, an E3-ubiquitin ligase. This promotes the conversion of LC3,which is cleaved after the C-terminal glycine, to LC3-I that subsequently it is conjugated to phosphatidylethanolamine (PE) to form LC3-II, causing elongation of AP [250].Furthermore, maturation of AP involves fabrication of APs throughout the cytoplasm, followed by the trafficking of APs by means of the dynein machinery on the

microtubules to carry APs into a juxtaposition with the lysosome [251]. After fusion of an AP with a lysosome, the contents of the AP are degraded into free amino acids by lysosomal hydrolases (Figure 6).

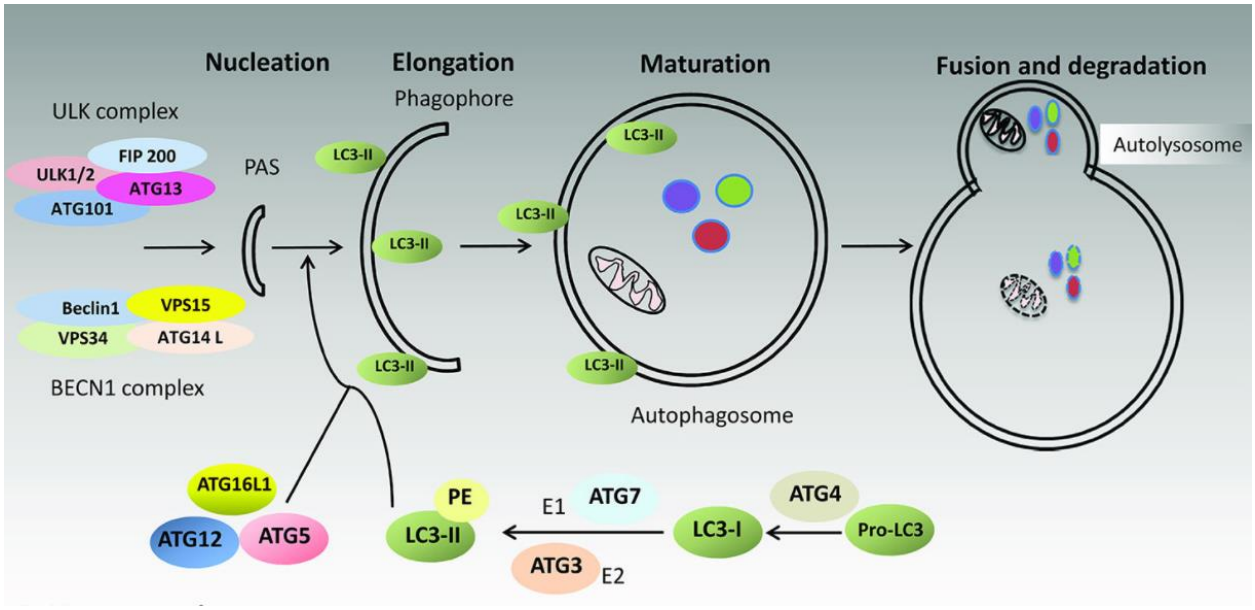


***Figure 6*** *: Macroautophagy consists of several steps of nucleation, elongation, maturation, and finally fusion and degradation. The process starts by the association of the ULK1 and BECN1 complexes that form the basis for recruiting other autophagy-related (ATG) proteins as well as the lipidated form of LC3 (LC3-II, i.e. LC3-I linked to phosphatidyl-ethanolamine). The ULK1 complex consists of the serine/threonine kinase UNC-51-like autophagy activating kinase (ULK1), focal adhesion kinase family interacting protein of 200 kDa (FIP200), ATG13, and ATG101. The PI3 kinase III nucleation complex (BECN1 complex) consists of Beclin-1, class III phosphoinositide 3-kinase [PI3K-III; also termed vacuolar protein sorting 34 (VPS34)] and its regulatory subunit VPS15. LC3-I protein is formed from its precursor protein, pro-LC3 with the contribution of ATG4. After attaching phosphatidyl-ethanolamine (PE) to LC3-I by ATG7 and ATG3, the lipophilic form (LC3-II) is created. The closed autophagosome fuses with a lysosome to form the autolysosome, where the proteins undergo degradation by different lysosomal enzymes. (adopted from [252])*

Microautophagy is mainly involved in the degradation of small cytosolic proteins, even under resting conditions. This term is reserved for removal of damaged or misfolded proteins and superfluous organelles that are directly engulfed by lysosomes or vacuoles in the case of yeast. In the early years it was known that microautophagy is not selective, but it was proven that cargo can be distinguished in the case of microautophagy, which gave genesis to new terms like micromitophagy, microlipophagy, and micropexophagy [253]. A link between microautophagy and αSyn is not yet clearly established.

Substantial evidence from human post-mortem studies shows that autophagy mechanisms are impaired in the PD brain The brain of PD is particularly susceptible to dysfunction of the autophagy

pathway, which may be due to the lack of formation of autophagosomes or the inability to bind with lysosomes due to a deficiency of lysozymes or dysfunction of HSC70 or LAMP2A [5, 254, 255]. Moreover, autophagy vacuole accumulation and levels of the AP marker microtubule-associated protein 1 light chain 3 (LC3) have been reported to increase in the SNpc area of the postmortem PD brain and temporal cortex of patients with DLB compared with age-matched controls, suggesting that autophagy dysfunction is associated with PD disease progression [256-258]. Recent transcriptome studies using postmortem tissue have shown that several autophagy-related downstream mechanisms, such as mTOR and PI3K/AKT signaling, were also severely impaired in PD brain [259, 260].

The mechanistic target of rapamycin complex 1 (mTORC1), a nutrient sensor and metabolic regulator heavily implicated in the process of aging and neurodegeneration [261-263]. mTORC1 is composed of the proteins mTOR kinase and its regulator protein, Raptor, as well as mLST8, PRAS40, and Deptor. Its primary function is to sense intracellular nutrient status and extracellular trophic factors, integrate these signals, and ultimately regulate the balance between cells' anabolic and catabolic processes. Particularly, mTORC1 is a positive regulator of protein synthesis and negative regulator of autophagy [264, 265] (Figure 7).

mTORC1 inhibits autophagy at multiple levels, including the inhibitory phosphorylation of ULK1 and transcription factor EB (TFEB), which respectively initiate autophagy and promote the lysosomal biogenesis required to break down the contents of autophagosomes the contents of autophagosomes [266, 267]

Although autophagy is extensively studied in PD, little information is available about alterations in protein synthesis in PD. Abnormal morphology and disruption of the nucleolus and reduced nucleolin expression have been reported in the substantia nigra in PD [268-270] and related experimental models [270, 271]. Mutations in DJ1,causative of familial PD, alter rRNA biogenesis [272]. Added to this limited input is the fact that nothing is known about the possible link between the machinery of protein synthesis and α-synuclein aggregates, particularly α-synuclein oligomers in PD. The hypothesis of translational deregulation as a key toxic mechanism in PD is a potential game changer in the field of the molecular pathogenesis of PD, with implications for the development of PD diagnostics and disease-modifying therapies.

In recent years, evidence has accumulated that mTOR signaling is altered during PD progression [259, 273]. However, the role of mTOR in PD seems to be controversial since it could be either neuroprotective or neurotoxic in different PD models. Several studies have shown that PD toxins (rotenone, 1-methyl-4-phenyl1,2,3,6-tetrahydropyridine (MPTP), 6-hydroxydopamine (6- OHDA), etc.)

suppress mTOR signaling and reduce cell viability [270, 274, 275]. Nevertheless, increased mTOR protein levels have also been found in postmortem brains of PD [276]. In En1 (engrailed 1) - mouse model of PD, heterozygous deletion of En1, a transcription factor important for the survival of mesencephalic dopaminergic neurons, results in up-regulation of mTOR signaling in dopaminergic neurons [277]. Additionally, maneb and paraquat, two environmental risk factors for PD, could significantly increase mTOR levels in mice [276]. Moreover, accumulating evidence suggests that inhibition of mTOR with rapamycin or its derivatives could be neuroprotective in cellular and animal models of PD [255, 278-281]. Interestingly, a common anti-Parkinsonian medication, L-DOPA (levodopa), elicits motor side effects (dyskinesia) via the activation of mTOR signaling in the striatum of mouse model of PD [282, 283]. Inhibition of mTOR with rapamycin or its derivatives prevents the development of L-DOPA-induced dyskinesia without significantly compromising the anti-akinetic potency of L-DOPA in animal models of PD [278, 282].Given these data and the clinical burden of neurodegenerative disease, it's reasonable that translational research generally focuses on the inhibition of mTOR, rather than on its activation.

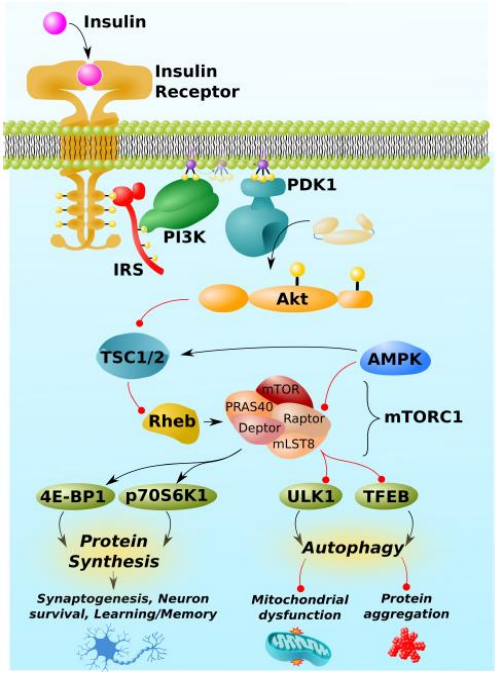


***Figure 7 :*** *mTORC1 pathway and regulation. mTORC1 is activated by insulin. Insulin/Akt signaling inhibits TSC1/2, thereby permitting the activation of the GTP-binding protein, Rheb. Rheb is the proximal activator of mTORC1. AMPK inhibits mTORC1 activity through indirect and direct mechanisms, phosphorylating TSC1/2 and the Raptor regulatory component of mTORC1. mTORC1 downstream targets include proteins involved the mRNA translation, 4E-BP1 and p70S6K1, and those involved in autophagy, such as the initiator of autophagy, ULK1, and the master regulator of lysosomal biogenesis, TFEB. By regulating the activity of these and other proteins, mTORC1 promotes protein synthesis, which is required for synaptogenesis, learning, and memory, but can also impair autophagy, leading to mitochondrial dysfunction and neurotoxic protein aggregation (Ab, phospho-tau, a-synuclein, etc.). Black arrows and red lines respectively represent positive and negative regulation.(adopted from [265])*

1.1.8. Drugs

1.1.8.1 Approved drugs.

Currently, there is not curative treatment to prevent or slow the progression of disease in PD patients. Therapies available aim at controlling symptoms and include both pharmacological replacement and surgical approaches but display severe side-effects [284]. Among these, the most effective and most commonly prescribed symptomatic pharmacotherapy remains the precursor of dopamine, L-3,4-dihydroxyphenylalanine(L-DOPA), which was developed in late 1960s[284]. However, chronic administration leads to an increase in motor fluctuations and abnormal movements termed dyskinesias in 80% of patients between 5 and 8 years of use, that are thought to arise because of the increasing loss of dopaminergic neurons over time and the intermittent availability of L-DOPA [285]. Other drugs currently used in PD treatment and their mechanism of action are shown in Table 2.

***Table 2 :*** *Drugs currently used in PD treatment and their mechanism of action*

| **Drug classes** | **Specific drugs** | **Mechanism of action** |
|---|---|---|
| Anticholinergic | Trihexyphenidy<br>Benztropine<br>Ethopropazine | Block acetylcholine receptors and prevents the dopamine degeneration |
| Monoamine oxidase (MAO) inhibitors | Selegiline | Blocks MAO-B receptors to reduce dopamine metabolism |
| Antiviral drugs | Amantadine | Blocks NMDA and acetylcholine receptors and promotes release of dopamine |
| Dopamine agonists | Bromocriptine<br>Pergolide<br>Ropinirole<br>Pramipexole | Directly stimulates dopamine receptors |
| L-dopa combinations | L-dopa/ Carbidopa<br>L-dopa/ Benserazide<br>Sinemet CR | Metabolism of dopamine in cells containing dopa-decarboxylase |

| | | |
|---|---|---|
| Catechol-O-methyl transferase (COMT) inhibitors | Entacapone | Blocks peripheral COMT activity to retain catecholamines |

1.1.8.2 Drug development

Development of therapeutic compounds and evaluation of their protective capacities may lead to identification of potential compounds/ strategies for clinical benefits of PD patients. Protection of dopaminergic neurons in pre-clinical studies by taurine, caffeine, Mfn2 overexpression, puerarin, progranulin gene delivery, nicotine receptor activation, estrogen in cell-culture study seems convincing and promising [286-290]. However, human clinical trials of coenzyme Q10 administration for slowing disease progression revealed no clinical benefits, thus convincing preclinical therapeutic investigations in animals are debatable for their relevance to human clinical situations [291]. Mounting evidence suggests a bunch of molecules with potential therapeutic value against oxidative stress, such as cinnamic aldehyde, curcumin and melatonin conferring protection to dopaminergic neurons in rodent models of PD [292-294]. Additionally, mitochondrial dysfunction mitigation strategies are reported to enhance neuronal cell survival in neurodegenerative disease [295].

The PD therapeutic strategies that are currently in clinical trials include dopamine receptor agonists, anti-synuclein aggregation therapy, convalescent plasma therapy, cell-based therapy, gene therapy, serotonin receptor agonists or antagonists, muscarinic and nicotinic acetylcholine receptor agonists, monoamine reuptake inhibitors, NMDAR modulators, anti-apoptotic drugs, kinase inhibitors, myeloperoxidase inhibitors, adenosine A2A receptor antagonists, antioxidants/botanical-based medication and others [296] (Figure 8).

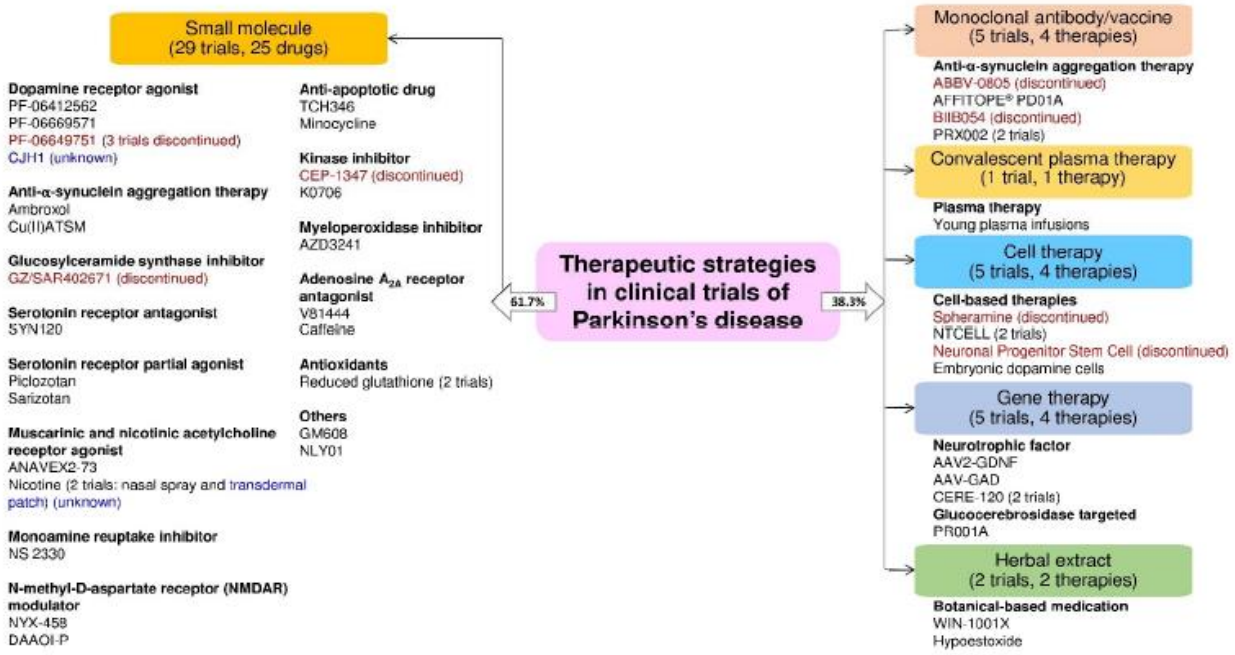


***Figure 8 :*** *The drug or therapy with its therapeutic strategy and trial status in the clinical trials for PD treatment. The blue and red text color indicates the trial status is unknown and discontinued, respectively (active as of 16 June 2021)(adopted from[296]).*

Kinases are an intensively studied drug target class in current pharmacological research as evidenced by the large number of kinase inhibitors being assessed in clinical trials [297]. Kinase-targeted therapies have potential for treatment of a broad array of indications including central nervous system (CNS) disorders. The rationale behind protein kinases as relevant targets for the discovery of drugs for neurodegenerative diseases are aligned with the fact that most cellular processes are tightly regulated by reversible phosphorylation by kinases. In disease conditions, this phosphorylation may become aberrant and this has been reported in many neurodegenerative diseases. A series of active compounds target specific kinases to control neurogenerative diseases and neuroinflammation (Figure 9).

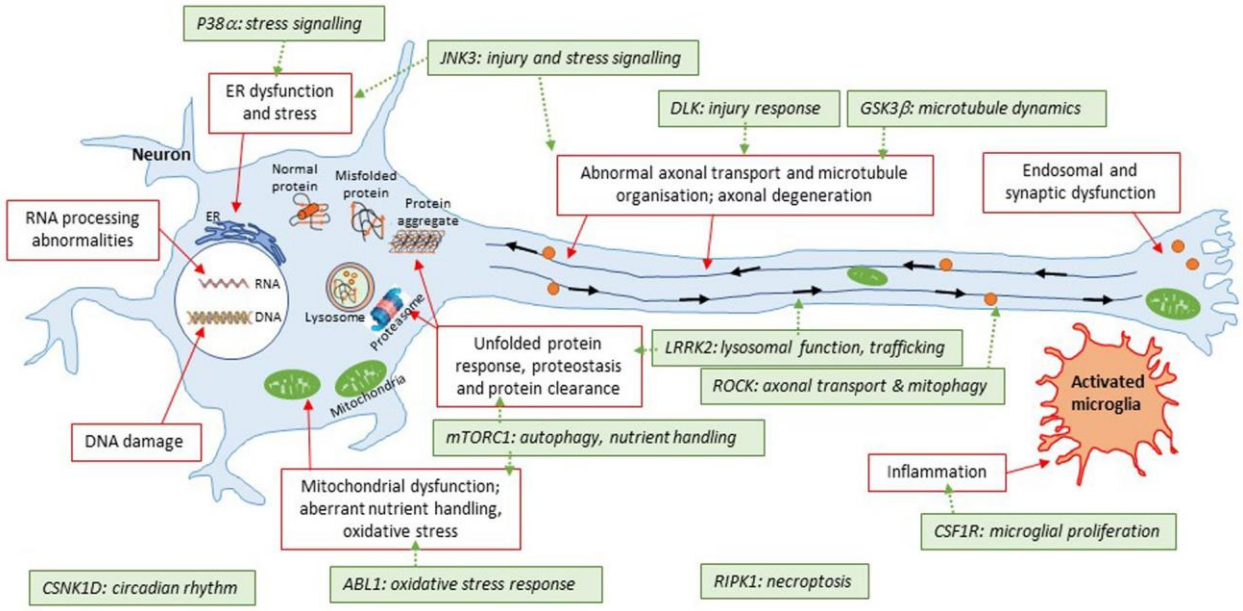


***Figure 9 :*** *Illustration of kinase targets with respect to converging pathways in neurodegeneration. This simplified schematic summarizes some of the common areas of pathophysiology in neurodegenerative diseases. The general theme is that the disease protein(s) are misfolded; which then triggers a number of downstream events such as protein aggregation, energy imbalances, altered proteostasis, stress responses to the unfolded proteins themselves or downstream consequences of events triggered by the unfolded proteins. Some of these pathways are further connected (e.g., diseased mitochondria can be removed by a specialized form of autophagy, known as mitophagy; furthermore, trafficking defects can apply to specific organelles illustrated here such as autolysosomes) (adopted from [297]).*

Drug discovery is an expensive, slow, and risky business. Although preclinical translational studies have uncovered the potential protective capacities of several molecules,the overall failure rate in drug development is more than 96%, in which 90% fail during clinical development [298]. Multifactorial and heterogeneous PD manifestations involving multiple cellular pathways make it an extremely challenging medical problem. Thus, development of clinical neuroprotective strategies remains elusive.

1.2 Modeling PD using in vitro human iPSC model

There is a variety of ways to study PD and the underlying mechanisms of neurodegeneration. Models range across the spectrum from in vitro cell lines, to flies and worms, to non-human primates and human patient samples with each system presenting advantages and disadvantages. Shortly after the groundbreaking discovery that human adult somatic cells could be reprogrammed back to an embryonic like state through the forced expression of a subset of pluripotency transcription factors [299, 300],

human disease modeling entered a new frontier. Scientists now have the capability of using patient-derived skin cells and other somatic cells (e.g. peripheral blood derived mononuclear cells and excreted kidney epithelial cells in urine) to generate iPSCs that offer a virtually endless source of human cells, retain the unique genetic background of each donor, can be chemically and/or transcriptionally coaxed to differentiate into the specific cell type(s) affected in disease, and can be used to specifically interrogate mechanistic processes involved in disease (Figure 10). In that regard, PD studies have preferentially used iPSCs differentiated towards a dopaminergic fate, as their loss triggers the typical motor signs of PD [301].

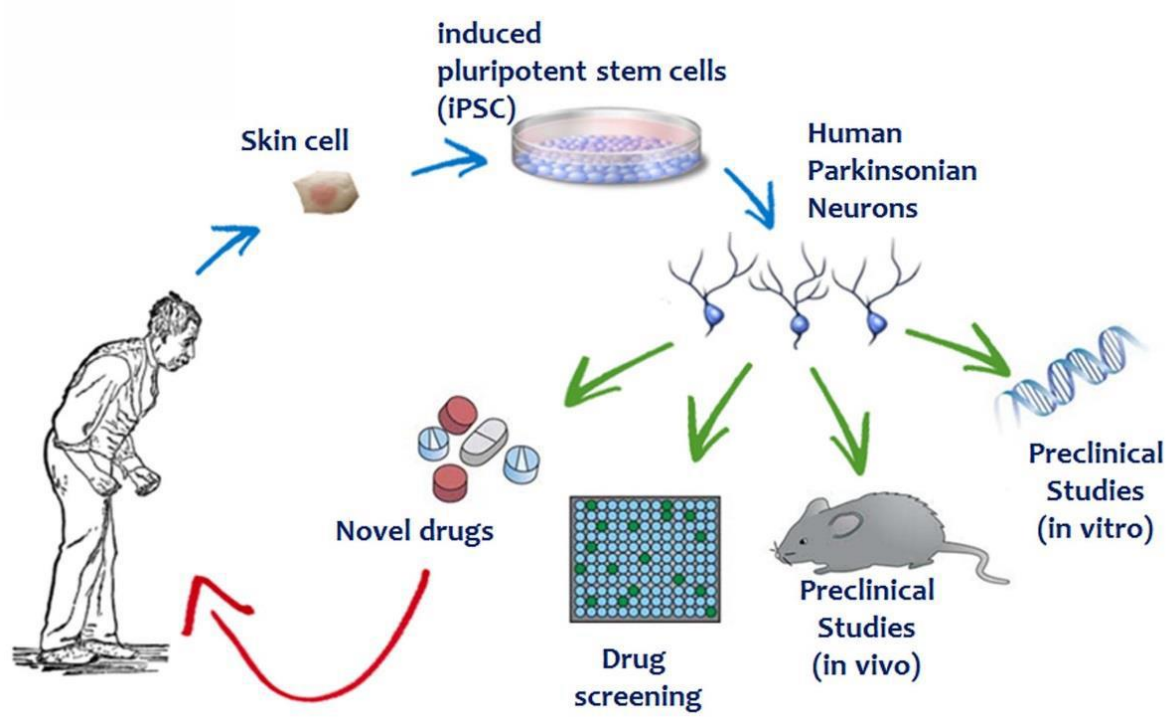


***Figure 10 :*** *Induced Pluripotent Stem Cells (iPSCs) as an in vitro system to model diseases such as Parkinson's disease and to discover new therapies.*

### 1.2.1 PD Relevant Phenotypes Identified from iPSC Models

In the PD field, intensive efforts have been made to generate high-purity human ventral midbrain dopaminergic neurons for in vitro maturation, but mainly for intracerebral transplantation that has long been an attractive prospect for PD treatment [302, 303]. To date, a number of sporadic and familial PD hiPSC-based models have been created displaying a variety of disease-relevant characteristics that could be exploited in either target-based or unbiased phenotypic screens (Figure 11).

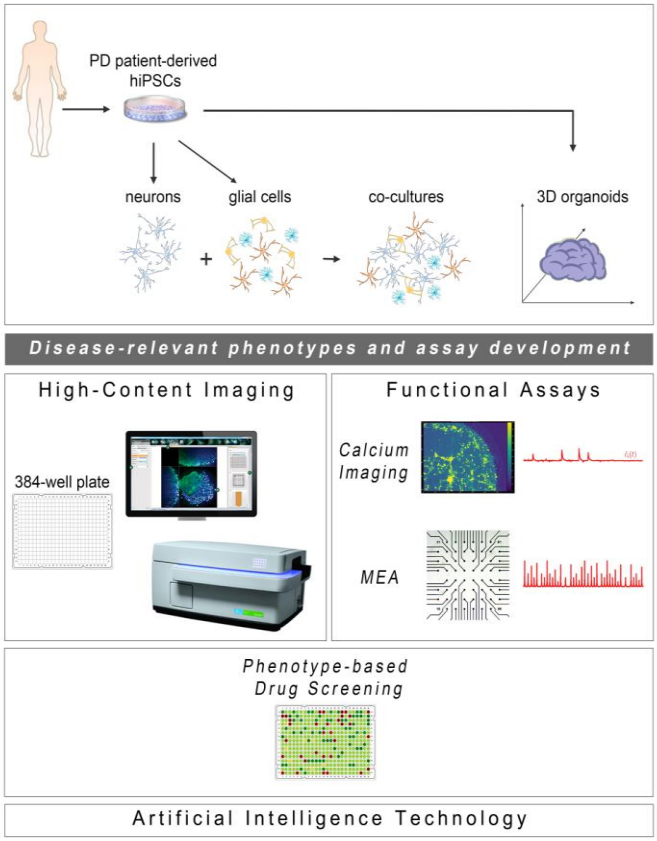


***Figure 11 :*** *Cell reprogramming technologies allowed the generation of Parkinson's disease (PD) patientderived hiPSCs that are further differentiated into neuronal and glial cell populations (astrocytes (shown), but also oligodendrocytes or microglia (not shown)) studied separately or in co-culture with neurons. hiPSC-derived brain organoids are being created to better simulate the human disease. The PD-relevant phenotypes identified in these cellular systems form the foundations for the development of drug discovery platforms encompassing high-content imaging/chemical library screening as well as functional assays, such as calcium imaging and high-resolution multi-electrode array (MEA) recordings (phenotypic drug screening). The application of artificial intelligence technologies will be critical for analysis of the resulting large and complex data sets.*

The first PD-patient specific iPSC lines were generated in 2008 by Park et al. [304] followed by a second group [305]. Both teams provided proof-of-principle that it is feasible to produce hiPSC-derived dopaminergic neurons from patients with sporadic PD, but did not proceed further to identify disease associated phenotypes. Since then, the majority of hiPSC-based PD models have been developed mostly from patients carrying various genetic mutations [306]. Most studied lines carry the G2019S mutation in the LRRK2 gene, one of the most prominent monogenetic risk factors for PD linked to both familial and sporadic forms of the disease [307]. hiPSC-derived cultures from patients bearing point mutations in the SNCA gene (A53T, A30P and E46K) or SNCA multiplications have also been extensively studied, while hiPSC-derived neurons carrying Parkin (PARK2), PINK1 or GBA mutations have been analyzed to a lesser

extent [301]. Overall morphological, biochemical and functional analyses have revealed a battery of disease-associated phenotypes, initially after induction of cellular stress and later—upon careful observations—at basal conditions. Some of these phenotypes were previously described in post-mortem PD brains or in relevant animal models, while a number were identified for the first time in hiPSC-based models.

***α-Synuclein Accumulation***. As discussed, Syn is the major protein associated with both sporadic and genetic PD [308, 309]. Syn accumulation and/or aggregation has been shown in hiPSC-derived neurons generated from PD patients carrying disease-associated mutations. In particular, increased Syn protein levels were detected in hiPSC-derived neurons carrying the A53T (G209A) point mutation [310-314] or SNCA duplication [315] and triplication [313, 316-321]. Accumulation of Syn has also been described in several other hiPSC models of familial PD, including LRRK2, Parkin, PINK1 and hiPSC-derived neurons from GBA patients, as well as, in hiPSC models of sporadic PD [301]. Detection of the pathological species relies largely on the presence of phosphorylated Syn, particularly at serine 129, but also on the presence of specific oligomeric and fibrillar forms as aggregation proceeds. The presence of cellular protein aggregates has also been observed using fluorescence-based assays. In particular, Kouroupi et al. [312] and Ryan et al. [314] have shown discrete Syn accumulations co-localizing with Tau and ubiquitin in both the soma and axons of hiPSC-derived neurons from patients bearing the A53T mutation.

***Mitochondrial Defects.*** Mitochondrial impairment is thought to be a key factor in PDpathology, with PD-associated mutations in Parkin, PINK1, DJ-1, GBA, LRRK2 and SNCA being linked to distortions in mitochondrial function [322]. Studies in hiPSC-derived neurons from PD patients have revealed mitochondrial defects, including morphological and functional alterations [301]. In particular, fragmented mitochondria or mitochondria with abnormal morphology have been observed in hiPSC-derived neurons carrying LRRK2-G2019S [323], Parkin [324-328], PINK1 [326, 329] or GBA mutations [330], but also SNCA-G209A or triplication [313]. Others have reported decreased mitochondrial content in patient neurons [331-333]. Altered mitochondrial functionality has also been demonstrated [328, 330, 332], with decreased ATP production [318, 323], reduced membrane potential [334] or dysfunctional mobility [335], affecting multiple cellular processes and altering the redox status of the neuron.

***Oxidative Stress.*** As mitochondrial respiration is the major source of reactive oxygen species (ROS) in the cell, mitochondrial defects should result in an increase in oxidative stress within patient neurons. A number of studies have demonstrated changes in mitochondrial and oxidative stress-related proteins observed in the human parkinsonian brain [258]. Similarly, oxidative stress phenotypes, such as increased ROS and carbonylated proteins or upregulation of proteins involved in dopamine oxidation,

have been observed in several hiPSC-based models carrying LRRK2 [336, 337], Parkin [324, 327, 338] and PINK1 [335, 339] mutations as well as in hiPSC-derived neurons with SNCA-triplication [320].

***Autophagy-Related Phenotypes and ER Stress.***Consistent with protein aggregation and cellular stress, studies in hiPSC models reveal that endoplasmic reticulum (ER) dysregulation and increased ER stress may be involved in PD pathogenesis promoting neuronal cell death [310, 319, 340]. Additionally, altered function of other cellular organelles, such as lysosomes, together with autophagy impairment, has been observed in LRRK2 [323, 337, 341], SNCA [321] and GBA [342, 343] mutant hiPSC-derived neurons, as well as in a hiPSC-based model of sporadic PD [341], resulting in defective clearance of aggregated proteins. Finally, several studies have shown that genetically diverse PD patient-derived neurons exhibit increased susceptibility to various forms of cellular stress, including proteotoxic [312, 336] or nitrosative stress [310, 314], linking specific cellular pathways to disease pathology that have not been previously described in other systems.

***Compromised Neuritic Growth, Axonal Degeneration and Decreased Synaptic Connectivity.*** Studies on LRRK2-G2019S [341, 344-347], on Parkin-mutated [348] and on SNCA-mutated [312, 321] hiPSC-derived neurons have revealed previously unrecognized morphological changes, including compromised neuritic outgrowth, reduced neurite complexity and axonal degeneration, resulting in impaired synaptic connectivity and network function. LRRK2-G2019S mutant neurons displayed shorter and less complex processes, reminiscent of immature neurons. Over time, these cells exhibited clear signs of degeneration, including very short or absent neurites, vacuolated soma, fragmented nucleus and positive staining for cleaved caspase-3. In the case of SNCA mutations, α-Syn overexpression due to triplication of the gene led to poor formation of the neuronal network that correlated with significantly lower generation of action potentials in response to current injections [321]. A later study have shown that, A53T α-Syn neurons had a profound downregulation of mRNAs associated with synaptic formation, maintenance and function. The neuronal network formed was also less complex with neurite number, length and morphology being compromised when compared to control cells [312].

***Table 3 :*** *Major phenotypes observed in PD hiPSC-derived neurons. This table summarizes key pathogenic phenotypes associated with PD mutant neurons as described in the cited publications. (adopted from [349])*

| **Major PD-relevant phenotypes** | **Patient-derived iPSC-based models in PD** | | | | | |
|---|---|---|---|---|---|---|
| | ***Gene mutations*** | | | | | |
| | ***SNCA*** | ***LRKK2*** | ***PARKIN*** | ***PINK1*** | ***GBA*** | ***OPA1*** |
| αSyn accumulation and/ or aggregation; increased phosphorylated αSyn (Ser 129); presence of oligomeric and fibrillar αSyn forms | *G209A* [310-314]<br>Duplication [315]<br>Triplication [313, 316-321] | *G2019S* [336, 341, 345-347] | Ex2–4 del and Ex6–7 del [327]<br>Ex3del, R42P, Ex3–4del, 1-BP del 255A, R275W, R42P [333]<br>V324A [326]<br>c.255delA [345] | *Q456X* [326] | L444P [343]<br>N370S [342] | |
| Mitochondrial defects: fragmented mitochondria or mitochondria with abnormal morphology; decreased mitochondrial content; decreased ATP production; reduced | *G209A*<br>Triplication [313] | *G2019S* [323, 332] | Ex2–4 del and Ex6–7 del [327] | Q456X [326] | N370S, L444P, and RecNcil [330] | p.G488R and p.A495V [331] |

| | | | | | | |
|---|---|---|---|---|---|---|
| membrane potential; dysfunctional mitochondrial mobility | | | Ex3, 5, and 6 del [324]<br><br>V324A [326]<br><br>c.1072delT, p.A324fsX110 [328]<br><br>Ex2–4 del and Ex6–7 del [325] | G309D; Ex7/del [329] | | |
| Oxidative stress: increased ROS and carbonylated proteins; upregulation of proteins involved in dopamine oxidation | Triplication [316, 318, 320] | *G2019S* [336]<br><br>*I2020T* [337] | Ex2–4 del & Ex6–7 del [327]<br><br>Ex3, 5, and 6 del [324]<br><br>Ex3 del / Ex5 del and Ex3 del / Ex 3 del [338] | *Q456X* [335, 339] | | |

| | | | | | | |
|---|---|---|---|---|---|---|
| ER dysregulation; increased ER stress; autophagy impairment | *G209A* [310, 340]<br><br>Triplication [319, 321] | *G2019S* [323, 341]<br><br>*I2020T* [337] | | | RecNcil, L444P and N370S [343]<br><br>N370S [342] | |
| Compromised neurite growth & complexity; neurite swellings; axonal degeneration; decreased synaptic connectivity; impaired axonal transport | *G209A* [312]<br>Triplication [321] | *G2019S* [341, 345-347] | Ex3 del / Ex5 del and Ex3 del / Ex 3 del [348] | | | |

1.2.2 Rescue of disease-related phenotypes in hiPSC-derived models of PD: setting the foundations towards drug discovery

Contrary to the initial skepticism regarding the potential of hiPSC-based systems to recapitulate age-related diseases such as PD, the identification of a wealth of cellular and molecular phenotypes, either previously known or novel, has prompted the use of such systems for early drug discovery. A number of candidate drugs have been tested for their ability to restore disease-related phenotypes in hiPSC-derived models of PD with promising results (Table 2). These studies have laid the groundwork for future application of hiPSC models in larger drug screening campaigns, assisting in the development of robust assays.

Analyses of hiPSC-derived neurons from patients with different PD-linked mutations have shown that αSyn accumulation presents a common theme regardless of the gene mutated, suggesting that it

could serve as a read-out when testing novel therapeutics. Accordingly in hiPSC-derived dopaminergic neurons from sporadic PD patients, as well as from patients carrying mutations in *GBA*, *LRRK2*, *DJ-1*, *Parkin* and *SNCA* (A53T, triplication) with decreased lysosomal β-glucocerebrosidase (GCase) activity, treatment with small-molecule enhancers of GCase has resulted in reduced αSyn levels and associated toxicity. These observations suggest that non-inhibitory small-molecule chaperones of GCase may prove promising for treatment of PD and related synucleinopathies [350-352]. Additionally, recent data in *GBA*-linked PD patient-derived dopaminergic neurons have implicated increased acid ceramidase activity in the context of decreased GCase. This led to intracellular accumulation of αSyn, the levels of which were reduced upon inhibition of acid ceramidase by carmofur [353]. In the same lines, Burbulla et al. have applied treatment with mitochondrial antioxidants to smooth out a pathological cascade instigated by mitochondrial oxidant stress causing lysosomal dysfunction and αSyn accumulation in dopaminergic neurons derived from patients with sporadic and familial PD [354].

Alterations in neuronal morphology, neurite outgrowth and complexity as well as axonal degeneration have been used as parameters to evaluate the potential efficacy of compounds in rescuing pathological phenotypes. One study has demonstrated that *LRRK2-G2019S* hiPSC-derived neurons display neurite shortening and fewer neurites compared to wild-type controls [347], a PD-associated phenotype previously linked to ERK signaling [355]. Interestingly, treatment with an inhibitor of ERK phosphorylation or a selective inhibitor of LRRK2 kinase activity increased neurite growth and rescued mutant cultures from degeneration [347]. Similarly, Korecka et al. demonstrated that exposure to a LRRK2 kinase inhibitor or application of a LRRK2-specific antisense oligonucleotide (ASO) rescued neurite collapse, also in a model of *LRRK2-G2019S* hiPSC-derived neurons [344].

In the patient-derived *SNCA-G209A* (A53T) hiPSC-based model that we developed, PD neurons exhibited distinct morphological features characterized by extensive neuritic pathology and degeneration [312]. By immunostaining for βIII-tubulin we observed contorted or fragmented axons with swollen varicosities and spheroid inclusions containing Tau and αSyn. Under morphological examination using a lentiviral vector for expression of the red fluorescent protein DsRed under the control of human synapsin 1 promoter (LV. SYN1.DsRed) to facilitate imaging of single neurons, we also observed a significant reduction in both total neurite length and the number of neurites extending from the soma. Three de novo in silico-designed compounds [356, 357] that all interact with and reduce αSyn toxicity by interfering with αSyn oligomer formation, could restore neurite length and rescue axonal pathology [312]. Interestingly, a small variation of one of these small molecules, NPT200-11, that was developed by the

company Neuropore Therapies in collaboration with UCB Biopharma, is the only αSyn-inhibiting compound that has reached clinical trials successfully completing phase I (https://clinical trials.gov).

Several studies with hiPSC-derived neurons have revealed dysregulation in the expression of genes involved in numerous cellular processes, rendering cells vulnerable to stressors that activate or modulate these pathways. Oxidative stress, mitochondrial impairment and proteasome inhibition are key factors that cause increased susceptibility and cell death of patient-derived neurons (reviewed in [301, 358]). The first study recapitulating PD-associated phenotypes has revealed that dopaminergic neurons derived from *LRRK2-G2019S* hiPSCs displayed increased expression of key oxidative stress-response genes. Moreover, these cells were highly sensitive to cell death caused by exposure to hydrogen peroxide, the proteosomal inhibitor MG-132 or the neurotoxin 6-hydroxydopamine (6-OHDA) [336]. In a similar manner, Reinhardt et al. have confirmed that *LRRK2-G2019S* hiPSC-derived dopaminergic neurons are susceptible to oxidative stress induced by the mitochondrial complex 1 inhibitor rotenone or the neurotoxin 6-OHDA resulting in increased apoptosis, preferentially of dopaminergic neurons [347]. The incurred cytotoxicity was rescued in the presence of the small molecule inhibitor of LRRK2 kinase, LRRK2-IN1, which increased the survival of dopaminergic neurons.

An association between PD and exposure to mitochondrial toxins, including rotenone, has also been reported in *SNCA-G209A* (A53T) mutant neurons [314]. Microarray analysis of *SNCA-G209A* hiPSC-derived dopaminergic neurons has highlighted a pathway where toxin-induced nitrosative/oxidative stress results in S-nitrosylation of the transcription factor MEF2C. High-throughput screening of a chemical library for small molecules capable of targeting the MEF2C-PGC1α pathway pinpointed isoxazole as a potential therapeutic, protecting *SNCA-G209A* neurons from apoptosis induced by mitochondrial toxins [314].

When exposing the A53T-αSyn hiPSC-based model that we generated to epoxomicin or MG132 both of which interfere with αSyn clearance via the proteasome, we observed a significant increase in cleaved caspase-3 immunoreactivity consistent with the levels of LDH release in mutant neurons. This was accompanied by a pronounced disruption of the MAP2+ neuronal network, confirming once again their susceptibility to proteotoxic stress [312]. The observed stress-induced vulnerability could also be reversed by the three small molecules targeting αSyn [356, 357], resulting in restoration of the MAP2+ network [312].

Finally, a recent study has revealed that increased oxidative stress and inflammation are associated with induction of the necroptotic pathway in hiPSC-derived neural cells from patients with a mutation in the OPA1 gene encoding a key player in mitochondrial fusion and structure [331] that has been associated

with an inherited form of PD and dementia [359]. Mutant cultures exhibited severe mitochondrial dysfunctions, impaired oxidative phosphorylation, and high oxidative stress levels, leading to neuronal cell loss. Pharmacological treatment of necroptosis with the specific inhibitor necrostatin-1 protected neurons from cell death [331].

The above paradigms provide evidence that despite the initial concerns in using human iPSC-based models for modeling age-related neurodegenerative pathologies, such systems show multiple disease-associated phenotypes with high relevance to PD pathogenesis and progression and can be of great value in drug discovery.

***Table 4.*** *Summary of hiPSC-based models of PD that have been used for drug testing. This table briefly describes the rescue of disease-related phenotypes in PD hiPSC-derived neurons by selected compounds.(adopted from [349])*

| **Gene** | **Phenotypes described** | **Compound testing** | **Phenotype restored** | **Reference** |
|---|---|---|---|---|
| *GBA* mutations | increased levels of αSyn; reduced lysosomal GCase levels, reduced lysosomal GCase activity | small-molecule noninhibitory chaperone of GCase NCGC607 | reduced αSyn levels and associated toxicity | [350] |
| *GBA* (N370S/c.84dupG), *SNCA*-triplication | presence of amyloidogenic αSyn within cell bodies and neurites; accumulation of insoluble αSyn; reduced neuronal viability; reduced lysosomal activity of GCase | small-molecule GCase modulator 758 | improved GCase activity; reduced αSyn levels | [351] |
| *GBA* (c.84dupG frameshift mutation) *LRRK2* and | reduced amounts of GCase; decreased GCase enzymatic activity; accumulation of oxidized dopamine | small-molecule GCase modulator S-181 | increased amounts of lysosomal GCase; enhanced GCase enzymatic activity; | [352] |

| | | | | |
|---|---|---|---|---|
| *Parkin* mutations | | | decreased dopamine oxidation | |
| *GBA* (c.84dupG frameshift mutation) | increased acid ceramidase activity in the context of decreased GCase, leading to intracellular accumulation of αSyn | carmofur, acid ceramidase inhibitor | reduced αSyn levels | [353] |
| *DJ-1* mutations | mitochondrial oxidant stress causing lysosomal dysfunction and αSyn accumulation | mitochondrial antioxidants | diminished accumulation of oxidized dopamine; improved lysosomal GCase activity and proteolysis | [354] |
| *LRRK2* (G2019S) | reduced neurite outgrowth; increased sensitivity to oxidative stress | ERK phosphorylation inhibitor PD0325901 or LRRK2 kinase inhibitor LRRK2-IN1 | increased neurite growth; reduced cytotoxicity | [347] |
| *LRRK2* (G2019S) | neurite collapse; altered ER calcium homeostasis | LRRK2 kinase inhibitor MLi-2 or LRRK2-ASO | rescued neurite collapse | [344] |
| *SNCA* (G209A) | αSyn aggregation; mitochondrial dysfunction; increased susceptibility to mitochondrial toxins | small molecule targeting MEF2C-PGC1α (isoxazole) | reduced apoptosis | [314] |

| | | | | |
|---|---|---|---|---|
| *SNCA* (G209A) | αSyn aggregation; compromised neurite outgrowth and axonal neuropathology; defective synaptic connectivity | small molecules targeting αSyn (NPT100-18A, NPT100-14A or ELN484228) | improved neurite outgrowth; rescue of axonal pathology and morphological restoration of the neuronal network | [312] |
| *OPA1* mutation | mitochondrial dysfunction; impaired oxidative phosphorylation and high oxidative stress levels leading to neuronal cell loss | necrostatin-1, specific necroptosis inhibitor | increased survival | [331] |

### 1.2.3 Phenotypic screens using hiPSC-derived models of PD: empowering drug discovery

#### 1.2.3.1.Target-based versus phenotype-based drug screening

The two main high-throughput screening approaches for discovering new disease-modifying therapeutics are either target-based or phenotype-based. Historically, phenotypic-based screening strategies shaped the foundations of pharmaceutical drug discovery long before molecular target-based approaches were applied [360]. However, in the past 25 years molecular target-based drug screening has become the main route to drug discovery in both the academia and the pharmaceutical industry. This change was mainly due to an accelerated progress in molecular biology and genomics that resulted in efficient mining of genes associated with various diseases [361]. The starting point in this approach is a well-defined molecular target with a predicted role in disease allowing the hypothesis that modulation of its activity would have beneficial effects. Screening of chemical libraries of small molecules is then used to identify lead compounds that interact with high affinity and specificity with the target [362]. Hits from such screens are then used for pharmacological target validation and lead compound optimization. The main advantage of the target-based approach is that the mechanism of action is known right from the start, which can accelerate preclinical assessment. Other advantages include the ability to facilitate optimization of the lead compound as there is a clear structure-activity relationship enabling improvement of its physicochemical properties, and the potential to predict target-associated safety liabilities and toxicity. However, knowledge of the molecular targets has not translated into identification

of disease-modifying agents for PD or other neurodegenerative diseases [363]. One reason could be that the underlying mechanism is not clear for PD, as for most neurodegenerative diseases, resulting in a universal lack of well-defined targets. Besides, neurodegenerative diseases including PD, are highly complex disorders and manipulating a single target may not be sufficient to restore the dysfunctional cellular network.

In phenotypic screens, on the other hand, disease-driving phenotypes can be used to determine compounds that change the outcome of multiple biological pathways without prior knowledge of the molecular mechanisms of the disease. Such screens are unbiased and may identify compounds targeting completely unexpected proteins or pathways. Consequently, phenotypic screens hold promise for identification of previously unrecognized disease pathways and the discovery of new therapeutic targets [364]. It is notable that during the past 20 years phenotypic screening has contributed to most of the first-in-class small-molecule drugs approved by FDA. Among all the new molecular entities approved from 1999 to 2008, 28 were identified through phenotypic screens whereas target-based approaches contributed to the discovery of 17 compounds [365]. In particular, in the central nervous system field phenotypic screening has yielded 7 out of 9 first-in-class drugs. Consequently, there is renewed interest in reinventing phenotypic screens as a means of drug discovery.

#### 1.2.3.2.Phenotypic-based drug screening in hiPSC-derived models of PD

Although the first PD patient-derived hiPSCs were generated in 2009 [305], surprisingly only two phenotypic screens have been reported so far in hiPSC-derived PD neurons. To identify disease-modifying agents, Yamaguchi et al. established an imaging-based, semi-automatic, high-throughput assay for quantitative detection of mitochondrial clearance and cell viability in dopaminergic neurons from patients with familial PD having Parkin or PINK1 mutations. After screening 320 pharmacologically active inhibitor compounds the researchers identified 4 hits, MRS1220, tranylcypromine, flunarizine and bromocriptine, that improved the pathological clearance of mitochondria possibly by promoting mitochondrial degradation through the lysosomal system, without further investigating the underlying mechanism [366]. In another study Tabata et al. [367] performed a phenotypic screen in Parkin (PARK2) patient-derived dopaminergic neurons displaying increased susceptibility to rotenone-induced mitochondrial stress, to identify neuroprotective compounds. From phenotypic screening of an FDA-approved drug library, one voltage-gated calcium channel antagonist, benidipine, was found to suppress rotenone-induced apoptosis [367]. The selective vulnerability of dopaminergic neurons was further attributed in

this study to dysregulation of intracellular calcium homeostasis via T-type calcium channels, revealing a previously unidentified pathway in PD and offering a potential treatment opportunity.

## 2. AIM OF THE STUDY

Parkinson's disease (PD) represents an enormous social and economic burden due to its high incidence, the severity of symptoms, and the lack of effective disease-modifying therapies. Our knowledge of the exact mechanisms of the disease is limited. Traditional mehods of studying the disease, such as the use of human tissue, are almost exclusively limited to postmortem brain for PD. Animal models, although commonly used, cannot totally represent the full range of symptoms, in part,due to significant divergence from human physiology. Measuring subtle changes in cognition and behavior is also difficult in animals.The emergence of human-induced pluripotent stem cell (hiPSC) technology added great value in the existing PD models. Together with advances in gene-editing technologies, hiPSC-derived neural cells from patients and healthy donors have created new methods of modeling neurological diseases in a human context that is just beginning to be exploited for therapeutic purposes.

Over the last twenty years, many differentiation protocols have been developed for the various cell types of the brain, such as neurons, astrocytes, microglia and oligodendrocytes. Different methods and modeling strategies determine which cell types are produced, which experimental questions can be addressed, and how compounds can be screened for drug development [368].

Kinases have emerged as one of the most intensively investigated drug targets in current pharmacological research, due to their pivotal roles in modulating a wide array of cellular processes [369]. A great effort has been directed toward the development of molecules specifically targeting the human kinome [370]. To date, the majority of molecules show a spectrum of kinase inhibitors, with >250 currently in clinical trials and 48 approved by U.S. FDA, mostly to treat malignancies [371]. Initially focused on cancer therapy, kinase drug discovery has recently broadened its focus to include an expanded range of therapeutic areas, such as autoimmune and inflammatory diseases, as well as neurodegenerative disorders [372], including PD. However, the contribution of the dysregulation of human kinome to neurodegeneration has not been clarified so far and the field of kinase-directed therapies is still immature compared to their application in cancer therapy. The neuronal functions of many kinases are still largely uncharacterized, with a sparse indication of how these targets influence the major signaling pathways involved in PD. Further investigations on human brains are needed to profile the changes in protein kinase activity in the different brain areas during aging and the progression of neurodegeneration.

As the main feature of PD is the death of dopaminergic neurons of the substantia nigra, in the present study we focus on the identification of molecules that enhance the differentiation and survival of these neurons using as an experimental model the induced stem cells (iPS) from healthy individuals and from PD patients harboring the p.A53T αSyn mutation (G209A in the SNCA gene).We utilize a small

molecule library of kinase inhibitors to perform a high-content screening in order to detect molecules that induce the differentiation and / or survival of dopaminergic neurons and reverse neurodegeneration.

We discovered that the multi-kinase inhibitor BX795 significantly reverts disease-associated phenotypes. A single treatment of patient neurons with BX795 has sustainable effects in supporting neuritic growth, restoring axonal pathology and limiting αSyn protein aggregate formation. Protection from p.A53T-associated pathology was also confirmed in human iPSC-derived neurons in which the mutation was introduced by genome editing, against isogenic wild-type controls. Strikingly, proteomics profiling by quantitative mass spectrometry revealed that BX795 treatment results in significant downregulation of a cohort of 118 proteins that are abnormally upregulated in p.A53T-neurons. Enrichment analysis demonstrated that these proteins are associated with mRNA metabolism, mRNA transport and translation, protein metabolism and degradation processes. Using neuronal cells expressing the human p.A53T-αSyn, we demonstrate that BX795 affects the mTORC1 pathway to restrict excessive protein synthesis and facilitate autophagy. Taken together, our data highlight the BX795 kinase inhibitor as a compelling compound and candidate therapeutic that ameliorates p.A53T-related pathology.

## 3. MATERIALS

### 3.1 Lab equipment

#### 3.1.1 Instruments and devices

•Laminar hood (Thermo Fisher Scientific)

•CO2 Incubator (Heracell 150; Marschall Scientific)

•Pipettes (1-10 µL, 2-20 µL, 20-200 µL, 100-1000 µL; Gilson)

•Freezers -20°C; -80°C

•Waterbath (Julabo)

•Neubauer counting chamber (Marienfeld)

•Freezing container (Thermo Fisher, 5100-0001)

•pH-measurer (Orion 3 Star; Thermo Electron Corporation)

•Light Cycler 96 (Roche)

•Pipette filler (Thermo Fisher)

•Mini rocker-shaker (MR-1; Kisker)

•Laboratory balance (Mettler)

#### 3.1.2 Microscopes and Image analysis software

•Confocal laser scanning microscopy platform TCS SP8 (Leica)

• Opera High-Content Screening System (Perkin Elmer)

• Image processing program ImageJ (NIH)

•Adobe Photoshop CS6

#### 3.1.3 Consumables

•Surgical gloves and mask

•Serological pipettes, sterile, single wrapped (1, 2, 5, 10ml; Greiner Bio-one)

• Tissue culture plates, sterile (6-, 12-, 24 well; Corning)

• Microscope slides B/50, 76 x 26 mm (Knittel)

•VWR Micro Cover Glasses, 24 x 50 mm (VWR, 48393-081)

**3.2 Reagents**

**3.2.1 Chemical reagents**

•Agarose (Sigma, A9539)

•Bisacrylamide(Promega,V314A)

•Protein Assay Dye Reagent Concentrate (Bio-Rad, 5000006)

•Glycine(Applichem, A37037.5000)

•TRI reagent (Sigma, T9424) for RNA extraction

•Isopropyl alcohol (Fisher Scientific, BP2618212)

•L-Ascorbic acid (Sigma, A4544)

•Normal donkey serum, NDS (S30, Merck)

•Triton X-100 (FLUKA)

•Tween-20(Applichem, A4974.0250)

•Sodium azide or NaN3 (Sigma)

•Ethanol (Panreac and Merck)

•Paraformaldehyde (Sigma, 1581127)

•Sodium hydroxide or NaOH (Merck)

•Hydrochloric acid or HCl (Merck)

•Sodium Chloride or NaCl (Panreac)

•Calcium- and magnesium-free Hanks' buffered salt solution (CMF-HBSS); containing 2 g/ liter glucose, ice cold

•1% (w/v) DNase in CMF-HBSS (store in small aliquots at −20°C)

•PBS, Phosphate buffer saline 1x (Gibco, 11594516)

•Prolong Gold Antifade Reagent with DAPI (CST, 8961)

•Hoechst 33343 Solution (Thermo Scientific, 62249)

**3.2.2 Cell culture**

Basic media, and supplements

Knockout DMEM (Gibco, 10829-018)

KSR (knockout serum replacement) (Gibco, 10828-028)

Penicillin/Streptomycin (Gibco, 11548876)

GlutaMAX Supplement (Gibco, 35050-038)

MEM-Non essential amino acids (Gibco, 11140-035)

Beta-mercaptoethanol (Gibco, 21985-023)

FGF basic rec human (Miltenyi, 130-093-842)

DMEM high glucose (Gibco, 11965092)

Fetal Bovine Serum (Gibco, 10500064)

F12 (Sigma, 51445C)

N2 Supplement (Gibco, 17502048)

B27 supplement (Gibco, 12587010)

Neurobasal (Gibco, 21103049)

SB431542 (Tocris, 1614)

SHH (R&D, 1314-SH)

FGF8 (R&D, 423-F8)

BDNF (brain-derived neurotrophic factor; R&D, 248-BD)

GDNF (glial cell line-derived neurotrophic factor; R&D, 212-GD)

Ascorbic acid (Sigma- Aldrich, A92902)

Dibutyryl cAMP (Sigma- Aldrich, P4890)

Y-27632 (ROCK inhibitor; Stem Cell Technologies, 72302)

Synth-a-Freeze (Cryopreservation medium, Gibco, A1254201)

<u>iPSC media on feeders</u>

Knockout DMEM

KSR (knockout serum replacement) 2%

Pen/Strep 1%

GlutaMAX 1%

MEM-Non essential amino acids 1%

Beta-mercaptoethanol 1000x

(Filter using Millipore stericup 0.22µm)

FGF basic rec human 10ng/ml

<u>MEF media</u>

DMEM high glucose

GlutaMAX Supplement 1%

Fetal Bovine Serum 10%

iPSC media feeder-free conditions

TeSR™-E8™ Basal Medium (Stem Cell technologies, 05990)

Pen/Strep 1%

N2 medium

DMEM high glucose /F12

N2 Supplement 1%

GlutaMAX Supplement 1%

Beta-mercaptoethanol 1000x

B27 medium

Neurobasal

B27 Supplement 2%

GlutaMAX Supplement 1%

DAergic differentiation media

DMEM/F12

GlutaMAX 2mM

FGF basic rec human 10 ng/ml

SHH 200 ng/ml

FGF8 100 ng/ml

Ascorbic acid 0.2 mM

Maturation media

BDNF 20 ng/ml

GDNF 20 ng/ml

Ascorbic acid 0.2 mM

dibutyryl cAMP 0.5 mM

Coating materials

Gelatin solution 0.1 % (Merck, ES-006-B)

Matrigel (BD, 354230)

Polyethylenimine (PLE, Sigma, 40877)

Laminin (Sigma, L2020)

Poly-L-ornithine (PLO, Sigma, P3655)

**3.2.3 Enzymes**

•Tsp45I (NEB, R0583S)

•Collagenase, Type IV (Invitrogen, 17104-019): for the dissociation of iPSC

•ReLesR (StemCell technologies, 05782): for the dissociation of iPSC

• StemPro Accutase Cell Dissociation Reagent (Gibco, A1110501): for the dissociation of iPSC

•RQ1 RNase-free DNase (Promega, M6101), for the removal of DNA in RNA samples

•ImProm-II Reverse Transcriptase (Promega, A3802) and random hexamers (Applied Biosystems, N8080127) for the RT-qPCR

•KAPA SYBR FAST qPCR Master Mix (KapaBiosystems)

<u>Other reagents</u>

•Mouse embryonic fibroblasts (MEFs, Gibco, A34180)

•iCell Dopa neurons and iCell DopaNeurons. PD SNCA A53T HZ(Fujifilm Cellular Dynamics International)

•PCR kit (Qiagen, 201203)

•Molecular Mass Ruler (BioRad, 1708207)

•Clean and Concentrator (Zymo Research, R1018)

• EndoFree Plasmid Maxi Kit (QIAGEN, 12362)

•QIAquick Gel Extraction Kit (QIAGEN, 28704)

•Random Hexamers (50mM) (Applied Biosystems, N8080127)

• PROTEOSTAT Aggresome Detection Kit (Enzo)

•One Shot® TOP10 Chemically Competent E. coli (Invitrogen,C4040-10)

• Amersham ECL Prime Western Blotting Detection Reagent (GE Healthcare,RPN2232)

•Cyto-ID® autophagy detection kit 2.0 (Enzo Life Sciences, ENZ-KIT175, Plymouth Meeting, PA)

• p70 S6K activity assay kit (ADI-EKS-470 Enzo Life Sciences)

• ProLong Gold antifade reagent with DAPI (Cell Signaling Techology,5297S)

### 3.2.4 Primer sequences

**Table 5. Primer sequences used for RT-qPCR in the current study**

| Gene name | Application | Forward | Reverse |
|---|---|---|---|
| TH | RT-PCR | TGTCTGAGGAGCCTGAGATTCG | GCTTGTCCTTGGCGTCACTG |
| Nurr1 | RT-PCR | TCGACATTTCTGCCTTCTCCTG | GGTTCCTTGAGCCCGTGTCT |
| AADC | RT-PCR | TGCGAGCAGAGAGGGAGTAG | TGAGTTCCATGAAGGCAGGATG |

### 3.2.5 Antibodies

**Table 6. Primary antibodies used in the current study**

| Name | Host | Dilution | Vendor | Catalog# |
|---|---|---|---|---|
| Anti-GAPDH | Mouse | 1/1000 | Santa Cruz Biotechnology | sc-365062 |
| Anti-beta actin | Mouse | 1/5000 | Abcam | ab8227 |
| Anti-MAP2 | Mouse | 1/200 | Merck-Millipore | MAB3418 |
| Anti-NESTIN | Rabbit | 1/200 | Merck-Millipore | ABD69 |
| Anti-α-Synuclein (αSyn) | Mouse | 1/500 | BD Biosciences | 610787 |
| Anti-phosphorylated α-Synuclein (Ser129) | Mouse | 1/10000 | WAKO | 015-25191 |
| Anti-TH | Rabbit | 1/500 | Merck-Millipore | AB152 |
| Anti-VGLUT1 | Mouse | 1/1000 | Merck-Millipore | MAB5502 |
| Anti-TUJ1 | Mouse | 1/1000 | Biolegend | 801202 |
| Anti-PAX6 | Mouse | 1/100 | DSHB | AB 528427 |
| Anti-ki67 | Rabbit | 1/400 | Abcam | ab15580 |
| Anti-Phospho-S6 Ribosomal Protein (Ser235/236) | Rabbit | 1/1000 | Cell Signalling | 4858 |
| Anti-S6 Ribosomal Protein (5G10) | Rabbit | 1/1000 | Cell Signalling | 2217 |
| Anti-Phospho-mTOR (Ser2448) (D9C2) | Rabbit | 1/1000 | Cell Signalling | 5536 |
| Anti- mTOR (7C10) | Rabbit | 1/1000 | Cell Signalling | 2983 |
| Anti-Phospho-PRAS40 (Thr246) (C77D7) | Rabbit | 1/1000 | Cell Signalling | 2997 |
| Anti-PRAS40 (D23C7) | Rabbit | 1/1000 | Cell Signalling | 2691 |
| Anti-TBK1/NAK | Rabbit | 1/1000 | Cell Signalling | 3013 |
| Anti-Phospho-TBK1/NAK (Ser172) (D52C2) | Rabbit | 1/1000 | Cell Signalling | 5483 |
| Anti-Phospho-PDK1 (Ser241) | Rabbit | 1/1000 | Cell Signalling | 3061 |
| Anti-PDK1 (D37A7) | Rabbit | 1/1000 | Cell Signalling | 5662 |

**Table 7. Secondary antibodies used in the current study**

| Antigen | Conjugate | Host | Dilution | Vendor | Catalog number |
|---|---|---|---|---|---|
| goat IgG | Alexa 488 | donkey | 1/1000(ICC) | Molecular Probes | A11055 |
| rabbit IgG | Alexa 488 | donkey | 1/1000(ICC) | Molecular Probes | A21206 |
| mouse IgG | Alexa 647 | donkey | 1/1000(ICC) | Molecular Probes | A31571 |
| rabbit IgG | Alexa 647 | donkey | 1/1000(ICC) | Molecular Probes | A31573 |
| mouse IgG | Alexa 546 | donkey | 1/1000(ICC) | Molecular Probes | A10036 |
| rabbit IgG | Alexa 546 | donkey | 1/1000(ICC) | Biotium | 20038 |
| chicken IgG | Alexa 546 | goat | 1/1000(ICC) | Molecular Probes | A11040 |
| mouse IgG | HRP | goat | 1/10000(WB) | Thermo | 31444 |
| rabbit IgG | HRP | goat | 1/10000(WB) | Thermo | 31460 |

### 3.2.6 Buffers

10x Phosphate buffered saline (PBS)

140 mM NaCl

8 mM Na2HPO4 (x2H2O)

1.5 mM NaH2PO4 και

3 mM KCl

10x Tris-buffered saline (TBS)

200mM Tris base

1.5 mM NaCl

8% paraformaldehyde (PFA STOCK)

80g parafolmadehyde in 1L 1x PBS

Antigen retrieval buffer pH 6

10 mM trisodium citrate dehydrate

Normal Donkey Serum Blocking solution or blocking buffer

5% (v/v) NDS in 0.01 M PBS (pH ~ 7.4) and 0.02% (v/v) NaN3

Lysis buffer (RIPA modified)

50mM Tris-HCl, PH=7.5

150mM Nacl

1% Triton-X100

1mM EDTA

1mM EGTA

0.1% SDS

0.5% NaDeoxycholate

Protease Inhibitors (add fresh)

Phosphatase Inhibitors (add fresh)

Stripping Buffer(mild)

200mM glycine

0.8 % SDS

Running/Transfer Buffer (10X)

30.3g Tris Base

114.2g Glycine

Add to 1L with ddH20

To make 1X SDS running buffer, make 1L of 1X (100mL of Tris/Gly buffer stock) then add 10mL of 10% SDS

To make 1L of 1X transfer, add: 100mL of Tris/Gly buffer stock, 200mL (20%) methanol and 700mL water

## 4.METHODS

### 4.1 Human iPSC culture and maintenance.

The PD patient-derived p.A53T-iPSC and healthy donor control lines used in this study were generated and characterized as previously described [312].

#### 4.1.1 Human iPSC culture and passaging.

iPSCs were maintained in culture either using feeders or in feeder-free conditions. Regarding feeders, irradiated mouse embryonic fibroblasts (MEFs) were used, which are ideal for supporting healthy undifferentiated human iPSCs. One to three days prior to iPSC passaging or thawing, MEFs were seeded on gelatin-treated 6-well plates at densities ranging from 2 x 104–5.3 x 104 cells/cm2 according to manufacturer's instructions (www.thermofisher.com), in MEF medium. The day of the passaging, MEF medium was removed and each well was washed one time with KO-DMEM, before the iPSCs were plated on it. When FGF2 was added, the iPSC medium was used within 5 days.

Regarding feeder-free conditions, matrigel as a surface coating matrix was used. The day of the passaging, matrigel aliquot stored at -20oC was allowed to thaw on ice. Upon thawing, matrigel was added to DMEM medium at 1:200 dilution and the diluted one was seeded immediately on 6-well plates. The plates were then incubated at room temperature for one hour and after gently washes with KO-DMEM, were ready for the plating of the iPSCs. For feeder-free conditions, mTeSR™-E8™ Medium was used. This medium were prepared as indicated (www.stemcell.com ) and stored in 50ml aliquots at -20oC for up to 6 months. The medium in use was stored in 4oC for up to 2 weeks.

iPSCs were passaged whenever full confluent colonies were produced (usually every 5-7 days), while media were changed every day. iPSC colonies were usually passaged using the enzyme-free passaging reagent ReLeSR™, which does not require manual selection of differentiated areas or scraping to remove cell aggregates. After washing the cells once with PBS, 1ml/well of ReLeSR was added and 1 minute later the ReLeSR was removed so that colonies are exposed to a thin film of liquid for additional 5 minutes. Next, 1 ml/well of medium was added and holding the plate with one hand and using the other hand to firmly tap the side of the plate, the cells were detached from it. The detached cell aggregates were transferred in the new plate containing medium. The plate was then placed in the incubator and was moved in several quick, short, back-and-forth and side-to-side motions to evenly distribute the cell aggregates. The plating density was adjusted each time to maintain the culture at the desired confluence. When the colonies were full confluent with very few spontaneous differentiation in the culture, they were

passaged using collagenase IV. More specifically, iPSC colonies were incubated with the enzyme for 10min at 37oC, which was then removed, the cells were gently scraped using a cell scraper, were centrifuged for 5 min at 900 x g and then replated either on feeders or without feeders. After plating the cells, the plates were gently rocked side to side, and back and forth to spread the cells evenly across the well.

**4.1.2 Thawing iPSCs.**

Cells were thawed rapidly by placing the cryovial in a water bath set to maintain 37°C. The cryovial were swirled gently to ensure rapid thaw. Upon thawing, the cells then transferred from the cryovial into a 15 mL centrifuge tube. The cryovial was rinsed once with 1 mL of appropriate medium. The cells were centrifuged at 200 x g for 5 minutes. In parallel, the plates were washed with KO-DMEM and 1ml/well of medium was added. The supernatant was discarded and cells were gently resuspended in the appropriate medium volume. After plating the cells, the plates were gently rocked side to side, and back and forth to spread the cells evenly across the well.

**4.1.3 Freezing iPSCs.**

The optimal time for harvest is normally when cells are approximately 70-80% confluent. After removing the medium, cells were incubated with collagenase IV, as described above. 1 ml/ well of cryoprotectant (Synth-a-Freeze) was used per cryovial. The cryovial was placed immentiately into a pre-chilled freezing container into a -80°C freezer. The next day, the cryovial was transferred to liquid hydrogen container.

**4.1.4 Detection of the G209A (A53T) mutation in patient-derived genomic DNA**

The primers used are:

Syna3 forward: 5’-GCTAATCAGCAATTTAAGGCTAG-3’

Syna13 reverse: 5’-GATATGTTCTTAGATGCTCAG-3’

(Primer stock 100µM, Working stock 10µM at -20oC)

Reaction:

| | |
|---|---|
| DNA template 200 ng/µl | 1 |
| 10x buffer | 2 |
| 5x Q Sol | 4 |
| Primer 3 (10 µM) | 4 |
| Primer 13 (10 µM) | 4 |
| dNTPs (10 mM) | 0.4 |
| Taq polymerase | 0.1 |
| ddH2O | 4.5 |
| Total volume | 20 µl |

PCR Cycling Conditions:

1) Denaturation 94oC for 4 min

2) Denaturation 94oC for 30 sec

3) Annealing 50oC for 30 sec

4) Elongation 72oC for 1 min

5) Go to step 2, 34 times

6) 72oC for 5 min

Digestion with Tsp45I enzyme and incubation in 65oC for 5 h was followed:

| | |
|---|---|
| DNA (PCR product) | 20 |
| NEB1 | 3 |
| BSA | 0.3 |
| Tsp45I | 1.3 |
| ddH2O | 5.4 |
| Total volume | 30 µl |

The digestion product was loaded in 3 % agarose gel, using 12 µl DNA ladder (Mass Ruler L).

**4.2 NPCs generation and freezing**

For generation of neural precursor cells (NPCs), iPSCs were allowed to form embryoid bodies and neural induction was initiated by applying a dual SMAD inhibition protocol in the presence of Noggin and TGFβ inhibitor [312]. NPCs were maintained and expanded in DMEM/F12/B27/N2-medium supplemented with HEPES, Glutamax, non-essential amino acids [NEAA] and 20ug/ml FGF2. At this stage NPCs were

dissociated either for further neuronal differentiation or for freezing. For freezing, NPCs medium was removed and cells were washed once with 1X PBS (without calcium and magnesium). Adequate volume of accutase were added to cover the cells for 10 minutes at 37°C. After 10 minutes, cells were collected using a pipette by gently pipetting up and down 10-15 times to resuspend the cells into single cells. Cells were centrifuged at 300g for 5 minutes and resuspended in fresh medium for counting. After counting, cells were centrifuged and resuspented in cryoprotectant. 1 ml/ well of cryoprotectant (Synth-a-Freeze) was used per cryovial and 3-4*$10^6$ cells per cryovial. The cryovial was placed immentiately into a pre-chilled freezing container into a -80°C freezer. The next day, the cryovial was transferred to liquid hydrogen container.

**4.3 Neuronal differentiation**.

For neuronal differentiation, NPCs were dissociated with accutase and 35*$10^3$ cells/$cm^2$ were seeded onto poly-L-ornithine (20 µg/ml; Sigma-Aldrich)/laminin (5 µg/ml; Sigma-Aldrich)-coated 35mm dishes in DMEM/F12/ B27/N2-medium supplemented with 200 ng/ml human recombinant sonic hedgehog (SHH, R&D Systems) and 100 ng/ml murine recombinant fibroblast growth factor 8b (FGF-8b, R&D Systems) for 7 days in vitro (DIV). On 7 DIV cells were dissociated with accutase and 14*$10^4$ cells / $cm^2$ were seeded onto poly-L-ornithine/ laminin-coated plates in DMEM/F12/B27/N2-medium supplemented with 20 ng/ml brain-derived neurotrophic factor (BDNF, R&D Systems), 20 ng/ml glial cell-derived neurotrophic factor (GDNF, R&D Systems), 200 µM ascorbic acid (AA, Sigma-Aldrich) and 0.5 mM cyclic AMP (cAMP, Sigma- Aldrich). The medium was changed every 2 to 3 days for 2 weeks.

**4.4 Compound screening and analysis**.

For high content screening, iPSC-derived NPCs at 7 DIV were dissociated with accutase and were seeded (9,000 cells/well) onto poly-L-ornithine/ laminin-coated 384-well optical bottom plates containing the kinase inhibitors (Greiner Bio-One, Kremsmünster, Austria) in DMEM/F12/B27/N2-medium supplemented with 20 ng/ml BDNF/GDNF/AA/cAMP). The medium was changed every 2 to 3 days for 2 weeks. A collection of 273 small molecule kinase inhibitors from Selleck Chemicals was used in this study. The list of molecules and their known targets according to the provider is shown in Table 8. Two week prior imaging the cells, the compounds were dispensed in duplicate in 384-well optical bottom plates at a final concentration of 1µM. After 2 weeks of neuronal maturation the cells were fixed in 4% paraformaldehyde (PFA) for 20 min followed by immunofluorescence staining for βIII-tubulin (TUJ1) and Tyrosine hydroxylase (TH) at 4oC overnight, followed by incubation with appropriate secondary antibodies

(Molecular Probes, Thermo Fisher Scientific) conjugated to AlexaFluor 488 (green) or 546 (red), for at least 1 h at room temperature. Nuclei were stained with Hoechst dye. Images per well were captured by automated confocal microscopy (Opera High-Content Screening System, Perkin Elmer, Hamburg, Germany). To quantify the fluorescence and texture of our images, we used Image Mining, a custom-made image processing and analysis application with an extendable "plug-in" infrastructure [373]. A total of 15 images per well were acquired using a 10X magnifying objective and analyzed with Image Mining software. The number of cell nuclei and fluorescence staining of cells were quantified by segmentation on 15 images per well in a duplicate experimental setup.

**4.5 RNA isolation.**

Total RNA was extracted from cell pellets using the TRI Reagent. The following steps were followed:

1. Add 1 ml of TRIzol to the cell pellet and transfer the cell suspension in a 2 ml tube.

2. Lyse cells by repetitive pipetting (pipette up and down 4-5 times using insulin syringe).

3. Incubate the samples at RT for 5 min to ensure complete homogenization.

4. Add 0.2 ml of chloroform to each tube and shake vigorously by hand for 15 sec to mix well.

5. Incubate the samples at RT for 2-3 min.

6. Centrifuge samples for 15 min at 12,000 x g at 4oC.

7. Transfer the upper aqueous/clear phase (~500-600 µl) to a new 1.5 ml tube. Be careful not to get any of the intermediate or the lower pink phase!

8. Add 0.5 ml of isopropyl alcohol to precipitate RNA and mix.

9. Incubate the samples at RT for 10 min.

10. Centrifuge at 12,000 x g for 10 minutes at 4oC.

11. Discard the supernatant (reverse the tube).

12. Wash pellet with 1 ml 75% ethanol.

13. Mix sample by vortexing (gently).

14. Centrifuge at 7500 x g for 5 min at 4oC.

15. Remove supernatant.

16. Air dry the pellet for 5-10 minutes. Do not completely dry out the pellet.

17. Dissolve pellet in 30 to 60 µl (50 µl) RNase free water. Do not vortex!

18. Incubate the samples at RT (or 55-60oC) for 10 min.

19. RNA can be frozen (-80oC). Run on a gel to test the RNA quality. Measure the concentration of RNA in each sample (260/280 ratio should be ~1.8-2.2).

Following digestion with DNaseI, 1 µg of total RNA was used for first strand cDNA synthesis with the ImProm-II Reverse Transcription System (Promega) according to the manufacturer's instructions.

**4.6 RNA cleaning and cDNA synthesis.**

RNA cleaning was performed using the columns of Clean and Concentrator kit. For the digestion with DNase I, for every µg RNA, 1 µl DNAase I was added, plus 10x buffer and ddH2O and incubation at 37oC for 30min was followed.

1 µg of total RNA was used for first strand cDNA synthesis with the ImProm-II Reverse Transcription System (Promega), following the steps:

1. Add 2 volumes RNA Binding Buffer to each sample 1 and mix.

2. Add an equal volume of ethanol (95-100%) and mix.

3. Transfer the sample to the Zymo-SpinII C Column in a Collection Tube and centrifuge for 30seconds. Discard the flow- through.

4. Add 400 µl RNA Prep Buffer to the column and centrifuge for 30 seconds. Discard the flow-through.

5. Add 700 µl RNA Wash Buffer to the column and centrifuge for 30 seconds. Discard the flow-through.

6. Add 400 µl RNA Wash Buffer to the column and centrifuge for 2 minutes to ensure complete removal of the wash buffer. Transfer the column carefully into an RNase-free tube.

7. Add 50 µl DNase/ RNase- Free Water directly to the column matrix and centrifuge for 30 seconds.

1 µg of total RNA was used for first strand cDNA synthesis with the ImProm-II Reverse Transcription System (Promega) according to the following protocol:

Target RNA and primer combination and denaturation (total 5 µl/ RT reaction)

On ice:

• RNA up to 1 µg (1-1.5 µg)

• Random Hexamers2 µl of 0.5µM (stock 50 µM; working dilution 1/100, 0.5 µM)

• Mix well (spin)

• Incubate at 70oC for 5 min (heat block)

• Incubate on ice for 5min

• Spin

• Add 15 µl RT mix

Reverse Transcription

RT mix:

| | |
|---|---|
| Nuclease-free water | until 15 µl |
| ImProm-II 5x reaction buffer | 4 µl |
| MgCl2 | 1.2 µl |
| dNTPs (stock 25 µM) | 1 µl |
| RNasin | 0.5 µl |
| ImProm-II Reverse Transcriptase | 1 µl |

**4.7 Real time quantitative PCR**

Quantitative PCR analyses were carried out in a Light Cycler 96 (Roche) Real time PCR detection system using KAPA SYBR FAST qPCR Master Mix (KapaBiosystems). The primers used are listed in Table 5. The mix of primers, the enzyme and the 1/10 diluted cDNA.

**4.8 Immunofluorescence staining**.

Cells were fixed with 4% paraformaldehyde (Sigma-Aldrich) for 20 min at room temperature. Samples were blocked with 0.1% Triton X-100 (Sigma-Aldrich) and 5% donkey serum in PBS for 30 min and were subsequently incubated with primary antibodies (Table S6) at 4oC overnight, followed by incubation with appropriate secondary antibodies (Molecular Probes, Thermo Fisher Scientific) conjugated to AlexaFluor 488 (green) or 546 (red), for at least 1 h at room temperature. Coverslips were mounted with

ProLong Gold antifade reagent with DAPI (Cell Signaling) and images were acquired using a Leica TCS SP8 confocal microscope (LEICA Microsystems) and analyzed using ImageJ software (NIH).

**4.9 Neurite analysis**.

Neurite analysis was performed on iPSC-derived neurons at 21 DIV. Immunofluorescence staining was performed for Tyrosine Hydroxylase (TH). The number of neurites extending from the soma of at least 50 single TH+ neurons per sample was determined. Neurite length was estimated by manually tracing the length of all neurites on TH-labeled neurons using the NeuronJ plugin of ImageJ (NIH).

**4.10 Axon degeneration index.**

Analysis of axon degeneration was performed by immunostaining for βIII-tubulin (TUJ1) in iPSC-derived PD neuronal cultures. The cultures were either untreated (in the presence of DMSO) or treated with BX795. The number of TUJ1+ spots in blebbed or fragmented axons was counted manually (ImageJ) on twenty randomly selected fields and the ratio between the number of spots and the total TUJ1+ staining area (ImageJ) was defined as axon degeneration index.

**4.11 Protein aggregates quantification.**

Protein aggregates were detected with the PROTEOSTAT Aggresome Detection Kit (Enzo) followed by immunolabeling for TUJ1 or Tyrosine Hydoxylase(TH) [18, 19] Manual analysis was performed by isolating individual cells from images (ROIs), applying a threshold, and utilizing the analyze particles ImageJ function.

**4.12 Proteomic Analysis.**

The same line of patient-derived neurons used for high content screening was used for proteomics analysis vis-à-vis a healthy control. At 21 DIV iPSC-derived neurons were suspended, lysed and the proteins reduced in 4% SDS, 100 mM DTT, 100 mM Tris pH 7.8 through heating for 5 min. Next, the proteins were alkylated by 100 mM iodoacetamide treatment for 30 min in the dark. Samples were further processed according to the Single-Pot Solid-Phase enhanced Sample Preparation (SP3) method of Hughes et al [374]. Digestion was carried out overnight at 37°C using Trypsin/LysC mix (Promega) at a protein/enzyme ratio of 50:1 in a ThermoMixer under continuous mixing at 1000 rpm. After digestion, the tubes were placed on a magnetic rack, and the supernatant containing the peptides was collected and dried down in a centrifugal evaporator (Savant SPD 1010, Thermo scientific). The peptide mixtures were

reconstituted in a solution of 2% (v/v) ACN/ 0.1% (v/v) formic acid and incubated for 3 min in a sonication water bath. Peptide concentration was determined by nanodrop absorbance measurement at 280 nm.

### 4.12.1 Ultra high pressure nanoLC.

2.5 µg peptides were pre-concentrated with a flow of 3 µL/min for 10 min using a C18 trap column (Acclaim PepMap100, 100 µm x 2 cm, Thermo Scientific) and then loaded onto a 50 cm long C18 column (75 µm ID, particle size 2 µm, 100Å, Acclaim PepMap100 RSLC, Thermo Scientific). The binary pumps of the HPLC (RSLCnano, Thermo Scientific) consisted of Solution A (2% (v/v) ACN in 0.1% (v/v) formic acid) and Solution B (80% (v/v) ACN in 0.1% (v/v) formic acid). The peptides were separated using a linear gradient of 4% B up to 40% B in 340 min with a flow rate of 300 nL/min. The column was placed in an oven operating at 35°C.

### 4.12.2 LC-MS/MS.

The eluted peptides were ionized by a nanospray source and detected by an LTQ Orbitrap XL mass spectrometer (Thermo Fisher Scientific, Waltham, MA, USA) operating in a data dependent mode (DDA). Full scan MS spectra were acquired in the orbitrap (m/z 300–1600) in profile mode with the resolution set to 60,000 at m/z 400 and automatic gain control target at 106 ions. The six most intense ions were sequentially isolated for collision-induced (CID) MS/MS fragmentation and detection in the linear ion trap. Dynamic exclusion was set to 1 min and activated for 90 sec. Ions with single charge states were excluded. Lockmass of m/z 445,120025 was used for continuous internal calibration. XCalibur (Thermo Scientific) was used to control the system and acquire the raw files.

### 4.12.3 Protein identification and quantification.

The mass spectral files (raw files) were processed using MaxQuant software (version 1.6.9.0). Default parameters were used for protein identification and quantification. Trypsin specificity was set to allow two missed cleavages and minimum peptide length was set to 7 amino acids. Cysteine carbamidomethylation was set as fixed, and methionine oxidation, deamidation of asparagine and glutamine and N-terminal acetylation were set as variable modifications. A maximum of 5 modifications per peptide was set. The false discovery rate both for peptide and protein was set to 1%. For calculation of protein abundances, label-free quantification (LFQ) was performed with both “second peptides” and “match between run” options enabled. The human FASTA files were from UniProt downloaded on 15 October 2019.

### 4.12.4 Proteomic data analysis.

Statistical analysis was performed using Perseus (1.6.6.0). Proteins identified as contaminants, "reverse" and "only identified by site" were filtered out. The LFQ intensities were transformed to logarithmic values [log2(x)]. The protein groups were filtered to obtain at least 2 valid values in at least one group. The label-free quantified proteins were subjected to statistical analysis with ANOVA test (permutation-based p-value with 0.05 cutoff). LC-MS/MS data after statistical analysis were plotted in a volcano graph based on the difference between the two samples expressed as log2(x) versus their statistical significance expressed as –Log10(p-value). Hierarchical clustering was carried out on Z-score transformed LFQ values using average linkage of Euclidian distance. For statistical and bioinformatics analysis, as well as for visualization, Perseus, which is part of Maxquant, was used [375]. GO Enrichment analysis for biological processes, molecular function and cellular compartment was performed using DAVID functional annotation tools with official gene symbol as identifiers, the Homo sapiens background and the GOTERM_DIRECT annotation categories. A P value of 0.05 was selected as the cutoff criterion. The enrichment of proteins involved in signaling pathways was performed using the Reactome pathway database. A P value of 0.01 was selected as the cutoff criterion.

### 4.13 Western blot.

iPSC-derived neurons or SH-SY5Y cell cultures were lysed at 4oC for 15 min in ice cold lysis buffer [150mMNaCl, 50 mM Tris (pH 7.5), 1%v/v Triton X-100, 1mM EDTA, 1mM EGTA, 0.1% SDS, 0.5% Nsodium deoxycholate containing PhosSTOP phosphatase inhibitors and a complete protease inhibitor mixture (Roche Life Science), and centrifuged at 20,000 g. Protein concentration was estimated in the supernatant by Bradford assay (Biorad). Proteins were separated by gel electrophoresis (PAGE) on 12% SDS- gels using running buffer (see Materilas) and transferred onto nitrocellulose membranes (Maine Manufacturing) using transfer buffer (see Materials). For phospho-(Ser129)-αSyn detection, the membrane was heated at 65 0C overnight in PBS. Nonspecific binding sites were blocked in TBS/ 0.1% Tween 20/5% skimmed milk for 1 hour at 20°C 0C followed by overnight incubation with primary antibodies diluted in TBS/0.1% Tween20/3% BSA or in TBS/0.1% Tween 20/5% skimmed milk. Incubation with appropriate HRP-conjugated secondary antibodies (Thermo) was performed for 2 hours at room temperature and protein bands were visualized using the Amersham ECL Prime Western Blotting Detection Reagent (GE Healthcare,RPN2232). Densitometric analysis was performed using ImageJ software (NIH).

### 4.14 Production of CMV.DsRed and CMV.DsRed.A53T lentiviral vectors.

Four plasmids were used for lentivirus generation: the lentiviral transfer vector and three lentiviral packaging vectors (pMDL, pRev and pVSVG; provided by Dr. Fred Gage, the Salk Institute for Biological Studies). The lentiviral transfer vectors for expression of either the red fluorescent protein DsRed under the control of CMV promoter (LV.CMV.DsRed) or for co-expression of the red fluorescent protein DsRed, a T2A bicistronic configuration and p.A53T-αSyn under the control of CMV promoter (LV.CMV.DsRed.T2A.A53T) were constructed by VectorBuilder. The preparation and purification of the lentiviral vectors were performed as previously described [376]. LV.CMV.DsRed and LV.CMV.DsRed.T2A.A53T were used for transduction of the human neuroblastoma cell line SH-SY5Y that was routinely maintained in regular RPMI 1640 medium (Gibco) supplemented with 10% FBS (Gibco) and 1% penicillin/streptomycin (Life Technologies) at 37°C in a humidified atmosphere containing 5% CO2 and 95% air.

### 4.15 Stably transfected SH-SY5Y culture.

SH-SY5Y cell line stable expressing the human p.A53T a-synuclein has been generated using CMV.DsRed and CMV.DsRed.A53T lentiviral vectors. SH-SY5Y cells transduced with either the control vector LV.CMV.DsRed or LV.CMV.DsRed.T2A.A53T for expression of p.A53T-αSyn and they were maintained in regular RPMI 1640 medium (Gibco) supplemented with 10% FBS (Gibco) and 1% penicillin/streptomycin (Life Technologies) at 37°C in a humidified atmosphere containing 5% CO2 and 95% air. After 24 h incubation, the culture medium was changed. Following another 24 h, cells were transferred in selective medium containing 300 µg/ml gentamycin-disulfate G418. After 3 weeks of G418 selection,when 100% of the cells were expressing the DsRED protein, they were frozen down as a polyclonal line.

#### 4.15.1 Differentiation of SH-SY5Y cells.

Cells were plated on PLL/Laminin coated plates (2*104 cells/cm2) in regular RPMI 1640 (Gibco) supplemented with 5% FBS (Gibco) and 1% penicillin/streptomycin (Life Technologies) at 37°C in a humidified atmosphere containing 5% CO2 and 95% air(DIV0). Next day, 10uM Retinoic Acid (RA) was added (DIV1).On DIV3, medium was changed to Neurobasal supplemented with B27,N2,Glutamax and BDNF (50ng/ml). Mediun was changed every 2-3 days until DIV9.

**4.16 Cell culture and transfection of the inducible SH-SY5Y line.**

The inducible SH-SY5Y cell line expressing human p.A53T-αSyn was created and characterized as previously described [377]. It was maintained in regular RPMI 1640 (Gibco) supplemented with 10% FBS (Gibco) and 1% penicillin/streptomycin (Life Technologies) at 37°C in a humidified atmosphere containing 5% CO2 and 95% air. The expression of p.A53T-αSyn was switched off by the addition of doxycycline (Dox) (2 µg/mL). Transfection with the GFP-LC3 and mCherry-GFP-p62 plasmids (a kind gift from Dr Tamotsu Yoshimori, Osaka University, Japan and Dr Terje Johansen, University of Tromso, Norway, respectively) was performed in the absence of Dox using Lipofectamine 2000 transfection reagent, according to the manufacturer's protocol (Invitrogen; Thermo Fisher Scientific, Inc.).

**4.17 iCell Dopa neurons and iCell DopaNeurons. PD SNCA A53T HZ.**

Commercially available neurons from Fujifilm Cellular Dynamics International (CDI) produce more than 90% MAP2+/Nes- and more than 80% pure midbrain DA neurons The catalog numbers for the cells used in this paper are iCell DopaNeurons, 01279, Catalog No C1028,and iCell DopaNeurons SNCA A53T HZ,01279, Catalog No C1113. The cells were defrosted according to the protocol on the User's Guide from CDI and plated on Poly-L-ornithine- and Laminin-coated coverslips (2x105 cells/cm2). The media used was supplied by Fujifilm Cellular Dynamics International (Neural Base Medium 1, iCell Nervous System Supplement, Neural Supplement B).Media was changed every 2 days for two weeks.

**4.18 Protein synthesis assay.**

For detection of total protein synthesis an assay Kit (ab239725) (Abcam) was used that utilizes a cell permeable analog of puromycin, O-Propargyl-puromycin which, once inside the cell, stops translation by forming covalent conjugates with nascent polypeptide chains. Truncated polypeptides are rapidly turned over by the proteasome and can be detected based on a click reaction with fluorescent azide. SH-SY5Y cells transduced with either the control vector LV.CMV.DsRed or LV.CMV.DsRed.T2A.A53T for expression of p.A53T-αSyn were pre-treated with DMSO vehicle or BX795 for 24h and were incubated for 2h with fresh aliquots of media containing either Protein Label or Protein Label and BX795. Cells were then fixed with 4% paraformaldehyde (Sigma-Aldrich) for 20 min at room temperature. Coverslips were mounted with ProLong Gold antifade reagent with DAPI (Cell Signaling) and images were acquired using a Leica TCSSP5II confocal microscope (LEICA Microsystems) and analyzed using ImageJ software (NIH).

**4.19 Autophagy detection assay.**

For detection of autophagosomes and monitoring autophagic flux, cells were seeded in 48-well plates on coverslips. After 7d incubation, the cells were treated with BX795 (1uM). The Cyto-ID® autophagy detection kit (Enzo Life Sciences, Plymouth Meeting, PA) was used according to the manufacturer's instructions in live cells. Samples were briefly exposed to Cyto-ID Green Dye and Hoechst 33342 at 37 °C for 30 min. The cells were then washed with 1× assay buffer and fixed with 4% parafolmadehyde. Coverslips were mounted with ProLong Gold antifade reagent with DAPI (Cell Signaling) and images were acquired using a Leica TCS SP8 confocal microscope (LEICA Microsystems) and analyzed using ImageJ software (NIH).

**4.20 P70 S6K activity.**

S6K1 activity was analyzed with an S6K activity assay kit (Enzo Life Sciences) according to the manufacturer's instructions. Briefly, the purified S6K1 was incubated in the presence of the BX795 inhibitor prior to initiating the kinase reaction for 30min. Rapamycin was used as a positive control.Then, the protein was added to reaction buffer and incubated in a 96-well plate coated with the S6K substrate, a synthesized peptide containing the S6 consensus peptide (KRRRLASLR). After removal of the reaction mixture and three washes with wash buffer, the plate was incubated with anti-phospho-S6 antibody (1:1000) for 1 h, followed by a secondary antibody conjugated to horseradish peroxidase (HRP) for 20 min. S6K1 kinase activity was monitored after color development by adding tetramethylbenzidine (TMB) substrate with a microplate reader (Bio-Rad 680) and measuring the absorbance at 450 nm.

**4.21 Statistics.**

All experiments were replicated at least three times and data from parallel cultures were acquired. Statistical analysis was performed using GraphPad Prism 6 software. Before performing parametric tests, data were assessed for normality with a D'Agostino–Pearson omnibus. Statistical significance was calculated for two groups using Student's t-tests or the Mann-Whitney test for non-parametric distribution. Group comparisons of data were performed by one-way ANOVA test followed by Tukey post hoc test using PRISM (Graph Pad). P-values < 0.05 were considered significant; *p < 0.05, **p<0.01,***p<0.001,****p<0.0001.

## 5. RESULTS

Disease-modifying therapies remain an important unmet need for neurodegenerative diseases, including Parkinson's disease (PD). The aim of this study was to use induced pluripotent stem cell-derived neurons generated from patients with PD in order to identify small molecules that revert previously identified pathological phenotypes [312, 378] and elucidate novel disease targets and pathways with potential therapeutic value. To address this aim, we combined high throughput screening approaches with induced pluripotent stem cell (iPSC)-based disease modeling. More specifically, we applied high content imaging on iPSC-derived neurons from patients with familial Parkinson's disease bearing the G209A (p.A53T) α-synuclein (αSyn) mutation and launched a screening campaign on a small kinase inhibitor library. Our search focused on kinases, since they are attractive clinical targets for treatment of various disorders, including cancer [379] and, more recently, CNS disorders and neurodegenerative diseases [297, 369].

### 5.1 Assay development for high content screening of p.A53T-iPSC derived neurons

iPSCs used in this study were generated from a PD patient bearing the p.A53T αSyn mutation and thoroughly characterized [312]. For directed differentiation a dual SMAD inhibition protocol was used in the presence of Noggin and TGFβ inhibitor [305, 312, 380], which favors the generation and expansion of Pax6+/Nestin+ neural progenitor cells (NPCs; Fig. 12a). NPCs were replated in neuronal differentiation medium for 7 days *in vitro* (DIV) and were allowed to further differentiate into βIII-tubulin (TUJ1)+ neurons for another two weeks (DIV 21) at which time point 15-20% of TUJ1+ neurons also expressed the dopaminergic marker TH (Fig. 12a). The expression of dopaminergic lineage markers, such as Nurr1, TH, and aromatic amino acid decarboxylase (AADC) was also confirmed by qRT-PCR (Fig. 12b).

For compound screening iPSC-derived NPCs were dissociated at DIV 7 and re-plated onto miniature 384-well plates at 9,000 cells/well, a density that was selected as the most suitable for quantitative image analysis by automated microscopy at DIV 21. As readout we assessed TH immunofluorescence, seeking to identify putative neuroprotective compounds enhancing dopaminergic neuron output (Figs. 12 and 13). To this end, the fluorescent signal for TH within a well was normalized to the fluorescent signal for the pan-neuronal marker βIII-tubulin (TUJ1) allowing to monitor changes in the TH population in a simple and effective way.

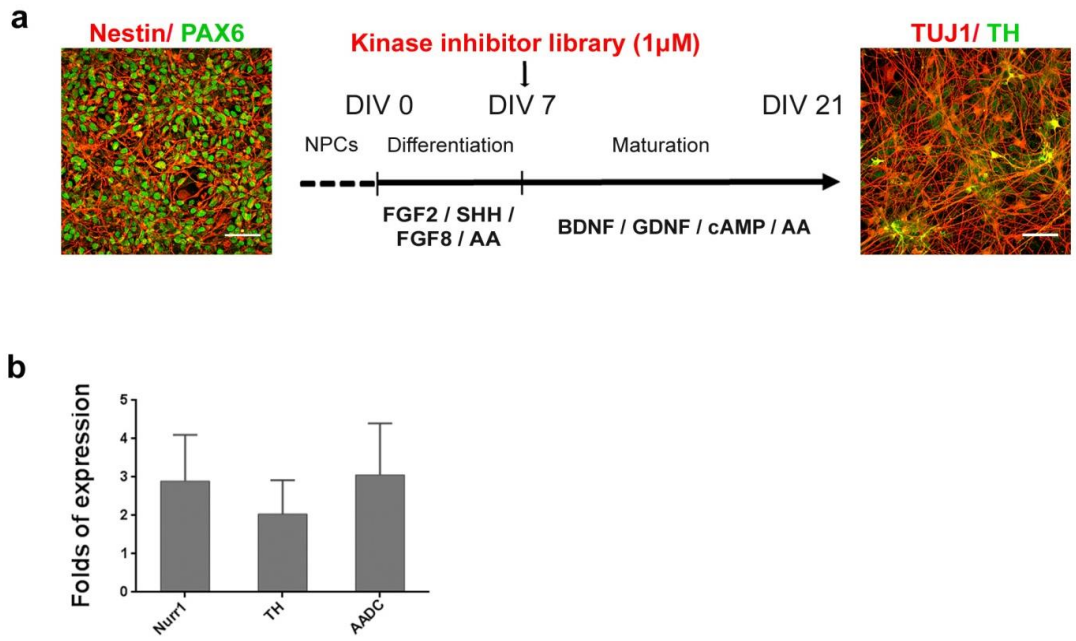


***Figure 12. Differentiation protocol. a****. Directed differentiation of Pax6+ (green)/ Nestin+ (red) neural precursor cells (NPCs; DIV 0, left) into TUJ1+ (red)/ TH+ (green) neurons (DIV 21, right). The differentiation protocol and timeline of analysis are shown in the drawing in the middle. Scale bar represents 150 µm* ***b****. RTqPCR analysis of selected domaminergic markers in iPSC-derived neurons at 21 DIV: Tyrosine Hydrosylase (TH), Nuclear receptor related 1 protein (Nurr1) and Aromatic L-amino acid decarboxylase (AADC) normalized to GAPDH levels. Data represent mean ± SEM (n = 3)*

### 5.2 High content screening of a kinase inhibitor library identifies BX795 as a compound that increases TH immunofluorescence in p.A53T-neurons

Protein kinases represent central molecular hubs that regulate numerous cell processes, thus constituting potentially attractive clinical targets. Indeed, the success of kinase inhibitors in treating cancer has spurred the evaluation of such compounds in phase II/III clinical trials as candidates for treatment of various neurodegenerative diseases [381, 382]. Since several kinases have been implicated in PD pathology [383], we screened a collection of 273 small molecule kinase inhibitors from Selleck Chemicals (Table 8) to identify compounds with prospective neuroprotective properties. p.A53T cells adapted in 384-well plate format were exposed once (7 DIV) to the library of kinase inhibitors at 1µM concentration and quantitative image analysis was performed two weeks later, at 21 DIV (Figs. 12 and 13). Hits were defined as compounds that robustly conferred an increase in TH expression compared to DMSO-treated p.A53T neurons within a well, normalized to the expression of the pan-neuronal marker βIII-tubulin (TUJ1) (Fig. 13a, b, c). Toxic compounds were excluded by assessing cellular viability (total nuclei count) of compound-treated as compared to DMSO-treated cells (Fig. 13d).

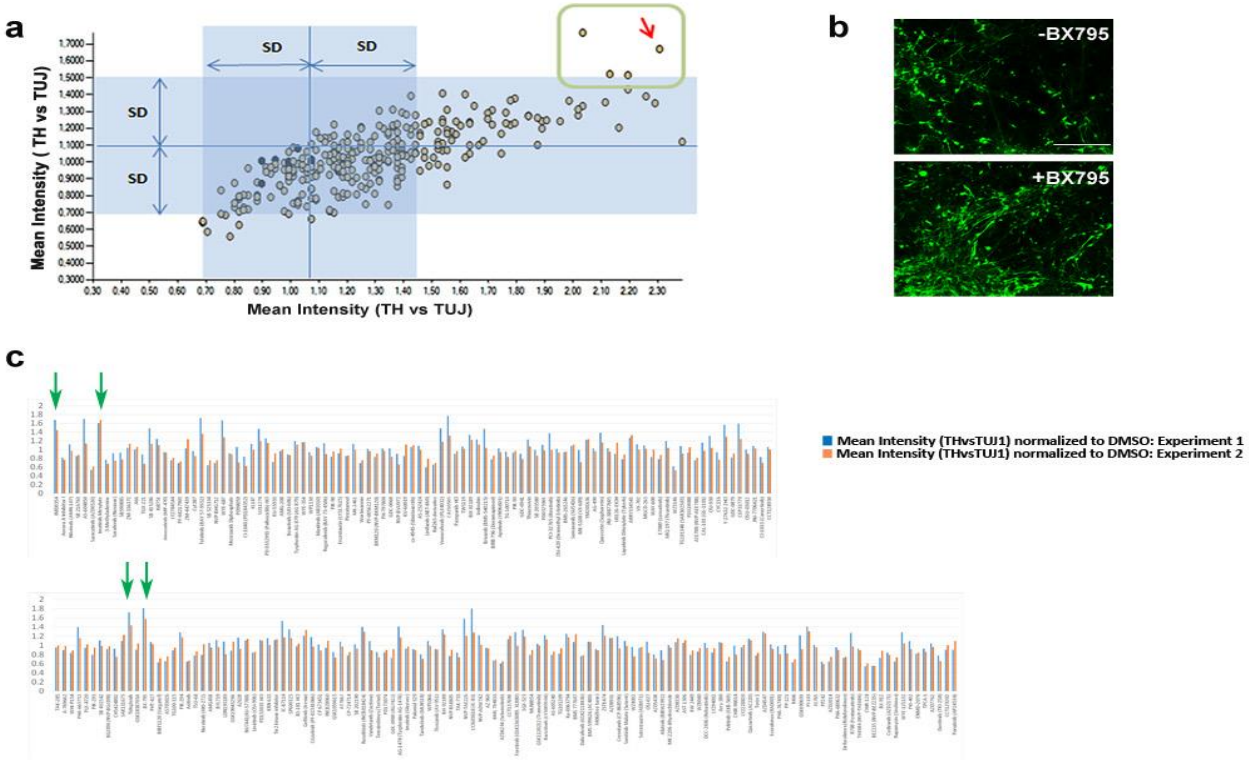
a
SD
SD
SD
SD
Mean Intensity ( TH vs TUJ)
Mean Intensity (TH vs TUJ)
b
-BX795
+BX795
c
Mean Intensity (THvsTUJ1) normalized to DMSO: Experiment 1
Mean Intensity (THvsTUJ1) normalized to DMSO: Experiment 2
d
Nuclei count (Norm): Experiment 2
Nuclei count (Norm): Experiment 1
Compounds
Toxic compounds
e
Imatinib Mesylate
IMD0354
Tideglusib
BX795
Mean Intensity ratio ( TH vs TUJ)
Concentration

***Figure 13. Identification of BX795 by high content screening of a kinase inhibitor library. a.*** *Scatter plot showing the ratio of TH versus Tuj1 expression in duplicate upon drug treatment with 273 small kinase molecule inhibitors. The dots inside the green square correspond to the 4 hit compounds show significant increase TH versus Tuj1 expression ratio as compared to the DMSO controls (blue dots). The red arrow indicates BX795.* ***b.*** *Representative images of p.A53T-neurons immunolabelled for TH in 384-well plates. Upper micrograph shows control DMSO-treated cells while lower micrograph represents BX795-treated cells. Scale bar represents 150 µm.* ***c.*** *Summary of total nuclei counts from two screening plates. Compounds in cells with low nuclei counts were considered toxic and where excluded from the analysis. Each assay plate was normalized to DMSO.****d.*** *Graph plot showing the ratio of TH versus Tuj1 expression in duplicate upon drug treatment with 273 small kinase molecule inhibitors. The arrows in green correspond to the 4 hit compounds show significant increase TH versus Tuj1 expression ratio as compared to the DMSO controls.* ***e.*** *Tests of the four hit compounds in a dose-response format. Data are presented as mean ± SEM. *P<0.05 control versus 1uM BX795.*

From the primary screen four hits were identified (Fig. 13a,c), which were re-tested for validation in a dose-response assay (Fig. 13e). Of these BX795, an aminopyrimidine compound that acts as a multi-kinase inhibitor with pro-survival and/or anti-inflammatory effects [384], significantly increased TH immunofluorescence at 1 µM concentration (Fig. 13e). BX795 was initially developed as an ATP-competitive inhibitor of 3-phosphoinositide-dependent kinase 1 (PDK1), and was later shown to also inhibit the IKK-related kinase, TANK-binding kinase 1 (TBK1) and IKKε, as well as to have numerous additional targets [385-387]. Based on the sustained neuroprotective effect of a single dose of BX795 on p.A53T dopaminergic neurons, we focused further on this compound to explore its function.

**5.3 BX795 rescues neuropathological features of p.A53T neurons**

The effects of BX795 on p.A53T-neurons were tested in cells that received a single treatment of the kinase inhibitor (1 µM) at 7 DIV and were analyzed two weeks later at 21 DIV, in accordance with the protocol applied during the screening procedure. In a first set of experiments a range of different drug concentrations from 0.1-2 µM was tried, including repeated drug additions every 2-3 days, with the selected scheme ensuring optimal efficacy and minimal toxicity. Then, we asked if the enhancement in TH immunofluorescence could be attributed to an increase in cell survival/proliferation or dopaminergic differentiation in p.A53T-cultures. We could not detect BX795-driven changes in either proliferation, as assessed by the percentage of Ki67+ cells (Fig. 14a; %ki67+ cells, DMSO: 43.3 $\pm$ 4.4, BX795: 50.3 $\pm$ 1.5, n=3), or in differentiation as estimated by the percentage of or TH+ cells in the culture (Fig. 14b; % TH+ cells out of all TUJ1+ cells, DMSO: 13.9 $\pm$ 3.1, BX795: 18.1.0 $\pm$ 2.3, n=3). Moreover, we did not detect any

change in total cell viability, as assessed by nuclei count (Fig. 14c, % of control, ctl: 100±19.4, p.A53T: 102.8±11.6, p.A53T+BX795:100.5±10.38). These observations indicate that the effect of BX795 on dopaminergic neurons is not related to an increase in either survival/proliferation or differentiation.

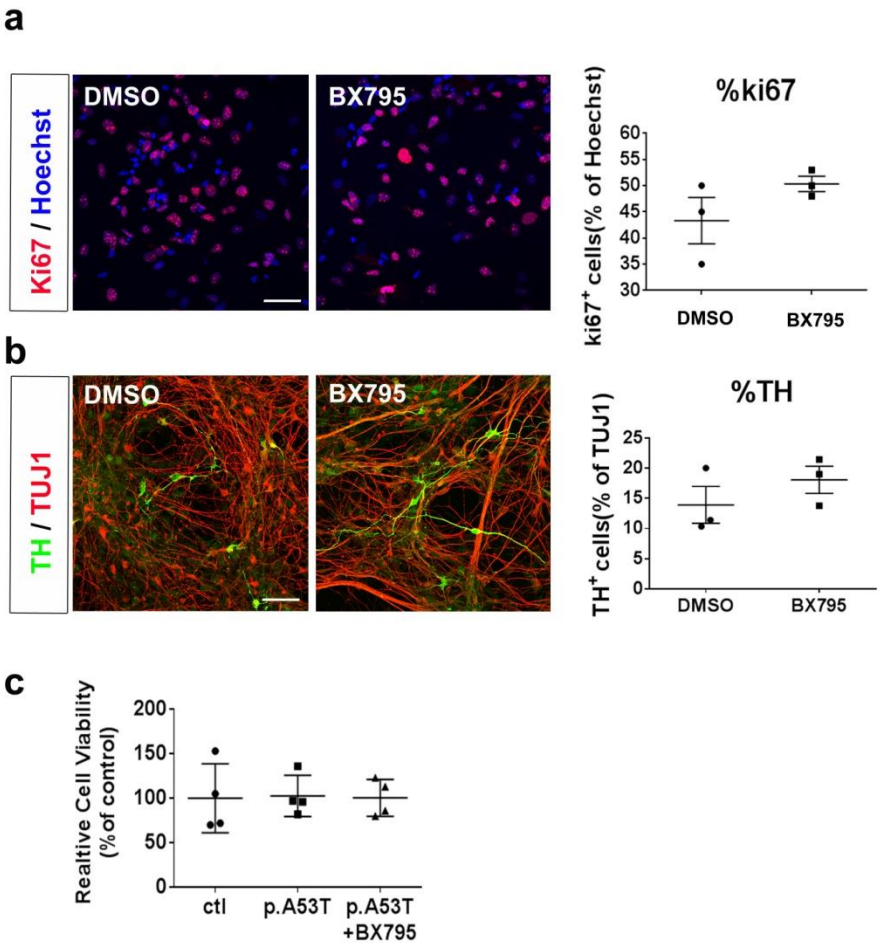


***Figure 14.Effect of BX795 on survival/proliferation and differentiation. a.*** *Representative images of p.A53T iPSC-derived neurons at 21 DIV immunostained for Ki67 (red) to label cycling cells. Hoechst+ nuclei are in blue (Scale bar, 50 µm).Quantification of the percentage of Ki67+ cells in the presence or absence of BX795. Data represent mean ± SEM (n = 3). Student's t-test was used.* ***b.*** *Representative images of p.A53T iPSC-derived neurons at 21 DIV immunostained for TUJ1(red) and Tyrosine Hydrozylase (TH)(green), (Scale bar, 50 µm).Quantification of the percentage of TH+ cells in the presence or absence of BX795. Data represent mean ± SEM (n = 3). Student's t-test was used.* ***c.*** *Quantification of total nuclei count. Data represent mean ± SEM (n = 4). Comparisons by ANOVA with Tukey correction.*

Next, we investigated if treatment with BX795 could rescue neuropathological features previously identified in p.A53T-neurons, such as compromised neuritic growth, dystrophic or fragmented neurites

and the presence of intracellular protein aggregates [312, 378]. Evaluation of total neurite length in p.A53T TH+ dopaminergic neurons revealed a significant increase in response to BX795 (length in µm, ctl: 221.7 ± 16.8, p.A53T:127.2 ± 13.5, p.A53T+ BX795: 196.8 ± 21.1, n=5, Fig. 15a) compatible with the observed increase in TH immunofluorescence. Moreover, examination of the distinct pathological morphology of TUJ1+ p.A53T neurons revealed an almost 50% reduction in axonal degeneration (axon degeneration index: ctl: 2.945 ± 1.325, p.A53T:13.03 ± 1.491, p.A53T+ BX795: 7.276 ± 1.017 n=3; Fig. 15b.

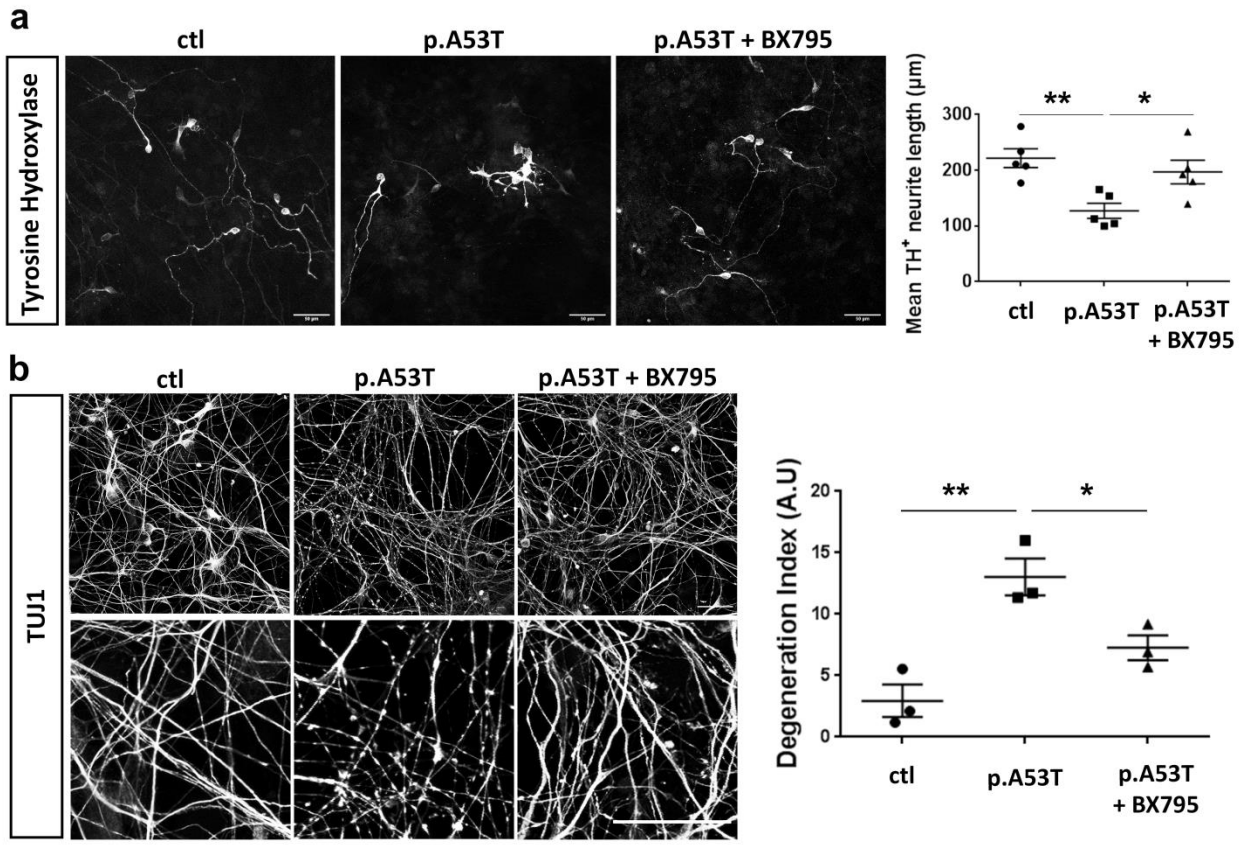


***Figure 15. Rescue of neuropathological features in patient-derived p.A53T neurons by BX795. a.*** *BX795 has a positive effect on neurite length of p.A53T-neurons. Representative confocal images of healthy control (ctl) and p.A53T-neurons immunostained for TH and quantification of total neurite length of TH+ cells. Data represent mean ± SEM. (Comparisons by ANOVA with Tukey correction *P<0.05, **P<0.01, n=4 independent experiments with at least 50 cells analyzed in each experiment). Scale bar, 50µm.* ***b.*** *BX795 alleviates axonal neuropathology in p.A53T-neurons. Higher magnification at the right (upper, DMSO-treated cells; lower, BX795-treated cells) shows neurites with swollen varicosities or fragmented processes (arrows). Scale bar, 30µm. Quantification of axonal degeneration is estimated in the accompanying graph by measuring the ratio of TUJ1+ spots over the total TUJ1+ area in untreated*

*(p.A53T) or BX795-treated p.A53T-neurons. Data represent mean ± SEM.(Comparisons by ANOVA with Tukey correction, *P< 0.05, **P<0.01, n = 20 randomly selected fields for each condition.Data was from three independent experiments.).*

Moreover, exposure to BX795 resulted in a notable 60% decrease in protein aggregate formation in p.A53T cells (number of aggregates per cell, p.A53T: 8.431 + 0.77, n= 51, p.A53T+ BX795: 3.242 + 0.40, n=62; Fig. 16a) accompanied by a consistent decline in the levels of (Ser129)-phosphorylated αSyn (Fig. 16b). It is known that increased formation of (Ser129)-phosphorylated αSyn changes its solubility properties enhancing its tendency to aggregate and disrupt normal function. This modification that renders αSyn prone to self-assembly is commonly associated with synucleinopathy [334, 388].

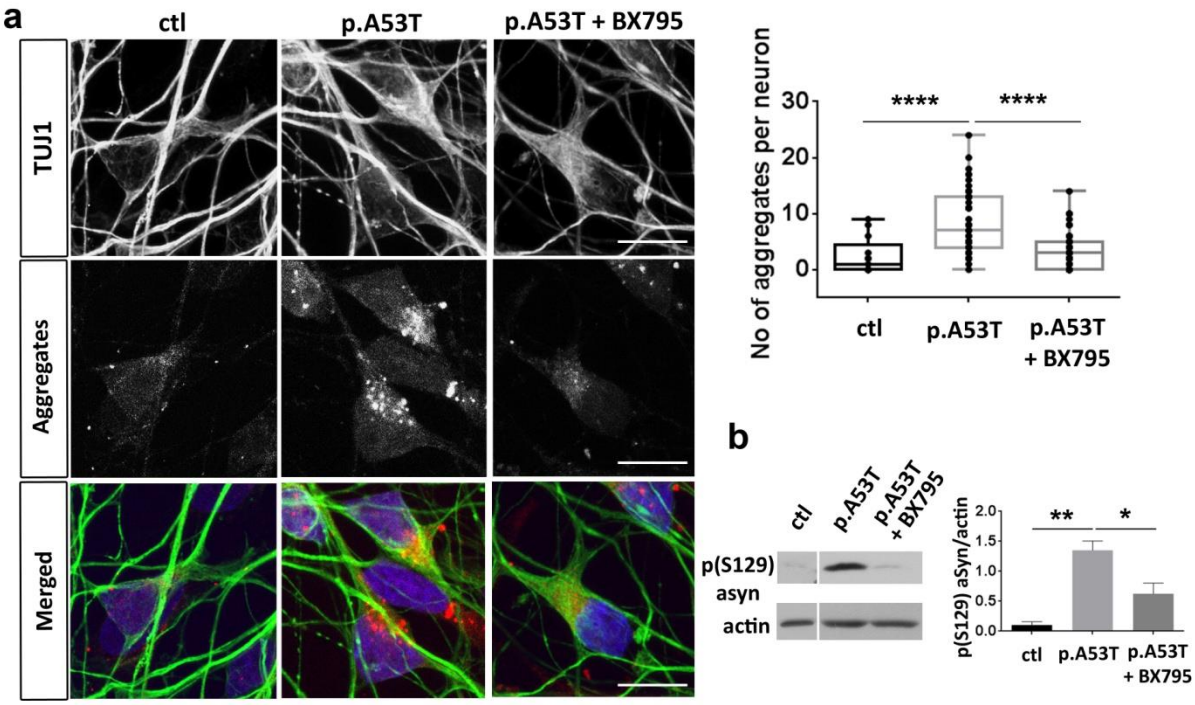


***Figure 16. Decrease of protein aggregate formation in patient-derived p.A53T neurons by BX795.a.*** *BX795 reduces protein aggregates in p.A53T-neurons. Representative confocal images showing protein aggregates in p.A53T TUJ1+ neurons (Scale bar, 10μm) and quantification in untreated or BX795-treated TUJ1+ cells (.Data was from three independent experiments. Mann–Whitney test; n=at least 30 cells per group; ****P< 0.0001).* ***b.*** *Detection and quantification of p(Ser129)αSyn by Western blot; Actin shows equal protein loading. Data represent mean ± SEM (t-test, *P<0.05, n=4 independent experiments).*

To exclude the possibility of a patient-specific effect, we confirmed that the BX795 enhancement in neuritic growth and the decrease in the neurodegeneration index were also observed in previously well characterized p.A53T-neurons derived from a second patient.(Fig. 17) [312, 378].

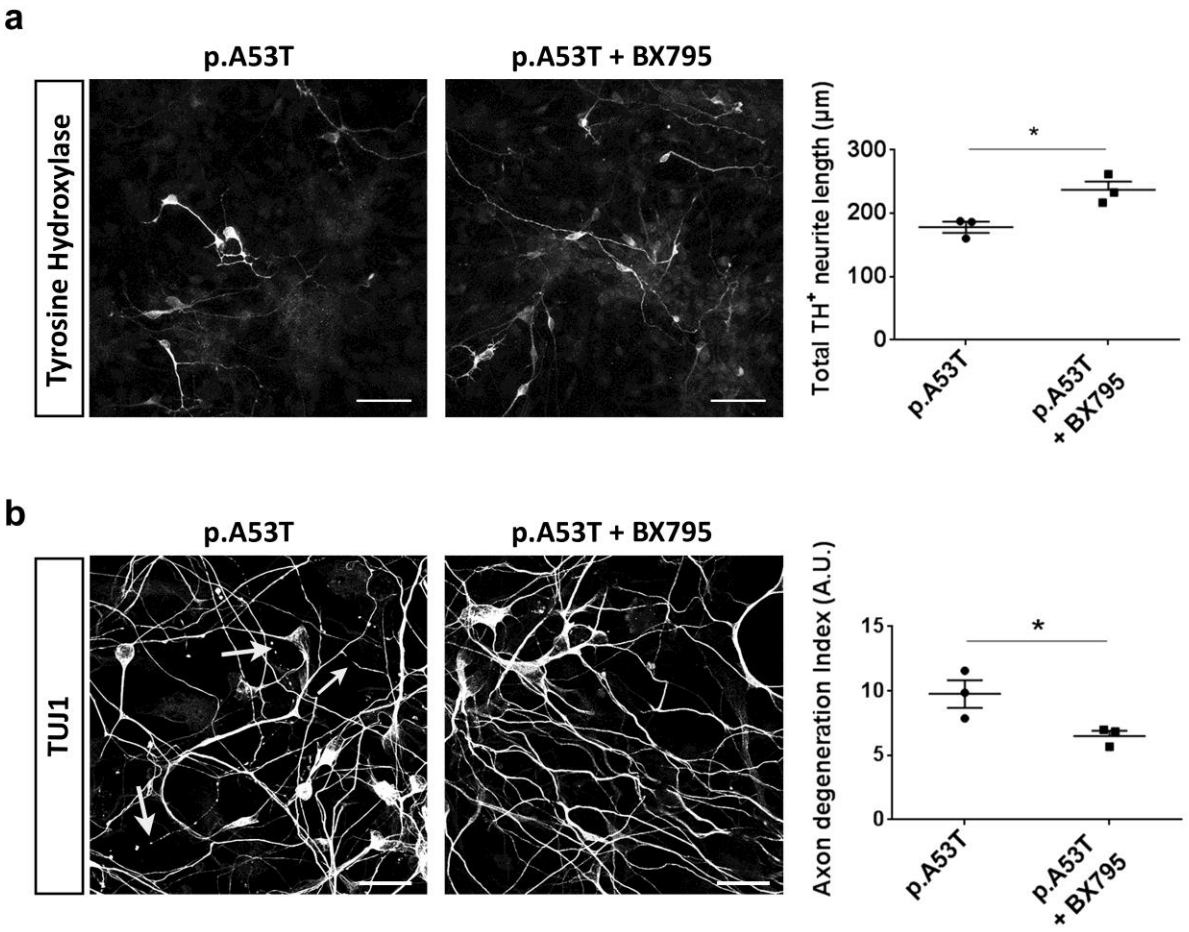


***Figure 17. Rescue of neuropathological features by BX795 in p.A53T neurons from a second patient. a.*** *BX795 has a positive effect on neurite length of p.A53T-neurons. Representative confocal images of p.A53T-neurons immunostained for TH and quantification of total neurite length of TH+ cells. Data represent mean ± SEM. (n=at least 50-60 cells per condition from two independent experiments). Scale bar, 50µm.* ***b.*** *BX795 alleviates axonal neuropathology in p.A53T-neurons as demonstrated by immunostaining for βIII-tubulin (TUJ1; confocal images). Neurites with swollen varicosities or fragmented processes are indicated with arrows. Scale bar, 30µm. Quantification of axonal degeneration is estimated in the accompanying graph by measuring the ratio of TUJ1+ spots over the total TUJ1+ area in untreated (DMSO) or BX795-treated p.A53T-neurons. Data represent mean ± SEM.*

To further exclude the influence of the genetic background in our observations, we also assessed the neuroprotective effects of BX795 in a highly enriched culture of mature human midbrain dopaminergic neurons (obtained from Fujifilm Cellular Dynamics Inc). These comprised an isogenic pair of wild-type (iCell DOPA) and gene-edited (iCell A53T DOPA) iPSC-derived neurons in which a heterozygous p.A53T mutation was inserted into one allele of the *SNCA* gene. After 14 days in culture, more than 90% of cells

were TUJ1+ and more than 80% were TH+ dopaminergic neurons (Fig. 18a). At this time and similarly to patient-derived cells, abundant protein aggregates were detected in the iCell A53T DOPA neurons compared to their isogenic control, and treatment with BX795 resulted in a significant reduction (number of aggregates per cell, iCell DOPA ctl:2.7±0.49, n=57, iCell A53T DOPA: 9.9 ± 1.1, n=76, iCell A53T DOPA + BX795:4.9 ±0.7, n=76; Fig. 18b,c).

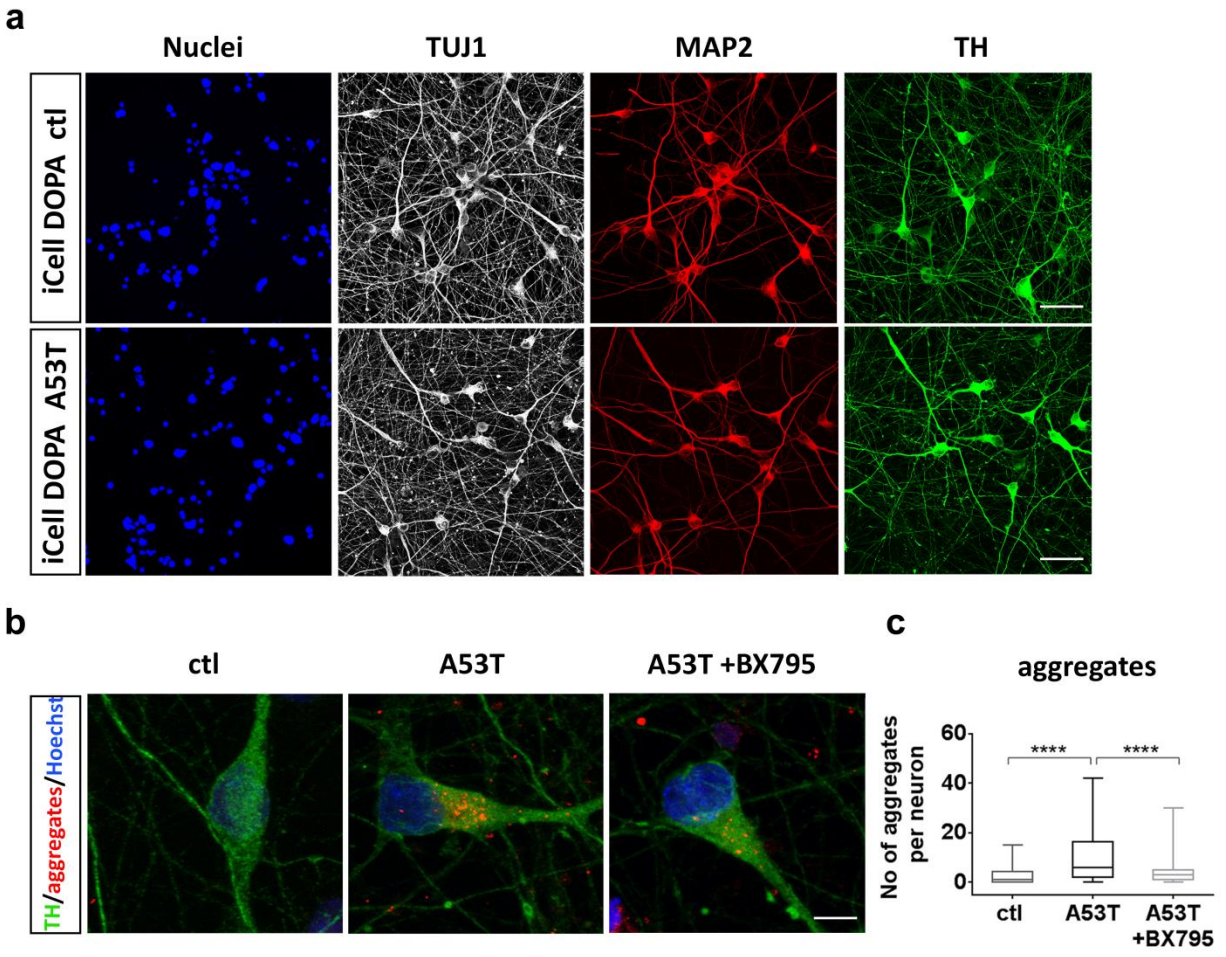


***Figure 18. BX795 reduces protein aggregates in a gene-edited p.A53T line of mature human iPSC-derived TH neurons*** ***a.*** *Representative confocal images of iCell Dopa neurons immunolabelled for Nuclei, TUJ1, MAP2 and TH. Scale bar,30 µm* ***b.*** *Representative confocal images of wild-type (ctl) and isogenic p.A53T iCellDopa neurons showing immunostaining for tyrosine hydroxylase (TH green) and protein aggregates (red). p.A53T cells were treated or not with BX795, as indicated. Scale bar, 5µm* ***c.*** *Quantification of aggregates in TH+ neurons. Data represent mean ± SEM. (Comparisons by ANOVA with Tukey correction, ****P<0.0001, n = at least 50 randomly selected TH+ cells for each condition).*

Taken together, our results from patient-derived and gene-edited neurons indicate that BX795 exerts prominent and sustainable neuroprotection in p.A53T neurons by improving neuritic growth,

limiting the levels of pathological αSyn and restricting aggregate formation whilst maintaining axonal integrity. Importanlty, the beneficial effects of BX795 were noted whether it was added early during neuronal differentiation (as in p.A53T patient-derived neurons) or at later stages of neuronal maturation (as in A53T iCell dopaminergic neurons) when disease-associated phenotypes were already established.

**5.4 Proteomics analysis identifies cellular pathways targeted by BX795 in p.A53T neurons**

Next we sought to investigate the cellular pathways affected by BX795 in neuronal cells, which is a challenging task given that these vary according to the biological system investigated [386, 387, 389]. Therefore, we decided to apply an unbiased approach based on comparative proteomics using LC-MS/MS and label-free quantification in p.A53T and control neurons (wild-type SNCA), treated or not with BX795. Similarly, to the screening procedure, BX795 was added once at DIV 7 and proteomics analysis was performed at DIV 21 when rescue of neuropathological phenotypes was noted. A total of 1652 proteins were identified and quantified using the MaxQuant software [390, 391], followed by filtering of low quality protein hits with the Perseus software. Initial comparison between p.A53T versus control neurons in the absence of BX795, revealed differential expression of 640 proteins (Fig. 19a) from which only 67 were down-regulated whilst the rest 573 were up-regulated (Fig. 19a, Table 9). This large increase in protein expression was linked by GO enrichment analysis mainly to the biological processes of transcription, translation, protein synthesis and modification (Fig. 19b).

**a**

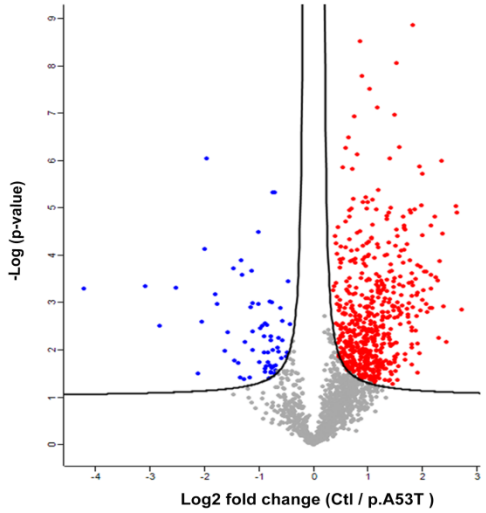
-Log (p-value)
Log2 fold change (Ctl / p.A53T )

**b**

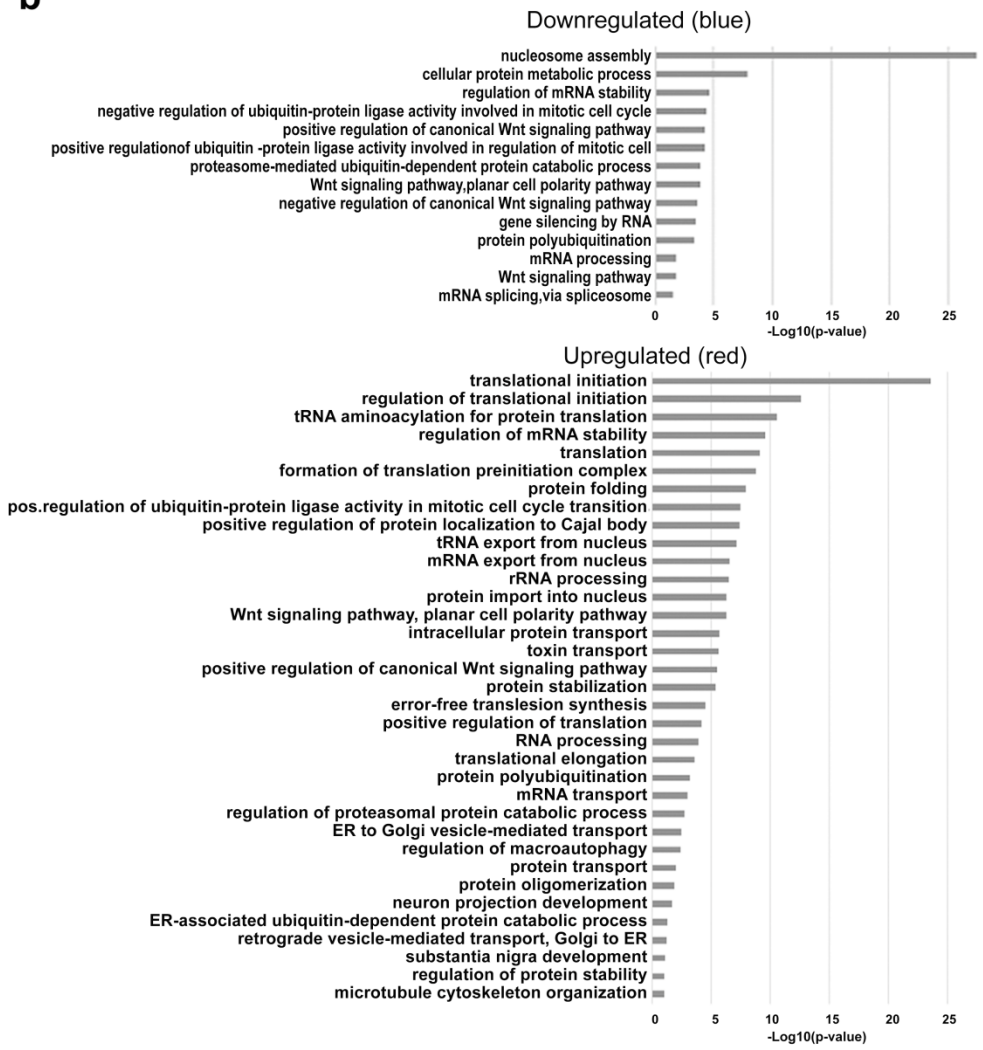
Downregulated (blue)
nucleosome assembly
cellular protein metabolic process
regulation of mRNA stability
negative regulation of ubiquitin-protein ligase activity involved in mitotic cell cycle
positive regulation of canonical Wnt signaling pathway
positive regulationof ubiquitin -protein ligase activity involved in regulation of mitotic cell
proteasome-mediated ubiquitin-dependent protein catabolic process
Wnt signaling pathway,planar cell polarity pathway
negative regulation of canonical Wnt signaling pathway
gene silencing by RNA
protein polyubiquitination
mRNA processing
Wnt signaling pathway
mRNA splicing,via spliceosome
0 5 10 15 20 25
-Log10(p-value)
Upregulated (red)
translational initiation
regulation of translational initiation
tRNA aminoacylation for protein translation
regulation of mRNA stability
translation
formation of translation preinitiation complex
protein folding
pos.regulation of ubiquitin-protein ligase activity in mitotic cell cycle transition
positive regulation of protein localization to Cajal body
tRNA export from nucleus
mRNA export from nucleus
rRNA processing
protein import into nucleus
Wnt signaling pathway, planar cell polarity pathway
intracellular protein transport
toxin transport
positive regulation of canonical Wnt signaling pathway
protein stabilization
error-free translesion synthesis
positive regulation of translation
RNA processing
translational elongation
protein polyubiquitination
mRNA transport
regulation of proteasomal protein catabolic process
ER to Golgi vesicle-mediated transport
regulation of macroautophagy
protein transport
protein oligomerization
neuron projection development
ER-associated ubiquitin-dependent protein catabolic process
retrograde vesicle-mediated transport, Golgi to ER
substantia nigra development
regulation of protein stability
microtubule cytoskeleton organization
0 5 10 15 20 25
-Log10(p-value)

***Figure 19. Identification of the biological processes that are dysregulated in p.A53T neurons**. **a.** Volcano plot of differentially expressed proteins between control and patient-derived p.A53T-neurons assessed by quantitative proteomics analysis. Each point represents the difference in expression (fold-change) between the two groups plotted against the level of statistical significance. Blue dots correspond to proteins downregulated in p.A53T neurons while red dots show proteins upregulated in p.A53T neurons (FDR=0.05, S0 = 0.1, as indicated by black lines). **b.** GO enrichment analysis for biological processes of the differentially expressed proteins was performed using DAVID software (p<0.05).*

Remarkably, the levels of a cohort of 118 proteins lying mostly within these biological processes and representing approximately 20% of the total dysregulated proteins in p.A53T neurons, were restored upon treatment with BX795 ($p<0.05$) (Fig. 20a, Table 10). Extensive data mining by GO enrichment analysis for biological processes, molecular function and cellular compartments ($p<0.01$), complemented by reactome pathway analysis ($p<0.01$), highlighted the affected core pathways in p.A53T-neurons and, amongst them, those targeted by BX795 to restore neuronal physiology (Fig. 20b).

Most important, this outcome was specific to p.A53T-neurons as BX795 had no significant effect on the proteome of control neurons (Fig. 21).

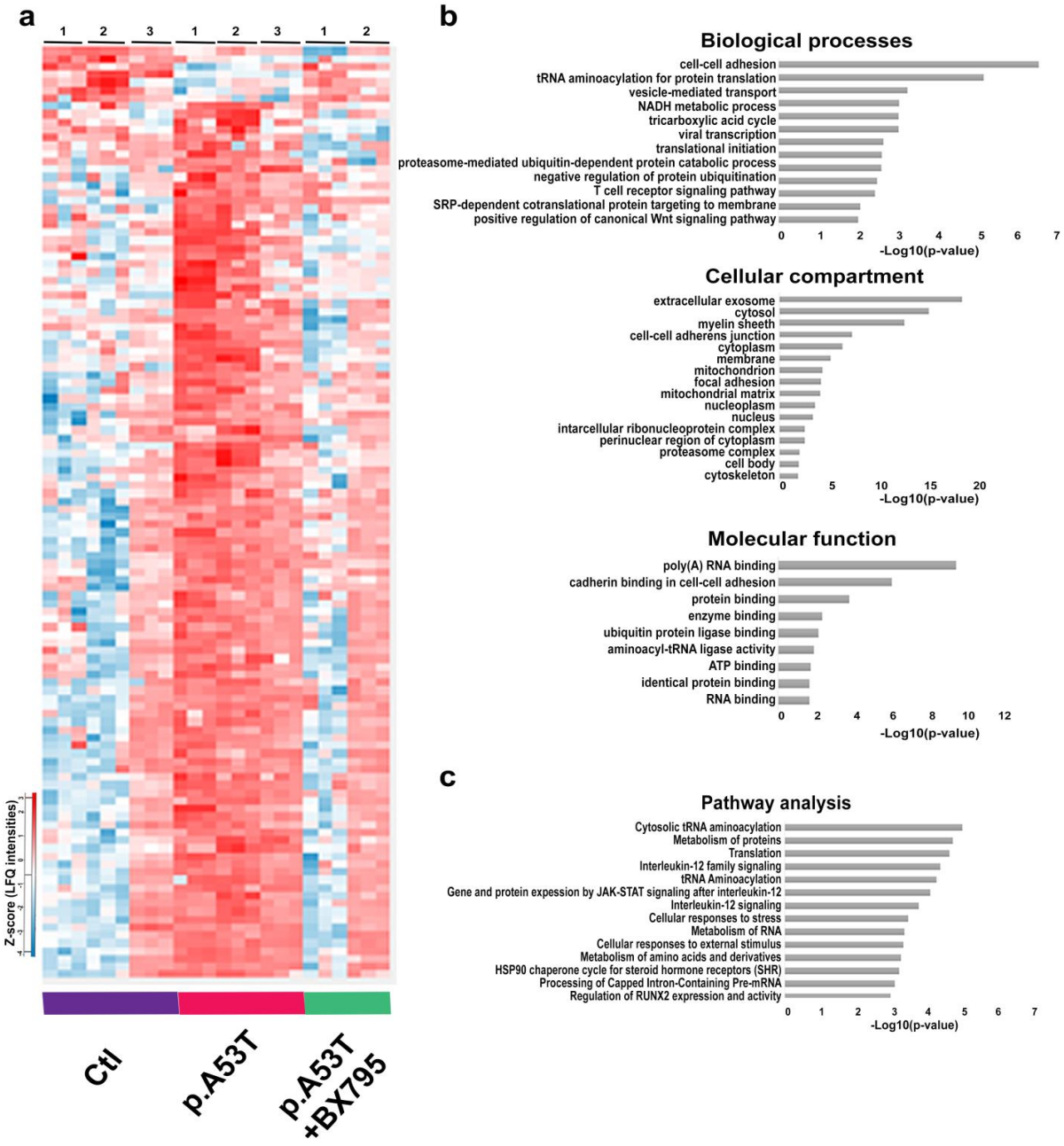


***Figure 20. Bioinformatics analysis of dysregulated proteins in p.A53T-neurons that are restored by BX795.a.*** *Hierarchical clustering of 118 upregulated proteins in patient-derived p.A53T-neurons that are restored upon treatment with BX795 (one-way ANOVA analysis). Columns in the different groups (control, p.A53T-neurons and p.A53T-neurons treated with BX795) correspond to individual samples tested and rows represent single proteins (blue, low expression; red, high expression; n=3 for control and p.A53T; n=2 for p.A53T+BX795).* ***b.*** *GO enrichment analysis for biological processes, molecular function and cellular compartments was performed using DAVID software (p<0.01).* ***c.*** *Pathway analysis using Reactome software (p<0.01).*

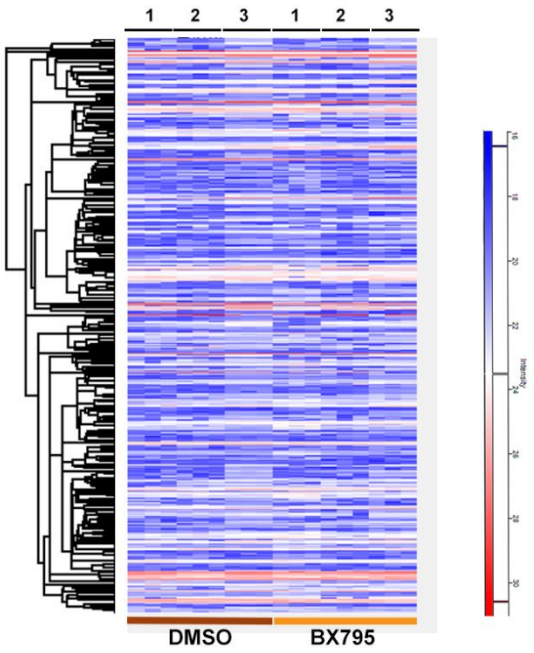


***Figure 21.Hierarchical clustering of proteins in ctl (WT) cells treated with BX795.****Hierarchical clustering shows that there is no change in the proteome of ctl-neurons upon treatment with BX795 (one-way ANOVA analysis). Columns in the different groups (control and crtl-neurons treated with BX795) correspond to individual samples tested and rows represent single proteins (blue, low expression; red, high expression; n=3).*

Extensive data mining by GO enrichment analysis for biological processes, molecular function and cellular compartments ($p < 0.01$), complemented by reactome pathway analysis ($p < 0.01$), highlighted the affected core pathways in p.A53T-neurons and, amongst them, those targeted by BX795 to restore neuronal physiology (Fig. 20c). These include proteins associated with RNA metabolism, protein synthesis, protein modification and transport, stress response, and neurodegeneration, as outlined below.

***RNA metabolism.*** The p.A53T proteome showed enrichment for proteins in subcellular compartments known to be associated with αSyn [392], including membrane bound organelles (204 proteins), mitochondria (118), ribosomal complexes (29), nucleus (292), and neuron projection/axon cytoplasm (10) (Table 11). Processes such as cellular metabolism, translational initiation and regulation, tRNA aminoacetylation and export from nucleus, mRNA stability and export from nucleus, rRNA processing, formation of pre-initiation complex and protein folding were among the top pathways

enriched in the p.A53T proteome (Fig. 19). A previous study has identified mRNA binding proteins (RBPs) and those involved in protein biosynthesis within the protein network residing in immediate vicinity of αSyn, suggesting that perturbation of these pathways may be directly related to pathology [392]. Herein, we provide evidence that these same pathways are altered when p.A53T is expressed in human neurons (Fig. 19). Specifically, a significant number of RBPs (60 proteins) were differentially expressed, including members with known neuronal localization and involvement in neuronal functions, such as ELAV-1, ELAV-3, RBBP7, RNPS1, RNMT, TARDBP, XPO1, XPO5, HNRNPA1, HNRNPA1L2, HNRNPF, HNRNPL, HNRPNPM, HRNNPUL1, PABPC1, PABPC4, PTBP2 and CELF1 (Table 9). Since even small changes in RBP expression or activity are amplified due to their broad impact on expression, splicing and translation of numerous RNA substrates, changes in such a large number of these RNA regulators suggest a severe perturbation in RNA homeostasis in p.A53T-neurons. Of these p.A53T-affected RBPs, a cluster implicated in splicing and adenylation events in the nuclear compartment was restored after BX795 treatment(Fig. 22a). These RBPs included DEK, involved in splice site selection, RBM4, a modulator of alternative 5'-splice site and exon selection, MYEF2, an mRNA stabilizer, UBTF, a critical protein in rRNA transcription, SNRPB, a component of small RNPs essential for pre-mRNA splicing, PCBP1 that binds ssDNA sequences to guide mRNA splicing and regulators of transcription, ZNF207 and HINT1. RAE1, that acts as a major mRNA export factor and attaches cytoplasmic RNPs to the cytoskeleton, and HNRNPUL1 that belongs to the hnRNP family and has been linked to ALS due to its aggregation-prone motif, were also restored by BX795.

Pre-mRNA splicing determines nucleosome organization [393], whilst nucleosomes assembled around specific splice sites regulate transcription [394]. Nucleosome assembly was the major category of proteins downregulated in p.A53T-neurons (23 proteins) including histones 1.2, 1.3, 1.4, 1.5, H2A, H2B, H3.3 and H4, nuclear pore NUP153 and nuclear organizers Lamin-B1 and Prelamin A/C (Table 12). These downregulated proteins were not affected by BX795, whereas only the upregulated HIST1H1E and NUP93 that are important for nuclear pore complex assembly and maintenance, were restored by BX795 (Table 10)

***Protein Synthesis.*** Disturbances in RBP dosage have detrimental consequences also outside the nucleus, as they control the targeted localization of mRNAs, either proximally in the cell soma or distally in the projecting axon, affecting whether an mRNA will be translated or remain translationally silent and whether it will be stored for local mRNA translation or degraded [395]. Aberrant expression of the translational machinery emerged in the p.A53T proteome with translational initiation and regulation processes being the most affected in mutant neurons (Fig. 19, Table 9). A total of 18 proteins involved in the formation of the pre-initiation complex were identified and included EIF2, 3, 4 and 5, of which EIF4G2

that functions as a general suppressor of translation by forming translationally inactive stress granules, was affected by BX795 (Fig. 22b). Ribosomal proteins (29 proteins), structural components of ribosome subunits, were upregulated in p.A53T-neurons (Table 9) and a significant fraction returned to near-control levels after BX795 treatment (Fig. 22b). These included RPL31 and RPL12, which are involved in 60S biogenesis, and RPS6, a component of the 40S subunit and downstream effector of the mTORC1 signaling pathway. tRNA processing represents another important part of the translational cascade that was altered in p.A53T-neurons (Table 9), while a significant fraction was restored by BX795, including the aminoacyl-tRNA synthetases RARS (arginyl-tRNA synthase), VARS (valyl-tRNA synthase), and WARS (tryptophanyl-tRNA synthase) together with regulatory or accessory proteins such as PPA1, EEF1D,PRMPT1, FAM98B and RTCB. Although mutations in aminoacyl-tRNA synthetases have been implicated in various recessive and dominant disorders [396] and growing evidence associates changes in tRNA gene biogenesis and processing with neurodegenerative diseases [397], our data reveal for the first time a link between p.A53T-αSyn expression and this molecular process. (Fig. 22b, Table 9).

***Protein modification and transport.*** p.A53T-αSyn toxicity has been attributed to problematic modifications at the ER membrane and disturbances in ER-Golgi and early endosomal/vesicle trafficking [310, 334, 340, 392]. In accordance, p.A53T-neurons exhibit altered protein levels in components of these pathways (Fig. 19, Table 9). Among these, five members of the adaptor protein complexes that function in transport-vesicle mediated transfer between membranous structures are increased by p.A53T-expression (AP1B1, AP2A2, AP3B1, AP3D1 and AP3M1). Another prominent category included members of the largest branch of Ras-like small GTPases involved in membrane trafficking, such as RAB2A, RAB2B and RAB6B, responsible for ER to Golgi transport; RAB18, important for early endosome formation as well as for macroautophagy, and strongly associated with neurodegeneration [398, 399]; and RAB21, regulator of integrin internalization and SNARE-mediated autophagosome-lysosome fusion [400]. Other dysregulated proteins involved in ER to Golgi trafficking included SEC22B and SEC31A whilst ARF1 and 3, two proteins required for vesicle budding/uncoating in the Golgi apparatus and required for synaptic stability of excitatory synapses [401] were also increased in p.A53T neurons. Finally, another affected process seems to be the retrograde Golgi to ER transport, as coatomer proteins COPA, COPB, COPG (Table 9) were also differentially expressed in p.A53T neurons.

BX795 had a selective effect on p.A53T-altered transport proteins like SRP9, a signal recognition particle assembly molecule that targets proteins to RER membranes, GDI2, a regulator of RABs, CKAP4, a post-translational modifier, ATP6VOD1, part of a multi-subunit acidification enzyme required for protein sorting, the DAD1 subunit of oligosaccahryl transferase complex and OGT, both functioning at the initial

steps of N-glycosylation, and NAPB, a SNAP protein with preferential expression in the brain involved in docking and fusion during ER to Golgi transfer (Fig. 22c). SAR1A, SEC22B and YKT6, all components of the SNARE complex, were also targeted by BX795 (Fig. 22c) whilst effects on molecules of the RAB, adaptor protein complex and coatomer remained largely unaffected.

***Stress Response.*** p.A53T-αSyn protein expression acts as a primary neurotoxin triggering a battery of stress responses in human neurons [402]. The proteomics analysis indicated that p.A53T neurons activate most of these mechanisms. Both the unfolded protein response (UPR), as evidenced by mis-expression of chaperones CCT2, 3, 4, 5, 7 and 8, as well as the heat shock protein response (HSP), with proteins such as DNAJA1, DNAJB11, DNAJC7, HSPA4L, HSP9 and HSPE1, were apparent in the p.A53T-proteome (Table 9). These stress response pathways were significantly downregulated in p.A53T neurons treated with BX795, which seems to target many stress response mediators (Fig. 22d). These included TCP-1, a member of the chaperonin TCP1 complex (CCT), PTPN1, a UPR regulator, STIP1, a coordinator of HSP70 and HSP90 function and the chaperone/ co-chaperone proteins DNAJB11, GCN1L1, CCT8, and DNAJA1.

Such a dysregulation of the UPR/HSP response systems in p.A53T neurons should result in the production of dangerous protein cargo and the formation of protein aggregates, as indeed identified by immunofluorescence (Fig. 16a). The p.A53T proteome also revealed alterations in protein clearance pathways with mediators of both proteasomal and autophagic systems being affected (Table 9). BX795 improved the expression of multiple ubiquitin-associated proteins suggesting partial restoration of proteasome targeting of aberrant protein products, in accordance with the decrease of protein aggregates in BX795-treated p.A53T neurons (Fig. 16). BX795 restored the expression of PSMA3, a component of the 20S core proteasome complex that is essential for removing misfolded or damaged proteins and can also act in a ubiquitin-independent manner, UCHL1, a thiol protease involved in processing of ubiquitinated proteins, OTUB1, a highly specific Ub-isopeptidase that interacts with E3 ligases to edit polyubiquitin chain growth, PSME3, a subunit of the proteasome PA28-gamma regulator activated by DNA damage, CUL1, a core component of the SKP1-CUL1-F- box E3 ligase complex, PSMD12, component of the 26S proteasome, and UBA6, an activator of ubiquitin required for E2 ligase binding. VCP, an AAA ATPase that extracts ubiquitinated proteins from large protein complexes for degradation and has been shown to co-localize with protein aggregates in various neurodegenerative diseases with proteasome inhibition, was another BX795-downregulated protein (Fig. 22d).

Components of the lysosomal pathway of autophagy targeted by BX795 included vacuole transport components such as ATG4B and proteins required for multivesicular body (MVB) biogenesis and

sorting (PDCD6IP, AP3M1 and DNM2) (Fig. 22d). Finally, BX795 also modulated oxidative stress response mechanisms, as the mitochondrial biosynthesis regulators TOMM70A and MDH2 were brought to near control levels. In addition, STOML2, a stimulator of cardiolipin biosynthesis recently shown to be associated with p.A53T neurotoxicity in human dopamine neurons was also positively targeted by BX795 [334].

When STRING analysis was used to assess the relatedness level of all 118 proteins affected by BX795, a network with strong functional linkage among the majority of these proteins was revealed (Fig. 23)

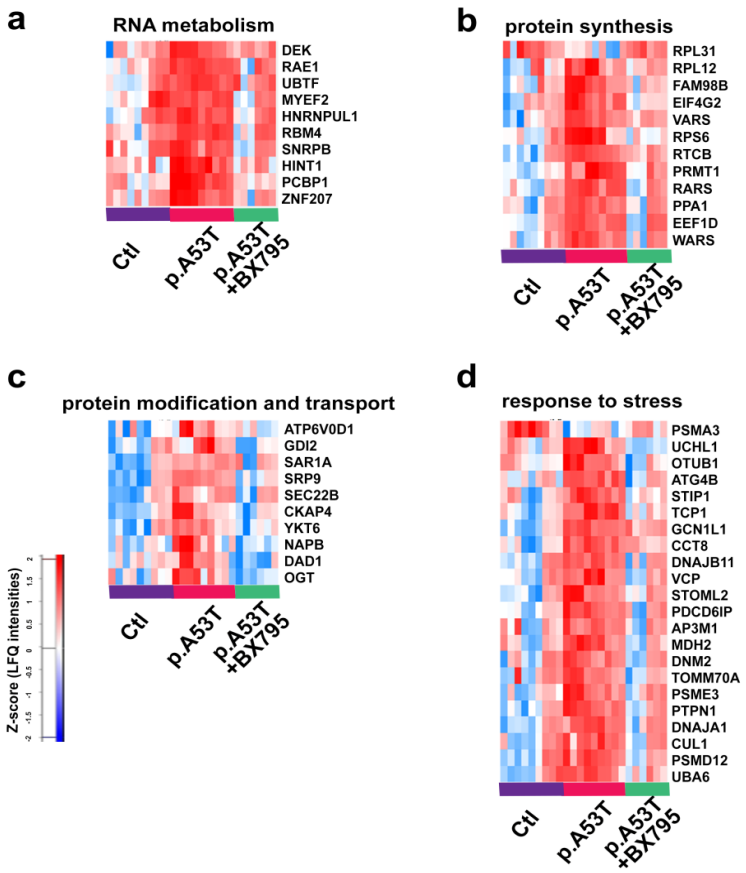


***Figure 22. Protein network of pathways and processes restored by BX795 treatment.*** *Heatmaps illustrating specific proteins upregulated in p.A53T-neurons that are involved* ***a.*** *in RNA metabolism,* ***b****. in protein synthesis,* ***c****. in protein modification and* ***d.*** *in transport and response to stress, which are restored after BX795 treatment. High expression is in red and low expression is in blue.*

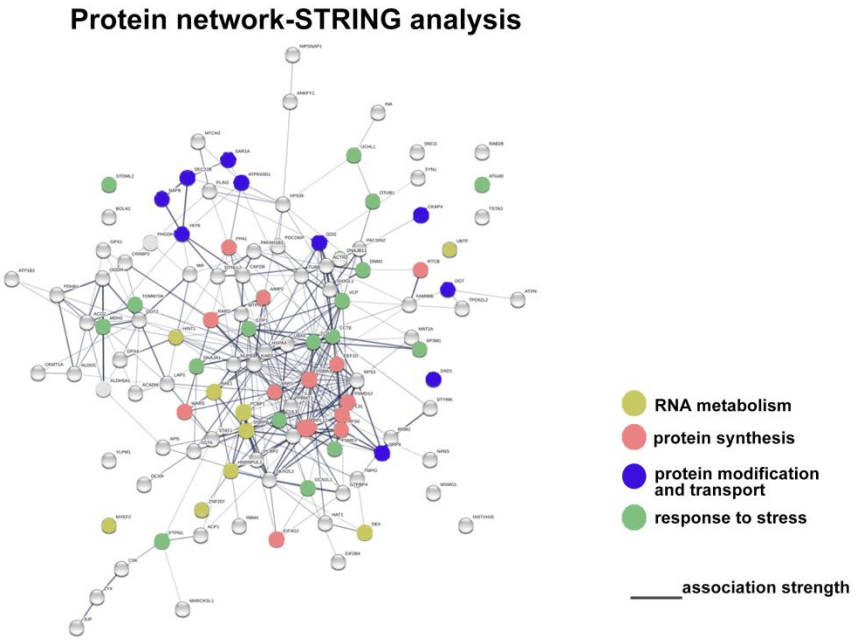


***Figure 23. STRING-analysis representation of the protein-protein interaction network of the 118 upregulated proteins in p.A53T-neurons that are restored by BX795.*** *Each circular node depicts one protein and the different colors represent the different pathways/processes as indicated. Connecting lines represent protein-protein associations and line intensity represents the confidence score of a functional association.*

***Proteins associated with neurodegeneration.*** An important measure of the biological significance of the proteomic profile of p.A53T neurons comes from comparisons with human genetic studies. Enrichment analysis for PD and other neurodegenerative diseases identified several proteins comprising both known and novel converging targets that were modified by BX795 (Fig. 24a). Among those, UCHL1/PARK5 is linked to lower susceptibility for PD, while a point mutation co-segregating with the disease has been identified in one family [403] and VPS35/PARK17-D620N mutated protein causes late-onset autosomal dominant PD [404]. FAM98B has been linked to SMA and ALS [405], VCP mutations can cause FTD, ALS and Charcot-Marie-Tooth diseases [406, 407], HINT1 autosomal recessive mutations lead to neuromytotonia and axonal neuropathy [408], PAFAHB1 mutations and gene deletions lead to lissencephaly syndrome [409] and RBM4 is linked to Down's syndrome [410] (Fig. 24a, b). STRING analysis of the BX795-modified protein network to which αSyn was also incorporated, demonstrated a strong association between αSyn and other neurodegeneration-linked proteins (Fig. 24c).

These findings collectively deepen our understanding of p.A53T-mediated neurotoxicity and reveal key biological processes that are targeted by BX795 to alleviate p.A53T-αSyn-related phenotypes in human neurons.

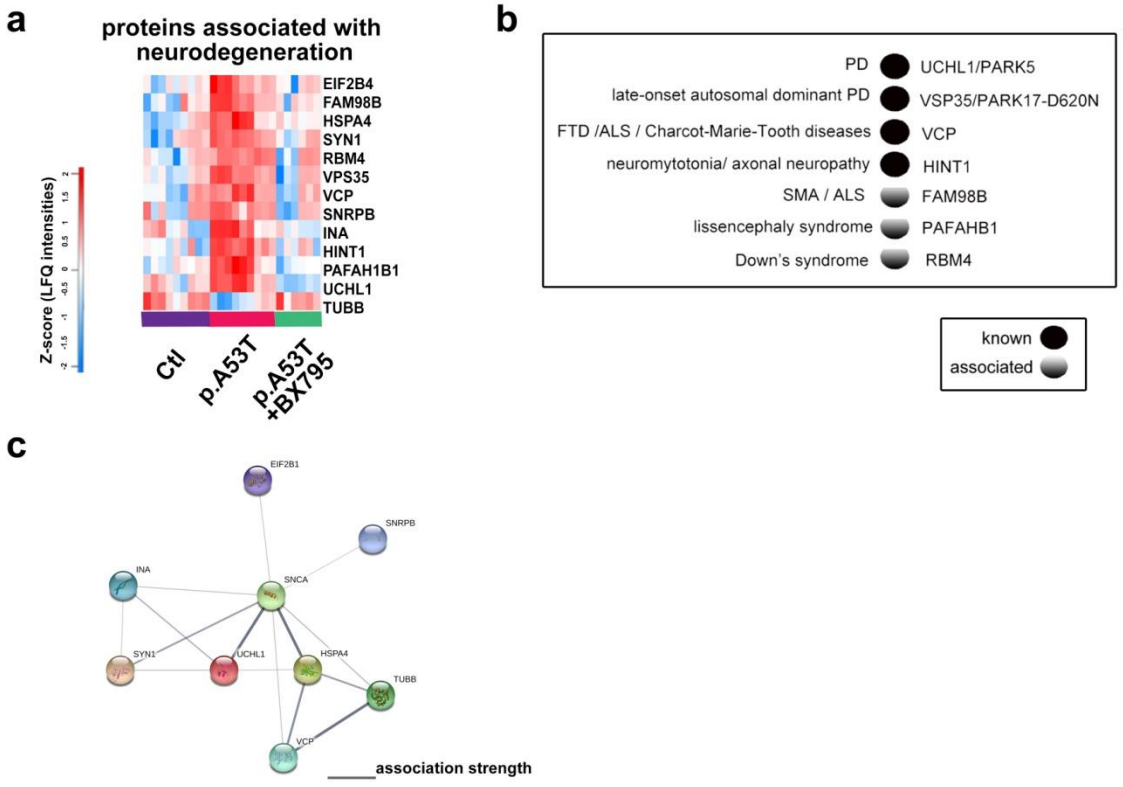


***Figure 24. Restoration of disease-associated proteins by BX795 in p.A53T-neurons. a.*** *Heatmap of proteins associated with neurodegeneration that are restored after BX795 treatment. High expression is in red and low expression is in blue.* ***b.*** *Disease-associated proteins that are modified by BX795 are either known or associated genetic risk factors for neurodegenerative diseases as revealed by human genetic studies.* ***c.*** *STRING network analysis of the neurodegeneration-associated proteins restored by BX795 in p.A53T-neurons and their interaction with αSyn. Each αSyn interactor is shown as a colored circle and connecting lines between proteins represent protein-protein associations. The intensity of lines represents the confidence score of a functional association.*

**5.5 BX795 affects the mTORC1 signaling pathway to attenuate protein synthesis and facilitate autophagic flux in p.A53T neurons**

The p.A53T proteome clearly indicates aberrant mRNA translation and protein clearance mechanisms, both linked to mammalian aging and neurodegenerative diseases that can be effectively restored by BX795. The mammalian target of rapamycin (mTOR) signaling pathway is a central regulator of proteostasis and the p.A53T proteome clearly indicates hyperfunctional overactive biosynthetic processes that could be associated with alterations in mTORC1 activation. Components of this signaling cascade have emerged in the proteomics analysis of p.A53T-neurons, including RPS6, a major downstream effector of mTORC1, together with several RAG GTPases like IQGAP1, required for efficient activation of mTORC1, which were largely restored after BX795 treatment (Table 3). To validate the activation of the mTORC1 pathway in p.A53T patient-derived neurons, we examined the levels of phosphorylated RPS6 (pRPS6), which is commonly used as a readout of mTOR signaling. Indeed, we observed significantly higher levels of pRPS6 in p.A53T neurons as compared to control that were efficiently downregulated upon BX795 treatment (Fig. 25a,b).

To confirm that the p.A53T mutation is causally related to dysregulation of protein metabolism and verify that BX795 can restore this effect in mature human neurons, we exploited the isogenic system of iCell DopaNeurons where we measured the levels of the activated form of RPS6, (phospho-RPS6; pRPS6), and the total protein synthesis rate. The presence of the p.A53T mutation led to a significant increase in the levels of pRPS6 (Fig. 25c,d) that correlated with a significant increase of global protein synthesis in iCell Dopa p.A53T neurons (Fig. 25c, d). BX795 could lower significantly the levels of pRPS6 and reverse the aberrantly increased protein synthesis rate (Fig. 25c, d). This data suggests that BX795 targets and restores dysregulated mRNA translation and protein synthesis pathways instigated by the p.A53T mutation in neuronal cells.

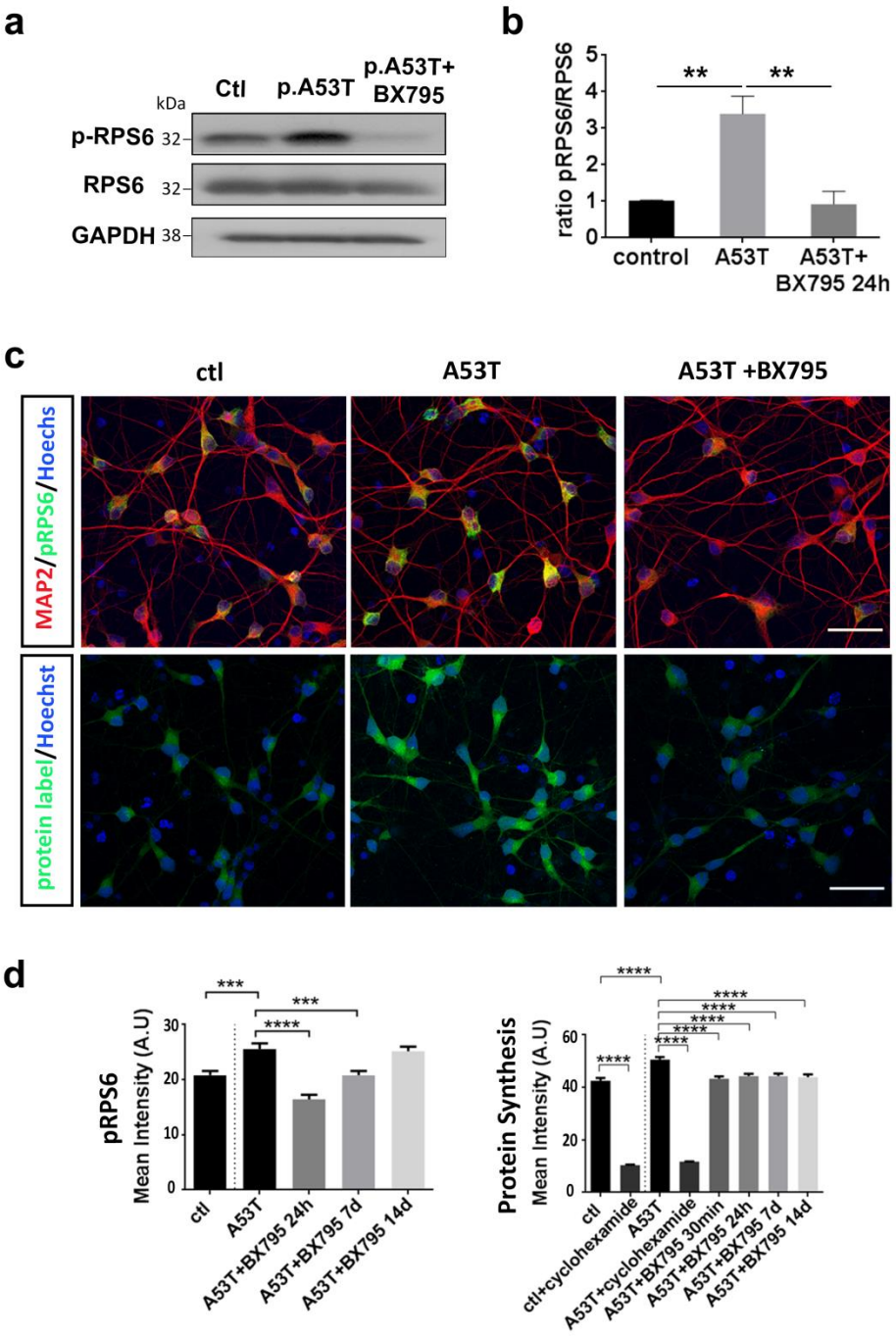


***Figure 25. BX795 affects the mTORC1 signaling pathway to attenuate protein synthesis a.*** *Western blot showing an acute reduction in the increased levels of p-RPS6 in p.A53T neurons, in the presence of BX795. Actin shows equal protein loading.* ***b.*** *Quantification of p-RPS6 levels in iPS-derived neurons. Data represent mean ± SEM. (Comparisons by ANOVA with Bonferroni's multiple comparisons test. **P<0.01,n=3 independent experiments.* ***c.****Representative confocal images of control (ctl) and isogenic gene-edited p.A53T iCellDopa neurons, either non-treated or treated*

*with BX795. Cells were immunolabeled for phosphorylated RPS6 (green) andmicrotubule associated protein 2 (MAP2; red)(upper panel) and labeled for total protein synthesis (protein label, green)(lower panel). Nuclei are seen with Hoechst dye (blue). Scale bar, 30μm* ***d.*** *BX795 reduces phosphorylated RPS6 levels and reduces total protein synthesis in p.A53T-neurons. Quantification of fluorescence intensity in control, untreated p.A53T or BX795-treated p.A53T neurons. Data represent mean ± SEM (Comparisons by ANOVA with Tukey correction, ***P< 0.001 ****P<0.0001, n = 100 randomly selected cells for each condition).*

To examine further the effect of the p.A53T mutation on mTORC1 activity and protein synthesis, we created stably transduced SH-SY5Y neuroblastoma cells co-expressing the human p.A53T-αSyn and the fluorescent protein DsRed or DsRed only as a control (Fig. 26a). Upon neuronal differentiation, SH-SY5Y cells expressing the human p.A53T-αSyn displayed a prominent upregulation in the levels of phosphorylated mTOR and pRPS6 as compared to control cells (Fig. 26b), whilst BX795 had an acute effect in downregulating their levels (Fig. 26c), as determined by Western blot analysis.

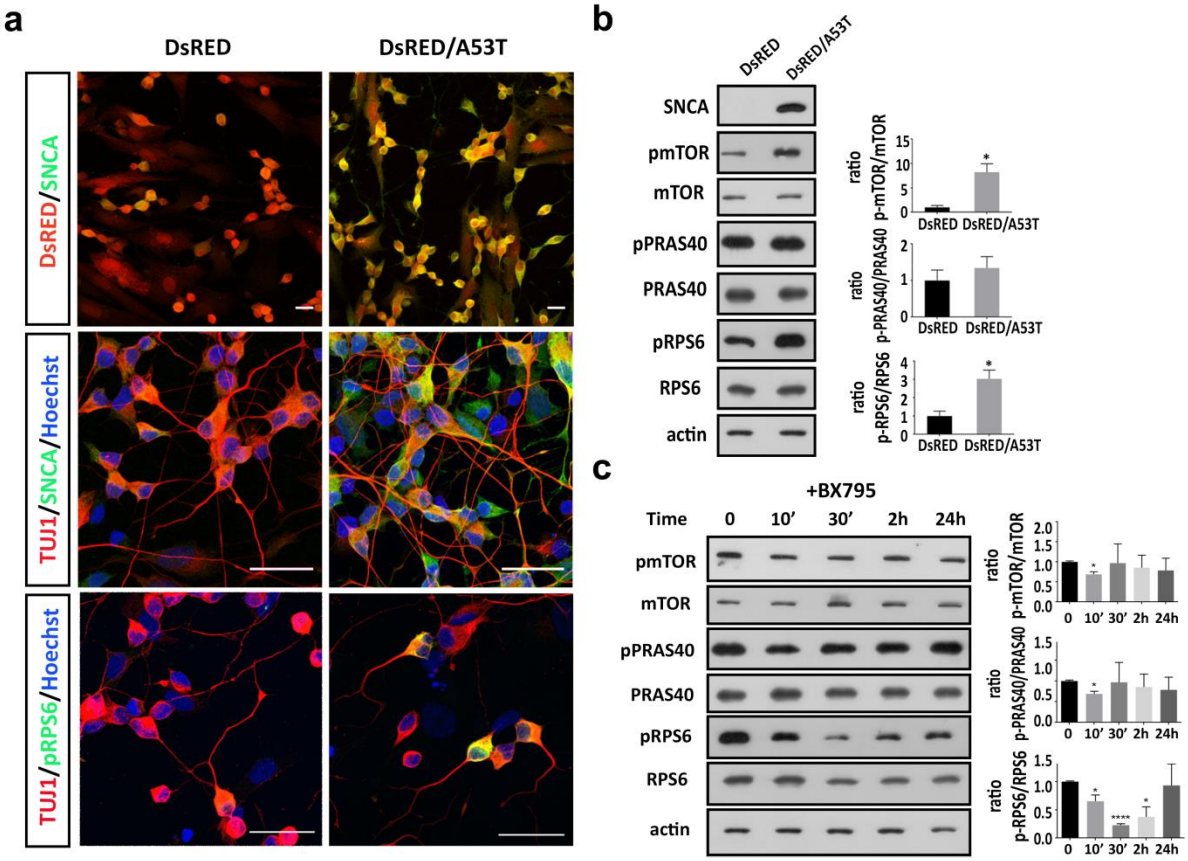


***Figure 26. BX795 affects the mTORC1 signaling pathway in SH-SY5Y cells over expressing p.A53T.a.*** *Representative images of SH-SY5Y cells stably transduced to express DsRed only or DsRed and human pA53T-αSyn. After neuronal*

*differentiation, cells were immunolabled for αSyn (SNCA), TUJ1 and pRPS6.* ***b.*** *Western blot showing that the presence of mutant SNCA in differentiated p.A53T-transduced SH-SY5Y cells, results in an increase in the levels p-mTOR and p-RPS6. Actin shows equal protein loading. Data represent mean ± SEM (t-test, *P<0.05, n=3 independent experiments).****c.*** *Western blot showing an acute reduction in the levels of p-mTOR and p-RPS6 in the above stably transduced and differentiated SH-SY5Y cells, in the presence of BX795. Actin shows equal protein loading. Data represent mean ± SEM (Comparisons by ANOVA with Tukey correction, *P<0.05, ****P<0.0001, n=3 independent experiments).*

Biochemical and genetic studies have identified the upstream p70 S6 kinase as the main *in vivo* kinase responsible for RPS6 phosphorylation [411]. Since a most prominent observation in all p.A53T-bearing cells tested in our study was an up-regulation of pRPS6 and its downregulation by BX795, we asked if the compound could inhibit the activity of p70 S6 kinase. To this end, we assessed the kinase activity of purified recombinant p70 S6K in the absence and presence of BX795 and found a notable dose-dependent inhibitory effect (Fig. 27a), indicating that BX795 may restore pRPS6 levels and protein synthesis by directly targeting p70 S6K. Finally, we checked if MHY-1485, a synthetic mTOR activator, could counteract the beneficial effects of BX795 in p.A53T cells. Consistently, we could not see a reduction in pathological p129S-αSyn levels in SH-SY5Y cells or a decrease in neuronal aggregates in p.A53T iPSC-derived neurons upon co-treatment with MHY-1485 and BX795 (Fig. 27e, f).

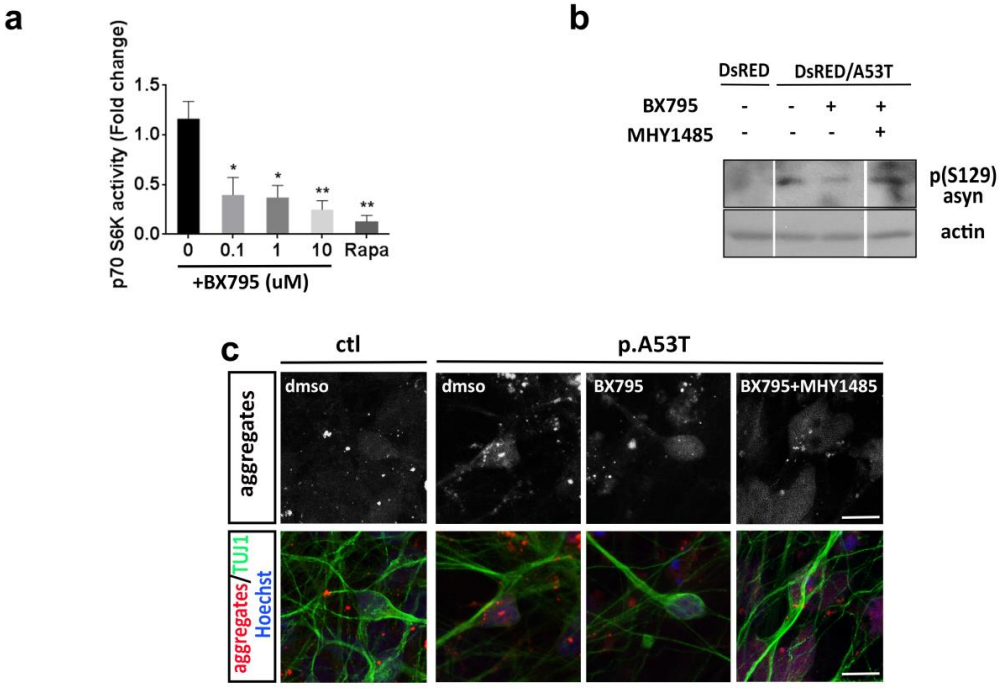


***Figure 27. BX795 affects the mTORC1 signaling pathway to attenuate neuroprotection.*** ***a.*** *Effect of BX795 on p70 S6K activity. p70 S6k activity was measured by using a S6 assay kit according to the manufacturer's instructions. The data were presented as relative p70S6k activity of the means. Data represent mean ± SEM (Comparisons by ANOVA with Tukey correction, *P<0.05, **P<0.01, n=3).****b*** *Western blot*

*showing the effect of BX795 treatment alone and in combination with mTOR activator MHY-1485 on the p-SNCA levels in SH-SY5Y cells.* ***c.*** *Representative confocal images show protein aggregates in control (ctl) and p.A53T neurons, either non-treated or treated with BX795 alone or in combination with mTOR activator MHY-1485. Scale bar, 10µm.*

mTORC1 also controls autophagy, the major degradation pathway essential for removing aggregation-prone αSyn [253, 412]. To test if BX795 could also affect this clearance pathway, we utilized a previously established inducible SH-SY5Y cell line that expresses the human p.A53T-αSyn upon withdrawal of Doxycycline (-Dox). In this model, expression of mutant p.A53T has been shown to cause perturbation of the autophagy lysosomal pathway resulting in increased steady-state levels of LC3II and p62 ([377]; Fig. 28a, b). p62 is a receptor for ubiquitinated cargo destined to be degraded by autophagy and is associated with LC3-II, the processed form of LC3, within autophagosomes and autolysosomes [413, 414]. To visualize LC3-II and quantify GFP-LC3-II+ puncta comprising brightly fluorescent autophagosomes and more weakly labeled autolysosomes (Fig. 28a), we transfected the inducible SH-SY5Y line with a fusion construct containing the green fluorescent protein tagged to LC3 (GFP-LC3) [415]. In agreement with the Western blot data, GFP-LC3-II+ puncta were scarce in p.A53T cells treated with DMSO while in the presence of BX795 there was a small, yet not significant increase (Fig. 28c, d). As expected, when DMSO-treated cells were exposed to bafilomycin, a blocker of autophagosome-lysosome fusion that prevents lysosome-mediated protein degradation, GFP-LC3-II+ puncta increased significantly (Fig. 28c, d)., Addition of both bafilomycin and BX795 further increased the number and brightness of GFP-LC3-II+ puncta, suggesting that BX795 acts as an autophagy inducer (Fig. 28c, d).

To distinguish labeled autophagosomes from autolysosomes and monitor the autophagic flux, we used a dual fluorophore probe consisting of a tandem fluorescent mCherry-GFP-p62 construct [416]. GFP fluorescence is sensitive to low-pH and labels only neutral-pH autophagosomes, while mCherry retains fluorescence in both autophagosomes and low-pH autolysosomes [414] (Fig. 28e). Calculation of the ratio of GFP+/mCherry+ puncta presents a measure of the autophagic flux, and a reduction in this ratio mirrors an increase in the progress of autophagy. Indeed, quantification of green and red puncta revealed a significantly lower GFP/mCherry ratio in the presence of BX795 as compared to DMSO-treated cells, indicating that BX795 facilitates the autophagic flux (Fig. 28f, g). In agreement, a decrease in the total levels of p62 was noted upon treatment with BX95 (Fig. 28h).

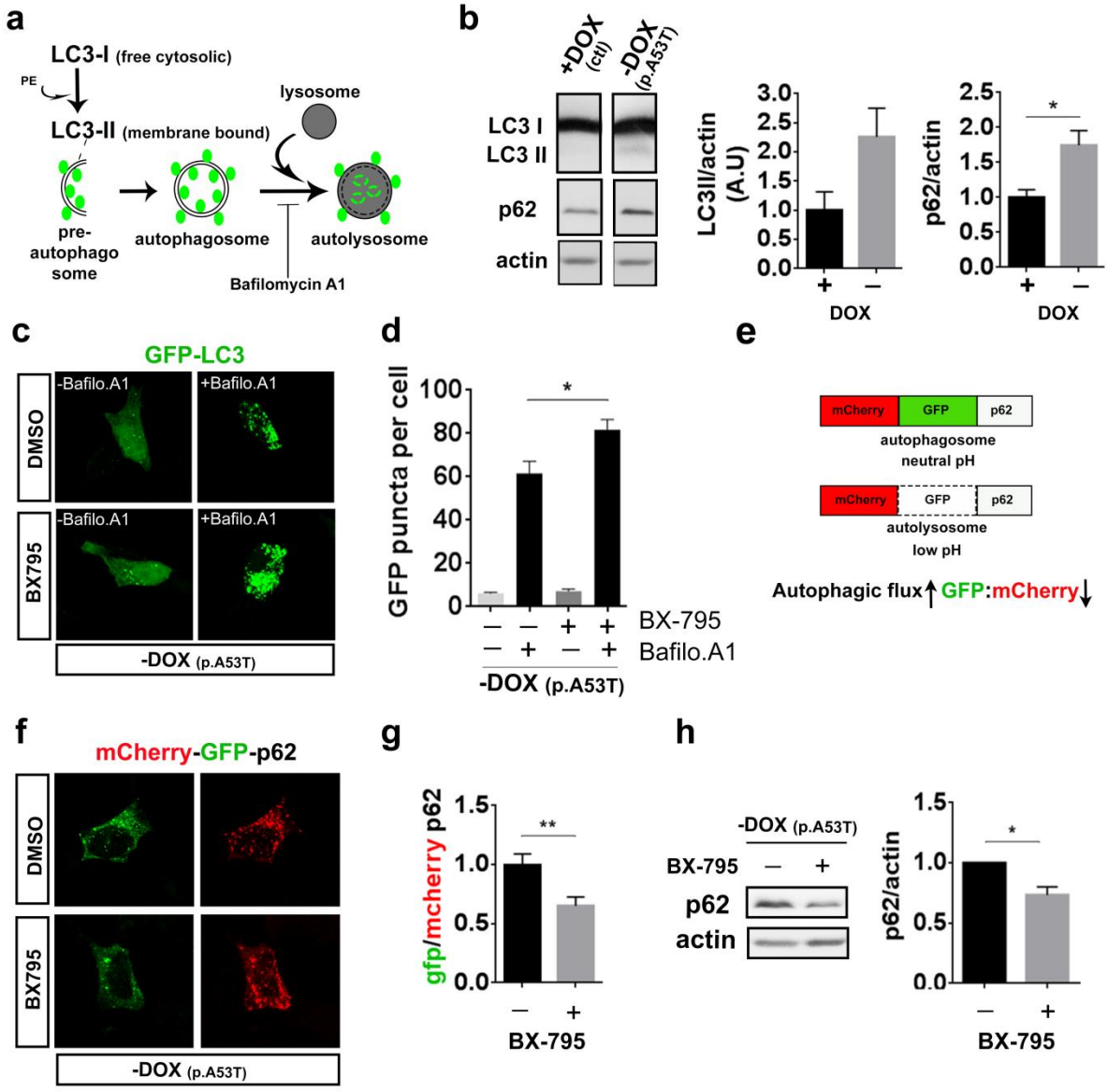


***Figure 28. BX795 facilitates autophagy in an inducible SH-SY5Y cell line expressing human p.A53T-αSyn a.*** *Schema illustrating that cytosolic LC3 is cleaved to yield LC3-I, which is subsequently conjugated to phosphatidylethanolamine (PE) to form membrane-bound LC3-II (green circles). Pre-autophagosomal structures engulfing protein cargo and organelles destined for degradation close to form double membrane spherical autophagosomes. These fuse with lysosomes to yield autolysosomes and their contents are degraded. Bafilomycin blocks autophagic flux by inhibiting autophagosome-lysosome fusion, which results in accumulation of LC3-II+ autophagosomes.* ***b.*** *Representative immunoblot showing steady-state levels of LC3-II and p62 in lysates of inducible SH-SY5Y cells expressing the human p.A53T-αSyn (-Dox) and quantification relative to actin. Data represent mean ± SEM, t-test, *P<0.05, n=3 independent experiments.* ***c.*** *Representative confocal images of individual p.A53T SH-SY5Y cells (-Dox) transfected with GFP-LC3*

*that were treated or not with bafilomycin A1 in the absence or presence of BX795.* ***d.*** *Quantification of GFP-LC3 puncta per cell. Comparisons by ANOVA with Tukey correction. *P < 0.05, n=72 cells (control DMSO), n=79 cells (BX795), n=67 cells (Bafilomycin A1), n=68 cells BX795+Bafilomycin A1. Data are representative of three independent experiments).* ***e.*** *Assessment of autophagic flux using mCherry-GFP-LC3 color change between autophagosomes and autolysosomes. Autophagic flux is induced when the GFP:mCherry ratio is reduced.* ***f, g****. Representative confocal images of individual cells [inducible SH-SY5Y cell line expressing p.A53T-αSyn (-Dox)] transfected with GFP-mCherry-p62 that were treated with DMSO (control) or BX795 and quantification of the ratio of GFP+/mCherry+ puncta (t-test,n= 60 (control DMSO), n=53 (BX795) **P < 0.01 Data are representative of three independent experiments).* ***h.*** *Representative immunoblot showing steady-state levels of p62 in cells [inducible SH-SY5Y cell line expressing p.A53T-αSyn (-Dox)] treated or not with BX795, and quantification relative to actin. Data represent mean ± SEM, t-test, n=3 independent experiments.*

Last, we examined if BX795 had a similar effect in facilitating autophagic flux in p.A53T patient-derived neurons. Electron microscopy observations have revealed that these cells have prominent autophagosomes exemplified by multi-lamellar vesicular bodies either empty (vacuoles) or encompassing mitochondrial or other organelles (Fig. 29a). Such structures were never detected in control cells from healthy donor (Fig. 29). These findings are consistent with an accumulation of autophagosomes resulting from stalled autophagic flux in p.A53T cells. To assess the effect of BX795, we used the Cyto-ID® autophagy detection kit that monitors autophagosomes and autophagic flux in lysosomally inhibited cells. As expected, p.A53T neurons showed an accumulation of autophagosomes that were effectively decreased upon BX795 treatment (Fig. 29b), indicative of restoration of autophagic flux.

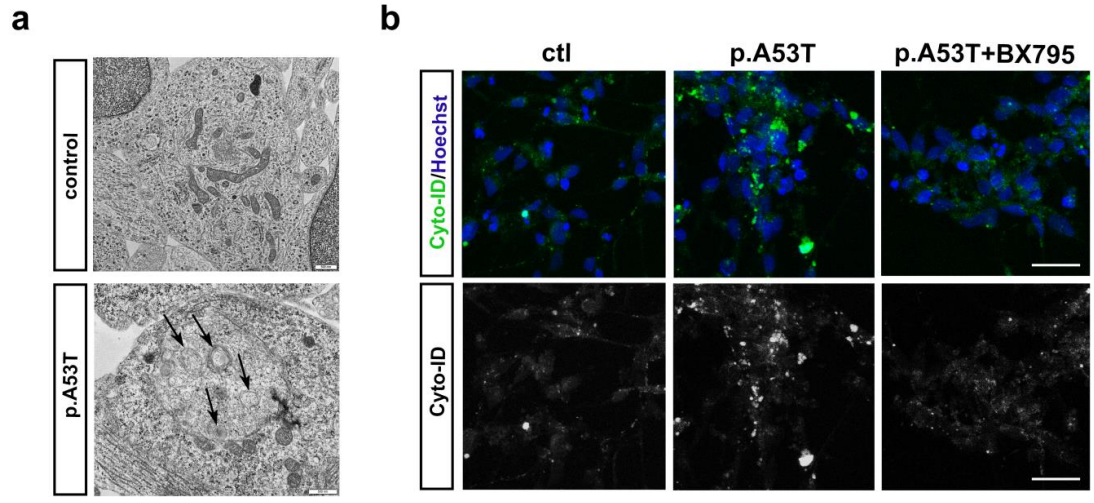


***Figure 29. BX795 facilitates autophagy in human p.A53T-neurons a.*** *Representative electron microscopy images depicting autophagosomes in p.A53T neurons. Scale bar 500nm.* ***b.*** *Representative confocal images show*

*autophagosome accumulation in control (ctl) and p.A53T neurons, either non-treated or treated with BX795. Scale bar, 30µm.*

Overall, our results indicate that disease-associated characteristics can be recapitulated in patient-derived p.A53T-neurons, including axonal degeneration and accumulation of protein inclusions resembling Lewy bodies and neurites. Moreover, the p.A53T proteome examined here revealed a profound increase in proteins related to the biological processes of RNA metabolism, protein synthesis, modification and transport, protein clearance and stress response, suggesting that the mechanisms for maintaining protein homeostasis are affected in p.A53T cells. Notably, we demonstrated that the p.A53T iPSC-based system we have established can be adapted for compound screening using automated high-content imaging in combination with small molecule chemical libraries. In this fashion we have identified a hit compound, BX795, with potent and sustainable neuroprotective properties, such that it restores pathological phenotypes in p.A53T neurons irrespective of patient genetic background. Mechanistically, BX795 can restore a cohort of 118 dysregulated proteins specifically in p.A53T-neurons which are associated with key cellular processes of proteostasis, elucidating the potential therapeutic significance of this molecule in p.A53T pathology and related disorders.

**List of Tables**

***Table 8.*** *Kinase Inhibitor Library (Selleck Chemicals) and targets.*

| **Item Name** | **Target** |
|---|---|
| Linifanib (ABT-869) | PDGFR, VEGFR |
| Axitinib | VEGFR, PDGFR, c-Kit |
| Saracatinib (AZD0530) | Src, Bcr-Abl |
| AZD6244 (Selumetinib) | MEK |
| BEZ235 (NVP-BEZ235) | mTOR, PI3K |
| BIBF1120 (Vargatef) | VEGFR, PDGFR, FGFR |
| Afatinib (BIBW2992) | EGFR, HER2 |
| Bosutinib (SKI-606) | Src |
| Cediranib (AZD2171) | VEGFR, Flt |
| CI-1033 (Canertinib) | EGFR, HER2 |
| CI-1040 (PD184352) | MEK |
| Dasatinib (BMS-354825) | Src, Bcr-Abl, c-Kit |
| Deforolimus (Ridaforolimus) | mTOR |
| Gefitinib (Iressa) | EGFR |
| Imatinib Mesylate | PDGFR, c-Kit, Bcr-Abl |
| Lapatinib Ditosylate (Tykerb) | EGFR, HER2 |
| Motesanib Diphosphate | VEGFR, PDGFR, c-Kit |
| Nilotinib (AMN-107) | Bcr-Abl |
| Pazopanib HCl | VEGFR, PDGFR, c-Kit |
| PD0325901 | MEK |

| | |
|---|---|
| PI-103 | DNA-PK, PI3K, mTOR |
| Rapamycin (Sirolimus) | mTOR |
| Sorafenib (Nexavar) | VEGFR, PDGFR, Raf |
| Sunitinib Malate (Sutent) | VEGFR, PDGFR, c-Kit, Flt |
| Tandutinib (MLN518) | Flt |
| Temsirolimus (Torisel) | mTOR |
| Vandetanib (Zactima) | VEGFR |
| VX-680 (MK-0457, Tozasertib) | Aurora Kinase |
| Enzastaurin (LY317615) | PKC |
| BMS-599626 (AC480) | EGFR, HER2 |
| Masitinib (AB1010) | c-Kit, PDGFR, FGFR, FAK |
| GDC-0941 | PI3K |
| SB 431542 | TGF-beta/Smad |
| Crizotinib (PF-02341066) | c-Met, ALK |
| ZSTK474 | PI3K |
| SB 216763 | GSK-3 |
| SB 203580 | p38 MAPK |
| SB 202190 | p38 MAPK |
| MK-2206 dihydrochloride | Akt |
| PD153035 HCl | EGFR |
| SU11274 | c-Met |
| NVP-ADW742 | IGF-1R |

| | |
|---|---|
| KU-55933 | ATM |
| PF-04217903 | c-Met |
| U0126-EtOH | MEK |
| ZM-447439 | Aurora Kinase |
| GDC-0879 | Raf |
| LY294002 | PI3K |
| Danusertib (PHA-739358) | Aurora Kinase, FGFR, Bcr-Abl, c-RET, Src |
| TAE684 (NVP-TAE684) | ALK |
| BI 2536 | PLK |
| Foretinib (GSK1363089, XL880) | c-Met, VEGFR |
| SGX-523 | c-Met |
| JNJ-38877605 | c-Met |
| PD 0332991 (Palbociclib) HCl | CDK |
| XL147 | PI3K |
| Everolimus (RAD001) | mTOR |
| MLN8237 (Alisertib) | Aurora Kinase |
| AT9283 | Bcr-Abl, JAK, Aurora Kinase |
| AG-490 | JAK, EGFR |
| SNS-032 (BMS-387032) | CDK |
| Barasertib (AZD1152-HQPA) | Aurora Kinase |
| PLX-4720 | Raf |
| SNS-314 | Aurora Kinase |

| | |
|---|---|
| CP-724714 | EGFR, HER2 |
| TGX-221 | PI3K |
| WZ3146 | EGFR |
| CYC116 | Aurora Kinase, VEGFR |
| WZ4002 | EGFR |
| PD98059 | MEK |
| Regorafenib (BAY 73-4506) | c-Kit, Raf, VEGFR |
| WZ8040 | EGFR |
| ENMD-2076 | Flt, Aurora Kinase, VEGFR |
| PIK-90 | PI3K |
| Tivozanib (AV-951) | VEGFR, c-Kit, PDGFR |
| OSI-930 | c-Kit, VEGFR |
| Ku-0063794 | mTOR |
| Amuvatinib (MP-470) | c-Met, c-Kit, PDGFR, Flt, c-RET |
| JNJ-7706621 | CDK, Aurora Kinase |
| WYE-354 | mTOR |
| IC-87114 | Others |
| TG100-115 | PI3K |
| GSK1059615 | PI3K, mTOR |
| MGCD-265 | c-Met, VEGFR, Tie-2 |
| Rigosertib (ON-01910) | PLK |
| Ki8751 | VEGFR, c-Kit, PDGFR |

| | |
|---|---|
| Pelitinib (EKB-569) | EGFR |
| AS-605240 | PI3K |
| Aurora A Inhibitor I | Aurora Kinase |
| PHA-680632 | Aurora Kinase |
| SP600125 | JNK |
| TSU-68 | VEGFR, PDGFR, FGFR |
| AS703026 | MEK |
| SB 525334 | TGF-beta/Smad |
| HMN-214 | PLK |
| AEE788 (NVP-AEE788) | EGFR, Flt, VEGFR, HER2 |
| PHA-793887 | CDK |
| PIK-93 | PI3K, VEGFR |
| Ponatinib (AP24534) | Bcr-Abl, VEGFR, FGFR, PDGFR, Flt |
| LY2228820 | p38 MAPK |
| CCT129202 | Aurora Kinase |
| XL765 | PI3K, mTOR |
| AT7519 | CDK |
| Quizartinib (AC220) | Flt |
| Hesperadin | Aurora Kinase |
| BIX 02188 | MEK |
| BIX 02189 | MEK |
| AZD7762 | Chk |

| | |
|---|---|
| R406(free base) | Syk |
| AZD8055 | mTOR |
| KRN 633 | VEGFR, PDGFR |
| AT7867 | Akt, S6 kinase |
| BMS 777607 | c-Met |
| PD318088 | MEK |
| KU-60019 | ATM |
| BS-181 HCl | CDK |
| BIRB 796 (Doramapimod) | p38 MAPK |
| NVP-BSK805 | JAK |
| DCC-2036 (Rebastinib) | Bcr-Abl |
| AZD8330 | MEK |
| Neratinib (HKI-272) | HER2, EGFR |
| KW 2449 | Flt, Bcr-Abl, Aurora Kinase |
| LY2784544 | JAK |
| AZD8931 | EGFR, HER2 |
| GSK461364 | PLK |
| R406 | Syk, Flt |
| Raf265 derivative | VEGFR, Raf |
| BMS 794833 | c-Met, VEGFR |
| NVP-BHG712 | VEGFR, Src, Raf, Bcr-Abl |
| OSI-420 (Desmethyl Erlotinib) | EGFR |

| | |
|---|---|
| PIK-293 | PI3K |
| AZ 960 | JAK |
| Mubritinib (TAK 165) | HER2 |
| PP242 | mTOR |
| Cyt387 | JAK |
| Indirubin | GSK-3 |
| Quercetin (Sophoretin) | PI3K, PKC, Src, Sirtuin |
| Imatinib (Gleevec) | |
| GSK2126458 | PI3K, mTOR |
| VX-702 | p38 MAPK |
| CAL-101 (GS-1101) | PI3K |
| BI6727 (Volasertib) | PLK |
| PIK-294 | PI3K |
| Telatinib (BAY 57-9352) | VEGFR, PDGFR, c-Kit |
| AZD5438 | CDK |
| OSI-027 | mTOR |
| PP-121 | DNA-PK, mTOR, PDGF |
| WP1130 | DUB, Bcr-Abl |
| BKM120 (NVP-BKM120) | PI3K |
| cx-4945 (Silmitasertib) | PKC |
| LDN193189 | TGF-beta/Smad |
| PF-05212384 (PKI-587) | mTOR, PI3K |

| | |
|---|---|
| TAK-733 | MEK |
| CCT128930 | Akt |
| A66 | PI3K |
| A-674563 | Akt, CDK, PKA |
| AS-252424 | PI3K |
| AS-604850 | PI3K |
| PF-00562271 | FAK |
| WAY-600 | mTOR |
| WYE-125132 | mTOR |
| WYE-687 | mTOR |
| Apatinib (YN968D1) | VEGFR |
| LY2603618 (IC-83) | Chk |
| GSK1120212 (Trametinib) | MEK |
| A-769662 | AMPK |
| KX2-391 | Src |
| PCI-32765 (Ibrutinib) | Src |
| TAK-901 | Aurora Kinase |
| TG101209 | Flt, JAK, c-RET |
| AMG 900 | Aurora Kinase |
| GSK1838705A | IGF-1, ALK |
| ZM 336372 | Raf |
| GDC-0980 (RG7422) | mTOR, PI3K |

| | |
|---|---|
| NU7441(KU-57788) | DNA-PK, PI3K |
| Flavopiridol hydrochloride | CDK |
| PH-797804 | p38 MAPK |
| Crenolanib (CP-868596) | PDGFR |
| PF-04691502 | mTOR, PI3K, Akt |
| Dovitinib (TKI-258) | c-Kit, FGFR, Flt, VEGFR, PDGFR |
| Y-27632 2HCl | ROCK |
| Brivanib (BMS-540215) | VEGFR, FGFR |
| GSK1904529A | IGF-1R |
| MLN8054 | Aurora Kinase |
| OSU-03012 | PDK-1 |
| PD173074 | FGFR, VEGFR |
| Vemurafenib (PLX4032) | Raf |
| AMG-208 | c-Met |
| Thiazovivin | ROCK |
| Palomid 529 | mTOR |
| PHT-427 | Akt, PDK-1 |
| Tie2 kinase inhibitor | Tie-2 |
| Baricitinib (LY3009104) | JAK |
| E7080 (Lenvatinib) | VEGFR |
| BGJ398 (NVP-BGJ398) | FGFR |
| SB590885 | Raf |

| | |
|---|---|
| R788 (Fostamatinib) | Syk |
| CAY10505 | PI3K |
| CHIR-124 | Chk |
| Linsitinib (OSI-906) | IGF-1R |
| GSK690693 | Akt |
| Ruxolitinib (INCB018424) | JAK |
| PHA-665752 | c-Met |
| GSK1070916 | Aurora Kinase |
| PKI-402 | PI3K |
| TG101348 (SAR302503) | JAK |
| PF-03814735 | Aurora Kinase, FAK |
| SB 415286 | GSK-3 |
| INK 128 | mTOR |
| Dinaciclib (SCH727965) | CDK |
| MK-5108 (VX-689) | Aurora Kinase |
| AG-1478 (Tyrphostin AG-1478) | EGFR |
| AMG458 | c-Met |
| Arry-380 | HER2, EGFR |
| PHA-848125 | CDK |
| AZ628 | Raf |
| CCT137690 | Aurora Kinase |
| CHIR-98014 | GSK-3 |

| | |
|---|---|
| NVP-BGT226 | PI3K, mTOR |
| YM201636 | PI3K |
| 3-Methyladenine | PI3K |
| BX-795 | PDK-1, IKK |
| BX-912 | PDK-1 |
| CH5424802 | ALK |
| NVP-BVU972 | c-Met |
| AST-1306 | EGFR |
| BMS-265246 | CDK |
| MK-2461 | c-Met, FGFR, PDGFR |
| AZD2014 | mTOR |
| TAK-285 | EGFR, HER2 |
| INCB28060 | c-Met |
| WP1066 | JAK |
| Piceatannol | Others |
| Sotrastaurin (AEB071) | PKC |
| AZD4547 | FGFR |
| GDC-0068 | Akt |
| Dabrafenib (GSK2118436) | Raf |
| Tyrphostin AG 879 (AG 879) | HER2 |
| Torin 2 | mTOR |
| BYL719 | PI3K |

| | |
|---|---|
| CEP33779 | JAK |
| NVP-TAE226 | FAK |
| CP 673451 | Others |
| PHA-767491 | CDK |
| Torin 1 | mTOR |
| TPCA-1 | IKK |
| Wortmannin | PI3K |
| Staurosporine | PKC |
| ARRY334543 | EGFR |
| Tideglusib | GSK-3 |
| Semaxanib (SU5416) | VEGFR |
| SAR131675 | VEGFR |
| IMD0354 | IKK |
| TG 100713 | PI3K |
| WHI-P154 | JAK, EGFR |
| ARQ 197 (Tivantinib) | c-Met |
| TWS119 | GSK-3 |

***Table 9.*** *Differentially expressed proteins between pA53T and control neurons*

| **Protein names** | **Gene names** | **Difference** | **Upregulated** | **Downregulated** |
|---|---|---|---|---|
| Prothymosin alpha;Prothymosin alpha, N- | PTMA | -4,22058974 | | + |

| | | | | |
|---|---|---|---|---|
| terminally processed;Thymosin alpha-1 | | | | |
| Protein transport protein Sec61 subunit alpha isoform 1 | SEC61A1 | -3,09643152 | | + |
| Histone H3.3;Histone H3.2;Histone H3.1t;Histone H3.1 | H3f3a;H3F3A;HIST2H3A;HIST3H3;Hist1h3b;Hist1h3a;HIST1H3A | -2,83120812 | | + |
| Fibronectin;Anastellin;Ugl-Y1;Ugl-Y2;Ugl-Y3 | FN1 | -2,52735837 | | + |
| 60S ribosomal protein L31 | RPL31 | -2,12383503 | | + |
| Glial fibrillary acidic protein | GFAP | -2,05050193 | | + |
| Golgi-associated plant pathogenesis-related protein 1 | GLIPR2 | -1,997111 | | + |
| Histone H1.4 | HIST1H1E | -1,96522289 | | + |
| Transgelin | TAGLN | -1,80209096 | | + |
| Radixin | RDX | -1,77318255 | | + |
| Collagen alpha-1(I) chain | COL1A1 | -1,63404274 | | + |

| | | | | |
|---|---|---|---|---|
| Ubiquitin-conjugating enzyme E2 variant 2 | UBE2V2 | -1,57051065 | | + |
| Histone H2A type 2-C;Histone H2A type 2-A | Hist2h2ac;HIST2H2AC;Hist2h2aa1;HIST2H2AA3 | -1,46609285 | | + |
| MARCKS-related protein | MARCKSL1 | -1,45300293 | | + |
| Chromobox protein homolog 1 | CBX1 | -1,35597377 | | + |
| Histone H2B type 1-L;Histone H2B type 1-M;Histone H2B type 1-N;Histone H2B type 1-H;Histone H2B type 1-P;Histone H2B type 1-K;Histone H2B type 1-C/E/G;Histone H2B type 2-B;Histone H2B type 1-B;Histone H2B type 2-F;Histone H2B type 1-C/E/F/G/I;Histone H2B type 1-D;Histone H2B | HIST1H2BL;HIST1H2BM;HIST1H2BN;HIST1H2BH;Hist1h2bp;Hist1h2bk;Hist1h2bc;Hist2h2bb;Hist1h2bh;Hist1h2bb;HIST2H2BF;HIST1H2BC;HIST1H2BD;Hist1h2bm;Hist1h2bf;HIST1H2BK;H2BFS;hist2h2l;Hist1h2ba;HIST1H2BA | -1,32357407 | | + |

| | | | | |
|---|---|---|---|---|
| type 1-F/J/L;Histone H2B type F-S;Histone H2B 3;Histone H2B type 1-A | | | | |
| Histone H1.5 | HIST1H1B | -1,32074398 | | + |
| TAR DNA-binding protein 43 | TARDBP | -1,28565174 | | + |
| Neutral amino acid transporter A | SLC1A4 | -1,26124043 | | + |
| Clathrin light chain A | CLTA | -1,16397328 | | + |
| Cytoplasmic dynein 1 intermediate chain 2 | DYNC1I2;Dync1i2 | -1,15378104 | | + |
| CDKN2A-interacting protein | CDKN2AIP | -1,13875198 | | + |
| Tropomyosin alpha-4 chain | TPM4 | -1,1163631 | | + |
| Tropomyosin alpha-1 chain | TPM1 | -1,11481222 | | + |
| Soluble lamin-associated protein of 75 kDa | FAM169A | -1,11439917 | | + |

| | | | | |
|---|---|---|---|---|
| Ribosome-binding protein 1 | RRBP1 | -1,01449564 | | + |
| Histone H1.2;Histone H1.3 | HIST1H1C;Hist1h1d;Hist1h1c | -1,00663524 | | + |
| Zinc finger RNA-binding protein | ZFR | -1,00062116 | | + |
| Cellular retinoic acid-binding protein 1 | CRABP1 | -0,97820261 | | + |
| 45 kDa calcium-binding protein | SDF4 | -0,93680615 | | + |
| Eukaryotic translation initiation factor 4 gamma 3 | EIF4G3 | -0,91687775 | | + |
| Protein phosphatase 1B | PPM1B | -0,90773561 | | + |
| Caldesmon | CALD1 | -0,89930958 | | + |
| Proteasome subunit alpha type-3 | PSMA3 | -0,89364327 | | + |
| Tubulin beta chain | TUBB | -0,89241261 | | + |
| Protein canopy homolog 2 | CNPY2 | -0,86795319 | | + |
| Nuclear pore complex protein Nup153 | NUP153 | -0,85966153 | | + |

| | | | | |
|---|---|---|---|---|
| Transmembrane emp24 domain-containing protein 10 | TMED10;Tmed10 | -0,84096781 | | + |
| Rho GTPase-activating protein 21 | ARHGAP21 | -0,83467611 | | + |
| Brain acid soluble protein 1 | BASP1 | -0,82571665 | | + |
| Heterochromatin protein 1-binding protein 3 | HP1BP3 | -0,81141747 | | + |
| Peroxiredoxin-2 | PRDX2 | -0,80545298 | | + |
| Plasma membrane calcium-transporting ATPase 1 | ATP2B1 | -0,78781933 | | + |
| Band 4.1-like protein 3;Band 4.1-like protein 3, N-terminally processed | EPB41L3 | -0,78772333 | | + |
| Actin, alpha cardiac muscle 1;Actin, alpha skeletal muscle | ACTC1;ACTA1 | -0,77967135 | | + |

| | | | | |
|---|---|---|---|---|
| Polypyrimidine tract-binding protein 2 | PTBP2;Ptbp2 | -0,77931235 | | + |
| Putative phospholipase B-like 2;Putative phospholipase B-like 2 32 kDa form;Putative phospholipase B-like 2 45 kDa form | PLBD2 | -0,76606115 | | + |
| Heterogeneous nuclear ribonucleoprotein A1;Heterogeneous nuclear ribonucleoprotein A1, N-terminally processed;Heterogeneous nuclear ribonucleoprotein A1-like 2 | HNRNPA1;HNRNPA1L2 | -0,76263936 | | + |
| Acyl-CoA dehydrogenase family member 9, mitochondrial | ACAD9 | -0,7569809 | | + |
| Kinectin | KTN1 | -0,74694803 | | + |

| | | | | |
|---|---|---|---|---|
| UBX domain-containing protein 1 | UBXN1 | -0,72750621 | | + |
| ATP synthase subunit d, mitochondrial | ATP5H | -0,72205056 | | + |
| Reticulon-4 | RTN4 | -0,71967845 | | + |
| Amyloid beta A4 protein;N-APP;Soluble APP-alpha;Soluble APP-beta;C99;Beta-amyloid protein 42;Beta-amyloid protein 40;C83;P3(42);P3(40);C80;Gamma-secretase C-terminal fragment 59;Gamma-secretase C-terminal fragment 57;Gamma-secretase C-terminal fragment 50;C31 | APP;App | -0,70541975 | | + |
| Formin-binding protein 1-like | FNBP1L | -0,69941372 | | + |

| | | | | |
|---|---|---|---|---|
| Ubiquitin-40S ribosomal protein S27a;Ubiquitin;40S ribosomal protein S27a;Ubiquitin-60S ribosomal protein L40;Ubiquitin;60S ribosomal protein L40;Polyubiquitin-B;Ubiquitin;Polyubiquitin-C;Ubiquitin;Polyubiquitin-A;Ubiquitin;Ubiquitin-related | RPS27A;Rps27a;UBA52;Uba52;RpL40;RpS27A;UBB;Ubb;UBC;ubq-2;ubq-1 | -0,66847505 | | + |
| Prelamin-A/C;Lamin-A/C | LMNA | -0,66254658 | | + |
| N(G),N(G)-dimethylarginine dimethylaminohydrolase 2 | DDAH2 | -0,64632734 | | + |
| U4/U6.U5 tri-snRNP-associated protein 1 | SART1;Sart1 | -0,63747215 | | + |
| Splicing factor, proline- and glutamine-rich | SFPQ | -0,61198764 | | + |

| | | | | |
|---|---|---|---|---|
| Delta-1-pyrroline-5-carboxylate dehydrogenase, mitochondrial | ALDH4A1 | -0,58621025 | | + |
| Pre-mRNA-processing factor 40 homolog A | PRPF40A | -0,57962841 | | + |
| Zyxin | ZYX | -0,56851408 | | + |
| Histone H4 | Hist1h4a;HIST1H4A | -0,49797291 | | + |
| Catenin delta-1 | CTNND1 | -0,48542023 | | + |
| Lamin-B1 | LMNB1 | -0,47633659 | | + |
| Reticulocalbin-1 | RCN1 | -0,44097794 | | + |
| Polyadenylate-binding protein 1 | PABPC1 | 0,36678696 | + | |
| T-complex protein 1 subunit eta | CCT7 | 0,37164391 | + | |
| ELAV-like protein 1 | ELAVL1 | 0,38943545 | + | |
| Nitric oxide synthase-interacting protein | NOSIP | 0,40467771 | + | |
| Lamina-associated polypeptide 2, isoform alpha;Thymopoietin;Thymopentin | TMPO | 0,41073651 | + | |

| | | | | |
|---|---|---|---|---|
| Chromobox protein homolog 5 | CBX5;Cbx5 | 0,41383574 | + | |
| Elongation factor 2 | EEF2;Eef2 | 0,42066256 | + | |
| 60S ribosomal protein L4 | RPL4 | 0,4245472 | + | |
| Cell cycle and apoptosis regulator protein 2 | CCAR2 | 0,43223847 | + | |
| Pre-mRNA-splicing factor ATP-dependent RNA helicase DHX15 | DHX15 | 0,44824028 | + | |
| Ubiquitin thioesterase OTUB1 | OTUB1 | 0,44847086 | + | |
| Myosin-10 | MYH10 | 0,44919946 | + | |
| Platelet-activating factor acetylhydrolase IB subunit alpha | PAFAH1B1;Pafah1b1 | 0,46440866 | + | |
| MICOS complex subunit MIC60 | IMMT | 0,47223282 | + | |
| General transcription factor II-I | GTF2I;Gtf2i | 0,47717624 | + | |
| Voltage-dependent anion- | VDAC2 | 0,47729916 | + | |

| | | | | |
|---|---|---|---|---|
| selective channel protein 2 | | | | |
| DNA topoisomerase 1 | TOP1 | 0,47934278 | + | |
| 60 kDa heat shock protein, mitochondrial | HSPD1 | 0,48447143 | + | |
| Far upstream element-binding protein 2 | KHSRP | 0,48472828 | + | |
| Stress-70 protein, mitochondrial | HSPA9 | 0,48504872 | + | |
| Dynamin-2 | DNM2 | 0,48548105 | + | |
| Hydroxymethylglutaryl-CoA synthase, cytoplasmic | HMGCS1 | 0,48664877 | + | |
| Sarcoplasmic/endoplasmic reticulum calcium ATPase 2 | ATP2A2 | 0,49363581 | + | |
| Multifunctional protein ADE2;Phosphoribosylaminoimidazole-succinocarboxamide synthase;Phospho | PAICS | 0,49574788 | + | |

| | | | | |
|---|---|---|---|---|
| ribosylaminoimidazole carboxylase | | | | |
| Bifunctional purine biosynthesis protein PURH;Phosphoribosylaminoimidazolecarboxamide formyltransferase; IMP cyclohydrolase | ATIC | 0,49794049 | + | |
| Isocitrate dehydrogenase [NADP], mitochondrial | IDH2 | 0,49905989 | + | |
| Adenosylhomocysteinase | AHCY | 0,50178507 | + | |
| Methionine--tRNA ligase, cytoplasmic | MARS | 0,50235918 | + | |
| Eukaryotic initiation factor 4A-III;Eukaryotic initiation factor 4A-III, N-terminally processed | EIF4A3 | 0,50351991 | + | |

| | | | | |
|---|---|---|---|---|
| Coatomer subunit alpha;Xenin;Proxenin | COPA | 0,50397809 | + | |
| Rab GDP dissociation inhibitor beta | GDI2 | 0,5050727 | + | |
| Oxysterol-binding protein 1 | OSBP | 0,50976329 | + | |
| Ras-related protein Rab-2A | RAB2A | 0,51790598 | + | |
| NADPH--cytochrome P450 reductase | POR | 0,52251604 | + | |
| Aspartate aminotransferase, mitochondrial | GOT2 | 0,52831353 | + | |
| Eukaryotic translation initiation factor 3 subunit E | EIF3E | 0,53256332 | + | |
| 40S ribosomal protein SA | Rpsa;RPSA | 0,53590287 | + | |
| Stress-induced-phosphoprotein 1 | STIP1 | 0,53696569 | + | |
| Serine-threonine kinase receptor-associated protein | STRAP | 0,53877873 | + | |

| | | | | |
|---|---|---|---|---|
| 2,4-dienoyl-CoA reductase, mitochondrial | DECR1 | 0,54022598 | + | |
| Malate dehydrogenase, mitochondrial | MDH2 | 0,54088974 | + | |
| Malectin | MLEC | 0,54325846 | + | |
| Coatomer subunit beta | COPB2 | 0,54395019 | + | |
| Septin-9 | SEPT9 | 0,54734124 | + | |
| CTP synthase 1 | CTPS1 | 0,55151049 | + | |
| Signal transducer and activator of transcription 3 | STAT3 | 0,55413225 | + | |
| Cysteine protease ATG4B | ATG4B;Atg4b | 0,55785137 | + | |
| Flap endonuclease 1 | FEN1 | 0,56196107 | + | |
| ATP-dependent RNA helicase DDX19A;ATP-dependent RNA helicase DDX19B | DDX19A;DDX19B | 0,56328519 | + | |
| Nuclear pore membrane glycoprotein 210 | NUP210 | 0,56637213 | + | |

| | | | | |
|---|---|---|---|---|
| Heat shock 70 kDa protein 4 | HSPA4 | 0,566942 | + | |
| Phosphoserine aminotransferase | PSAT1 | 0,57374679 | + | |
| Pyruvate dehydrogenase E1 component subunit beta, mitochondrial | PDHB | 0,57605701 | + | |
| Transitional endoplasmic reticulum ATPase | Vcp;VCP | 0,58135562 | + | |
| Arginine--tRNA ligase, cytoplasmic | RARS | 0,58195093 | + | |
| X-ray repair cross-complementing protein 6 | XRCC6 | 0,58255429 | + | |
| Bifunctional glutamate/proline --tRNA ligase;Glutamate--tRNA ligase;Proline--tRNA ligase | EPRS | 0,58510844 | + | |
| Peroxiredoxin-6 | PRDX6 | 0,58962144 | + | |
| CAD protein;Glutamine -dependent | CAD | 0,59100299 | + | |

| | | | | |
|---|---|---|---|---|
| carbamoyl-phosphate synthase;Aspartate carbamoyltransferase;Dihydroorotase | | | | |
| Farnesyl pyrophosphate synthase | FDPS | 0,59512181 | + | |
| Cyclin-dependent-like kinase 5 | CDK5 | 0,60137918 | + | |
| Ran GTPase-activating protein 1 | RANGAP1 | 0,60225423 | + | |
| Heterogeneous nuclear ribonucleoprotein D-like | HNRNPDL | 0,60320918 | + | |
| NEDD8-activating enzyme E1 catalytic subunit | UBA3 | 0,60380046 | + | |
| T-complex protein 1 subunit beta | CCT2 | 0,60664368 | + | |
| Cytoskeleton-associated protein 5 | CKAP5 | 0,60961533 | + | |
| Prohibitin | PHB | 0,61144045 | + | |

| | | | | |
|---|---|---|---|---|
| Unconventional myosin-VI | MYO6 | 0,61296166 | + | |
| Cleavage stimulation factor subunit 3 | CSTF3 | 0,61377652 | + | |
| Importin-5 | IPO5 | 0,61648496 | + | |
| Very-long-chain (3R)-3-hydroxyacyl-CoA dehydratase 3 | HACD3 | 0,61995697 | + | |
| Glycine--tRNA ligase | GARS | 0,62528377 | + | |
| Thioredoxin-like protein 1 | TXNL1 | 0,62663396 | + | |
| Isoleucine--tRNA ligase, cytoplasmic | IARS | 0,62683529 | + | |
| Pyruvate carboxylase, mitochondrial | PC | 0,63483853 | + | |
| T-complex protein 1 subunit gamma | CCT3 | 0,6354794 | + | |
| 40S ribosomal protein S10;Putative 40S ribosomal protein S10-like | RPS10;RPS10P5 | 0,63819567 | + | |

| | | | | |
|---|---|---|---|---|
| 182 kDa tankyrase-1-binding protein | TNKS1BP1 | 0,64544317 | + | |
| ATP-citrate synthase | ACLY;Acly | 0,64815733 | + | |
| Inositol-3-phosphate synthase 1 | ISYNA1 | 0,65151003 | + | |
| Guanine nucleotide-binding protein subunit beta-2-like 1;Guanine nucleotide-binding protein subunit beta-2-like 1, N-terminally processed | GNB2L1 | 0,6532597 | + | |
| Probable ATP-dependent RNA helicase DDX6;ATP-dependent RNA helicase ddx6 | DDX6;Ddx6;ddx6 | 0,65331353 | + | |
| Gem-associated protein 5 | GEMIN5 | 0,65372573 | + | |
| Mitochondrial-processing peptidase subunit alpha | PMPCA | 0,65491528 | + | |

| | | | | |
|---|---|---|---|---|
| ATP-dependent RNA helicase DDX1 | DDX1 | 0,65614933 | + | |
| Neurofilament light polypeptide | NEFL | 0,65656302 | + | |
| 40S ribosomal protein S6 | RPS6 | 0,65667152 | + | |
| Methylmalonate-semialdehyde dehydrogenase [acylating], mitochondrial | ALDH6A1 | 0,65771061 | + | |
| Heterogeneous nuclear ribonucleoprotein L | HNRNPL | 0,65942128 | + | |
| Exportin-1 | XPO1;Xpo1 | 0,66231028 | + | |
| T-complex protein 1 subunit theta | CCT8 | 0,66265233 | + | |
| Heterogeneous nuclear ribonucleoprotein M | HNRNPM | 0,66267946 | + | |
| T-complex protein 1 subunit epsilon | CCT5 | 0,66413583 | + | |
| Lysine--tRNA ligase | KARS | 0,66436916 | + | |

| | | | | |
|---|---|---|---|---|
| Carboxymethylene butenolidase homolog | CMBL | 0,66666497 | + | |
| Uncharacterized protein C7orf50 | C7orf50 | 0,66734335 | + | |
| Neurofilament medium polypeptide | NEFM | 0,6674739 | + | |
| Dynamin-1-like protein | DNM1L | 0,66997189 | + | |
| Nuclear pore complex protein Nup50 | NUP50 | 0,67132717 | + | |
| Peroxiredoxin-1 | PRDX1 | 0,67464023 | + | |
| Ubiquitin carboxyl-terminal hydrolase 5 | USP5 | 0,67514716 | + | |
| Chloride intracellular channel protein 1 | CLIC1 | 0,67566193 | + | |
| T-complex protein 1 subunit delta | CCT4 | 0,6770969 | + | |
| Elongation factor 1-beta | EEF1B2 | 0,67718993 | + | |
| AP-2 complex subunit alpha-2 | AP2A2 | 0,68129052 | + | |
| Septin-2 | SEPT2 | 0,68638208 | + | |

| | | | | |
|---|---|---|---|---|
| High mobility group protein B1;Putative high mobility group protein B1-like 1 | HMGB1;Hmgb1;HMGB1P1 | 0,6891399 | + | |
| Replication factor C subunit 1 | RFC1 | 0,69490157 | + | |
| MICOS complex subunit MIC19 | CHCHD3 | 0,69938045 | + | |
| Alpha-internexin | INA | 0,7001809 | + | |
| RNA polymerase II-associated factor 1 homolog | PAF1 | 0,70027139 | + | |
| 60S ribosomal protein L5 | RPL5 | 0,7005859 | + | |
| Sideroflexin-1 | SFXN1 | 0,701732 | + | |
| Poly(rC)-binding protein 2 | PCBP2 | 0,70254792 | + | |
| Protein crumbs homolog 2 | CRB2 | 0,70587688 | + | |
| 39S ribosomal protein L22, mitochondrial | MRPL22 | 0,70988634 | + | |
| Cytoskeleton-associated protein 4 | CKAP4 | 0,70989778 | + | |
| Tumor protein D54 | TPD52L2 | 0,71015655 | + | |

| | | | | |
|---|---|---|---|---|
| Metastasis-associated protein MTA2 | MTA2;Mta2 | 0,71304385 | + | |
| mRNA cap guanine-N7 methyltransferase | RNMT | 0,71329859 | + | |
| Ubiquitin carboxyl-terminal hydrolase isozyme L1 | UCHL1 | 0,71483188 | + | |
| Cytochrome b-c1 complex subunit 2, mitochondrial | UQCRC2 | 0,715438 | + | |
| YLP motif-containing protein 1 | YLPM1 | 0,71668392 | + | |
| ATP-dependent DNA helicase Q1 | RECQL | 0,71730084 | + | |
| Vacuolar protein sorting-associated protein 35 | VPS35;Vps35 | 0,71786329 | + | |
| Chromobox protein homolog 3 | CBX3 | 0,71830495 | + | |
| 60S ribosomal protein L12 | RPL12 | 0,72048357 | + | |
| Sodium/potassium -transporting | ATP1B1 | 0,72105302 | + | |

| | | | | |
|---|---|---|---|---|
| ATPase subunit beta-1 | | | | |
| Protein LSM14 homolog B | LSM14B | 0,72187487 | + | |
| C-1-tetrahydrofolate synthase, cytoplasmic;Methylenetetrahydrofolate dehydrogenase;Methenyltetrahydrofolate cyclohydrolase;Formyltetrahydrofolate synthetase;C-1-tetrahydrofolate synthase, cytoplasmic, N-terminally processed | MTHFD1 | 0,72321616 | + | |
| 40S ribosomal protein S25 | RPS25 | 0,72731739 | + | |
| FACT complex subunit SSRP1 | SSRP1 | 0,72842047 | + | |
| Huntingtin-interacting protein 1 | HIP1 | 0,72859001 | + | |

| | | | | |
|---|---|---|---|---|
| Pyrroline-5-carboxylate reductase 1, mitochondrial | PYCR1 | 0,72987959 | + | |
| Pre-mRNA-processing-splicing factor 8 | PRPF8 | 0,7321896 | + | |
| HBS1-like protein | HBS1L | 0,73350504 | + | |
| Adenylosuccinate synthetase isozyme 2 | ADSS | 0,73512416 | + | |
| Protein arginine N-methyltransferase 1 | PRMT1 | 0,7378042 | + | |
| Alanine--tRNA ligase, cytoplasmic | AARS | 0,73953523 | + | |
| O-acetyl-ADP-ribose deacetylase 1 | OARD1 | 0,74088754 | + | |
| SUMO-activating enzyme subunit 2 | UBA2 | 0,74310282 | + | |
| Nuclear pore complex protein Nup205 | NUP205 | 0,74427859 | + | |
| Ataxin-10 | ATXN10 | 0,75490401 | + | |
| Glutathione peroxidase 1 | GPX1 | 0,75532087 | + | |

| | | | | |
|---|---|---|---|---|
| Calcyclin-binding protein | CACYBP | 0,75540161 | + | |
| F-actin-capping protein subunit beta | CAPZB | 0,75865576 | + | |
| Alpha-aminoadipic semialdehyde dehydrogenase | ALDH7A1 | 0,76025094 | + | |
| Calcium-binding mitochondrial carrier protein Aralar1 | SLC25A12 | 0,76159901 | + | |
| Aconitate hydratase, mitochondrial | ACO2 | 0,76345507 | + | |
| Sorting nexin-6;Sorting nexin-6, N-terminally processed | SNX6 | 0,76497332 | + | |
| Heat shock 70 kDa protein 12A | HSPA12A | 0,76612684 | + | |
| Basic leucine zipper and W2 domain-containing protein 1 | BZW1 | 0,77025922 | + | |
| Enhancer of mRNA-decapping protein 4 | EDC4 | 0,78210153 | + | |

| | | | | |
|---|---|---|---|---|
| Nuclear protein localization protein 4 homolog | NPLOC4 | 0,78391669 | + | |
| Tyrosine-protein kinase CSK | CSK | 0,78742769 | + | |
| Translation initiation factor eIF-2B subunit delta | EIF2B4 | 0,78922335 | + | |
| E3 ubiquitin-protein ligase UHRF1 | UHRF1 | 0,78940964 | + | |
| 60S ribosomal protein L27a | RPL27A;Rpl27a | 0,79095183 | + | |
| 26S proteasome non-ATPase regulatory subunit 4 | PSMD4 | 0,79130618 | + | |
| FACT complex subunit SPT16 | SUPT16H | 0,79339176 | + | |
| Trifunctional purine biosynthetic protein adenosine-3;Phosphoribosylamine--glycine ligase;Phosphoribosylformylglycinamidine cyclo- | GART | 0,79848162 | + | |

| | | | | |
|---|---|---|---|---|
| ligase;Phosphoribosylglycinamide formyltransferase | | | | |
| Eukaryotic translation initiation factor 4 gamma 2 | EIF4G2 | 0,80582746 | + | |
| E2/E3 hybrid ubiquitin-protein ligase UBE2O | UBE2O | 0,80629285 | + | |
| Eukaryotic translation initiation factor 3 subunit C;Eukaryotic translation initiation factor 3 subunit C-like protein | EIF3C;EIF3CL | 0,80635749 | + | |
| DNA ligase 3 | LIG3 | 0,80947198 | + | |
| ATP-binding cassette sub-family F member 1 | ABCF1 | 0,81026226 | + | |
| Nuclear pore complex protein Nup88 | NUP88 | 0,8166737 | + | |

| | | | | |
|---|---|---|---|---|
| Adipocyte plasma membrane-associated protein | APMAP | 0,81971105 | + | |
| Cysteine and glycine-rich protein 1 | CSRP1 | 0,8229582 | + | |
| Nucleoporin p54 | NUP54 | 0,82570903 | + | |
| ATP-dependent 6-phosphofructokinase, muscle type | PFKM | 0,83510272 | + | |
| Protein kinase C and casein kinase substrate in neurons protein 2 | PACSIN2 | 0,83510399 | + | |
| DNA repair protein XRCC1 | XRCC1 | 0,83597565 | + | |
| Succinate-semialdehyde dehydrogenase, mitochondrial | ALDH5A1 | 0,83830134 | + | |
| Aflatoxin B1 aldehyde reductase member 2 | AKR7A2 | 0,8383984 | + | |
| E3 ubiquitin-protein ligase BRE1A | RNF20 | 0,83881548 | + | |

| | | | | |
|---|---|---|---|---|
| PHD finger protein 6 | PHF6 | 0,8417937 | + | |
| 28S ribosomal protein S31, mitochondrial | MRPS31 | 0,8446863 | + | |
| Probable global transcription activator SNF2L1 | SMARCA1;Smarca 1 | 0,84491963 | + | |
| Regulator of chromosome condensation | RCC1 | 0,84653388 | + | |
| Cyclin-dependent kinase 11A;Cyclin-dependent kinase 11B | CDK11A;CDK11B | 0,84698232 | + | |
| 39S ribosomal protein L1, mitochondrial | MRPL1 | 0,84698423 | + | |
| Pinin | PNN | 0,8496774 | + | |
| Fatty acid synthase;[Acyl-carrier-protein] S-acetyltransferase;[Acyl-carrier-protein] S-malonyltransferase;3-oxoacyl-[acyl-carrier-protein] synthase;3- | FASN | 0,85016759 | + | |

| | | | | |
|---|---|---|---|---|
| oxoacyl-[acyl-carrier-protein] reductase;3-hydroxyacyl-[acyl-carrier-protein] dehydratase;Enoyl-[acyl-carrier-protein] reductase;Oleoyl-[acyl-carrier-protein] hydrolase | | | | |
| Protein transport protein Sec31A | SEC31A | 0,85054546 | + | |
| Structural maintenance of chromosomes protein 1A | SMC1A;smc1a | 0,85207791 | + | |
| Protein transport protein Sec23A | SEC23A | 0,85275926 | + | |
| Kinesin-like protein KIF1A | KIF1A | 0,8551178 | + | |
| Squalene synthase | FDFT1 | 0,85576375 | + | |
| Eukaryotic translation initiation factor 2 subunit 3;Putative eukaryotic translation initiation factor 2 | EIF2S3;Eif2s3;EIF2S3L;Eif2s3x;Eif2s3y | 0,85691494 | + | |

| | | | | |
|---|---|---|---|---|
| subunit 3-like protein;Eukaryotic translation initiation factor 2 subunit 3, X-linked;Eukaryotic translation initiation factor 2 subunit 3, Y-linked | | | | |
| Heterogeneous nuclear ribonucleoprotein F;Heterogeneous nuclear ribonucleoprotein F, N-terminally processed | HNRNPF | 0,85778597 | + | |
| Squalene monooxygenase | SQLE | 0,85792033 | + | |
| T-complex protein 1 subunit alpha | TCP1;Tcp1 | 0,86092822 | + | |
| 10 kDa heat shock protein, mitochondrial | HSPE1 | 0,86157121 | + | |
| Quinone oxidoreductase | CRYZ | 0,86160787 | + | |
| Glycylpeptide N-tetradecanoyltransferase 1 | NMT1 | 0,87303861 | + | |

| | | | | |
|---|---|---|---|---|
| Glutaredoxin-3 | GLRX3 | 0,8834112 | + | |
| Heat shock protein 105 kDa | HSPH1 | 0,88477092 | + | |
| Probable glutathione peroxidase 8 | GPX8 | 0,88546732 | + | |
| Intraflagellar transport protein 27 homolog | IFT27 | 0,88639641 | + | |
| Protein O-GlcNAcase | MGEA5;Mgea5 | 0,8876614 | + | |
| Importin-4 | IPO4 | 0,8891076 | + | |
| Exosome complex component RRP43 | EXOSC8 | 0,89599164 | + | |
| Protein DEK | DEK | 0,89820035 | + | |
| ADP-ribosylation factor-like protein 8A | ARL8A | 0,89923392 | + | |
| Synaptobrevin homolog YKT6 | YKT6 | 0,89995914 | + | |
| Eukaryotic initiation factor 4A-I | EIF4A1 | 0,90034993 | + | |
| N-acetylserotonin O-methyltransferase -like protein | ASMTL | 0,90054046 | + | |

| | | | | |
|---|---|---|---|---|
| Histidine--tRNA ligase, cytoplasmic | HARS | 0,90092129 | + | |
| Glutamine--tRNA ligase | QARS | 0,90180757 | + | |
| Apoptosis regulator BAX | BAX | 0,90222761 | + | |
| Cysteine and histidine-rich domain-containing protein 1 | CHORDC1 | 0,90228123 | + | |
| Calcium-binding mitochondrial carrier protein Aralar2 | SLC25A13 | 0,90638924 | + | |
| Atlastin-1 | ATL1 | 0,90722953 | + | |
| 26S proteasome non-ATPase regulatory subunit 8 | PSMD8 | 0,90734715 | + | |
| Uridine 5-monophosphate synthase;Orotate phosphoribosyltransferase;Orotidine 5-phosphate decarboxylase | UMPS | 0,91802639 | + | |
| Ras-related protein Rab-18 | RAB18 | 0,92116186 | + | |

| | | | | |
|---|---|---|---|---|
| 26S proteasome non-ATPase regulatory subunit 10 | PSMD10 | 0,921548 | + | |
| Lanosterol 14-alpha demethylase | CYP51A1 | 0,92195278 | + | |
| Membrane-associated progesterone receptor component 2 | PGRMC2 | 0,92723952 | + | |
| THO complex subunit 4 | ALYREF | 0,92735121 | + | |
| Filamin-C | FLNC | 0,92777104 | + | |
| Valine--tRNA ligase | VARS | 0,92905405 | + | |
| Cleavage and polyadenylation specificity factor subunit 5 | NUDT21 | 0,93198013 | + | |
| Heterogeneous nuclear ribonucleoprotein U-like protein 1 | HNRNPUL1 | 0,93243514 | + | |
| Eukaryotic translation initiation factor 3 subunit F | EIF3F | 0,93482166 | + | |

| | | | | |
|---|---|---|---|---|
| Septin-5 | SEPT5 | 0,93491491 | + | |
| Eukaryotic translation initiation factor 3 subunit H | EIF3H | 0,9407408 | + | |
| NEDD8-activating enzyme E1 regulatory subunit | NAE1 | 0,94177945 | + | |
| Sideroflexin-3 | SFXN3 | 0,94284206 | + | |
| Alcohol dehydrogenase class-3 | ADH5 | 0,94287194 | + | |
| Dolichyl-diphosphooligosaccharide--protein glycosyltransferase subunit STT3B | STT3B | 0,94328859 | + | |
| 40S ribosomal protein S9 | RPS9 | 0,945062 | + | |
| Poly(rC)-binding protein 1 | PCBP1 | 0,94605361 | + | |
| Nuclear pore complex protein Nup85 | NUP85 | 0,95299551 | + | |
| Lysine-specific histone demethylase 1A | KDM1A | 0,95578766 | + | |

| | | | | |
|---|---|---|---|---|
| Sister chromatid cohesion protein PDS5 homolog B | PDS5B | 0,95589892 | + | |
| 26S proteasome non-ATPase regulatory subunit 11 | PSMD11 | 0,95619117 | + | |
| Histone acetyltransferase type B catalytic subunit | HAT1 | 0,95839225 | + | |
| Nuclear pore complex protein Nup155 | NUP155;Nup155 | 0,95919906 | + | |
| Vacuolar protein sorting-associated protein 4B | VPS4B | 0,95933194 | + | |
| Eukaryotic translation initiation factor 3 subunit M | EIF3M | 0,95983484 | + | |
| Spermine synthase | SMS | 0,95988231 | + | |
| Actin-related protein 2;Actin-related protein 2-B | ACTR2;actr2b | 0,96049881 | + | |
| Adenine phosphoribosyltransferase | APRT | 0,96247821 | + | |

| | | | | |
|---|---|---|---|---|
| Ankycorbin | RAI14 | 0,96523158 | + | |
| Transmembrane protein 33 | TMEM33 | 0,96590932 | + | |
| 40S ribosomal protein S3 | RPS3 | 0,96805848 | + | |
| Eukaryotic translation initiation factor 3 subunit B | EIF3B | 0,96913613 | + | |
| Myosin regulatory light chain 12A;Myosin regulatory light chain 12B | MYL12A;MYL12B | 0,97154744 | + | |
| Eukaryotic translation initiation factor 3 subunit D | EIF3D | 0,97200288 | + | |
| Protein phosphatase methylesterase 1 | PPME1 | 0,9724297 | + | |
| DNA replication licensing factor MCM6 | MCM6 | 0,97616132 | + | |
| Anamorsin | CIAPIN1 | 0,9777209 | + | |
| ADP-sugar pyrophosphatase | NUDT5 | 0,97962591 | + | |

| | | | | |
|---|---|---|---|---|
| Cullin-1 | Cul1;CUL1 | 0,98065461 | + | |
| Splicing factor 45 | RBM17 | 0,98133341 | + | |
| Syntaxin-12 | STX12 | 0,9816316 | + | |
| Hsc70-interacting protein;Putative protein FAM10A5;Putative protein FAM10A4 | ST13;ST13P5;ST13P4 | 0,98399353 | + | |
| V-type proton ATPase subunit d 1 | ATP6V0D1 | 0,98763635 | + | |
| Methionine adenosyltransferase 2 subunit beta | MAT2B | 0,98799621 | + | |
| Probable ATP-dependent RNA helicase DDX5 | DDX5 | 0,9885966 | + | |
| Nucleoside diphosphate kinase B | NME2 | 0,98965306 | + | |
| Mycophenolic acid acyl-glucuronide esterase, mitochondrial | ABHD10 | 0,99094348 | + | |
| Ubiquitin-conjugating enzyme E2 E3;Ubiquitin- | UBE2E3;Ube2e3;UBE2E2 | 0,99097697 | + | |

| | | | | |
|---|---|---|---|---|
| conjugating enzyme E2 E2 | | | | |
| Nuclear pore complex protein Nup133 | NUP133 | 0,99205356 | + | |
| 5-3 exoribonuclease 2 | XRN2 | 0,99258635 | + | |
| GDP-L-fucose synthase | TSTA3 | 0,99589411 | + | |
| Syntenin-1 | SDCBP | 0,99601788 | + | |
| U2 snRNP-associated SURP motif-containing protein | U2SURP | 0,99694697 | + | |
| UDP-N-acetylglucosamine --peptide N-acetylglucosaminyl transferase 110 kDa subunit | OGT | 0,99701733 | + | |
| Proteasome subunit alpha type-1 | PSMA1 | 0,99923706 | + | |
| Myosin light polypeptide 6 | MYL6 | 0,99941953 | + | |
| Condensin complex subunit 3 | NCAPG | 1,00285445 | + | |

| | | | | |
|---|---|---|---|---|
| Agrin;Agrin N-terminal 110 kDa subunit;Agrin C-terminal 110 kDa subunit;Agrin C-terminal 90 kDa fragment;Agrin C-terminal 22 kDa fragment | AGRN | 1,00335926 | + | |
| Exportin-2 | CSE1L | 1,00356144 | + | |
| Fanconi anemia group I protein | FANCI | 1,00651783 | + | |
| Isopentenyl-diphosphate Delta-isomerase 1 | IDI1 | 1,0073897 | + | |
| Mitochondrial import receptor subunit TOM70 | TOMM70A | 1,00825564 | + | |
| Selenide, water dikinase 1 | SEPHS1 | 1,0087293 | + | |
| Synaptic vesicle membrane protein VAT-1 homolog-like | VAT1L | 1,01057137 | + | |
| Laminin subunit gamma-1 | LAMC1 | 1,0107265 | + | |

| | | | | |
|---|---|---|---|---|
| DnaJ homolog subfamily C member 7 | DNAJC7 | 1,01387151 | + | |
| Nucleolar GTP-binding protein 1 | GTPBP4 | 1,01682303 | + | |
| Mesencephalic astrocyte-derived neurotrophic factor | MANF | 1,02139431 | + | |
| Proliferating cell nuclear antigen | PCNA | 1,02184698 | + | |
| Signal recognition particle receptor subunit beta | SRPRB | 1,0224639 | + | |
| Casein kinase II subunit alpha | CSNK2A2 | 1,0233061 | + | |
| Ephrin type-A receptor 2 | EPHA2 | 1,02584394 | + | |
| Ubiquitin-conjugating enzyme E2 K | UBE2K | 1,03290727 | + | |
| ELAV-like protein 3 | ELAVL3 | 1,03751861 | + | |
| Apoptosis inhibitor 5 | API5 | 1,03793229 | + | |
| Peptidyl-prolyl cis-trans isomerase FKBP10 | FKBP10 | 1,04088169 | + | |

| | | | | |
|---|---|---|---|---|
| Translocon-associated protein subunit delta | SSR4 | 1,04090563 | + | |
| AP-3 complex subunit delta-1 | AP3D1 | 1,04234166 | + | |
| Ubiquitin carboxyl-terminal hydrolase 14 | USP14 | 1,04278119 | + | |
| 28 kDa heat- and acid-stable phosphoprotein | PDAP1 | 1,04491382 | + | |
| Serine/threonine-protein phosphatase 2A catalytic subunit alpha isoform | PPP2CA | 1,04501343 | + | |
| NADH dehydrogenase [ubiquinone] iron-sulfur protein 2, mitochondrial | NDUFS2 | 1,04504479 | + | |
| Electron transfer flavoprotein subunit beta | ETFB | 1,04917781 | + | |
| NADH dehydrogenase [ubiquinone] iron- | NDUFS3 | 1,05075328 | + | |

| | | | | |
|---|---|---|---|---|
| sulfur protein 3, mitochondrial | | | | |
| Serine/threonine-protein phosphatase 2A activator | PPP2R4 | 1,0543357 | + | |
| Golgi-specific brefeldin A-resistance guanine nucleotide exchange factor 1 | GBF1 | 1,05519549 | + | |
| Acetyl-CoA carboxylase 1;Biotin carboxylase | ACACA | 1,05589909 | + | |
| Replication factor C subunit 5 | RFC5 | 1,05746905 | + | |
| NAD-dependent malic enzyme, mitochondrial | ME2 | 1,06008848 | + | |
| Protein PBDC1 | PBDC1 | 1,06041993 | + | |
| Regulator of nonsense transcripts 1 | UPF1 | 1,0617307 | + | |
| Methylmalonyl-CoA mutase, mitochondrial | MUT | 1,06339433 | + | |

| | | | | |
|---|---|---|---|---|
| ATP-binding cassette sub-family D member 3 | ABCD3 | 1,06370862 | + | |
| Structural maintenance of chromosomes protein 4 | SMC4 | 1,06396378 | + | |
| Alcohol dehydrogenase [NADP(+)] | AKR1A1 | 1,06649611 | + | |
| BTB/POZ domain-containing protein KCTD12 | KCTD12;Kctd12 | 1,06699498 | + | |
| DNA polymerase delta catalytic subunit | POLD1 | 1,06902334 | + | |
| Band 4.1-like protein 2 | EPB41L2 | 1,07153087 | + | |
| 26S protease regulatory subunit 10B | PSMC6 | 1,07276196 | + | |
| Regulation of nuclear pre-mRNA domain-containing protein 1B | RPRD1B | 1,07551363 | + | |
| Cyclin-dependent kinase 1 | CDK1 | 1,08203782 | + | |

| | | | | |
|---|---|---|---|---|
| Synapsin-1 | SYN1 | 1,08556345 | + | |
| Ornithine aminotransferase, mitochondrial;Ornithine aminotransferase, hepatic form;Ornithine aminotransferase, renal form | OAT | 1,08617592 | + | |
| 28S ribosomal protein S22, mitochondrial | MRPS22 | 1,08682378 | + | |
| tRNA-splicing ligase RtcB homolog | RTCB;rtcb | 1,08863449 | + | |
| Succinate dehydrogenase [ubiquinone] flavoprotein subunit, mitochondrial | SDHA | 1,08875423 | + | |
| SUMO-activating enzyme subunit 1;SUMO-activating enzyme subunit 1, N-terminally processed | SAE1 | 1,08953815 | + | |

| | | | | |
|---|---|---|---|---|
| 3-mercaptopyruvate sulfurtransferase | MPST | 1,09141858 | + | |
| cAMP-dependent protein kinase catalytic subunit alpha | PRKACA | 1,09949705 | + | |
| Inosine-5-monophosphate dehydrogenase 2 | IMPDH2 | 1,10493978 | + | |
| Glucosamine-6-phosphate isomerase 1 | GNPDA1 | 1,10534392 | + | |
| Endoplasmic reticulum resident protein 44 | ERP44 | 1,1056508 | + | |
| ER membrane protein complex subunit 1 | EMC1 | 1,10666614 | + | |
| Delta-1-pyrroline-5-carboxylate synthase;Glutamate 5-kinase;Gamma-glutamyl phosphate reductase | ALDH18A1 | 1,10695733 | + | |
| 26S proteasome non-ATPase | PSMD1 | 1,10745769 | + | |

| | | | | |
|---|---|---|---|---|
| regulatory subunit 1 | | | | |
| Replication factor C subunit 4 | RFC4 | 1,1082628 | + | |
| Glutathione S-transferase omega-1 | GSTO1 | 1,10830943 | + | |
| Cytoplasmic dynein 1 light intermediate chain 1 | DYNC1LI1 | 1,10837788 | + | |
| NADH-ubiquinone oxidoreductase 75 kDa subunit, mitochondrial | NDUFS1 | 1,10967467 | + | |
| Endophilin-A2 | SH3GL1 | 1,11236042 | + | |
| Elongation factor 1-delta | EEF1D | 1,11504322 | + | |
| Calpain-2 catalytic subunit | CAPN2 | 1,11789682 | + | |
| Cytosol aminopeptidase | LAP3 | 1,11820115 | + | |
| Probable ATP-dependent RNA helicase DDX46 | DDX46 | 1,11878671 | + | |
| Copine-3 | CPNE3 | 1,12190289 | + | |

| | | | | |
|---|---|---|---|---|
| Nucleolar transcription factor 1 | UBTF | 1,12599924 | + | |
| GTPase NRas | NRAS | 1,13142776 | + | |
| 60S ribosomal protein L19 | RPL19 | 1,13175625 | + | |
| Ras-related protein Rab-21 | RAB21 | 1,13661808 | + | |
| Polyadenylate-binding protein 4 | PABPC4 | 1,13796128 | + | |
| DNA replication licensing factor MCM4 | MCM4 | 1,14170096 | + | |
| Low molecular weight phosphotyrosine protein phosphatase | ACP1 | 1,14384058 | + | |
| Protein RER1 | RER1 | 1,14668761 | + | |
| Nuclear cap-binding protein subunit 1 | NCBP1 | 1,14675395 | + | |
| Sorting and assembly machinery component 50 homolog | SAMM50 | 1,14759827 | + | |

| | | | | |
|---|---|---|---|---|
| Serine/threonine-protein kinase 26 | STK26 | 1,14860047 | + | |
| Aminopeptidase B | RNPEP | 1,15134536 | + | |
| Diablo homolog, mitochondrial | DIABLO | 1,15148841 | + | |
| Cleft lip and palate transmembrane protein 1 | CLPTM1 | 1,15618854 | + | |
| Bleomycin hydrolase | BLMH | 1,15647719 | + | |
| RNA-binding protein with serine-rich domain 1 | RNPS1 | 1,15653102 | + | |
| Coronin-1A | CORO1A;Coro1a | 1,15791215 | + | |
| Sialic acid synthase | NANS | 1,15846146 | + | |
| DNA replication licensing factor MCM2 | MCM2;Mcm2 | 1,1607009 | + | |
| Transaldolase | TALDO1 | 1,16363313 | + | |
| Synaptotagmin-1 | Syt1;SYT1 | 1,16573736 | + | |
| Eukaryotic translation initiation factor 5B | EIF5B | 1,16850323 | + | |

| | | | | |
|---|---|---|---|---|
| Glycine cleavage system H protein, mitochondrial | GCSH | 1,16958915 | + | |
| Vacuolar protein sorting-associated protein 29 | VPS29;vps29 | 1,17153422 | + | |
| Exportin-T | XPOT | 1,17379231 | + | |
| Stomatin-like protein 2, mitochondrial | STOML2 | 1,17472013 | + | |
| Nck-associated protein 1 | NCKAP1;nckap1 | 1,17568694 | + | |
| Chloride intracellular channel protein 4 | CLIC4 | 1,17719523 | + | |
| 26S protease regulatory subunit 8 | PSMC5 | 1,17812665 | + | |
| Importin subunit alpha-1 | KPNA2 | 1,1813221 | + | |
| DNA (cytosine-5)-methyltransferase 1 | DNMT1 | 1,18229421 | + | |
| Calcium-binding mitochondrial carrier protein SCaMC-1 | SLC25A24 | 1,1828732 | + | |

| | | | | |
|---|---|---|---|---|
| Proteasome activator complex subunit 3 | PSME3 | 1,18618562 | + | |
| Serine/threonine-protein phosphatase PGAM5, mitochondrial | PGAM5 | 1,18735949 | + | |
| C-terminal-binding protein 1 | CTBP1 | 1,18810251 | + | |
| Ubiquitin-like modifier-activating enzyme 6 | UBA6 | 1,18917169 | + | |
| Mitochondrial carrier homolog 2 | MTCH2 | 1,18970256 | + | |
| Ribonucleoside-diphosphate reductase subunit M2 | RRM2 | 1,19053099 | + | |
| S-phase kinase-associated protein 1 | SKP1 | 1,19096947 | + | |
| Coatomer subunit gamma-1 | COPG1 | 1,19160737 | + | |
| Exportin-5 | XPO5 | 1,19247754 | + | |

| | | | | |
|---|---|---|---|---|
| Histidine triad nucleotide-binding protein 1 | HINT1 | 1,19640308 | + | |
| Transforming protein RhoA | Rhoa;RHOA;rhoab | 1,20195495 | + | |
| Structural maintenance of chromosomes protein 2 | SMC2 | 1,20228174 | + | |
| LETM1 and EF-hand domain-containing protein 1, mitochondrial | LETM1 | 1,20574273 | + | |
| Double-stranded RNA-binding protein Staufen homolog 1 | STAU1 | 1,21546872 | + | |
| SWI/SNF complex subunit SMARCC1 | SMARCC1;Smarcc1 | 1,21738921 | + | |
| Macrophage migration inhibitory factor | MIF;Mif | 1,21811401 | + | |
| Trifunctional enzyme subunit beta, mitochondrial;3-ketoacyl-CoA thiolase | HADHB | 1,21991603 | + | |

| | | | | |
|---|---|---|---|---|
| E3 ubiquitin-protein ligase UBR4 | UBR4 | 1,22438007 | + | |
| Mitochondrial import receptor subunit TOM40 homolog | TOMM40 | 1,22960154 | + | |
| Structural maintenance of chromosomes flexible hinge domain-containing protein 1 | SMCHD1 | 1,23066839 | + | |
| SUMO-conjugating enzyme UBC9 | Ube2i;UBE2I | 1,23218918 | + | |
| Eukaryotic translation initiation factor 5 | EIF5 | 1,2381293 | + | |
| 1-phosphatidylinositol 4,5-bisphosphate phosphodiesterase gamma-1 | PLCG1 | 1,24022484 | + | |
| Methylsterol monooxygenase 1 | MSMO1 | 1,24659877 | + | |
| Tryptophan--tRNA ligase, | WARS | 1,24817318 | + | |

| | | | | |
|---|---|---|---|---|
| cytoplasmic;T1-TrpRS;T2-TrpRS | | | | |
| Microtubule-associated protein RP/EB family member 2 | MAPRE2 | 1,24869453 | + | |
| Symplekin | SYMPK | 1,24962786 | + | |
| Glyoxylate reductase/hydroxypyruvate reductase | GRHPR | 1,24965096 | + | |
| 4-trimethylaminobutyraldehyde dehydrogenase | ALDH9A1 | 1,25107638 | + | |
| N-alpha-acetyltransferase 15, NatA auxiliary subunit | NAA15 | 1,26060253 | + | |
| tRNA (cytosine(34)-C(5))-methyltransferase | NSUN2 | 1,26419301 | + | |
| Ribose-phosphate pyrophosphokinase 1 | PRPS1 | 1,26651658 | + | |

| | | | | |
|---|---|---|---|---|
| Eukaryotic translation initiation factor 5A-1;Eukaryotic translation initiation factor 5A-1-like;Eukaryotic translation initiation factor 5A-2 | EIF5A;EIF5AL1;EIF5A2;Eif5a2 | 1,26715575 | + | |
| Gamma-glutamyl hydrolase | GGH | 1,26757537 | + | |
| Rab GTPase-activating protein 1 | RABGAP1 | 1,26782735 | + | |
| CUGBP Elav-like family member 1 | CELF1;Celf1 | 1,27082994 | + | |
| Nuclear pore complex protein Nup93 | NUP93 | 1,27744166 | + | |
| Tubulin polymerization-promoting protein family member 3 | TPPP3 | 1,27820799 | + | |
| Importin subunit alpha-4 | Kpna3;KPNA3 | 1,27962981 | + | |
| Double-stranded RNA-binding | STAU2 | 1,28062312 | + | |

| | | | | |
|---|---|---|---|---|
| protein Staufen homolog 2 | | | | |
| Small nuclear ribonucleoprotein Sm D1 | SNRPD1 | 1,28078588 | + | |
| 26S proteasome non-ATPase regulatory subunit 7 | PSMD7 | 1,29013634 | + | |
| SH3 and PX domain-containing protein 2B | SH3PXD2B | 1,29430347 | + | |
| EH domain-containing protein 1 | EHD1 | 1,29486889 | + | |
| Creatine kinase U-type, mitochondrial | CKMT1A | 1,29677412 | + | |
| AP-1 complex subunit beta-1 | AP1B1;Ap1b1 | 1,29709562 | + | |
| Echinoderm microtubule-associated protein-like 4 | EML4 | 1,29756249 | + | |
| Transportin-1 | TNPO1 | 1,2988063 | + | |
| Junction plakoglobin | JUP | 1,30739339 | + | |

| | | | | |
|---|---|---|---|---|
| Polyadenylate-binding protein-interacting protein 1 | PAIP1 | 1,3093124 | + | |
| Spermidine synthase | SRM | 1,31046973 | + | |
| Superoxide dismutase [Mn], mitochondrial | SOD2 | 1,31601312 | + | |
| Calponin-2 | CNN2 | 1,32280413 | + | |
| Proline-, glutamic acid- and leucine-rich protein 1 | PELP1 | 1,32325384 | + | |
| Nodal modulator 2;Nodal modulator 3;Nodal modulator 1 | NOMO2;NOMO3; NOMO1 | 1,33712133 | + | |
| DNA replication licensing factor MCM5 | MCM5 | 1,34007666 | + | |
| Fructose-bisphosphate aldolase C | ALDOC | 1,34261025 | + | |
| Phosphomevalonate kinase | PMVK | 1,3451182 | + | |
| Leucine--tRNA ligase, cytoplasmic | LARS | 1,3463548 | + | |

| | | | | |
|---|---|---|---|---|
| GMP synthase [glutamine-hydrolyzing] | GMPS | 1,34731123 | + | |
| Vacuolar protein sorting-associated protein 26A | VPS26A | 1,34943602 | + | |
| Acylglycerol kinase, mitochondrial | AGK | 1,35339419 | + | |
| Sterol-4-alpha-carboxylate 3-dehydrogenase, decarboxylating | NSDHL | 1,35563893 | + | |
| Replication factor C subunit 2 | RFC2;Rfc2 | 1,36727333 | + | |
| Phosphoribosyl pyrophosphate synthase-associated protein 2 | PRPSAP2 | 1,37010574 | + | |
| Translationally-controlled tumor protein | TPT1 | 1,37118318 | + | |
| L-lactate dehydrogenase A chain | LDHA | 1,37382317 | + | |
| Serotransferrin | TF | 1,37452168 | + | |

| | | | | |
|---|---|---|---|---|
| rRNA 2-O-methyltransferase fibrillarin | FBL | 1,37890095 | + | |
| Cilia- and flagella-associated protein 20 | CFAP20 | 1,38244353 | + | |
| Asparagine synthetase [glutamine-hydrolyzing] | ASNS | 1,38304392 | + | |
| Myelin expression factor 2 | MYEF2 | 1,38640277 | + | |
| Ubiquitin carboxyl-terminal hydrolase isozyme L5 | UCHL5 | 1,3929437 | + | |
| NAD(P) transhydrogenase, mitochondrial | NNT | 1,39506065 | + | |
| Serine/threonine-protein kinase VRK1 | VRK1 | 1,3966287 | + | |
| BolA-like protein 2 | BOLA2 | 1,39900398 | + | |
| Serine/threonine-protein phosphatase PP1-alpha catalytic subunit | PPP1CA | 1,40087403 | + | |

| | | | | |
|---|---|---|---|---|
| 40S ribosomal protein S15a | RPS15A | 1,40176688 | + | |
| DNA replication licensing factor MCM3 | MCM3 | 1,4035812 | + | |
| Programmed cell death 6-interacting protein | PDCD6IP | 1,40365707 | + | |
| Aldose reductase | AKR1B1 | 1,40620316 | + | |
| Protein ERGIC-53 | LMAN1 | 1,40865495 | + | |
| Amidophosphoribosyltransferase | PPAT | 1,40898344 | + | |
| AP-3 complex subunit beta-1 | AP3B1 | 1,40919198 | + | |
| V-type proton ATPase 116 kDa subunit a isoform 1 | ATP6V0A1 | 1,4100469 | + | |
| Dihydrofolate reductase | DHFR | 1,41320165 | + | |
| 60S ribosomal protein L10 | RPL10 | 1,42001449 | + | |
| Casein kinase II subunit alpha;Casein kinase II subunit alpha 3 | Csnk2a1;CSNK2A1; CSNK2A3 | 1,42455716 | + | |
| Rabankyrin-5 | ANKFY1 | 1,430201 | + | |

| | | | | |
|---|---|---|---|---|
| Lactoylglutathione lyase | GLO1 | 1,44422616 | + | |
| ATP-dependent 6-phosphofructokinase, liver type | PFKL | 1,44787788 | + | |
| DnaJ homolog subfamily B member 11 | DNAJB11 | 1,44850201 | + | |
| Cytochrome b5 type B | CYB5B | 1,4577891 | + | |
| ATP-binding cassette sub-family E member 1 | ABCE1 | 1,46688165 | + | |
| Neural cell adhesion molecule L1 | L1CAM | 1,46708934 | + | |
| Beta-soluble NSF attachment protein | NAPB | 1,46821361 | + | |
| Superkiller viralicidic activity 2-like 2 | SKIV2L2 | 1,47076183 | + | |
| Histone-arginine methyltransferase CARM1 | CARM1 | 1,47321447 | + | |
| AP-3 complex subunit mu-1 | AP3M1 | 1,47604307 | + | |

| | | | | |
|---|---|---|---|---|
| Signal transducer and activator of transcription 1-alpha/beta | STAT1 | 1,4764542 | + | |
| Copine-1 | CPNE1 | 1,48263359 | + | |
| Single-stranded DNA-binding protein, mitochondrial | SSBP1 | 1,48416011 | + | |
| Thioredoxin reductase 1, cytoplasmic | TXNRD1 | 1,48630291 | + | |
| Lethal(2) giant larvae protein homolog 1 | LLGL1;Llgl1 | 1,48706245 | + | |
| Glutamine--fructose-6-phosphate aminotransferase [isomerizing] 1 | GFPT1 | 1,4924433 | + | |
| Plastin-3 | PLS3 | 1,49344381 | + | |
| Ankyrin-2 | ANK2 | 1,49850718 | + | |
| 3-ketoacyl-CoA thiolase, mitochondrial | ACAA2 | 1,49996482 | + | |
| Dolichyl-diphosphooligosaccharide--protein | Dad1;DAD1 | 1,50628026 | + | |

| | | | | |
|---|---|---|---|---|
| glycosyltransferase subunit DAD1 | | | | |
| Cysteine and glycine-rich protein 2 | CSRP2 | 1,51664988 | + | |
| Ribonucleoside-diphosphate reductase large subunit | RRM1 | 1,51934963 | + | |
| Ras-related protein Rab-2B | RAB2B | 1,52369372 | + | |
| Small nuclear ribonucleoprotein Sm D3 | SNRPD3 | 1,52862612 | + | |
| Vesicle-trafficking protein SEC22b | SEC22B | 1,53125276 | + | |
| Ubiquitin carboxyl-terminal hydrolase 10 | USP10 | 1,53869883 | + | |
| Eukaryotic peptide chain release factor subunit 1 | ETF1 | 1,54195086 | + | |
| Ras GTPase-activating-like protein IQGAP1 | IQGAP1 | 1,54405997 | + | |
| Aminoacyl tRNA synthase complex-interacting | AIMP1 | 1,55432426 | + | |

| | | | | |
|---|---|---|---|---|
| multifunctional protein 1;Endothelial monocyte-activating polypeptide 2 | | | | |
| ADP-ribosylation factor 1;ADP-ribosylation factor 3 | Arf1;ARF1;ARF3 | 1,562301 | + | |
| ATPase family AAA domain-containing protein 1;ATPase family AAA domain-containing protein 1-B | ATAD1;atad1b | 1,56366009 | + | |
| Condensin complex subunit 1 | NCAPD2 | 1,57342254 | + | |
| Putative ATP-dependent RNA helicase DHX30 | DHX30 | 1,57458687 | + | |
| DnaJ homolog subfamily A member 1 | DNAJA1;Dnaja1 | 1,57503446 | + | |
| Transcription elongation factor B polypeptide 1 | TCEB1 | 1,58280585 | + | |

| | | | | |
|---|---|---|---|---|
| 2-oxoglutarate dehydrogenase, mitochondrial | OGDH | 1,59054989 | + | |
| RNA-binding protein 4 | RBM4 | 1,59804175 | + | |
| CDGSH iron-sulfur domain-containing protein 2 | CISD2;Cisd2 | 1,60473484 | + | |
| COP9 signalosome complex subunit 2 | COPS2 | 1,61503855 | + | |
| Four and a half LIM domains protein 1 | FHL1;Fhl1 | 1,61602105 | + | |
| 26S proteasome non-ATPase regulatory subunit 12 | PSMD12 | 1,61712053 | + | |
| Eukaryotic translation initiation factor 3 subunit I | EIF3I | 1,63669247 | + | |
| NHP2-like protein 1;NHP2-like protein 1, N-terminally processed | NHP2L1 | 1,64543682 | + | |
| mRNA export factor | RAE1 | 1,64564217 | + | |

| | | | | |
|---|---|---|---|---|
| Cancer-related nucleoside-triphosphatase | NTPCR | 1,65407817 | + | |
| Serine/threonine-protein phosphatase 2A 56 kDa regulatory subunit epsilon isoform | PPP2R5E | 1,65412649 | + | |
| DNA replication licensing factor MCM7 | MCM7 | 1,66373634 | + | |
| 60S ribosomal protein L27 | RPL27 | 1,66913626 | + | |
| 26S proteasome non-ATPase regulatory subunit 5 | PSMD5 | 1,67783546 | + | |
| Acetyl-CoA acetyltransferase, cytosolic | ACAT2 | 1,68484137 | + | |
| Solute carrier family 2, facilitated glucose transporter member 1 | SLC2A1 | 1,7083274 | + | |
| Perilipin-3 | PLIN3 | 1,71646457 | + | |

| | | | | |
|---|---|---|---|---|
| Delta(24)-sterol reductase | DHCR24 | 1,73236232 | + | |
| FAS-associated factor 2 | FAF2 | 1,73505211 | + | |
| Heat shock 70 kDa protein 4L | HSPA4L | 1,7407928 | + | |
| Glypican-4;Secreted glypican-4 | GPC4 | 1,75487497 | + | |
| Small nuclear ribonucleoprotein-associated proteins B and B | SNRPB | 1,75680796 | + | |
| Importin subunit alpha-5;Importin subunit alpha-5, N-terminally processed | KPNA1;Kpna1 | 1,76424514 | + | |
| Myotrophin | MTPN | 1,7719858 | + | |
| Aminoacyl tRNA synthase complex-interacting multifunctional protein 2 | AIMP2 | 1,78462558 | + | |
| Thioredoxin | TXN | 1,79231008 | + | |

| | | | | |
|---|---|---|---|---|
| Actin-related protein 2/3 complex subunit 4 | Arpc4;ARPC4 | 1,79283778 | + | |
| 40S ribosomal protein S27-like | RPS27L | 1,79476293 | + | |
| Eukaryotic initiation factor 4A-II;Eukaryotic initiation factor 4A-II, N-terminally processed | EIF4A2 | 1,8018411 | + | |
| S-adenosylmethionine synthase isoform type-2 | MAT2A | 1,80378787 | + | |
| Leucine-rich repeat-containing protein 40 | LRRC40 | 1,80677817 | + | |
| LIM and SH3 domain protein 1 | LASP1 | 1,80794885 | + | |
| Elongation factor 1-alpha 2 | EEF1A2;Eef1a2 | 1,80938085 | + | |
| Small glutamine-rich tetratricopeptide repeat-containing protein alpha | SGTA | 1,82048522 | + | |

| | | | | |
|---|---|---|---|---|
| D-3-phosphoglycerate dehydrogenase | PHGDH | 1,82128949 | + | |
| Actin-like protein 6A | ACTL6A;Actl6a | 1,82179472 | + | |
| Histone-binding protein RBBP7 | RBBP7 | 1,86049122 | + | |
| Ran-specific GTPase-activating protein | RANBP1;Ranbp1 | 1,8705438 | + | |
| BUB3-interacting and GLEBS motif-containing protein ZNF207 | ZNF207 | 1,87806087 | + | |
| Unconventional myosin-Ib | MYO1B | 1,88188214 | + | |
| Pyruvate dehydrogenase E1 component subunit alpha, somatic form, mitochondrial | PDHA1 | 1,88665432 | + | |
| Ras-related protein Rab-6B | RAB6B | 1,91266653 | + | |
| Mitochondrial glutamate carrier 1;Mitochondrial glutamate carrier 2 | SLC25A22;SLC25A18 | 1,91282908 | + | |

| | | | | |
|---|---|---|---|---|
| Gamma-synuclein | SNCG | 1,91344664 | + | |
| Tyrosine-protein phosphatase non-receptor type 1 | PTPN1 | 1,91481972 | + | |
| Ras-related protein Rab-10 | RAB10 | 1,94398859 | + | |
| Translational activator GCN1 | GCN1L1 | 1,94721307 | + | |
| DNA mismatch repair protein Msh6 | MSH6 | 1,95109749 | + | |
| Activator of 90 kDa heat shock protein ATPase homolog 1 | AHSA1 | 1,95730146 | + | |
| Aldehyde dehydrogenase family 16 member A1 | ALDH16A1 | 1,98171404 | + | |
| Phosphoribosylformylglycinamidine synthase | PFAS | 1,99841309 | + | |
| Thymidylate synthase | TYMS | 1,99952147 | + | |
| Medium-chain specific acyl-CoA dehydrogenase, mitochondrial | ACADM | 2,0000568 | + | |

| | | | | |
|---|---|---|---|---|
| Peptidyl-prolyl cis-trans isomerase-like 1 | PPIL1 | 2,01126713 | + | |
| Inorganic pyrophosphatase | PPA1 | 2,02653122 | + | |
| Protein FAM98B | FAM98B | 2,05904028 | + | |
| Phospholipid hydroperoxide glutathione peroxidase, mitochondrial | GPX4 | 2,06965658 | + | |
| Protein NipSnap homolog 1 | NIPSNAP1;Nipsnap 1 | 2,08286815 | + | |
| Histone deacetylase 2 | HDAC2;Hdac2 | 2,13791275 | + | |
| Cellular retinoic acid-binding protein 2 | CRABP2 | 2,14412202 | + | |
| Eukaryotic translation initiation factor 2 subunit 2 | EIF2S2 | 2,14471118 | + | |
| 26S proteasome non-ATPase regulatory subunit 6 | PSMD6 | 2,15996827 | + | |

| | | | | |
|---|---|---|---|---|
| Adenylate kinase isoenzyme 1 | AK1 | 2,16386965 | + | |
| Dynein light chain 2, cytoplasmic | DYNLL2 | 2,23186874 | + | |
| GTP-binding protein SAR1a | SAR1A | 2,24796465 | + | |
| Tricarboxylate transport protein, mitochondrial | SLC25A1 | 2,28178279 | + | |
| Ubiquitin-conjugating enzyme E2 N;Ubiquitin-conjugating enzyme E2 35;Ubiquitin-conjugating enzyme E2 36;Putative ubiquitin-conjugating enzyme E2 N-like | UBE2N;Ube2n;UBC35;UBC36;UBE2NL | 2,29580328 | + | |
| Signal recognition particle 9 kDa protein | SRP9 | 2,31755235 | + | |
| DNA topoisomerase 2-alpha | TOP2A | 2,34728707 | + | |

| | | | | |
|---|---|---|---|---|
| Saccharopine dehydrogenase-like oxidoreductase | SCCPDH | 2,37124464 | + | |
| Peroxiredoxin-4 | PRDX4;Prdx4 | 2,38741154 | + | |
| 60S ribosomal protein L26;60S ribosomal protein L26-like 1 | RPL26;RPL26L1 | 2,44196616 | + | |
| Thymidylate kinase | DTYMK | 2,60647668 | + | |
| L-xylulose reductase | DCXR | 2,62080744 | + | |
| Tubulin alpha-1B chain;Tubulin alpha-4A chain | TUBA1B;TUBA4A | 2,72059165 | + | |

***Table 10.*** *List of the 118 dysregulated proteins in p.A53T neurons that were restored upon treatment with BX795.*

| **Gene Name** | **Protein Name** | **Biological Process** | **-Log ANOVA p value** | **ANOVA q-value** |
|---|---|---|---|---|
| SH3GL1 | Endophilin-A2 | Cell Membrane | 256.133 | 0,011476 |
| MIF | Macrophage migration inhibitory factor | Cytokine | 180.931 | 0,0363767 |
| ACTR2 | Actin-related protein 2 | Cytoskeleton | 194.818 | 0,030058 |

| | | | | |
|---|---|---|---|---|
| CAPZB | F-actin-capping protein subunit beta | Cytoskeleton | 46.958 | 0,000648649 |
| DYNLL2 | Dynein light chain 2, cytoplasmic | Cytoskeleton | 278.624 | 0,00791795 |
| JUP | Junction plakoglobin | Cytoskeleton | 184.446 | 0,0338618 |
| MARCKSL1 | MARCKS-related protein | Cytoskeleton | 182.146 | 0,0355364 |
| SNCG | Gamma-synuclein | Cytoskeleton | 369.107 | 0,0025 |
| TUBB | Tubulin beta chain | Cytoskeleton | 328.033 | 0,004 |
| HAT1 | Histone acetyltransferase type B catalytic subunit | DNA Organization | 193.087 | 0,0303367 |
| ACO2 | Aconitate hydratase, mitochondrial | Metabolism | 239.553 | 0,0147068 |
| ACP1 | Low molecular weight phosphotyrosine protein phosphatase | Metabolism | 223.884 | 0,0187195 |
| ALDOC | Fructose-bisphosphate aldolase C | Metabolism | 19.283 | 0,0305445 |

| | | | | |
|---|---|---|---|---|
| DCXR | L-xylulose reductase | Metabolism | 450.627 | 0,000888889 |
| DTYMK | Thymidylate kinase | Metabolism | 429.648 | 0,00128302 |
| GPX4 | Phospholipid hydroperoxide glutathione peroxidase, mitochondrial | Metabolism | 313.215 | 0,00468571 |
| MSMO1 | Methylsterol monooxygenase 1 | Metabolism | 23.571 | 0,0159706 |
| NANS | Sialic acid synthase | Metabolism | 197.987 | 0,0284313 |
| OGDH | 2-oxoglutarate dehydrogenase, mitochondrial | Metabolism | 189.588 | 0,0314673 |
| TSTA3 | GDP-L-fucose synthase | Metabolism | 471.268 | 0,000666667 |
| ALDH5A1 | Succinate-semialdehyde dehydrogenase, mitochondrial | Neuronal | 281.456 | 0,00780645 |
| ATXN10 | Ataxin-10 | Neuronal | 36.278 | 0,00266667 |
| INA | Alpha-internexin | Neuronal | 261.725 | 0,0103014 |
| NIPSNAP1 | Protein NipSnap homolog 1 | Neuronal | 201.319 | 0,0272045 |
| PAFAH1B1 | Platelet-activating factor | Neuronal | 416.529 | 0,00144262 |

| | | | | |
|---|---|---|---|---|
| | acetylhydrolase IB subunit alpha | | | |
| SYN1 | Synapsin-1 | Neuronal | 282.487 | 0,00773913 |
| HIST1H1E | Histone H1.4 | Nuclear Assembly | 462.922 | 0,000682927 |
| TMPO | Lamina-associated polypeptide 2, isoform alpha;Thymopoietin;Thymopentin | Nuclear Assembly | 273.826 | 0,00829268 |
| ACADM | Medium-chain specific acyl-CoA dehydrogenase, mitochondrial | Oxidative Stress | 361.925 | 0,00273684 |
| CKMT1A | Creatine kinase U-type, mitochondrial | Oxidative Stress | 169.957 | 0,0433538 |
| GOT2 | Aspartate aminotransferase, mitochondrial | Oxidative Stress | 195.739 | 0,0293862 |
| GPX1 | Glutathione peroxidase 1 | Oxidative Stress | 256.414 | 0,0115088 |
| MDH2 | Malate dehydrogenase, mitochondrial | Oxidative Stress | 325.647 | 0,00410256 |
| MTCH2 | Mitochondrial carrier homolog 2 | Oxidative Stress | 2.402 | 0,0146818 |

| | | | | |
|---|---|---|---|---|
| PDHA1 | Pyruvate dehydrogenase E1 component subunit alpha, somatic form, mitochondrial | Oxidative Stress | 222.971 | 0,0189673 |
| STOML2 | Stomatin-like protein 2, mitochondrial | Oxidative Stress | 313.378 | 0,00475362 |
| TOMM70A | Mitochondrial import receptor subunit TOM70 | Oxidative Stress | 181.295 | 0,0362534 |
| ATP1B1 | Sodium/potassium -transporting ATPase subunit beta-1 | Plasma Membrane | 192.654 | 0,0305888 |
| ANKFY1 | Rabankyrin-5 | Protein Modification and Transport | 23.323 | 0,0163 |
| AP3M1 | AP-3 complex subunit mu-1 | Protein Modification and Transport | 178.641 | 0,0375263 |
| ATP6V0D1 | V-type proton ATPase subunit d 1 | Protein Modification and Transport | 186.993 | 0,0326792 |
| CCT8 | T-complex protein 1 subunit theta | Protein Modification and Transport | 449.206 | 0,000956522 |

| | | | | |
|---|---|---|---|---|
| CKAP4 | Cytoskeleton-associated protein 4 | Protein Modification and Transport | 271.468 | 0,00867308 |
| DAD1 | Dolichyl-diphosphooligosaccharide--protein glycosyltransferase subunit DAD1 | Protein Modification and Transport | 270.969 | 0,00872381 |
| GDI2 | Rab GDP dissociation inhibitor beta | Protein Modification and Transport | 194.495 | 0,0300524 |
| LAP3 | Cytosol aminopeptidase | Protein Modification and Transport | 19.891 | 0,0281967 |
| NAPB | Beta-soluble NSF attachment protein | Protein Modification and Transport | 263.779 | 0,00978802 |
| OGT | UDP-N-acetylglucosamine--peptide N-acetylglucosaminyl transferase 110 kDa subunit | Protein Modification and Transport | 216.824 | 0,0208777 |
| PACSIN2 | Protein kinase C and casein kinase substrate in neurons protein 2 | Protein Modification and Transport | 286.533 | 0,00715556 |

| | | | | |
|---|---|---|---|---|
| PLIN3 | Perilipin-3 | Protein Modification and Transport | 167.058 | 0,0455219 |
| RAB2B | Ras-related protein Rab-2B | Protein Modification and Transport | 377.583 | 0,00245783 |
| SAR1A | GTP-binding protein SAR1a | Protein Modification and Transport | 227.985 | 0,0173559 |
| SEC22B | Vesicle-trafficking protein SEC22b | Protein Modification and Transport | 189.207 | 0,0317391 |
| SRP9 | Signal recognition particle 9 kDa protein | Protein Modification and Transport | 357.866 | 0,00273469 |
| YKT6 | Synaptobrevin homolog YKT6 | Protein Modification and Transport | 201.411 | 0,0271685 |
| AIMP2 | Aminoacyl tRNA synthase complex-interacting multifunctional protein 2 | Protein Synthesis | 540.207 | 0,00032 |
| EEF1D | Elongation factor 1-delta | Protein Synthesis | 24.002 | 0,0146566 |
| EIF2B4 | Translation initiation factor | Protein Synthesis | 277.038 | 0,00814141 |

| | | | | |
|---|---|---|---|---|
| | eIF-2B subunit delta | | | |
| EIF4G2 | Eukaryotic translation initiation factor 4 gamma 2 | Protein Synthesis | 325.565 | 0,00403361 |
| FAM98B | Protein FAM98B | Protein Synthesis | 302.174 | 0,00571795 |
| GTPBP4 | Nucleolar GTP-binding protein 1 | Protein Synthesis | 178.873 | 0,0375154 |
| KARS | Lysine--tRNA ligase | Protein Synthesis | 359.204 | 0,00272165 |
| MAT2A | S-adenosylmethionine synthase isoform type-2 | Protein Synthesis | 350.993 | 0,00290196 |
| PHGDH | D-3-phosphoglycerate dehydrogenase | Protein Synthesis | 106.486 | 0 |
| PPA1 | Inorganic pyrophosphatase | Protein Synthesis | 203.525 | 0,0261486 |
| PRMT1 | Protein arginine N-methyltransferase 1 | Protein Synthesis | 558.198 | 0,000190476 |
| RARS | Arginine--tRNA ligase, cytoplasmic | Protein Synthesis | 34.511 | 0,00316981 |
| RPL12 | 60S ribosomal protein L12 | Protein Synthesis | 236.748 | 0,0156444 |

| | | | | |
|---|---|---|---|---|
| RPL31 | 60S ribosomal protein L31 | Protein Synthesis | 241.579 | 0,0145385 |
| RPS3 | 40S ribosomal protein S3 | Protein Synthesis | 321.674 | 0,0043252 |
| RPS6 | 40S ribosomal protein S6 | Protein Synthesis | 295.529 | 0,0064878 |
| RTCB | tRNA-splicing ligase RtcB homolog | Protein Synthesis | 347.921 | 0,00303846 |
| VARS | Valine--tRNA ligase | Protein Synthesis | 302.941 | 0,00571429 |
| WARS | Tryptophan--tRNA ligase, cytoplasmic;T1-TrpRS;T2-TrpRS | Protein Synthesis | 233.632 | 0,0162437 |
| DEK | Protein DEK | RNA Metabolism | 19.105 | 0,0308276 |
| HINT1 | Histidine triad nucleotide-binding protein 1 | RNA Metabolism | 417.925 | 0,00135593 |
| HNRNPUL1 | Heterogeneous nuclear ribonucleoprotein U-like protein 1 | RNA Metabolism | 213.047 | 0,0220917 |
| MYEF2 | Myelin expression factor 2 | RNA Metabolism | 178.281 | 0,0377856 |
| NHP2L1 | NHP2-like protein 1;NHP2-like protein 1, N- | RNA Metabolism | 395.001 | 0,00191781 |

| | | | | |
|---|---|---|---|---|
| | terminally processed | | | |
| NUP93 | Nuclear pore complex protein Nup93 | RNA Metabolism | 290.302 | 0,00691954 |
| PCBP1 | Poly(rC)-binding protein 1 | RNA Metabolism | 617.692 | 0 |
| PCBP2 | Poly(rC)-binding protein 2 | RNA Metabolism | 242.141 | 0,0143938 |
| RAE1 | mRNA export factor | RNA Metabolism | 231.102 | 0,0169645 |
| RBM4 | RNA-binding protein 4 | RNA Metabolism | 23.421 | 0,0162464 |
| RRM2 | Ribonucleoside-diphosphate reductase subunit M2 | RNA Metabolism | 311.101 | 0,00472222 |
| SKIV2L2 | Superkiller viralicidic activity 2-like 2 | RNA Metabolism | 395.007 | 0,00194444 |
| SNRPB | Small nuclear ribonucleoprotein-associated proteins B and B | RNA Metabolism | 19.464 | 0,0300842 |
| UBTF | Nucleolar transcription factor 1 | RNA Metabolism | 252.596 | 0,0123729 |

| | | | | |
|---|---|---|---|---|
| YLPM1 | YLP motif-containing protein 1 | RNA Metabolism | 347.249 | 0,00304762 |
| ZNF207 | BUB3-interacting and GLEBS motif-containing protein ZNF207 | RNA Metabolism | 280.434 | 0,00785263 |
| API5 | Apoptosis inhibitor 5 | Signal Transduction | 192.253 | 0,03041 |
| BOLA2 | BolA-like protein 2 | Signal Transduction | 243.992 | 0,0139765 |
| CRABP2 | Cellular retinoic acid-binding protein 2 | Signal Transduction | 652.555 | 0 |
| CSK | Tyrosine-protein kinase CSK | Signal Transduction | 302.647 | 0,00570323 |
| MTPN | Myotrophin | Signal Transduction | 536.379 | 0,000307692 |
| STAT1 | Signal transducer and activator of transcription 1-alpha/beta | Signal Transduction | 250.904 | 0,0127197 |
| ZYX | Zyxin | Signal Transduction | 323.528 | 0,00406557 |
| ATG4B | Cysteine protease ATG4B | Stress Response | 30.765 | 0,00512752 |
| CUL1 | Cullin-1 | Stress Response | 205.844 | 0,0253684 |

| | | | | |
|---|---|---|---|---|
| DNAJA1 | DnaJ homolog subfamily A member 1 | Stress Response | 264.155 | 0,00980465 |
| DNAJB11 | DnaJ homolog subfamily B member 11 | Stress Response | 234.026 | 0,0161727 |
| DNM2 | Dynamin-2 | Stress Response | 185.961 | 0,0332459 |
| GCN1L1 | Translational activator GCN1 | Stress Response | 57.176 | 0 |
| HSPA4 | Heat shock 70 kDa protein 4 | Stress Response | 325.383 | 0,004 |
| OTUB1 | Ubiquitin thioesterase OTUB1 | Stress Response | 351.675 | 0,00289109 |
| PDCD6IP | Programmed cell death 6-interacting protein | Stress Response | 300.728 | 0,00585987 |
| PSMA3 | Proteasome subunit alpha type-3 | Stress Response | 318.164 | 0,00443077 |
| PSMD12 | 26S proteasome non-ATPase regulatory subunit 12 | Stress Response | 269.053 | 0,00904265 |
| PSME3 | Proteasome activator complex subunit 3 | Stress Response | 331.891 | 0,00378947 |

| | | | | |
|---|---|---|---|---|
| PTPN1 | Tyrosine-protein phosphatase non-receptor type 1 | Stress Response | 349.068 | 0,00291262 |
| SGTA | Small glutamine-rich tetratricopeptide repeat-containing protein alpha | Stress Response | 191.864 | 0,0304814 |
| STIP1 | Stress-induced-phosphoprotein 1 | Stress Response | 303.961 | 0,00565789 |
| TCP1 | T-complex protein 1 subunit alpha | Stress Response | 480.438 | 0,000685714 |
| UBA6 | Ubiquitin-like modifier-activating enzyme 6 | Stress Response | 226.136 | 0,0179532 |
| UCHL1 | Ubiquitin carboxyl-terminal hydrolase isozyme L1 | Stress Response | 555.947 | 0,000181818 |
| VCP | Transitional endoplasmic reticulum ATPase | Stress Response | 263.882 | 0,00983333 |
| VPS35 | Vacuolar protein sorting-associated protein 35 | Stress Response | 303.784 | 0,00564706 |
| TPD52L2 | Tumor protein D54 | Unknown | 19.239 | 0,0305592 |

***Table 11.*** *GO analysis for cellular compartment between pA53T and control neurons.*

| Cellular Compartment | No of genes | P-Value | Bonferroni |
|---|---|---|---|
| extracellular exosome | 299 | 1,6E-75 | 1,0E-72 |
| membrane | 204 | 2,8E-38 | 1,7E-35 |
| nucleoplasm | 230 | 7,9E-36 | 4,8E-33 |
| cytoplasm | 334 | 2,2E-32 | 1,3E-29 |
| mitochondrion | 118 | 1,6E-19 | 9,5E-17 |
| nucleus | 292 | 6,3E-15 | 3,9E-12 |
| nuclear pore | 22 | 6,7E-14 | 4,1E-11 |
| intracellular ribonucleoprotein complex | 29 | 7,5E-14 | 4,6E-11 |
| nucleosome | 23 | 2,4E-12 | 1,4E-9 |
| nuclear chromosome, telomeric region | 26 | 8,1E-12 | 4,9E-9 |
| nuclear nucleosome | 16 | 2,1E-11 | 1,3E-8 |
| nuclear envelope | 28 | 2,5E-11 | 1,5E-8 |
| proteasome complex | 18 | 2,8E-11 | 1,7E-8 |
| focal adhesion | 43 | 4,4E-10 | 2,7E-7 |
| eukaryotic translation initiation factor 3 complex | 10 | 2,1E-9 | 1,3E-6 |
| proteasome accessory complex | 9 | 5,6E-8 | 3,4E-5 |
| chaperonin-containing T-complex | 7 | 1,8E-7 | 1,1E-4 |
| nuclear membrane | 27 | 3,3E-7 | 2,0E-4 |
| cell body | 14 | 3,6E-7 | 2,2E-4 |
| proteasome regulatory particle | 7 | 9,3E-7 | 5,7E-4 |

| | | | |
|---|---|---|---|
| eukaryotic translation initiation factor 3 complex, eIF3m | 6 | 1,3E-6 | 7,8E-4 |
| axon cytoplasm | 10 | 3,40E-06 | 7,3E-5 |

***Table 12.*** *Nucleosome assembly proteins.*

| **Protein Name** | **Gene Name** | **Difference** |
|---|---|---|
| H3 histone family member 3A(H3F3A) | H3F3A | -2,8312081 |
| histone cluster 1 H3 family member a(HIST1H3A) | HIST1H3A | -2,8312081 |
| histone cluster 1 H3 family member b(HIST1H3B) | Hist1h3b | -2,8312081 |
| histone cluster 2 H3 family member a(HIST2H3A) | HIST2H3A | -2,8312081 |
| histone cluster 3 H3(HIST3H3) | HIST3H3 | -2,8312081 |
| histone cluster 1 H1 family member e(HIST1H1E) | HIST1H1E | -1,9652229 |
| H2B histone family member S(H2BFS) | H2BFS | -1,3235741 |
| histone cluster 1 H2B family member a(HIST1H2BA) | HIST1H2BA | -1,3235741 |
| histone cluster 1 H2B family member b(HIST1H2BB) | Hist1h2bb | -1,3235741 |

| | | |
|---|---|---|
| histone cluster 1 H2B family member c(HIST1H2BC) | HIST1H2BC | -1,3235741 |
| histone cluster 1 H2B family member d(HIST1H2BD) | HIST1H2BD | -1,3235741 |
| histone cluster 1 H2B family member f(HIST1H2BF) | Hist1h2bf | -1,3235741 |
| histone cluster 1 H2B family member h(HIST1H2BH) | Hist1h2bh | -1,3235741 |
| histone cluster 1 H2B family member k(HIST1H2BK) | HIST1H2BK | -1,3235741 |
| histone cluster 1 H2B family member l(HIST1H2BL) | HIST1H2BL | -1,3235741 |
| histone cluster 1 H2B family member m(HIST1H2BM) | Hist1h2bm | -1,3235741 |
| histone cluster 1 H2B family member n(HIST1H2BN) | HIST1H2BN | -1,3235741 |
| histone cluster 2 H2B family member f(HIST2H2BF) | HIST2H2BF | -1,3235741 |
| histone cluster 1 H1 family member b(HIST1H1B) | HIST1H1B | -1,320744 |
| histone cluster 1 H1 family member c(HIST1H1C) | Hist1h1c | -1,0066352 |
| histone cluster 1 H1 family member d(HIST1H1D) | Hist1h1d | -1,0066352 |
| heterochromatin protein 1 binding protein 3(HP1BP3) | HP1BP3 | -0,8114175 |

| | | |
|---|---|---|
| histone cluster 1 H4 family member a(HIST1H4A) | HIST1H4A | -0,4979729 |

## 6. DISCUSSION

### 6.1 Main findings and discussion

The generation of human models based on patient-derived iPSCs has opened up new perspectives for investigation of disease mechanisms and the discovery of new therapeutics. Importantly, it allows for identification of early, potentially instigating, disease mechanisms that cannot be observed in human post-mortem brain, which reflects an end-point of the pathology. Given that PD starts many years before the onset of clinical manifestations, iPSC-based models provide an opportunity to understand the early phases of pathology and identify the primary pathways affected. In this work, we used a well-characterized human model of p.A53T pathology that displays early disease-associated phenotypes [312], to screen for small molecules with neuroprotective function. Using a phenotypic screen in combination with proteomics profiling, we aimed to illuminate novel disease targets and pathways with potential therapeutic value. We thus identified the multi-kinase inhibitor BX795 as a compound that exerts a consistent and sustainable beneficial effect on patient-derived p.A53T-neurons. Remarkably, we found that a single treatment with BX795 has long-lasting consequences in supporting neuritic growth, limiting αSyn protein aggregate formation and restoring axonal neuropathology

This study represents the first high-content drug discovery screen performed in human p.A53T iPSC-derived neurons to identify candidate therapeutics for PD. Although the first PD patient-derived hiPSCs were generated in 2009 [305], surprisingly only two phenotypic screens have been reported so far in hiPSC-derived PD neurons. To identify disease-modifying agents, Yamaguchi et al. established an imaging-based, semi-automatic, high-throughput assay for quantitative detection of mitochondrial clearance and cell viability in dopaminergic neurons from patients with familial PD having *Parkin* or *PINK1* mutations. After screening 320 pharmacologically active inhibitor compounds the researchers identified 4 hits, MRS1220, tranylcypromine, flunarizine and bromocriptine, that improved the pathological clearance of mitochondria possibly by promoting mitochondrial degradation through the lysosomal system, without further investigating the underlying mechanism [366]. In another study Tabata et al. [367] performed a phenotypic screen in *Parkin* (*PARK2*) patient-derived dopaminergic neurons displaying increased susceptibility to rotenone-induced mitochondrial stress, to identify neuroprotective compounds. From phenotypic screening of an FDA-approved drug library, one voltage-gated calcium channel antagonist, benidipine, was found to suppress rotenone-induced apoptosis [367]. Our study is the third phenotypic screen performed in human iPSC-derived neurons in the field of PD and the only one related to p.A53T pathology.

Using an unbiased screening approach in combination with quantitative proteomics profiling, we were able to show that treatment with BX795 restored proteins associated with key cellular processes, most notably RNA metabolism, protein synthesis and degradation processes, as well as stress response, suggesting that restoration of proteostasis is key for rescuing the neuropathological features in p.A53T-neurons. Dissecting further the pathways affected by BX795, we demonstrated that BX795 modulates the mTORC1 pathway to restrict excessive protein synthesis and facilitate autophagy. Taken together, our data highlight the BX795 kinase inhibitor as a promising compound and candidate therapeutic that ameliorates p.A53T-associated pathology. Moreover, our results show that restoring proteostasis downstream mTOR signaling can have long-term beneficial consequences in cellular health by instigating sustainable constitutive changes.

Considerable progress in understanding the neurotoxic properties of α-Syn has been achieved by exploiting causal mutations resulting in rare familial forms of PD, most notably the p.A53T-αSyn mutation (G209A in the *SNCA* gene) [417, 418]. We and others have shown that disease-associated characteristics can be recapitulated in patient-derived p.A53T-neurons, including axonal degeneration and accumulation of protein inclusions resembling Lewy bodies and neurites [312]. These have been linked to multiple molecular defects in mRNA processing and translation, endocytic and retrograde trafficking [340, 392], protein misfolding, redox homeostasis [314, 334] and the synaptic protein machinery [312]. The p.A53T proteome examined here revealed a profound increase in proteins related to the biological processes of RNA metabolism, protein synthesis, modification and transport, protein clearance and stress response. Notably, the cohort of 118 proteins that was specifically restored in p.A53T-neurons upon treatment with BX795, was associated with these key cellular processes. Whether the dysregulated p.A53T proteome reflects cellular responses to αSyn-mediated pathology or causal defects induced by the expression of mutant αSyn remains an open question that deserves further investigation. Nevertheless, the early neuronal differentiation stage at which our study was conducted argues in favor of causality rather than consequence, further illustrating the value of BX795 as potential therapeutic.

The pathways affected by mutant αSyn in our study have a high similarity with the αSyn connectome reported by Chung et al [392] for mouse neurons, and the predictions of the *in silico* "humanized" map of αSyn proteotoxicity reported in the accompanying study of Khurana et al [340]. Our proteomics analysisidentified perturbations in RNA metabolic processes that initiate at the nucleus and reach the ribosome. Among these, dysregulation of RBPs that has been linked to aggregation processes and the formation of stress granules in multiple neurodegenerative disorders is very prominent [419-422]. In the p.A53T-proteome, proteins involved in mRNA splicing, elongation and export from the nucleus were

significantly upregulated, indicating that a re-organization of nucleosomal components occurs within the nucleus, regulating splicing site accessibility [393, 423]. Nucleosome assembly components were largely downregulated in p.A53T-neurons but all 24 proteins in this group were not affected by BX795 and remained at abnormally low levels compared to control. Looking at these categories collectively along with the strong nuclear component depicted by cellular component enrichment, we speculate that p.A53T-αSyn may affect nuclear processes through its suspected role as a DNA-binding protein or DNA-damage response modulator [424-426].

Alternative mRNA processing greatly increases the dimensions of gene expression through splicing, polyadenylation, targeted localization and post-transcriptional silencing. Neurons take advantage of all these strategies as the brain has the highest levels of alternative splicing compared to any other human tissue [427]. This process has recently been shown to be defective in the PS19 Tau model of Alzheimer's disease, where alternative splicing events affected genes particularly involved in synaptic transmission [428]. Similarly, the p.A53T-proteome suggests that this process could be excessively induced in p.A53T-neurons as a number of RBPs known to be linked to αSyn aggregation have emerged, including ELAV1, ELAV3 and CELF, suggesting a possible association with the abnormal expression of synaptic genes and the defective synaptic connectivity we have previously reported in p.A53T neurons- [312].An excess of mRNAs coming out of the nucleus in p.A53T-neurons could explain the abnormal expression of proteins involved in translation The significant increase of components of the tRNA splicing ligase complex, various aminoacyl-tRNA synthetases, ribosomal subunits and eukaryotic translation initiation factors indicate an enhanced translation of spliced mRNAs. Aberrant protein synthesis has been reported in p.A53T-derived neurons, but in the opposite direction by Khurana et al [340] that might reflect differences in maturation stage.

The mTOR kinase is a master regulator of cellular metabolism that functions in two distinct complexes: mTORC1 and mTORC2 [429] with the first implicated in protein and lipid biosynthesis through a signaling cascade that includes SK6 and 4E-BP1 proteins [430]. Unlike proliferating cells where this pathway is utilized for growth and division, in neurons it acts as a regulator of healthy metabolism and aging [262] with its restriction being associated with prolonged life span and delay of age-related pathologies. p.A53T neurons have increased RPS6, IQGAP1 and RAG-GTPases, components of mTORC1 pathway and this seems to be associated with an increased translation of a subset of mRNAs that are linked to RNA metabolism and the stress response. Similarly, a quantitative proteomics study of a pre-symptomatic p.A53T-αSyn Drosophila model shows significant upregulation of ribosomal proteins in the p.A53T flies [431]. Although the mechanistic link between p.A53T-αSyn and mTORC1 remains to be

established, recent evidence shows that genetic variability in the mTOR pathway contributes to SNCA effects in disease pathogenesis [432].

Concomitantly with promoting protein synthesis mTORC1 acts to repress autophagy through ULK1 phosphorylation. Autophagy has a central role in promoting health and longevity while this process is impaired in neurodegenerative diseases and αSyn pathology [433, 434]. The p.A53T-proteome shows that neurons are under stress as proteins involved in the UPR or the heat-shock stress response, proteasome assembly and regulation, known to be orchestrated by mTORC1 in neurons, are significantly upregulated [262]. Restoration of numerous components of RNA metabolism and protein translation cascades by BX795 is directly related to the diminished stress response that emerges by the lower levels of UPR and heat-shock-associated proteins also conferred by this molecule. In parallel, a significant number of ubiquitin/proteasome-associated proteins were brought back to near control levels. Considering that both the ubiquitin/proteasome system and autophagy share multiple molecular determinants, including ULK1, ATG5, ATG8 and p62, which can be simultaneously and mutually affected in neurodegenerative diseases [435, 436], it becomes evident that BX795 helps misfolded protein clearance by limiting protein synthesis. This is in agreement with its demonstrated ability to decrease protein aggregates in p.A53T-neurons, as shown in this study, along with facilitation of autophagy both in SYSH-5Y cells expressing p.A53T and in patient-derived neurons.

BX795 is a multi-kinase inhibitor that targets numerous pathways, including the kinases TBK1 and PDK1 [385-387, 389]. Although in our system differences in the total or phosphorylated levels of these two kinases were not observed in the presence of BX795 (data not shown), we cannot exclude that its effects are mediated through these two kinases as both are involved in neurodegeneration, mTOR signaling and autophagy [437, 438]. Yet four other PDK1 inhibitors that were included in the Selleck library did not emerge as hits during the screening campaign. TBK1 was recently suggested as a new player linking autophagy and neuroinflammation in ALS [437] and has been shown to activate mTOR directly in response to growth factors [439]. Interestingly, we found that BX795 could inhibit purified recombinant p70 S6K, the major kinase that phosphorylates RPS6 *in vivo*, indicating that the acute effect of the compound on RPS6 in p.A53T-expressing cells could be mediated through inhibition of p70 S6K. It is notable that multiple other inhibitors of mTOR phosphorylation present in the kinase inhibitor library tested (26 in total, including rapamycin), failed to show any protective effects in our system. Considering that BX795 has been proposed to act through distinct mechanisms in different pathologies, future mechanistic studies should reveal its direct targets in p.A53T neurons. Whether these lie within or beyond the kinome is a matter of investigation, as emerging evidence suggests that kinase inhibitors may unintendedly exert their

therapeutic action through non-kinase targets (Nature Reviews Drug Discovery volume 16, pages424–440 2017). Collectively, the work presented here identifies BX795 as a promising compound with therapeutic potential for PD patients and other protein conformational disorders. Further, our experimental approach shed light into the molecular and cellular pathways of αSyn proteotoxicity unveiling new disease targets for the development of combined therapeutics.

**6.2 Future perspectives**

The true translational potential of patient-derived iPSC platforms is just emerging as more large-scale unbiased drug screens are performed that validate the reproducibility and predictive ability of human based cellular systems. The work performed within the framework of this thesis demonstrates that human neurons with disease-associated phenotypic characteristics can be effectively adapted for use in high throughput drug screens. Current advances in the field of iPSC technology including improved protocols for neuronal differentiation, development of co-culture and three-dimensional (3D) systems, or the use of microfluidics or brain-on-chip devices chips could be combined with the current cellular system described here, to increase its value in high throughput screening approaches [440, 441] [349]. An important addition in compound library screening would be to include read-outs for rescue of neuronal functionality, as for example when assessing electrophysiological parameters by high throughput multi-electrode array systems. In combination with genome-wide siRNA libraries, machine learning and better *in silico* predictive tools, such platforms may be further exploited to select novel, more efficient and safer drugs that will enter clinical trials with confidence.

Importantly, our study advocates that human iPSC-based platforms used in early drug discovery can also be instrumental for uncovering disease mechanisms. We could thus identify a neuroprotective molecule that rescues core metabolic pathways, essential for neuronal function. Further *in vitro* and *in vivo* studies in PD models, should provide additional insight into the mechanism of action and the efficacy of BX795 to reveal its full translational potential as a lead PD therapeutic.

To conclude, many hiPSC lines have been generated from patients with familial or sporadic PD uncovering known or previously unrecognized disease-relevant phenotypes that, in many cases, could be effectively restored using small molecules. These investigations have laid the foreground for developing bioassays for screening small or larger chemical libraries in the search of lead compounds that may evolve into PD disease-modifying therapeutics. However, robust assays are still need to be established before hiPSC-based systems become more easily amenable to high-throughput technologies. In the meantime, more advanced co-culture systems encompassing neurons and glial cells or 3D brain organoids mimicking

more closely the in vivo human situation, are being developed to assist in PD studies and drug discovery. The necessity for functional assays to predict drug efficacy is also being recognized while technological advancements render complicated screens more feasible. Last but not least, the emergence of artificial intelligence over the past few years may prove to be a game-changing technology in drug discovery. Nevertheless, opportunities and challenges still remain ahead before these young technologies come to fruition and fulfill their promise for understanding and treating neurodegeneration in PD.

.

## 7. EXTENDED ABSTRACT

Parkinson's disease (PD) is a complex neurodegenerative disorder affecting 2% of the world population over 65 years of age [442]. PD is characterized by motor dysfunction related to the progressive loss of midbrain dopamine neurons [443] while a wide range of non-motor symptoms are also present such as psychiatric manifestations and cognitive impairment [444]. The neuropathological hallmark of PD is the presence of intracytoplasmic inclusions in neuronal cell bodies and neurites, respectively termed Lewy bodies and Lewy neurites [445, 446]. These are protein aggregates composed mainly of α-synuclein (αSyn), the major protein linked to sporadic PD [447]. αSyn belongs to a class of intrinsically disordered amyloid proteins that form specific forms of oligomeric and fibrillar aggregates and exert neurotoxicity through various molecular pathways [448]. Several point mutations (A30P, E46K, A53T, G51D) and multiplications of the *SNCA* locus encoding for αSyn cause autosomal dominant forms of PD [139, 308, 309]. Among the different variants, the p.A53TαSyn mutation is generally considered to accelerate aggregation [449] resulting in widespread accumulation of insoluble α-syn deposits that have been identified in the post-mortem p.A53T human brain [450, 451]. Despite extensive efforts in understanding PD pathogenesis, no disease modifying drugs exist. Currently only symptomatic or palliative treatments are available with none capable to prevent or slow-down disease progression. Dopamine-replacement drugs, such as levodopa, which was identified 55 years ago [452], are used to ameliorate motor symptoms and remain the primary and most effective treatment despite the undesired side-effects and deterioration of efficacy with disease progression. Therefore, the development of disease-modifying drugs is an urgent unmet need. Most present-day efforts in identifying novel PD therapeutics target the aggregation of misfolded αSyn as the major pathogenic factor that causes cellular toxicity [173, 447, 453, 454]. Alternative strategies to tackle early steps in neurodegeneration, particularly in an unbiased approach, have lagged behind. Recent advances in patient-derived induced pluripotent stem cell (iPSC)-based models for neurodegenerative diseases permit the detection of early, potentially triggering, pathologic phenotypes and provide amenable systems for drug discovery. In combination with high throughput high content screening technologies, these approaches open new perspectives for identification of disease-modifying compounds [314, 335, 455, 456].

We have previously established a model of iPSC-derived neurons from patients with familial PD harboring the p.A53T αSyn mutation (G209A in the *SNCA* gene) that displays disease-relevant phenotypes at basal conditions [312].In this study, we successfully adapted this cellular system to perform the first small molecule screen on human p.A53T-neurons. Since several kinases have been implicated in PD

pathology [383], we screened a collection of 273 small molecule kinase inhibitors to identify compounds with prospective neuroprotective properties.

We discovered that the multi-kinase inhibitor BX795 significantly reverts disease-associated phenotypes. A single treatment of patient neurons with BX795 has sustainable effects in supporting neuritic growth, restoring axonal pathology and limiting αSyn protein aggregate formation. Protection from p.A53T-associated pathology was also confirmed in human iPSC-derived neurons in which the mutation was introduced by genome editing, against isogenic wild-type controls. Strikingly, proteomics profiling by quantitative mass spectrometry revealed that BX795 treatment results in significant downregulation of a cohort of 118 proteins that are abnormally upregulated in p.A53T-neurons. To our knowledge, this study represents the first high-content drug discovery screen ans proteomics analysis performed in human p.A53T iPSC-derived neurons to identify candidate therapeutics for PD.

The p.A53T proteome examined here revealed a profound increase in proteins related to the biological processes of RNA metabolism, protein synthesis, modification and transport, protein clearance and stress response. Our proteomics analysis, identified perturbations in RNA metabolic processes that started from the nucleus and reached the ribosome. Alternative mRNA processing greatly increases the dimensions of gene expression through splicing, polyadenylation, targeted localization and post-transcriptional silencing. Neurons take advantage of all these strategies as the brain has the highest levels of alternative splicing compared to any other human tissue [427]. This process has recently been shown to be defective in the PS19 Tau model of Alzheimer's disease, where alternative splicing events affected genes particularly involved in synaptic transmission [428]. Similarly, the p.A53T-proteome suggests that this process could be excessively induced in p.A53T-neurons as a number of RBPs known to be linked to αSyn aggregation have emerged, including ELAV1, ELAV3 and CELF, suggesting a possible association with the abnormal expression of synaptic genes and the defective synaptic connectivity we have previously reported in p.A53T neurons- [312].

An excess of mRNAs coming out of the nucleus in p.A53T-neurons could explain the abnormal expression of proteins involved in translation, the next step of mRNA processing. The significant increase of components of the tRNA splicing ligase complex, various aminoacyl-tRNA synthetases, ribosomal subunits and eukaryotic translation initiation factors indicate an enhanced translation of spliced mRNAs. Moreover, in post-mortem PD brains, region and stage-dependent alterations in the machinery of protein synthesis have been reported and have been associated with α-synuclein oligomers in remaining neurons [457].

Dissecting further the pathways affected by BX795, we demonstrated that BX795 modulates the mTORC1 pathway to restrict excessive protein synthesis and facilitate autophagy. The mTOR kinase is a master regulator of cellular metabolism that functions in two distinct complexes: mTORC1 and mTORC2 [429] with the first implicated in protein and lipid biosynthesis through a signaling cascade that includes SK6 and 4E-BP1 proteins [430]. Unlike proliferating cells where this pathway is utilized for growth and division, in neurons it acts as a regulator of healthy metabolism and aging [262] with its restriction being associated with prolonged life span and delay of age-related pathologies. p.A53T neurons have increased RPS6, IQGAP1 and RAG-GTPases, components of mTORC1 pathway and this seems to be associated with an increased translation of a subset of mRNAs that are linked to RNA metabolism and the stress response.

Concomitantly with promoting protein synthesis mTORC1 acts to repress autophagy through ULK1 phosphorylation. Autophagy has a central role in promoting health and longevity while this process is impaired in neurodegenerative diseases and αSyn pathology [433, 434]. The p.A53T-proteome shows that neurons are under stress as proteins involved in the UPR or the heat-shock stress response, proteasome assembly and regulation, known to be orchestrated by mTORC1 in neurons, are significantly upregulated [262]. Restoration of numerous components of RNA metabolism and protein translation cascades by BX795 is directly related to the diminished stress response that emerges by the lower levels of UPR and heat-shock-associated proteins also conferred by this molecule. In parallel, a significant number of ubiquitin/proteasome-associated proteins were brought back to near control levels suggesting that BX795 helps misfolded protein clearance by limiting protein synthesis. This is in agreement with its demonstrated ability to decrease protein aggregates in p.A53T-neurons, as shown in this study, along with facilitation of autophagy both in SYSH-5Y cells expressing p.A53T and in patient-derived neurons.

BX795 is a multi-kinase inhibitor that targets numerous pathways, including the kinases TBK1 and PDK1 [385-387, 389]. Although in our system differences in the total or phosphorylated levels of these two kinases were not observed in the presence of BX795, we cannot exclude that its effects are mediated through these two kinases as both are involved in neurodegeneration, mTOR signaling and autophagy [437, 438]. Interestingly, we found that BX795 could inhibit purified recombinant p70 S6K, the major kinase that phosphorylates RPS6 *in vivo*, indicating that the acute effect of the compound on RPS6 in p.A53T-expressing cells could be mediated through inhibition of p70 S6K. Considering that BX795 has been proposed to act through distinct mechanisms in different pathologies, future mechanistic studies should reveal its direct targets in p.A53T neurons. Nevertheless, the work presented here uniquely identifies BX795 as a promising compound that may have therapeutic potential for patients with PD and other protein conformational disorders. Further, our collective data along with previous proteomics and

systems approaches shed light into the molecular and cellular pathways of αSyn proteotoxicity unveiling new disease targets for the development of combined therapeutics.

## 8.ΕΚΤΕΤΑΜΕΝΗ ΠΕΡΙΛΗΨΗ

Η νόσος του Πάρκινσον (ΝΠ) είναι μια πολύπλοκη νευροεκφυλιστική διαταραχή που επηρεάζει το 2% του παγκόσμιου πληθυσμού άνω των 65 ετών [442]. Η ΝΠ χαρακτηρίζεται από κινητικές διαταραχές που σχετίζονται με την προοδευτική απώλεια των ντοπαμινεργικών νευρώνων της συμπαγούς μοίρας της μέλαινας ουσίας [443], ενώ ένα ευρύ φάσμα μη κινητικών συμπτωμάτων είναι επίσης παρόντα, όπως ψυχιατρικές διαταραχές και νοητική δυσλειτουργία [444]. Το νευροπαθολογικό χαρακτηριστικό της ΝΠ είναι η ανώμαλη εναποθέση πρωτεϊνών σε νευρικά κύτταρα και νευρίτες, που ονομάζονται αντιστοίχως σωμάτια και νευρίτες Lewy [445, 446]. Αυτά είναι πρωτεϊνικά συσσωματώματα που αποτελούνται κυρίως από την πρωτεΐνη α-συνουκλεΐνη, που είναι η κύρια πρωτεΐνη που συνδέεται με την σποραδική μορφή της νόσου[447]. Η α-συνουκλεΐνη ανήκει στην κατηγορία αμυλοειδών πρωτεϊνών που σχηματίζουν ειδικές ολιγομερείς μορφές και συσσωματωμάτα με αποτέλεσμα να οδηγεί σε νευροτοξικότητα μέσω διαφόρων μοριακών οδών [448]. Αρκετές σημειακές μεταλλάξεις (A30P, E46K, A53T, G51D) και διπλασιασμοί/τριπλασιασμοί του γονιδίου της α-συνουκλεΐνης ( SNCA) οδηγούν σε οικογενείς μορφές της νόσου [139,308,309].Μεταξύ των διαφόρων μεταλλάξεων, η μετάλλαξη A53T παρουσιάζει μειωμένη διαλυτότητα, ύστερα από επώαση σε υδατικό διάλυμα, σε φυσιολογική θερμοκρασία και αυτό οδηγεί στην δημιουργία ινιδίων [449] με αποτέλεσμα την εκτεταμένη συσσώρευση αδιάλυτων αποθέσεων στον ανθρώπινο εγκέφαλο [450, 451].

Παρά τις εκτεταμένες προσπάθειες για την κατανόηση της παθογένεσης της ΝΠ, δεν υπάρχουν φάρμακα για την θεραπεία της νόσου. Επί του παρόντος, διατίθενται μόνο συμπτωματικές ή ανακουφιστικές θεραπείες χωρίς καμία να είναι ικανή να αποτρέψει ή να επιβραδύνει την πρόοδο της νόσου. Η λεβοντόπα (σε συνδυασμό με καρβιντόπα/βενζεραζίδη) αποτελεί την πιο αποτελεσματική φαρμακευτική θεραπεία, η οποία εντοπίστηκε πριν από 55 χρόνια [452]. Ωστόσο, η χρόνια χορήγηση της οδηγεί σε σοβαρές παρενέργειες. Ως εκ τούτου, η ανάπτυξη νέων φαρμάκων που να τροποποιούν την πορεία της νόσου είναι μια επείγουσα ανάγκη. Οι περισσότερες σύγχρονες προσπάθειες για τον εντοπισμό νέων θεραπειών στοχεύουν τη συσσώρευση της α-συνουκλεΐνης ως τον κύριο παθογόνο παράγοντα που προκαλεί κυτταρική τοξικότητα [173,447,453,454]. Οι εναλλακτικές στρατηγικές για την αντιμετώπιση των πρώιμων σταδίων του νευροεκφυλισμού, ιδιαίτερα με αμερόληπτο τρόπο, έχουν προχωρήσει με σχετικά αργό ρυθμό. Οι πρόσφατες εξελίξεις στα μοντέλα της ασθένειας που βασίζονται στα επαγόμενα πολυδύναμα βλαστοκύτταρα (iPSCs) που προέρχονται από ασθενείς, επιτρέπουν τον εντοπισμό πρώιμων παθολογικών φαινοτύπων και παρέχουν συστήματα για την ανακάλυψη νέων φαρμάκων. Σε συνδυασμό με τεχνολογίες ελέγχου υψηλής απόδοσης, αυτές οι προσεγγίσεις ανοίγουν νέες προοπτικές για την ανακάλυψη εν δυνάμει θεραπευτικών μορίων[314,335,455,456].

Οι γνώσεις μας για τους ακριβείς μηχανισμούς της νόσου είναι περιορισμένες. Οι παραδοσιακές μέθοδοι μελέτης της νόσου, όπως η χρήση ανθρώπινων ιστών, περιορίζονται σχεδόν αποκλειστικά στον μεταθανάτιο εγκέφαλο για την ΝΠ. Τα ζωικά μοντέλα, αν και χρησιμοποιούνται συνήθως, δεν μπορούν να αντιπροσωπεύσουν πλήρως το πλήρες φάσμα των συμπτωμάτων, εν μέρει, λόγω της σημαντικής απόκλισης από την ανθρώπινη φυσιολογία. Η μέτρηση των λεπτών αλλαγών στη νόηση και τη συμπεριφορά είναι επίσης δύσκολη στα ζώα. Η εμφάνιση της τεχνολογίας των ανθρώπινων πολυδύναμων βλαστικών κυττάρων (hiPSC) προσέδωσε μεγάλη αξία στα υπάρχοντα μοντέλα ΝΠ. Μαζί με τις προόδους στις τεχνολογίες γονιδιακής επεξεργασίας, τα νευρικά κύτταρα iPSC που προέρχονται από ασθενείς και υγιείς δότες δημιούργησαν νέες μεθόδους μοντελοποίησης νευρολογικών ασθενειών σε ανθρώπινο πλαίσιο που μόλις τώρα αρχίζει να αξιοποιείται για θεραπευτικούς σκοπούς.

Τα τελευταία είκοσι χρόνια έχουν αναπτυχθεί πολλά πρωτόκολλα διαφοροποίησης για τους διάφορους κυτταρικούς τύπους του εγκεφάλου, όπως οι νευρώνες, τα αστροκύτταρα, η μικρογλοία και τα ολιγοδενδροκύτταρα. Διαφορετικές μέθοδοι και στρατηγικές μοντελοποίησης καθορίζουν ποιοι κυτταρικοί τύποι παράγονται, ποια πειραματικά ερωτήματα μπορούν να αντιμετωπιστούν και πώς μπορούν να ελεγχθούν ενώσεις για την ανάπτυξη φαρμάκων [368].

Οι κινάσες έχουν αναδειχθεί ως ένας από τους πιο εντατικά διερευνώμενους φαρμακευτικούς στόχους στην τρέχουσα φαρμακολογική έρευνα, λόγω του κομβικού τους ρόλου στη διαμόρφωση ενός ευρέος φάσματος κυτταρικών διεργασιών [369]. Μεγάλη προσπάθεια έχει καταβληθεί για την ανάπτυξη μορίων που στοχεύουν ειδικά το ανθρώπινο κίνωμα (human kinome) [370]. Μέχρι σήμερα, η πλειονότητα των μορίων παρουσιάζει ένα φάσμα αναστολέων των κινασών, με >250 να βρίσκονται σήμερα σε κλινικές δοκιμές και 48 να έχουν εγκριθεί από τον FDA των ΗΠΑ, κυρίως για τη θεραπεία κακοηθειών [371]. Ενώ αρχικά η χρήση των αναστολέων κινασών επικεντρώθηκε στη θεραπεία του καρκίνου, πλέον συμπεριλαμβάνει ένα διευρυμένο φάσμα θεραπευτικών περιοχών, όπως οι αυτοάνοσες και φλεγμονώδεις νόσοι, καθώς και νευροεκφυλιστικές διαταραχές [372], συμπεριλαμβανομένης της ΝΠ. Ωστόσο, η συμβολή της απορρύθμισης του ανθρώπινου κινώματος στη νευροεκφύλιση δεν έχει αποσαφηνιστεί μέχρι στιγμής και ο τομέας των θεραπειών που κατευθύνονται από κινάσες είναι ακόμη σε πρώιμο στάδιο σε σύγκριση με την εφαρμογή τους στη θεραπεία του καρκίνου. Οι νευρωνικές λειτουργίες πολλών κινασών είναι ακόμη σε μεγάλο βαθμό αχαρακτήριστες, με λίγες ενδείξεις για το πώς αυτοί οι στόχοι επηρεάζουν τα κύρια σηματοδοτικά μονοπάτια που εμπλέκονται στην ΝΠ. Απαιτούνται περαιτέρω έρευνες σε ανθρώπινους εγκεφάλους για να σκιαγραφηθούν οι αλλαγές στη δραστηριότητα των πρωτεϊνικών κινασών στις διάφορες περιοχές του εγκεφάλου κατά τη γήρανση και την εξέλιξη του νευροεκφυλισμού.

Καθώς το κύριο χαρακτηριστικό της ΝΠ είναι ο θάνατος των ντοπαμινεργικών νευρώνων της μέλανας ουσίας, στην παρούσα μελέτη εστιάζουμε στον εντοπισμό μορίων που ενισχύουν τη διαφοροποίηση και την επιβίωση αυτών των νευρώνων χρησιμοποιώντας ως πειραματικό μοντέλο τα επαγόμενα βλαστικά κύτταρα (iPS) από υγιή άτομα και από ασθενείς με ΝΠ που φέρουν την A53T μετάλλαξη στην α-συνουκλεΐνη (G209A στο γονίδιο SNCA).Χρησιμοποιήσαμε μια βιβλιοθήκη μικρών μορίων αναστολέων κινασών για να πραγματοποιήσουμε διαλογή υψηλού περιεχομένου προκειμένου να ανιχνεύσουμε μόρια που επάγουν τη διαφοροποίηση ή/και την επιβίωση των ντοπαμινεργικών νευρώνων και αναστρέφουν τη νευροεκφύλιση.

Προηγούμενη μελέτη του εργαστηρίου οδήγησε στην δημιουργία ενός μοντέλου νευρώνων που προέρχονται από επαγόμενα πολυδύναμα βλαστοκύτταρα ασθενών με οικογενή ΝΠ που φέρουν τη μετάλλαξη A53T της α-συνουκλεΐνης. Στο μοντέλο αυτό οι νευρώνες εμφανίζουν φαινοτύπους σχετικούς με τη νόσο, συμπεριλαμβανομένης της συσσώρευσης πρωτεϊνών, της μειωμένης νευριτικής ανάπτυξης και των παραμορφωμένων ή κατακερματισμένων νευραξόνων που περιέχουν α-συνουκλεΐνη και tau. [312]. Στην παρούσα μελέτη, προσαρμόσαμε επιτυχώς αυτό το κυτταρικό σύστημα σε πλάκες 384 φρεατίων για να πραγματοποιήσουμε την πρώτη σάρωση μικρών μορίων σε ανθρώπινους νευρώνες με την μετάλλαξη A53T. Δεδομένου ότι πολλές κινάσες έχουν εμπλακεί στην παθολογία της ΝΠ [383], εξετάσαμε μια συλλογή 273 αναστολέων κινασών για να ανακαλύψουμε ενώσεις με εν δυνάμει νευροπροστατευτικές ιδιότητες.

Ανακαλύψαμε ότι ο αναστολέας πολλαπλών κινασών BX795 αναστρέφει σημαντικά τους φαινότυπους που σχετίζονται με τη νόσο. Μια μεμονωμένη δόση με BX795 παρέχει νευροπροστασία στους A53T νευρώνες βελτιώνοντας τη νευριτική ανάπτυξη, περιορίζοντας τα επίπεδα της παθολογικής α-συνουκλεΐνης και περιορίζοντας τον σχηματισμό συσσωματωμάτων, διατηρώντας παράλληλα την αξονική ακεραιότητα. Η νευροπροστασία επιβεβαιώθηκε επίσης σε ανθρώπινους νευρώνες που προέρχονται από iPSC στους οποίους η μετάλλαξη εισήχθη με επεξεργασία γονιδιώματος. Για τον εντοπισμό των κυτταρικών μονοπατιών που επηρεάζονται από το BX795, χρησιμοποιήσαμε μια αμερόληπτη προσέγγιση που βασίζεται στη συγκριτική πρωτεϊνική. Η αρχική σύγκριση μεταξύ A53T και νευρώνων ελέγχου απουσία BX795, αποκάλυψε διαφορική έκφραση 640 πρωτεϊνών από τις οποίες μόνο 67 εμφάνισαν μείωση, ενώ οι υπόλοιπες 573 αύξηση. Αυτή η μεγάλη αύξηση στην έκφραση πρωτεϊνών συνδέθηκε κυρίως με τις βιολογικές διεργασίες του μεταβολισμού του RNA, τη σύνθεση πρωτεϊνών, την τροποποίηση και μεταφορά, την αποικοδόμηση των πρωτεϊνών και την απόκριση στο στρες. Είναι ενδιαφέρον, ότι τα επίπεδα 118 πρωτεϊνών που βρίσκονται κυρίως εντός αυτών των βιολογικών διεργασιών και αντιπροσωπεύουν περίπου το 20% των συνολικών απορυθμισμένων πρωτεϊνών στους

A53T νευρώνες, αποκαταστάθηκαν κατά τη θεραπεία με BX795. Η παρούσα μελέτη αποτελεί την πρώτη, καθόσον γνωρίζουμε, σάρωση υψηλού περιεχομένου και πρωτεϊνικής ανάλυσης που πραγματοποιήθηκε σε ανθρώπινους νευρώνες που προέρχονται από iPSC με την μετάλλαξη A53T για τον εντοπισμό νέων θεραπευτικών ουσιών για την ΝΠ.

Το πρωτέωμα των νευρώνων με την μετάλλαξη A53T παρουσίασε εμπλουτισμό σε πρωτεΐνες υποκυτταρικών διαμερισμάτων που είναι γνωστό ότι σχετίζονται με την α-συνουλεΐνη [392], συμπεριλαμβανομένων των οργανιδίων που συνδέονται με τη μεμβράνη (204 πρωτεΐνες), των μιτοχονδρίων (118 πρωτεΐνες), των ριβοσωμικών συμπλεγμάτων (29 πρωτεΐνες), του πυρήνα (292 πρωτεΐνες) και του κυτταροπλάσματος των νευρικών αξόνων (10 πρωτεΐνες). Διαδικασίες όπως ο κυτταρικός μεταβολισμός, η έναρξη και η ρύθμιση της μετάφρασης, η αμινοακετυλίωση του tRNA και η εξαγωγή από τον πυρήνα, η σταθερότητα του mRNA και η εξαγωγή από τον πυρήνα, η επεξεργασία του rRNA, ο σχηματισμός του συμπλόκου προ-έναρξης και η αναδίπλωση των πρωτεϊνών ήταν μεταξύ των κορυφαίων μονοπατιών στο πρωτέωμα των νευρώνων με την μετάλλαξη A53T. Μια προηγούμενη μελέτη έχει εντοπίσει πρωτεΐνες πρόσδεσης mRNA (RBPs) και μόρια που εμπλέκονται στη βιοσύνθεση πρωτεϊνών εντός του πρωτεϊνικού δικτύου που βρίσκεται σε άμεση γειτνίαση με την α-συνουλεΐνη, γεγονός που υποδηλώνει ότι η διαταραχή αυτών των μονοπατιών μπορεί να σχετίζεται άμεσα με την παθολογία [392]. Εδώ, παρέχουμε αποδείξεις ότι αυτά τα ίδια μονοπάτια μεταβάλλονται όταν η A53T μετάλλαξη εκφράζεται σε ανθρώπινους νευρώνες. Συγκεκριμένα, ένας σημαντικός αριθμός RBPs (60 πρωτεΐνες) εκφράστηκαν διαφορετικά παρουσία της A53T μετάλλαξης, συμπεριλαμβανομένων μελών με γνωστή νευρωνική εντόπιση και συμμετοχή σε νευρωνικές λειτουργίες, όπως οι ELAV-1, ELAV-3, RBBP7, RNPS1, RNMT, TARDBP, XPO1, XPO5, HNRNPA1, HNRNPA1L2, HNRNPF, HNRNPL, HNRPNPM, HRNNPUL1, PABPC1, PABPC4, PTBP2 και CELF1. Δεδομένου ότι ακόμη και μικρές μεταβολές στην έκφραση ή τη δραστηριότητα των RBPs είναι κρίσιμες λόγω της ευρείας επίδρασής τους στην έκφραση, το μάτισμα και τη μετάφραση πολυάριθμων υποστρωμάτων RNA, οι μεταβολές σε έναν τόσο μεγάλο αριθμό αυτών των ρυθμιστών RNA υποδηλώνουν σοβαρή διαταραχή της ομοιόστασης του RNA στους νευρώνες p.A53T. Από αυτές τις RBPs, ένα σύμπλεγμα που εμπλέκεται σε γεγονότα μάτισης και αδενυλίωσης στο πυρηνικό διαμέρισμα αποκαταστάθηκε μετά την επίδραση με BX795. Αυτές οι RBPs περιελάμβαναν την DEK, που εμπλέκεται στην επιλογή της θέσης συρραφής, την RBM4, έναν ρυθμιστή της εναλλακτικής επιλογής της θέσης 5'-συρραφής και του εξωνίου, την MYEF2, έναν σταθεροποιητή του mRNA, την UBTF, μια κρίσιμη πρωτεΐνη στη μεταγραφή του rRNA, την SNRPB, ένα συστατικό των μικρών RNPs που είναι απαραίτητο για τη συρραφή του προ-mRNA, την PCBP1 που δεσμεύει αλληλουχίες ssDNA για να καθοδηγεί τη συρραφή του mRNA και τους ρυθμιστές της μεταγραφής, ZNF207 και HINT1. Το

RAE1, που δρα ως σημαντικός παράγοντας εξαγωγής mRNA και συνδέει τα κυτταροπλασματικά RNPs με τον κυτταροσκελετό, και το HNRNPUL1 που ανήκει στην οικογένεια hnRNP και έχει συνδεθεί με την ALS λόγω του μοτίβου του που είναι επιρρεπές στη συσσωμάτωση, αποκαταστάθηκαν επίσης από το BX795.

Η ωρίμανση του προ-mRNA καθορίζει την οργάνωση των νουκλεοσωμάτων [393], ενώ τα νουκλεοσώματα που συγκεντρώνονται γύρω από συγκεκριμένες θέσεις ωρίμανσης ρυθμίζουν τη μεταγραφή [394]. Η συγκρότηση των νουκλεοσωμάτων ήταν η κύρια κατηγορία πρωτεϊνών που υπορυθμίστηκε στους A53T-νευρώνες (23 πρωτεΐνες), συμπεριλαμβανομένων των ιστονών 1.2, 1.3, 1.4, 1.5, H2A, H2B, H3.3 και H4, του πυρηνικού πόρου NUP153 και των πυρηνικών οργανωτών Lamin-B1 και Prelamin A/C. Αυτές οι πρωτεΐνες δεν επηρεάστηκαν από το BX795, ενώ μόνο οι HIST1H1E και NUP93 που είναι σημαντικές για τη συγκρότηση και τη συντήρηση του συμπλόκου του πυρηνικού πόρου, αποκαταστάθηκαν από το BX795.

Οι διαταραχές στη δοσολογία των RBPs έχουν επιζήμιες συνέπειες και εκτός του πυρήνα, καθώς ελέγχουν τον στοχευμένο εντοπισμό των mRNAs, είτε εγγύς στο σώμα του κυττάρου είτε απομακρυσμένα στον προβαλλόμενο άξονα, επηρεάζοντας το αν ένα mRNA θα μεταφραστεί ή θα παραμείνει μεταφραστικά σιωπηλό και αν θα αποθηκευτεί για τοπική μετάφραση του mRNA ή θα αποικοδομηθεί [395]. Η ανώμαλη έκφραση του μεταφραστικού μηχανισμού αναδύθηκε στο A53T πρωτέωμα, με τις διαδικασίες έναρξης και ρύθμισης της μετάφρασης να είναι οι πιο επηρεασμένες στους μεταλλαγμένους νευρώνες. Εντοπίστηκαν συνολικά 18 πρωτεΐνες που εμπλέκονται στο σχηματισμό του συμπλόκου προ-έναρξης και περιελάμβαναν τους EIF2, 3, 4 και 5, εκ των οποίων ο EIF4G2 που λειτουργεί ως γενικός καταστολέας της μετάφρασης σχηματίζοντας μεταφραστικά ανενεργά κοκκία στρες, επηρεάστηκε από το BX795. Οι ριβοσωμικές πρωτεΐνες (29 πρωτεΐνες), δομικά συστατικά των υπομονάδων του ριβοσώματος, ήταν ρυθμισμένες προς τα πάνω σε A53T νευρώνες και ένα σημαντικό κλάσμα επέστρεψε σε σχεδόν στα επίπεδα ελέγχου μετά την επίδρασημε BX795. Σε αυτές περιλαμβάνονταν οι RPL31 και RPL12, οι οποίες εμπλέκονται στη βιογένεση της 60S, και η RPS6, συστατικό της υπομονάδας 40S και μεταγενέστερος παράγοντας της σηματοδοτικής οδού mTORC1. Η επεξεργασία του tRNA αποτελεί ένα άλλο σημαντικό μέρος του μεταφραστικού καταρράκτη που μεταβλήθηκε στους A53T-νευρώνες, ενώ ένα σημαντικό κλάσμα αποκαταστάθηκε από το BX795, συμπεριλαμβανομένων των αμινοακυλο-tRNA συνθετασών RARS (αργινυλο-tRNA συνθετάση), VARS (βαλυλο-tRNA συνθετάση) και WARS (τρυπτοφανυλο-tRNA συνθετάση) μαζί με ρυθμιστικές ή βοηθητικές πρωτεΐνες όπως οι PPA1, EEF1D,PRMPT1, FAM98B και RTCB. Αν και οι μεταλλάξεις στις αμινοακυλο-tRNA συνθετάσες έχουν ενοχοποιηθεί για διάφορες υπολειπόμενες και επικρατούσες διαταραχές [396] και ολοένα και περισσότερα στοιχεία συσχετίζουν τις αλλαγές στη βιογένεση και την

επεξεργασία των γονιδίων tRNA με νευροεκφυλιστικές ασθένειες [397], τα δεδομένα μας αποκαλύπτουν για πρώτη φορά μια σύνδεση μεταξύ της έκφρασης της A53T α-συνουκλεΐνης και αυτής της μοριακής διαδικασίας.

Η τοξικότητα της A53T α-συνουκλεΐνης έχει αποδοθεί σε προβληματικές τροποποιήσεις στη μεμβράνη του ενδοπλασματικού δικτύου (ER) και σε διαταραχές στη διακίνηση ER-Golgi και στην πρώιμη ενδοσωματική/ λυσοσωμική διακίνηση [310, 334, 340, 392]. Οι A53T-νευρώνες παρουσιάζουν τροποποιημένα επίπεδα πρωτεϊνών σε συστατικά αυτών των οδών. Μεταξύ αυτών, πέντε μέλη των πρωτεϊνικών συμπλεγμάτων που συμμετέχουν στη μεταφορά μεταξύ μεμβρανικών δομών αυξάνονται παρουσία της A53T (AP1B1, AP2A2, AP3B1, AP3D1 και AP3M1). Μια άλλη εξέχουσα κατηγορία περιλαμβάνει μέλη του μεγαλύτερου κλάδου των μικρών GTPασών τύπου Ras που εμπλέκονται στη διακίνηση μεμβρανών, όπως οι RAB2A, RAB2B και RAB6B, υπεύθυνες για τη μεταφορά από το ER στο Golgi, η RAB18, σημαντική για τον πρώιμο σχηματισμό ενδοσώματος καθώς και για τη μακροαυτοφαγία και έντονα συνδεδεμένη με τον νευροεκφυλισμό [398, 399], και η RAB21, ρυθμιστής της εσωτερίκευσης των ιντεγκρινών και της συγχώνευσης αυτοφαγοσώματος-λυσοσώματος με τη μεσολάβηση SNARE [400]. Άλλες απορρυθμισμένες πρωτεΐνες που εμπλέκονται στη διακίνηση από το ER προς το Golgi περιελάμβαναν τις SEC22B και SEC31A, ενώ οι ARF1 και 3, δύο πρωτεΐνες που απαιτούνται για την εκβλάστηση/αποκόλληση κυστιδίων στο Golgi και απαιτούνται για τη συναπτική σταθερότητα των διεγερτικών συνάψεων [401] ήταν επίσης αυξημένες στους A53T νευρώνες. Τέλος, μια άλλη επηρεαζόμενη διαδικασία φαίνεται να είναι η ανάδρομη μεταφορά από το Golgi προς το ER, καθώς οι πρωτεΐνες COPA, COPB, COPG εκφράστηκαν επίσης διαφορετικά στους p.A53T νευρώνες.

Η έκφραση της A53T πρωτεΐνης  δρα ως πρωτογενής νευροτοξίνη που πυροδοτεί μια σειρά από αποκρίσεις στρες στους ανθρώπινους νευρώνες [402]. Η ανάλυση πρωτεομικής έδειξε ότι οι A53T νευρώνες ενεργοποιούν τους περισσότερους από αυτούς τους μηχανισμούς. Τόσο η απόκριση των αναδιπλούμενων πρωτεϊνών (UPR), όπως αποδεικνύεται από την εσφαλμένη έκφραση των συνοδών CCT2, 3, 4, 5, 7 και 8, όσο και η απόκριση των πρωτεϊνών θερμικού σοκ (HSP), με πρωτεΐνες όπως οι DNAJA1, DNAJB11, DNAJC7, HSPA4L, HSP9 και HSPE1, ήταν εμφανείς στο A53T πρωτέωμα. Αυτά τα μονοπάτια απόκρισης στο στρες ρυθμίστηκαν σημαντικά σε A53T νευρώνες υπό την επίδραση του BX795, το οποίο φαίνεται να στοχεύει πολλούς μεσολαβητές της απόκρισης στο στρες. Σε αυτούς περιλαμβάνονταν το TCP-1, μέλος του συμπλόκου της συνοδού TCP1 (CCT), το PTPN1, ρυθμιστής του UPR, το STIP1, συντονιστής της λειτουργίας των HSP70 και HSP90 και οι πρωτεΐνες συνοδού/συν-συν-συντηρητή DNAJB11, GCN1L1, CCT8 και DNAJA1.

Μια τέτοια απορρύθμιση των συστημάτων απόκρισης UPR/HSP στους A53T νευρώνες θα πρέπει να έχει ως αποτέλεσμα την παραγωγή επικίνδυνου πρωτεϊνικού φορτίου και το σχηματισμό πρωτεϊνικών συσσωματωμάτων, όπως πράγματι εντοπίστηκε με ανοσοφθορισμό. Το A53T πρωτέωμα αποκάλυψε επίσης μεταβολές στα μονοπάτια κάθαρσης των πρωτεϊνών με τους μεσολαβητές τόσο του πρωτεασωμικού όσο και του αυτοφαγικού συστήματος να επηρεάζονται. Το BX795 βελτίωσε την έκφραση πολλαπλών πρωτεϊνών που σχετίζονται με την ουβικουιτίνη, υποδηλώνοντας μερική αποκατάσταση της στόχευσης του πρωτεασώματος σε προϊόντα ανώμαλων πρωτεϊνών, σύμφωνα με τη μείωση των πρωτεϊνικών συσσωματωμάτων σε νευρώνες υπό την επίδραση του BX795.Το BX795 αποκατέστησε την έκφραση του PSMA3, ενός συστατικού του συμπλόκου του πυρήνα του 20S πρωτεασώματος που είναι απαραίτητο για την απομάκρυνση των κακώς διπλωμένων ή κατεστραμμένων πρωτεϊνών και μπορεί επίσης να δράσει με τρόπο ανεξάρτητο από την ουβικουιτίνη, της UCHL1, μιας πρωτεάσης θειόλης που εμπλέκεται στην επεξεργασία των ουβικουιτινιωμένων πρωτεϊνών, της OTUB1, μια εξαιρετικά ειδική Ub-ισοπεπτιδάση που αλληλεπιδρά με τις E3 λιγάσες για την επεξεργασία της ανάπτυξης της αλυσίδας πολυουβικουιτίνης, της PSME3, μια υπομονάδα του ρυθμιστή του πρωτεασώματος PA28-gamma που ενεργοποιείται από βλάβη του DNA, της CUL1, ένα βασικό συστατικό του συμπλόκου SKP1-CUL1-F- box E3 λιγάσης, της PSMD12, συστατικό του 26S πρωτεασώματος, και της UBA6, ένας ενεργοποιητής της ουβικουιτίνης που απαιτείται για τη δέσμευση της E2 λιγάσης. Η VCP, μια AAA ATPάση που εξάγει τις ουβικουιτινιωμένες πρωτεΐνες από μεγάλα πρωτεϊνικά σύμπλοκα για αποικοδόμηση και έχει αποδειχθεί ότι συν-εντοπίζεται με πρωτεϊνικά συσσωματώματα σε διάφορες νευροεκφυλιστικές ασθένειες με αναστολή του πρωτεασώματος, ήταν μια άλλη πρωτεΐνη που ρυθμίστηκε από τον BX795. Τα συστατικά της λυσοσωματικής οδού της αυτοφαγίας που στοχεύει το BX795 περιλάμβαναν πρωτεΐνες όπως η ATG4B και πρωτεΐνες που απαιτούνται για τη βιογένεση και τη διαλογή των Multivesicular Bodies (MVB) (PDCD6IP, AP3M1 και DNM2). Τέλος, το BX795 στόχευσε επίσης τους μηχανισμούς απόκρισης στο οξειδωτικό στρες, καθώς οι πρωτεΐνες της μιτοχονδριακής βιοσύνθεσης TOMM70A και MDH2 επανήλθαν στα φυσιολογικά επίπεδα. Επιπλέον, το STOML2, ένας διεγέρτης της βιοσύνθεσης τησ καρδιολιπίνης που πρόσφατα αποδείχθηκε ότι σχετίζεται με την A53T νευροτοξικότητα σε ανθρώπινους ντοπαμινεργικούς νευρώνες, επίσης επηρεάστηκε θετικά από τον BX795 [334].

Αυτή η μελέτη αποτελεί την πρώτη μελέτη υψηλού περιεχομένου για την ανακάλυψη φαρμάκων που πραγματοποιείται σε ανθρώπινους νευρώνες που προέρχονται από A53T iPSC για τον εντοπισμό υποψήφιων θεραπευτικών ουσιών για την ΝΠ. Παρόλο που οι πρώτοι iPSC που προήλθαν από ασθενείς με ΝΠ δημιουργήθηκαν το 2009 [305], παραδόξως μόνο δύο φαινοτυπικές σαρώσεις έχουν αναφερθεί

μέχρι σήμερα σε νευρώνες που προήλθαν από iPSC για την ΝΠ. Για τον εντοπισμό τροποποιητικών παραγόντων της νόσου, οι Yamaguchi et al. καθιέρωσαν μια βασισμένη στην απεικόνιση, ημιαυτόματη, υψηλής απόδοσης δοκιμασία για την ποσοτική ανίχνευση της μιτοχονδριακής κάθαρσης και της κυτταρικής βιωσιμότητας σε ντοπαμινεργικούς νευρώνες από ασθενείς με οικογενή ΝΠ που έχουν μεταλλάξεις Parkin ή PINK1. Μετά από έλεγχο 320 φαρμακολογικά δραστικών ενώσεων αναστολέων οι ερευνητές εντόπισαν 4 ουσίες, την MRS1220, την τρανυλκυπρομίνη, τη φλουναριζίνη και τη βρωμοκρυπτίνη, οι οποίες βελτίωσαν την παθολογική κάθαρση των μιτοχονδρίων πιθανώς προωθώντας τη μιτοχονδριακή αποικοδόμηση μέσω του λυσοσωματικού συστήματος, χωρίς να διερευνήσουν περαιτέρω τον υποκείμενο μηχανισμό [366]. Σε μια άλλη μελέτη οι Tabata κ.ά. [367] πραγματοποίησαν φαινοτυπική διαλογή σε ντοπαμινεργικούς νευρώνες που προέρχονται από ασθενείς με Parkin (PARK2) και εμφανίζουν αυξημένη ευαισθησία στο μιτοχονδριακό στρες που προκαλείται από τη ροτενόνη, για τον εντοπισμό νευροπροστατευτικών ενώσεων. Από τη φαινοτυπική διαλογή μιας εγκεκριμένης από τον FDA βιβλιοθήκης φαρμάκων, βρέθηκε ότι ένας ανταγωνιστής των διαύλων ασβεστίου, η βενιδιπίνη, καταστέλλει την απόπτωση που προκαλείται από τη ροτενόνη [367]. Η μελέτη μας είναι η τρίτη φαινοτυπική διαλογή που πραγματοποιείται σε ανθρώπινους νευρώνες που προέρχονται από iPSC στον τομέα της ΝΠ και η μόνη που σχετίζεται με την A53T παθολογία.

Τα μονοπάτια που επηρεάζονται από τη μεταλλαγμένη α-συνουκλεΐνη στη μελέτη μας έχουν μεγάλη ομοιότητα με το συνάπτωμα που αναφέρθηκε από τους Chung et al [392] για νευρώνες ποντικών και τις προβλέψεις του in silico "ανθρωποποιημένου" χάρτη της πρωτεοτοξικότητας που αναφέρθηκε στη συνοδευτική μελέτη των Khurana et al [340].

Αναλύοντας περαιτέρω τις οδούς που επηρεάζονται από το BX795, αποδείξαμε ότι το BX795 ρυθμίζει την οδό mTORC1 για τον περιορισμό της υπερβολικής πρωτεϊνοσύνθεσης και τη διευκόλυνση της αυτοφαγίας. Επιπλέον, τα αποτελέσματά μας δείχνουν ότι η αποκατάσταση της πρωτεόστασης που ακολουθεί την σηματοδότηση mTOR μπορεί να έχει μακροπρόθεσμες ευεργετικές συνέπειες στην κυτταρική υγεία, υποκινώντας μόνιμες βασικές αλλαγές.

Η κινάση mTOR είναι ένας κύριος ρυθμιστής του κυτταρικού μεταβολισμού που λειτουργεί σε δύο διακριτά σύμπλοκα: mTORC1 και mTORC2 [429] με το πρώτο να εμπλέκεται στη βιοσύνθεση πρωτεϊνών και λιπιδίων μέσω ενός καταρράκτη σηματοδότησης που περιλαμβάνει τις πρωτεΐνες SK6 και 4E-BP1 [430]. Σε αντίθεση με τα πολλαπλασιαζόμενα κύτταρα όπου το μονοπάτι αυτό χρησιμοποιείται για την ανάπτυξη και τη διαίρεση, στους νευρώνες δρα ως ρυθμιστής του υγιούς μεταβολισμού και της γήρανσης [262] με τον περιορισμό του να σχετίζεται με την παράταση της διάρκειας ζωής και την καθυστέρηση των παθολογιών που σχετίζονται με την ηλικία. Οι A53T νευρώνες έχουν αυξημένες RPS6,

IQGAP1 και RAG-GTPases, συστατικά του μονοπατιού mTORC1 και αυτό φαίνεται να σχετίζεται με αυξημένη μετάφραση ενός υποσυνόλου mRNAs που σχετίζονται με τον μεταβολισμό του RNA και την απόκριση στο στρες. Ομοίως, μια μελέτη ποσοτικής πρωτεομικής σε ένα προ-συμπτωματικό μοντέλο A53T Drosophila δείχνει σημαντική ρύθμιση των ριβοσωμικών πρωτεϊνών στις A53T μύγες [431]. Παρόλο που η μηχανιστική σύνδεση μεταξύ της A53T α-συνουκλεΐνης και του mTORC1 δεν έχει ακόμη τεκμηριωθεί, πρόσφατα στοιχεία δείχνουν ότι η γενετική ποικιλομορφία στο μονοπάτι mTOR συμβάλλει στις επιδράσεις του γονιδίου SNCA στην παθογένεια της νόσου [432].

Ταυτόχρονα με την προώθηση της πρωτεϊνοσύνθεσης ο mTORC1 δρα για την καταστολή της αυτοφαγίας μέσω της φωσφορυλίωσης του ULK1. Η αυτοφαγία έχει κεντρικό ρόλο στην προαγωγή της υγείας και της μακροζωίας, ενώ η διαδικασία αυτή διαταράσσεται στις νευροεκφυλιστικές νόσους και στην παθολογία αSyn [433, 434]. Το A53T-πρωτέωμα δείχνει ότι οι νευρώνες βρίσκονται υπό στρες, καθώς οι πρωτεΐνες που εμπλέκονται στην UPR ή στην απόκριση στρες λόγω θερμικού σοκ, στη συναρμολόγηση και ρύθμιση του πρωτεασώματος, που είναι γνωστό ότι ενορχηστρώνεται από το mTORC1 στους νευρώνες, είναι σημαντικά ρυθμισμένες [262]. Η αποκατάσταση πολυάριθμων συστατικών του μεταβολισμού του RNA και των καταρρακτών πρωτεϊνικής μετάφρασης από το BX795 σχετίζεται άμεσα με τη μειωμένη απόκριση στο στρες που προκύπτει από τα χαμηλότερα επίπεδα των πρωτεϊνών που σχετίζονται με την UPR και το θερμικό σοκ που επίσης προσδίδονται από αυτό το μόριο. Παράλληλα, ένας σημαντικός αριθμός πρωτεϊνών που σχετίζονται με την ουβικουιτίνη/πρωτεάσωμα επανήλθε σε επίπεδα σχεδόν ελέγχου. Λαμβάνοντας υπόψη ότι τόσο το σύστημα ουβικουιτίνης/πρωτεασώματος όσο και η αυτοφαγία μοιράζονται πολλαπλούς μοριακούς καθοριστικούς παράγοντες, συμπεριλαμβανομένων των ULK1, ATG5, ATG8 και p62, οι οποίοι μπορούν να επηρεαστούν ταυτόχρονα και αμοιβαία στις νευροεκφυλιστικές νόσους [435, 436], καθίσταται προφανές ότι το BX795 βοηθά στην εκκαθάριση των κακώς διπλωμένων πρωτεϊνών περιορίζοντας την πρωτεϊνοσύνθεση. Αυτό συμφωνεί με την αποδεδειγμένη ικανότητά του να μειώνει τα συσσωματώματα πρωτεϊνών σε p.A53T-νευρώνες, όπως φάνηκε στην παρούσα μελέτη, μαζί με τη διευκόλυνση της αυτοφαγίας τόσο σε κύτταρα SYSH-5Y που εκφράζουν την A53T α-συνουκλεΐνη όσο και σε νευρώνες που προέρχονται από ασθενείς.

Το BX795 είναι ένας αναστολέας πολλαπλών κινασών που στοχεύει πολυάριθμες οδούς, συμπεριλαμβανομένων των κινασών TBK1 και PDK1 [385-387, 389]. Παρόλο που στο σύστημά μας δεν παρατηρήθηκαν διαφορές στα συνολικά ή φωσφορυλιωμένα επίπεδα αυτών των δύο κινασών παρουσία του BX795 (τα δεδομένα δεν παρουσιάζονται), δεν μπορούμε να αποκλείσουμε ότι οι επιδράσεις του διαμεσολαβούνται μέσω αυτών των δύο κινασών, καθώς και οι δύο εμπλέκονται στη νευροεκφύλιση, τη

σηματοδότηση mTOR και την αυτοφαγία [437, 438]. Ωστόσο, τέσσερις άλλοι αναστολείς της PDK1 που περιλαμβάνονταν στη βιβλιοθήκη Selleck δεν αναδείχθηκαν κατά τη διάρκεια της διαλογής. Η TBK1 προτάθηκε πρόσφατα ως ένας νέος παράγοντας που συνδέει την αυτοφαγία και τη νευροφλεγμονή στην ALS [437] και έχει αποδειχθεί ότι ενεργοποιεί άμεσα το mTOR σε απόκριση σε αυξητικούς παράγοντες [439]. Είναι ενδιαφέρον ότι διαπιστώσαμε ότι το BX795 μπορούσε να αναστείλει την καθαρισμένη ανασυνδυασμένη p70 S6K, τη σημαντικότερη κινάση που φωσφορυλιώνει την RPS6 in vivo, υποδεικνύοντας ότι η οξεία επίδραση της ένωσης στην RPS6 σε κύτταρα που εκφράζουν p.A53T θα μπορούσε να μεσολαβείται μέσω της αναστολής της p70 S6K. Είναι αξιοσημείωτο ότι πολλαπλοί άλλοι αναστολείς της φωσφορυλίωσης του mTOR που υπάρχουν στη βιβλιοθήκη αναστολέων κινάσης που εξετάστηκε (26 συνολικά, συμπεριλαμβανομένης της ραπαμυκίνης), απέτυχαν να επιδείξουν προστατευτικές επιδράσεις στο σύστημά μας. Λαμβάνοντας υπόψη ότι το BX795 έχει προταθεί να δρα μέσω διαφορετικών μηχανισμών σε διαφορετικές παθολογίες, μελλοντικές μηχανιστικές μελέτες θα πρέπει να αποκαλύψουν τους άμεσους στόχους του στους A53T νευρώνες. Το κατά πόσον αυτοί βρίσκονται εντός ή εκτός του κινώματος είναι ένα θέμα προς διερεύνηση, καθώς τα αναδυόμενα στοιχεία υποδεικνύουν ότι οι αναστολείς κινάσης μπορεί ακούσια να ασκούν τη θεραπευτική τους δράση μέσω μη κινάσης στόχων. Συλλογικά, η εργασία που παρουσιάζεται εδώ προσδιορίζει το BX795 ως μια πολλά υποσχόμενη ένωση με θεραπευτικό δυναμικό για ασθενείς με ΝΠ και άλλες διαταραχές διαμόρφωσης πρωτεϊνών. Περαιτέρω, η πειραματική μας προσέγγιση έριξε φως στα μοριακά και κυτταρικά μονοπάτια της πρωτεοτοξικότητας αποκαλύπτοντας νέους στόχους νόσου για την ανάπτυξη συνδυασμένων θεραπευτικών ουσιών.

Οι πραγματικές μεταφραστικές δυνατότητες των πλατφορμών iPSC που προέρχονται από ασθενείς μόλις αναδύονται, καθώς πραγματοποιούνται περισσότερες αμερόληπτες σαρώσεις φαρμάκων μεγάλης κλίμακας. Οι εργασίες που πραγματοποιήθηκαν στο πλαίσιο της παρούσας διατριβής καταδεικνύουν ότι οι ανθρώπινοι νευρώνες με φαινοτυπικά χαρακτηριστικά που σχετίζονται με ασθένειες μπορούν να προσαρμοστούν αποτελεσματικά για χρήση σε σαρώσεις φαρμάκων υψηλής απόδοσης. Οι τρέχουσες εξελίξεις στον τομέα της τεχνολογίας iPSC, συμπεριλαμβανομένων βελτιωμένων πρωτοκόλλων για τη διαφοροποίηση των νευρώνων, της ανάπτυξης συστημάτων συν-καλλιέργειας και τρισδιάστατων (3D) συστημάτων ή της χρήσης μικρορρευστονικής ή τσιπ συσκευών brain-on-chip, θα μπορούσαν να συνδυαστούν με το τρέχον κυτταρικό σύστημα που περιγράφεται εδώ, ώστε να αυξηθεί η αξία του σε προσεγγίσεις διαλογής υψηλής απόδοσης [440, 441] [349]. Μια σημαντική προσθήκη στον έλεγχο βιβλιοθηκών ενώσεων θα ήταν να συμπεριληφθούν ενδείξεις ανάγνωσης της λειτουργικότητας των νευρώνων, όπως για παράδειγμα η αξιολόγηση ηλεκτροφυσιολογικών παραμέτρων με συστήματα

συστοιχιών πολλαπλών ηλεκτροδίων υψηλής απόδοσης. Σε συνδυασμό με βιβλιοθήκες siRNA σε όλο το γονιδίωμα, μηχανική μάθηση και καλύτερα εργαλεία πρόβλεψης in silico, τέτοιες πλατφόρμες μπορούν να αξιοποιηθούν περαιτέρω για την επιλογή νέων, αποτελεσματικότερων και ασφαλέστερων φαρμάκων που θα εισέλθουν με εμπιστοσύνη στις κλινικές δοκιμές.

Είναι σημαντικό ότι η μελέτη μας υποστηρίζει ότι οι πλατφόρμες που βασίζονται σε ανθρώπινα iPSC και χρησιμοποιούνται στην πρώιμη ανακάλυψη φαρμάκων μπορούν επίσης να συμβάλουν στην αποκάλυψη μηχανισμών ασθενειών. Θα μπορούσαμε έτσι να εντοπίσουμε ένα νευροπροστατευτικό μόριο που διασώζει βασικές μεταβολικές οδούς, απαραίτητες για τη νευρωνική λειτουργία. Περαιτέρω μελέτες *in vitro* και *in vivo* σε μοντέλα ΝΠ, θα πρέπει να παράσχουν πρόσθετη εικόνα του μηχανισμού δράσης και της αποτελεσματικότητας του BX795 για να αποκαλύψουν πλήρως το μεταφραστικό δυναμικό του ως κορυφαίο θεραπευτικό φάρμακο για την ΝΠ.

Συμπερασματικά, πολλές σειρές hiPSC έχουν παραχθεί από ασθενείς με οικογενή ή σποραδική ΝΠ αποκαλύπτοντας γνωστούς ή προηγουμένως μη αναγνωρισμένους φαινότυπους σχετικούς με τη νόσο, οι οποίοι, σε πολλές περιπτώσεις, θα μπορούσαν να αποκατασταθούν αποτελεσματικά με τη χρήση μικρών μορίων. Αυτές οι έρευνες έχουν θέσει το υπόβαθρο για την ανάπτυξη βιοδοκιμών για τον έλεγχο μικρών ή μεγαλύτερων χημικών βιβλιοθηκών σε αναζήτηση κύριων ενώσεων που μπορεί να εξελιχθούν σε θεραπευτικά προϊόντα που τροποποιούν τη ΝΠ. Ωστόσο, πρέπει ακόμη να καθιερωθούν ισχυρές δοκιμασίες προτού τα συστήματα που βασίζονται σε iPSC γίνουν πιο εύκολα προσιτά σε τεχνολογίες υψηλής απόδοσης. Εν τω μεταξύ, αναπτύσσονται πιο προηγμένα συστήματα συν-καλλιέργειας που περιλαμβάνουν νευρώνες και γλοιακά κύτταρα ή τρισδιάστατα εγκεφαλικά οργανοειδή που μιμούνται περισσότερο την *in vivo* ανθρώπινη κατάσταση, για να βοηθήσουν στις μελέτες της ΝΠ και στην ανακάλυψη φαρμάκων. Σημαντική είναι επίσης η ανάγκη για λειτουργικές δοκιμασίες για την πρόβλεψη της αποτελεσματικότητας των φαρμάκων, ενώ οι τεχνολογικές εξελίξεις καθιστούν πιο εφικτές τις πολύπλοκες σαρώσεις μορίων. Τέλος, η εμφάνιση της τεχνητής νοημοσύνης τα τελευταία χρόνια μπορεί να αποδειχθεί μια τεχνολογία που θα αλλάξει τα δεδομένα στην ανακάλυψη φαρμάκων. Παρ' όλα αυτά, οι ευκαιρίες και οι προκλήσεις παραμένουν ακόμη μπροστά μας προτού αυτές οι νέες τεχνολογίες καρποφορήσουν για την κατανόηση και τη θεραπεία του νευροεκφυλισμού στη ΝΠ.

## 9.REFERENCES


1. Parkinson, J., *An essay on the shaking palsy. 1817.* J Neuropsychiatry Clin Neurosci, 2002. **14**(2): p. 223-36; discussion 222.
2. Charcot, J.M., *Lectures on the Diseases of the Nervous System.* The British and Foreign Medico-Chirurgical Review, 1877. **60**(119): p. 180-181.
3. Tysnes, O.B. and A. Storstein, *Epidemiology of Parkinson's disease.* J Neural Transm (Vienna), 2017. **124**(8): p. 901-905.
4. Poewe, W., et al., *Parkinson disease.* Nat Rev Dis Primers, 2017. **3**: p. 17013.
5. Dauer, W. and S. Przedborski, *Parkinson's disease: mechanisms and models.* Neuron, 2003. **39**(6): p. 889-909.
6. Frucht, S.J., *Parkinson disease: an update.* The neurologist, 2004. **10**(4): p. 185-194.
7. Han, J.W., et al., *Psychiatric Manifestation in Patients with Parkinson's Disease.* J Korean Med Sci, 2018. **33**(47): p. e300.
8. Massano, J. and K.P. Bhatia, *Clinical approach to Parkinson's disease: features, diagnosis, and principles of management.* Cold Spring Harb Perspect Med, 2012. **2**(6): p. a008870.
9. Bain, P.G., *Parkinsonism & related disorders. Tremor.* Parkinsonism Relat Disord, 2007. **13 Suppl 3**: p. S369-74.
10. Deuschl, G., P. Bain, and M. Brin, *Consensus statement of the Movement Disorder Society on Tremor. Ad Hoc Scientific Committee.* Mov Disord, 1998. **13 Suppl 3**: p. 2-23.
11. Edwards, M., N. Quinn, and K. Bhatia, *Tremor Parkinson's Disease and Other Movement Disorders (Oxford Specialist Handbooks in Neurology)*, 2011, Oxford University Press: Oxford, UK.
12. Jankovic, J., *Parkinson's disease: clinical features and diagnosis.* J Neurol Neurosurg Psychiatry, 2008. **79**(4): p. 368-76.
13. Rodriguez-Oroz, M.C., et al., *Initial clinical manifestations of Parkinson's disease: features and pathophysiological mechanisms.* Lancet Neurol, 2009. **8**(12): p. 1128-39.
14. Marsden, C.D., *The mysterious motor function of the basal ganglia: the Robert Wartenberg Lecture.* Neurology, 1982. **32**(5): p. 514-39.
15. Sethi, K., *Levodopa unresponsive symptoms in Parkinson disease.* Mov Disord, 2008. **23 Suppl 3**: p. S521-33.
16. Zesiewicz, T.A., K.L. Sullivan, and R.A. Hauser, *Nonmotor symptoms of Parkinson's disease.* Expert Rev Neurother, 2006. **6**(12): p. 1811-22.
17. Pursiainen, V., et al., *Sweating in Parkinsonian patients with wearing-off.* Mov Disord, 2007. **22**(6): p. 828-32.
18. Senard, J.M., et al., *Prevalence of orthostatic hypotension in Parkinson's disease.* J Neurol Neurosurg Psychiatry, 1997. **63**(5): p. 584-9.
19. Swinn, L., et al., *Sweating dysfunction in Parkinson's disease.* Mov Disord, 2003. **18**(12): p. 1459-63.
20. Hely, M.A., et al., *Sydney Multicenter Study of Parkinson's disease: non-L-dopa-responsive problems dominate at 15 years.* Mov Disord, 2005. **20**(2): p. 190-9.
21. Aarsland, D., et al., *Neuropsychiatric symptoms in patients with Parkinson's disease and dementia: frequency, profile and associated care giver stress.* J Neurol Neurosurg Psychiatry, 2007. **78**(1): p. 36-42.
22. Palmiter, R.D., *Is dopamine a physiologically relevant mediator of feeding behavior?* Trends Neurosci, 2007. **30**(8): p. 375-81.
23. Miyasaki, J.M., et al., *Punding prevalence in Parkinson's disease.* Mov Disord, 2007. **22**(8): p. 1179-81.

24. Weintraub, D., et al., *Association of dopamine agonist use with impulse control disorders in Parkinson disease.* Arch Neurol, 2006. **63**(7): p. 969-73.
25. Ondo, W.G., et al., *Daytime sleepiness and other sleep disorders in Parkinson's disease.* Neurology, 2001. **57**(8): p. 1392-6.
26. Gjerstad, M.D., et al., *Excessive daytime sleepiness in Parkinson disease: is it the drugs or the disease?* Neurology, 2006. **67**(5): p. 853-8.
27. Borek, L.L., R. Kohn, and J.H. Friedman, *Phenomenology of dreams in Parkinson's disease.* Mov Disord, 2007. **22**(2): p. 198-202.
28. Gagnon, J.F., et al., *Rapid-eye-movement sleep behaviour disorder and neurodegenerative diseases.* Lancet Neurol, 2006. **5**(5): p. 424-32.
29. Plazzi, G., et al., *REM sleep behavior disorders in multiple system atrophy.* Neurology, 1997. **48**(4): p. 1094-7.
30. Schenck, C.H., S.R. Bundlie, and M.W. Mahowald, *Delayed emergence of a parkinsonian disorder in 38% of 29 older men initially diagnosed with idiopathic rapid eye movement sleep behaviour disorder.* Neurology, 1996. **46**(2): p. 388-93.
31. Boeve, B.F., et al., *Pathophysiology of REM sleep behaviour disorder and relevance to neurodegenerative disease.* Brain, 2007. **130**(Pt 11): p. 2770-88.
32. Gjerstad, M.D., et al., *Insomnia in Parkinson's disease: frequency and progression over time.* J Neurol Neurosurg Psychiatry, 2007. **78**(5): p. 476-9.
33. Fronczek, R., et al., *Hypocretin (orexin) loss in Parkinson's disease.* Brain, 2007. **130**(Pt 6): p. 1577-85.
34. Thannickal, T.C., Y.Y. Lai, and J.M. Siegel, *Hypocretin (orexin) cell loss in Parkinson's disease.* Brain, 2007. **130**(Pt 6): p. 1586-95.
35. Friedman, J.H., et al., *Fatigue in Parkinson's disease: a review.* Mov Disord, 2007. **22**(3): p. 297-308.
36. Comella, C.L. and C.G. Goetz, *Akathisia in Parkinson's disease.* Mov Disord, 1994. **9**(5): p. 545-9.
37. Djaldetti, R., et al., *Quantitative measurement of pain sensation in patients with Parkinson disease.* Neurology, 2004. **62**(12): p. 2171-5.
38. Ford, B., et al., *Oral and genital pain syndromes in Parkinson's disease.* Mov Disord, 1996. **11**(4): p. 421-6.
39. Lee, P.H., et al., *Correlation between cardiac 123I-MIBG and odor identification in patients with Parkinson's disease and multiple system atrophy.* Mov Disord, 2006. **21**(11): p. 1975-7.
40. Stamey, W., A. Davidson, and J. Jankovic, *Shoulder pain: a presenting symptom of Parkinson disease.* J Clin Rheumatol, 2008. **14**(4): p. 253-4.
41. Stern, M.B., et al., *Olfactory function in Parkinson's disease subtypes.* Neurology, 1994. **44**(2): p. 266-8.
42. Tinazzi, M., et al., *Pain and motor complications in Parkinson's disease.* J Neurol Neurosurg Psychiatry, 2006. **77**(7): p. 822-5.
43. Harding, A.J., et al., *Clinical correlates of selective pathology in the amygdala of patients with Parkinson's disease.* Brain, 2002. **125**(Pt 11): p. 2431-45.
44. Blandini, F., et al., *Functional changes of the basal ganglia circuitry in Parkinson's disease.* Prog Neurobiol, 2000. **62**(1): p. 63-88.
45. Bolam, J.P., et al., *Basal Ganglia: Internal Organization*, in *Encyclopedia of Neuroscience*, L.R. Squire, Editor 2009, Academic Press: Oxford. p. 97-104.
46. Gerfen, C.R., *The Neostriatal Mosaic: Multiple Levels of Compartmental Organization in the Basal Ganglia.* Annual Review of Neuroscience, 1992. **15**(1): p. 285-320.
47. Graybiel, A.M., *Neurotransmitters and neuromodulators in the basal ganglia.* Trends Neurosci, 1990. **13**(7): p. 244-54.

48. Chavkin, C., *Dynorphins are endogenous opioid peptides released from granule cells to act neurohumorly and inhibit excitatory neurotransmission in the hippocampus.* Prog Brain Res, 2000. **125**: p. 363-7.
49. Maiti, P., J. Manna, and G.L. Dunbar, *Current understanding of the molecular mechanisms in Parkinson's disease: Targets for potential treatments.* Transl Neurodegener, 2017. **6**: p. 28.
50. Bostan, A.C., R.P. Dum, and P.L. Strick, *Cerebellar networks with the cerebral cortex and basal ganglia.* Trends Cogn Sci, 2013. **17**(5): p. 241-54.
51. Caligiore, D., et al., *Consensus Paper: Towards a Systems-Level View of Cerebellar Function: the Interplay Between Cerebellum, Basal Ganglia, and Cortex.* Cerebellum, 2017. **16**(1): p. 203-229.
52. Caligiore, D., et al., *The contribution of brain sub-cortical loops in the expression and acquisition of action understanding abilities.* Neurosci Biobehav Rev, 2013. **37**(10 Pt 2): p. 2504-15.
53. Yin, H.H. and B.J. Knowlton, *The role of the basal ganglia in habit formation.* Nat Rev Neurosci, 2006. **7**(6): p. 464-76.
54. G E Alexander, a. M R DeLong, and P.L. Strick, *Parallel Organization of Functionally Segregated Circuits Linking Basal Ganglia and Cortex.* Annual Review of Neuroscience, 1986. **9**(1): p. 357-381.
55. Middleton, F.A. and P.L. Strick, *Basal ganglia output and cognition: evidence from anatomical, behavioral, and clinical studies.* Brain Cogn, 2000. **42**(2): p. 183-200.
56. Ichinohe, N., F. Mori, and K. Shoumura, *A di-synaptic projection from the lateral cerebellar nucleus to the laterodorsal part of the striatum via the central lateral nucleus of the thalamus in the rat.* Brain Res, 2000. **880**(1-2): p. 191-7.
57. Hoshi, E., et al., *The cerebellum communicates with the basal ganglia.* Nat Neurosci, 2005. **8**(11): p. 1491-3.
58. Milardi, D., et al., *Extensive Direct Subcortical Cerebellum-Basal Ganglia Connections in Human Brain as Revealed by Constrained Spherical Deconvolution Tractography.* Front Neuroanat, 2016. **10**: p. 29.
59. Pelzer, E.A., et al., *Cerebellar networks with basal ganglia: feasibility for tracking cerebello-pallidal and subthalamo-cerebellar projections in the human brain.* Eur J Neurosci, 2013. **38**(8): p. 3106-14.
60. Caligiore, D., et al., *Parkinson's disease as a system-level disorder.* NPJ Parkinsons Dis, 2016. **2**: p. 16025.
61. German, D.C., et al., *Midbrain dopaminergic cell loss in Parkinson's disease: computer visualization.* Ann Neurol, 1989. **26**(4): p. 507-14.
62. German, D.C., et al., *Midbrain dopaminergic cell loss in Parkinson's disease and MPTP-induced parkinsonism: sparing of calbindin-D28k-containing cells.* Ann N Y Acad Sci, 1992. **648**: p. 42-62.
63. Alexander, G.E., *Biology of Parkinson's disease: pathogenesis and pathophysiology of a multisystem neurodegenerative disorder.* Dialogues Clin Neurosci, 2004. **6**(3): p. 259-80.
64. Grillner, P. and N.B. Mercuri, *Intrinsic membrane properties and synaptic inputs regulating the firing activity of the dopamine neurons.* Behav Brain Res, 2002. **130**(1-2): p. 149-69.
65. Conn, P.J., et al., *Metabotropic glutamate receptors in the basal ganglia motor circuit.* Nat Rev Neurosci, 2005. **6**(10): p. 787-98.
66. Bonsi, P., et al., *Distinct roles of group I mGlu receptors in striatal function.* Neuropharmacology, 2008. **55**(4): p. 392-5.
67. Lange, K.W., J. Kornhuber, and P. Riederer, *Dopamine/glutamate interactions in Parkinson's disease.* Neurosci Biobehav Rev, 1997. **21**(4): p. 393-400.
68. Rodriguez, M.C., J.A. Obeso, and C.W. Olanow, *Subthalamic nucleus-mediated excitotoxicity in Parkinson's disease: a target for neuroprotection.* Ann Neurol, 1998. **44**(3 Suppl 1): p. S175-88.

69. O'Neill, M.J. and S. Dix, *AMPA receptor potentiators as cognitive enhancers.* IDrugs, 2007. **10**(3): p. 185-92.
70. Allaman, I., M. Belanger, and P.J. Magistretti, *Astrocyte-neuron metabolic relationships: for better and for worse.* Trends Neurosci, 2011. **34**(2): p. 76-87.
71. Hurley, M.J., et al., *Parkinson's disease is associated with altered expression of CaV1 channels and calcium-binding proteins.* Brain, 2013. **136**(Pt 7): p. 2077-97.
72. Stefanis, L., *alpha-Synuclein in Parkinson's disease.* Cold Spring Harb Perspect Med, 2012. **2**(2): p. a009399.
73. Ibanez, C.F. and J.O. Andressoo, *Biology of GDNF and its receptors - Relevance for disorders of the central nervous system.* Neurobiol Dis, 2017. **97**(Pt B): p. 80-89.
74. Blaszczyk, J.W., *Parkinson's Disease and Neurodegeneration: GABA-Collapse Hypothesis.* Front Neurosci, 2016. **10**: p. 269.
75. Huot, P., et al., *Serotonergic Approaches in Parkinson's Disease: Translational Perspectives, an Update.* ACS Chem Neurosci, 2017. **8**(5): p. 973-986.
76. Doder, M., et al., *Tremor in Parkinson's disease and serotonergic dysfunction: an 11C-WAY 100635 PET study.* Neurology, 2003. **60**(4): p. 601-5.
77. Tan, S.K., et al., *Serotonin-dependent depression in Parkinson's disease: a role for the subthalamic nucleus?* Neuropharmacology, 2011. **61**(3): p. 387-99.
78. Tagliavini, F. and G. Pilleri, *Basal nucleus of Meynert. A neuropathological study in Alzheimer's disease, simple senile dementia, Pick's disease and Huntington's chorea.* J Neurol Sci, 1983. **62**(1-3): p. 243-60.
79. Liu, A.K., et al., *Nucleus basalis of Meynert revisited: anatomy, history and differential involvement in Alzheimer's and Parkinson's disease.* Acta Neuropathol, 2015. **129**(4): p. 527-40.
80. Dickson, D.W., *Parkinson's disease and parkinsonism: neuropathology.* Cold Spring Harb Perspect Med, 2012. **2**(8).
81. Cheng, H.C., C.M. Ulane, and R.E. Burke, *Clinical progression in Parkinson disease and the neurobiology of axons.* Ann Neurol, 2010. **67**(6): p. 715-25.
82. Fearnley, J.M. and A.J. Lees, *Ageing and Parkinson's disease: substantia nigra regional selectivity.* Brain, 1991. **114 ( Pt 5)**: p. 2283-301.
83. Greffard, S., et al., *Motor score of the Unified Parkinson Disease Rating Scale as a good predictor of Lewy body-associated neuronal loss in the substantia nigra.* Arch Neurol, 2006. **63**(4): p. 584-8.
84. Ma, S.Y., et al., *Correlation between neuromorphometry in the substantia nigra and clinical features in Parkinson's disease using disector counts.* J Neurol Sci, 1997. **151**(1): p. 83-7.
85. Rudow, G., et al., *Morphometry of the human substantia nigra in ageing and Parkinson's disease.* Acta Neuropathol, 2008. **115**(4): p. 461-70.
86. Kordower, J.H., et al., *Disease duration and the integrity of the nigrostriatal system in Parkinson's disease.* Brain, 2013. **136**(Pt 8): p. 2419-31.
87. Spillantini, M.G., et al., *Alpha-synuclein in Lewy bodies.* Nature, 1997. **388**(6645): p. 839-40.
88. Kouli, A., K.M. Torsney, and W.L. Kuan, *Parkinson's Disease: Etiology, Neuropathology, and Pathogenesis.* 2018.
89. Spillantini, M.G., et al., *alpha-Synuclein in filamentous inclusions of Lewy bodies from Parkinson's disease and dementia with lewy bodies.* Proc Natl Acad Sci U S A, 1998. **95**(11): p. 6469-73.
90. Goedert, M., et al., *100 years of Lewy pathology.* Nat Rev Neurol, 2013. **9**(1): p. 13-24.
91. Xia, Q., et al., *Proteomic identification of novel proteins associated with Lewy bodies.* Front Biosci, 2008. **13**: p. 3850-6.
92. Braak, H., et al., *Staging of brain pathology related to sporadic Parkinson's disease.* Neurobiol Aging, 2003. **24**(2): p. 197-211.

93. Chaudhuri, K.R. and A.H. Schapira, *Non-motor symptoms of Parkinson's disease: dopaminergic pathophysiology and treatment.* Lancet Neurol, 2009. **8**(5): p. 464-74.
94. Khoo, T.K., et al., *The spectrum of nonmotor symptoms in early Parkinson disease.* Neurology, 2013. **80**(3): p. 276-81.
95. Pavese, N., et al., *Progression of monoaminergic dysfunction in Parkinson's disease: a longitudinal 18F-dopa PET study.* Neuroimage, 2011. **56**(3): p. 1463-8.
96. Hawkes, C.H., K. Del Tredici, and H. Braak, *Parkinson's disease: a dual-hit hypothesis.* Neuropathol Appl Neurobiol, 2007. **33**(6): p. 599-614.
97. Kalaitzakis, M.E., et al., *The dorsal motor nucleus of the vagus is not an obligatory trigger site of Parkinson's disease: a critical analysis of alpha-synuclein staging.* Neuropathol Appl Neurobiol, 2008. **34**(3): p. 284-95.
98. Parkkinen, L., T. Pirttila, and I. Alafuzoff, *Applicability of current staging/categorization of alpha-synuclein pathology and their clinical relevance.* Acta Neuropathol, 2008. **115**(4): p. 399-407.
99. Jellinger, K.A., *A critical evaluation of current staging of alpha-synuclein pathology in Lewy body disorders.* Biochim Biophys Acta, 2009. **1792**(7): p. 730-40.
100. Surmeier, D.J., J.A. Obeso, and G.M. Halliday, *Parkinson's Disease Is Not Simply a Prion Disorder.* J Neurosci, 2017. **37**(41): p. 9799-9807.
101. Braak, H., et al., *Stages in the development of Parkinson's disease-related pathology.* Cell Tissue Res, 2004. **318**(1): p. 121-34.
102. Lees, A.J., J. Hardy, and T. Revesz, *Parkinson's disease.* Lancet, 2009. **373**(9680): p. 2055-66.
103. Bower, J.H., et al., *Incidence and distribution of parkinsonism in Olmsted County, Minnesota, 1976-1990.* Neurology, 1999. **52**(6): p. 1214-20.
104. de Rijk, M.C., et al., *Prevalence of Parkinson's disease in the elderly: the Rotterdam Study.* Neurology, 1995. **45**(12): p. 2143-6.
105. Kalia, L.V. and A.E. Lang, *Parkinson's disease.* Lancet, 2015. **386**(9996): p. 896-912.
106. Mappin-Kasirer, B., et al., *Tobacco smoking and the risk of Parkinson disease: A 65-year follow-up of 30,000 male British doctors.* Neurology, 2020. **94**(20): p. e2132-e2138.
107. Bordia, T., et al., *The alpha7 nicotinic receptor agonist ABT-107 protects against nigrostriatal damage in rats with unilateral 6-hydroxydopamine lesions.* Exp Neurol, 2015. **263**: p. 277-84.
108. Srinivasan, R., et al., *Smoking-Relevant Nicotine Concentration Attenuates the Unfolded Protein Response in Dopaminergic Neurons.* J Neurosci, 2016. **36**(1): p. 65-79.
109. Ritz, B., et al., *Parkinson disease and smoking revisited: ease of quitting is an early sign of the disease.* Neurology, 2014. **83**(16): p. 1396-402.
110. Hong, C.T., L. Chan, and C.H. Bai, *The Effect of Caffeine on the Risk and Progression of Parkinson's Disease: A Meta-Analysis.* Nutrients, 2020. **12**(6).
111. Ross, G.W., et al., *Association of coffee and caffeine intake with the risk of Parkinson disease.* JAMA, 2000. **283**(20): p. 2674-9.
112. Noyce, A.J., et al., *Meta-analysis of early nonmotor features and risk factors for Parkinson disease.* Ann Neurol, 2012. **72**(6): p. 893-901.
113. Ascherio, A., et al., *Prospective study of caffeine consumption and risk of Parkinson's disease in men and women.* Ann Neurol, 2001. **50**(1): p. 56-63.
114. Ascherio, A., et al., *Coffee consumption, gender, and Parkinson's disease mortality in the cancer prevention study II cohort: the modifying effects of estrogen.* Am J Epidemiol, 2004. **160**(10): p. 977-84.
115. Xu, K., et al., *Estrogen prevents neuroprotection by caffeine in the mouse 1-methyl-4-phenyl-1,2,3,6-tetrahydropyridine model of Parkinson's disease.* J Neurosci, 2006. **26**(2): p. 535-41.
116. Langston, J.W., *The MPTP Story.* J Parkinsons Dis, 2017. **7**(s1): p. S11-S19.

117. Langston, J.W., et al., *Chronic Parkinsonism in humans due to a product of meperidine-analog synthesis.* Science, 1983. **219**(4587): p. 979-80.
118. Di Monte, D., et al., *Comparative studies on the mechanisms of paraquat and 1-methyl-4-phenylpyridine (MPP+) cytotoxicity.* Biochem Biophys Res Commun, 1986. **137**(1): p. 303-9.
119. Betarbet, R., et al., *Chronic systemic pesticide exposure reproduces features of Parkinson's disease.* Nat Neurosci, 2000. **3**(12): p. 1301-6.
120. Tanner, C.M., et al., *Rotenone, paraquat, and Parkinson's disease.* Environ Health Perspect, 2011. **119**(6): p. 866-72.
121. Goldman, S.M., et al., *Concordance for Parkinson's disease in twins: A 20-year update.* Ann Neurol, 2019. **85**(4): p. 600-605.
122. Keller, M.F., et al., *Using genome-wide complex trait analysis to quantify 'missing heritability' in Parkinson's disease.* Hum Mol Genet, 2012. **21**(22): p. 4996-5009.
123. Nalls, M.A., et al., *Identification of novel risk loci, causal insights, and heritable risk for Parkinson's disease: a meta-analysis of genome-wide association studies.* Lancet Neurol, 2019. **18**(12): p. 1091-1102.
124. Nalls, M.A., et al., *Large-scale meta-analysis of genome-wide association data identifies six new risk loci for Parkinson's disease.* Nat Genet, 2014. **46**(9): p. 989-93.
125. Escott-Price, V., et al., *Polygenic risk of Parkinson disease is correlated with disease age at onset.* Ann Neurol, 2015. **77**(4): p. 582-91.
126. Foo, J.N., et al., *Identification of Risk Loci for Parkinson Disease in Asians and Comparison of Risk Between Asians and Europeans: A Genome-Wide Association Study.* JAMA Neurol, 2020. **77**(6): p. 746-754.
127. Ibanez, L., et al., *Parkinson disease polygenic risk score is associated with Parkinson disease status and age at onset but not with alpha-synuclein cerebrospinal fluid levels.* BMC Neurol, 2017. **17**(1): p. 198.
128. Jacobs, B.M., et al., *Parkinson's disease determinants, prediction and gene-environment interactions in the UK Biobank.* J Neurol Neurosurg Psychiatry, 2020. **91**(10): p. 1046-1054.
129. Li, W.W., et al., *Association of the Polygenic Risk Score with the Incidence Risk of Parkinson's Disease and Cerebrospinal Fluid alpha-Synuclein in a Chinese Cohort.* Neurotox Res, 2019. **36**(3): p. 515-522.
130. Day, J.O. and S. Mullin, *The Genetics of Parkinson's Disease and Implications for Clinical Practice.* Genes (Basel), 2021. **12**(7).
131. Pankratz, N., et al., *Meta-analysis of Parkinson's disease: identification of a novel locus, RIT2.* Ann Neurol, 2012. **71**(3): p. 370-84.
132. Deng, H., P. Wang, and J. Jankovic, *The genetics of Parkinson disease.* Ageing Res Rev, 2018. **42**: p. 72-85.
133. Klein, C. and A. Westenberger, *Genetics of Parkinson's disease.* Cold Spring Harb Perspect Med, 2012. **2**(1): p. a008888.
134. Schulte, C. and T. Gasser, *Genetic basis of Parkinson's disease: inheritance, penetrance, and expression.* Appl Clin Genet, 2011. **4**: p. 67-80.
135. Polymeropoulos, M.H., et al., *Mutation in the alpha-synuclein gene identified in families with Parkinson's disease.* Science, 1997. **276**(5321): p. 2045-7.
136. Ki, C.S., et al., *The Ala53Thr mutation in the alpha-synuclein gene in a Korean family with Parkinson disease.* Clin Genet, 2007. **71**(5): p. 471-3.
137. Kang, L., et al., *The A53T mutation is key in defining the differences in the aggregation kinetics of human and mouse alpha-synuclein.* J Am Chem Soc, 2011. **133**(34): p. 13465-70.
138. Appel-Cresswell, S., et al., *Alpha-synuclein p.H50Q, a novel pathogenic mutation for Parkinson's disease.* Mov Disord, 2013. **28**(6): p. 811-3.

139. Chartier-Harlin, M.C., et al., *Alpha-synuclein locus duplication as a cause of familial Parkinson's disease.* Lancet, 2004. **364**(9440): p. 1167-9.
140. Kruger, R., et al., *Ala30Pro mutation in the gene encoding alpha-synuclein in Parkinson's disease.* Nat Genet, 1998. **18**(2): p. 106-8.
141. Lesage, S., et al., *G51D alpha-synuclein mutation causes a novel parkinsonian-pyramidal syndrome.* Ann Neurol, 2013. **73**(4): p. 459-71.
142. Singleton, A.B., et al., *alpha-Synuclein locus triplication causes Parkinson's disease.* Science, 2003. **302**(5646): p. 841.
143. Zarranz, J.J., et al., *The new mutation, E46K, of alpha-synuclein causes Parkinson and Lewy body dementia.* Ann Neurol, 2004. **55**(2): p. 164-73.
144. Healy, D.G., et al., *Phenotype, genotype, and worldwide genetic penetrance of LRRK2-associated Parkinson's disease: a case-control study.* Lancet Neurol, 2008. **7**(7): p. 583-90.
145. Pickrell, A.M. and R.J. Youle, *The roles of PINK1, parkin, and mitochondrial fidelity in Parkinson's disease.* Neuron, 2015. **85**(2): p. 257-73.
146. Di Fonzo, A., et al., *FBXO7 mutations cause autosomal recessive, early-onset parkinsonian-pyramidal syndrome.* Neurology, 2009. **72**(3): p. 240-5.
147. Olgiati, S., et al., *DNAJC6 Mutations Associated With Early-Onset Parkinson's Disease.* Ann Neurol, 2016. **79**(2): p. 244-56.
148. Paisan-Ruiz, C., et al., *Characterization of PLA2G6 as a locus for dystonia-parkinsonism.* Ann Neurol, 2009. **65**(1): p. 19-23.
149. Ramirez, A., et al., *Hereditary parkinsonism with dementia is caused by mutations in ATP13A2, encoding a lysosomal type 5 P-type ATPase.* Nat Genet, 2006. **38**(10): p. 1184-91.
150. Puschmann, A., et al., *A Swedish family with de novo alpha-synuclein A53T mutation: evidence for early cortical dysfunction.* Parkinsonism Relat Disord, 2009. **15**(9): p. 627-32.
151. Kitada, T., et al., *Mutations in the parkin gene cause autosomal recessive juvenile parkinsonism.* Nature, 1998. **392**(6676): p. 605-8.
152. Nishikawa, K., et al., *Alterations of structure and hydrolase activity of parkinsonism-associated human ubiquitin carboxyl-terminal hydrolase L1 variants.* Biochem Biophys Res Commun, 2003. **304**(1): p. 176-83.
153. Valente, E.M., et al., *PINK1 mutations are associated with sporadic early-onset parkinsonism.* Ann Neurol, 2004. **56**(3): p. 336-41.
154. Bonifati, V., et al., *Mutations in the DJ-1 gene associated with autosomal recessive early-onset parkinsonism.* Science, 2003. **299**(5604): p. 256-9.
155. Zimprich, A., et al., *Mutations in LRRK2 cause autosomal-dominant parkinsonism with pleomorphic pathology.* Neuron, 2004. **44**(4): p. 601-7.
156. Williams, D.R., et al., *Kufor Rakeb disease: autosomal recessive, levodopa-responsive parkinsonism with pyramidal degeneration, supranuclear gaze palsy, and dementia.* Mov Disord, 2005. **20**(10): p. 1264-71.
157. Lautier, C., et al., *Mutations in the GIGYF2 (TNRC15) gene at the PARK11 locus in familial Parkinson disease.* Am J Hum Genet, 2008. **82**(4): p. 822-33.
158. Strauss, K.M., et al., *Loss of function mutations in the gene encoding Omi/HtrA2 in Parkinson's disease.* Hum Mol Genet, 2005. **14**(15): p. 2099-111.
159. Wider, C., et al., *Autosomal dominant dopa-responsive parkinsonism in a multigenerational Swiss family.* Parkinsonism Relat Disord, 2008. **14**(6): p. 465-70.
160. Chartier-Harlin, M.C., et al., *Translation initiator EIF4G1 mutations in familial Parkinson disease.* Am J Hum Genet, 2011. **89**(3): p. 398-406.
161. Quadri, M., et al., *Mutation in the SYNJ1 gene associated with autosomal recessive, early-onset Parkinsonism.* Hum Mutat, 2013. **34**(9): p. 1208-15.

162. Vilarino-Guell, C., et al., *DNAJC13 mutations in Parkinson disease.* Hum Mol Genet, 2014. **23**(7): p. 1794-801.
163. Lesage, S., et al., *Loss of VPS13C Function in Autosomal-Recessive Parkinsonism Causes Mitochondrial Dysfunction and Increases PINK1/Parkin-Dependent Mitophagy.* Am J Hum Genet, 2016. **98**(3): p. 500-513.
164. Soto, C. and S. Pritzkow, *Protein misfolding, aggregation, and conformational strains in neurodegenerative diseases.* Nat Neurosci, 2018. **21**(10): p. 1332-1340.
165. Kim, W.S., K. Kagedal, and G.M. Halliday, *Alpha-synuclein biology in Lewy body diseases.* Alzheimers Res Ther, 2014. **6**(5): p. 73.
166. Sweeney, P., et al., *Protein misfolding in neurodegenerative diseases: implications and strategies.* Transl Neurodegener, 2017. **6**: p. 6.
167. Cardinale, A., R. Chiesa, and M. Sierks, *Protein misfolding and neurodegenerative diseases.* Int J Cell Biol, 2014. **2014**: p. 217371.
168. Mehra, S., S. Sahay, and S.K. Maji, *alpha-Synuclein misfolding and aggregation: Implications in Parkinson's disease pathogenesis.* Biochim Biophys Acta Proteins Proteom, 2019. **1867**(10): p. 890-908.
169. Lazaro, D.F., et al., *Systematic comparison of the effects of alpha-synuclein mutations on its oligomerization and aggregation.* PLoS Genet, 2014. **10**(11): p. e1004741.
170. Ranjan, P. and A. Kumar, *Perturbation in Long-Range Contacts Modulates the Kinetics of Amyloid Formation in alpha-Synuclein Familial Mutants.* ACS Chem Neurosci, 2017. **8**(10): p. 2235-2246.
171. Sahay, S., et al., *Alteration of Structure and Aggregation of alpha-Synuclein by Familial Parkinson's Disease Associated Mutations.* Curr Protein Pept Sci, 2017. **18**(7): p. 656-676.
172. Conway, K.A., J.D. Harper, and P.T. Lansbury, *Accelerated in vitro fibril formation by a mutant alpha-synuclein linked to early-onset Parkinson disease.* Nat Med, 1998. **4**(11): p. 1318-20.
173. Ghosh, D., et al., *The Parkinson's disease-associated H50Q mutation accelerates alpha-Synuclein aggregation in vitro.* Biochemistry, 2013. **52**(40): p. 6925-7.
174. Greenbaum, E.A., et al., *The E46K mutation in alpha-synuclein increases amyloid fibril formation.* J Biol Chem, 2005. **280**(9): p. 7800-7.
175. Ghosh, D., et al., *The newly discovered Parkinson's disease associated Finnish mutation (A53E) attenuates alpha-synuclein aggregation and membrane binding.* Biochemistry, 2014. **53**(41): p. 6419-21.
176. Li, J., V.N. Uversky, and A.L. Fink, *Effect of familial Parkinson's disease point mutations A30P and A53T on the structural properties, aggregation, and fibrillation of human alpha-synuclein.* Biochemistry, 2001. **40**(38): p. 11604-13.
177. Yoshino, H., et al., *Homozygous alpha-synuclein p.A53V in familial Parkinson's disease.* Neurobiol Aging, 2017. **57**: p. 248 e7-248 e12.
178. Mohite, G.M., et al., *Comparison of Kinetics, Toxicity, Oligomer Formation, and Membrane Binding Capacity of alpha-Synuclein Familial Mutations at the A53 Site, Including the Newly Discovered A53V Mutation.* Biochemistry, 2018. **57**(35): p. 5183-5187.
179. Karpinar, D.P., et al., *Pre-fibrillar alpha-synuclein variants with impaired beta-structure increase neurotoxicity in Parkinson's disease models.* EMBO J, 2009. **28**(20): p. 3256-68.
180. Winner, B., et al., *In vivo demonstration that alpha-synuclein oligomers are toxic.* Proc Natl Acad Sci U S A, 2011. **108**(10): p. 4194-9.
181. Volles, M.J. and P.T. Lansbury, Jr., *Vesicle permeabilization by protofibrillar alpha-synuclein is sensitive to Parkinson's disease-linked mutations and occurs by a pore-like mechanism.* Biochemistry, 2002. **41**(14): p. 4595-602.
182. Volles, M.J. and P.T. Lansbury, Jr., *Zeroing in on the pathogenic form of alpha-synuclein and its mechanism of neurotoxicity in Parkinson's disease.* Biochemistry, 2003. **42**(26): p. 7871-8.

183. Luk, K.C., et al., *Pathological alpha-synuclein transmission initiates Parkinson-like neurodegeneration in nontransgenic mice.* Science, 2012. **338**(6109): p. 949-53.
184. Luk, K.C., et al., *Exogenous alpha-synuclein fibrils seed the formation of Lewy body-like intracellular inclusions in cultured cells.* Proc Natl Acad Sci U S A, 2009. **106**(47): p. 20051-6.
185. Volpicelli-Daley, L.A., K.C. Luk, and V.M. Lee, *Addition of exogenous alpha-synuclein preformed fibrils to primary neuronal cultures to seed recruitment of endogenous alpha-synuclein to Lewy body and Lewy neurite-like aggregates.* Nat Protoc, 2014. **9**(9): p. 2135-46.
186. Chauhan, A. and A.F. Jeans, *Is Parkinson's disease truly a prion-like disorder? An appraisal of current evidence.* Neurol Res Int, 2015. **2015**: p. 345285.
187. Rietdijk, C.D., et al., *Exploring Braak's Hypothesis of Parkinson's Disease.* Front Neurol, 2017. **8**: p. 37.
188. Chandra, R., et al., *alpha-Synuclein in gut endocrine cells and its implications for Parkinson's disease.* JCI Insight, 2017. **2**(12).
189. Volpicelli-Daley, L.A., et al., *Exogenous alpha-synuclein fibrils induce Lewy body pathology leading to synaptic dysfunction and neuron death.* Neuron, 2011. **72**(1): p. 57-71.
190. Raposo, G. and W. Stoorvogel, *Extracellular vesicles: exosomes, microvesicles, and friends.* J Cell Biol, 2013. **200**(4): p. 373-83.
191. Rajendran, L., et al., *Alzheimer's disease beta-amyloid peptides are released in association with exosomes.* Proc Natl Acad Sci U S A, 2006. **103**(30): p. 11172-7.
192. Sharples, R.A., et al., *Inhibition of gamma-secretase causes increased secretion of amyloid precursor protein C-terminal fragments in association with exosomes.* FASEB J, 2008. **22**(5): p. 1469-78.
193. Danzer, K.M., et al., *Exosomal cell-to-cell transmission of alpha synuclein oligomers.* Molecular Neurodegeneration, 2012. **7**(1): p. 42.
194. Emmanouilidou, E., et al., *Cell-produced alpha-synuclein is secreted in a calcium-dependent manner by exosomes and impacts neuronal survival.* J Neurosci, 2010. **30**(20): p. 6838-51.
195. Ngolab, J., et al., *Brain-derived exosomes from dementia with Lewy bodies propagate α-synuclein pathology.* Acta Neuropathologica Communications, 2017. **5**(1): p. 46.
196. Gerdes, H.H., A. Rustom, and X. Wang, *Tunneling nanotubes, an emerging intercellular communication route in development.* Mech Dev, 2013. **130**(6-8): p. 381-7.
197. Onfelt, B., et al., *Long-distance calls between cells connected by tunneling nanotubules.* Sci STKE, 2005. **2005**(313): p. pe55.
198. Rustom, A., et al., *Nanotubular highways for intercellular organelle transport.* Science, 2004. **303**(5660): p. 1007-10.
199. Abounit, S., et al., *Tunneling nanotubes spread fibrillar alpha-synuclein by intercellular trafficking of lysosomes.* EMBO J, 2016. **35**(19): p. 2120-2138.
200. Rostami, J., et al., *Human Astrocytes Transfer Aggregated Alpha-Synuclein via Tunneling Nanotubes.* J Neurosci, 2017. **37**(49): p. 11835-11853.
201. Tardivel, M., et al., *Tunneling nanotube (TNT)-mediated neuron-to neuron transfer of pathological Tau protein assemblies.* Acta Neuropathologica Communications, 2016. **4**(1): p. 117.
202. Wang, Y., et al., *Tunneling-nanotube development in astrocytes depends on p53 activation.* Cell Death Differ, 2011. **18**(4): p. 732-42.
203. Gomperts, S.N., *Lewy Body Dementias: Dementia With Lewy Bodies and Parkinson Disease Dementia.* Continuum (Minneap Minn), 2016. **22**(2 Dementia): p. 435-63.
204. Hepp, D.H., et al., *Distribution and Load of Amyloid-beta Pathology in Parkinson Disease and Dementia with Lewy Bodies.* J Neuropathol Exp Neurol, 2016. **75**(10): p. 936-945.

205. Schraen-Maschke, S., et al., *Tau as a biomarker of neurodegenerative diseases.* Biomark Med, 2008. **2**(4): p. 363-84.
206. Arima, K., et al., *Cellular co-localization of phosphorylated tau- and NACP/alpha-synuclein-epitopes in lewy bodies in sporadic Parkinson's disease and in dementia with Lewy bodies.* Brain Res, 1999. **843**(1-2): p. 53-61.
207. Walker, L., et al., *Neuropathologically mixed Alzheimer's and Lewy body disease: burden of pathological protein aggregates differs between clinical phenotypes.* Acta Neuropathol, 2015. **129**(5): p. 729-48.
208. Wang, X. and E.K. Michaelis, *Selective neuronal vulnerability to oxidative stress in the brain.* Front Aging Neurosci, 2010. **2**: p. 12.
209. Parker, W.D., Jr., J.K. Parks, and R.H. Swerdlow, *Complex I deficiency in Parkinson's disease frontal cortex.* Brain Res, 2008. **1189**: p. 215-8.
210. Anderson, R.F. and T.A. Harris, *Dopamine and uric acid act as antioxidants in the repair of DNA radicals: implications in Parkinson's disease.* Free Radic Res, 2003. **37**(10): p. 1131-6.
211. Lotharius, J. and P. Brundin, *Pathogenesis of Parkinson's disease: dopamine, vesicles and alpha-synuclein.* Nat Rev Neurosci, 2002. **3**(12): p. 932-42.
212. Dong, X.X., Y. Wang, and Z.H. Qin, *Molecular mechanisms of excitotoxicity and their relevance to pathogenesis of neurodegenerative diseases.* Acta Pharmacol Sin, 2009. **30**(4): p. 379-87.
213. Mark, L.P., et al., *Pictorial review of glutamate excitotoxicity: fundamental concepts for neuroimaging.* AJNR Am J Neuroradiol, 2001. **22**(10): p. 1813-24.
214. Bjorling-Poulsen, M., H.R. Andersen, and P. Grandjean, *Potential developmental neurotoxicity of pesticides used in Europe.* Environ Health, 2008. **7**: p. 50.
215. Bove, J., et al., *Toxin-induced models of Parkinson's disease.* NeuroRx, 2005. **2**(3): p. 484-94.
216. Perier, C. and M. Vila, *Mitochondrial biology and Parkinson's disease.* Cold Spring Harb Perspect Med, 2012. **2**(2): p. a009332.
217. Amor, S., et al., *Inflammation in neurodegenerative diseases.* Immunology, 2010. **129**(2): p. 154-69.
218. Meredith, G.E. and D.J. Rademacher, *MPTP mouse models of Parkinson's disease: an update.* J Parkinsons Dis, 2011. **1**(1): p. 19-33.
219. Bartels, A.L. and K.L. Leenders, *Cyclooxygenase and neuroinflammation in Parkinson's disease neurodegeneration.* Curr Neuropharmacol, 2010. **8**(1): p. 62-8.
220. McNaught, K.S., et al., *Failure of the ubiquitin-proteasome system in Parkinson's disease.* Nat Rev Neurosci, 2001. **2**(8): p. 589-94.
221. Ciechanover, A. and Y.T. Kwon, *Degradation of misfolded proteins in neurodegenerative diseases: therapeutic targets and strategies.* Exp Mol Med, 2015. **47**: p. e147.
222. Larsen, K.E. and D. Sulzer, *Autophagy in neurons: a review.* Histol Histopathol, 2002. **17**(3): p. 897-908.
223. Rubinsztein, D.C., *The roles of intracellular protein-degradation pathways in neurodegeneration.* Nature, 2006. **443**(7113): p. 780-6.
224. Pukass, K. and C. Richter-Landsberg, *Inhibition of UCH-L1 in oligodendroglial cells results in microtubule stabilization and prevents alpha-synuclein aggregate formation by activating the autophagic pathway: implications for multiple system atrophy.* Front Cell Neurosci, 2015. **9**: p. 163.
225. Ding, Q., et al., *Characterization of chronic low-level proteasome inhibition on neural homeostasis.* J Neurochem, 2003. **86**(2): p. 489-97.
226. Sullivan, P.G., et al., *Proteasome inhibition alters neural mitochondrial homeostasis and mitochondria turnover.* J Biol Chem, 2004. **279**(20): p. 20699-707.

227. Saigoh, K., et al., *Intragenic deletion in the gene encoding ubiquitin carboxy-terminal hydrolase in gad mice.* Nat Genet, 1999. **23**(1): p. 47-51.
228. Cha, G.H., et al., *Parkin negatively regulates JNK pathway in the dopaminergic neurons of Drosophila.* Proc Natl Acad Sci U S A, 2005. **102**(29): p. 10345-50.
229. Greene, J.C., et al., *Mitochondrial pathology and apoptotic muscle degeneration in Drosophila parkin mutants.* Proc Natl Acad Sci U S A, 2003. **100**(7): p. 4078-83.
230. Dokladny, K., O.B. Myers, and P.L. Moseley, *Heat shock response and autophagy--cooperation and control.* Autophagy, 2015. **11**(2): p. 200-13.
231. Maiti, P., et al., *Molecular chaperone dysfunction in neurodegenerative diseases and effects of curcumin.* Biomed Res Int, 2014. **2014**: p. 495091.
232. Karunanithi, S. and I.R. Brown, *Heat shock response and homeostatic plasticity.* Front Cell Neurosci, 2015. **9**: p. 68.
233. Bercovich, B., et al., *Ubiquitin-dependent degradation of certain protein substrates in vitro requires the molecular chaperone Hsc70.* J Biol Chem, 1997. **272**(14): p. 9002-10.
234. Wyttenbach, A., *Role of heat shock proteins during polyglutamine neurodegeneration: mechanisms and hypothesis.* J Mol Neurosci, 2004. **23**(1-2): p. 69-96.
235. Kaushik, S. and A.M. Cuervo, *Chaperone-mediated autophagy: a unique way to enter the lysosome world.* Trends Cell Biol, 2012. **22**(8): p. 407-17.
236. Cuervo, A.M., et al., *Impaired degradation of mutant alpha-synuclein by chaperone-mediated autophagy.* Science, 2004. **305**(5688): p. 1292-5.
237. Levine, B. and D.J. Klionsky, *Development by self-digestion: molecular mechanisms and biological functions of autophagy.* Dev Cell, 2004. **6**(4): p. 463-77.
238. Bandyopadhyay, U. and A.M. Cuervo, *Chaperone-mediated autophagy in aging and neurodegeneration: lessons from alpha-synuclein.* Exp Gerontol, 2007. **42**(1-2): p. 120-8.
239. Webb, J.L., et al., *Alpha-Synuclein is degraded by both autophagy and the proteasome.* J Biol Chem, 2003. **278**(27): p. 25009-13.
240. Glick, D., S. Barth, and K.F. Macleod, *Autophagy: cellular and molecular mechanisms.* J Pathol, 2010. **221**(1): p. 3-12.
241. Juste, Y.R. and A.M. Cuervo, *Analysis of Chaperone-Mediated Autophagy.* Methods Mol Biol, 2019. **1880**: p. 703-727.
242. Crotzer, V.L. and J.S. Blum, *Autophagy and intracellular surveillance: Modulating MHC class II antigen presentation with stress.* Proc Natl Acad Sci U S A, 2005. **102**(22): p. 7779-80.
243. Komatsu, M., et al., *Loss of autophagy in the central nervous system causes neurodegeneration in mice.* Nature, 2006. **441**(7095): p. 880-4.
244. Kuma, A., et al., *The role of autophagy during the early neonatal starvation period.* Nature, 2004. **432**(7020): p. 1032-6.
245. Alvarez-Erviti, L., et al., *Chaperone-mediated autophagy markers in Parkinson disease brains.* Arch Neurol, 2010. **67**(12): p. 1464-72.
246. Murphy, K.E., et al., *Lysosomal-associated membrane protein 2 isoforms are differentially affected in early Parkinson's disease.* Mov Disord, 2015. **30**(12): p. 1639-47.
247. Hayashi-Nishino, M., et al., *A subdomain of the endoplasmic reticulum forms a cradle for autophagosome formation.* Nat Cell Biol, 2009. **11**(12): p. 1433-7.
248. Wei, Y., et al., *Origin of the Autophagosome Membrane in Mammals.* Biomed Res Int, 2018. **2018**: p. 1012789.
249. Itakura, E. and N. Mizushima, *Characterization of autophagosome formation site by a hierarchical analysis of mammalian Atg proteins.* Autophagy, 2010. **6**(6): p. 764-76.
250. Ravikumar, B., et al., *Mammalian macroautophagy at a glance.* J Cell Sci, 2009. **122**(Pt 11): p. 1707-11.

251. Jahreiss, L., F.M. Menzies, and D.C. Rubinsztein, *The itinerary of autophagosomes: from peripheral formation to kiss-and-run fusion with lysosomes.* Traffic, 2008. **9**(4): p. 574-87.
252. Kaleağasıoğlu, F., D.M. Ali, and M.R. Berger, *Multiple Facets of Autophagy and the Emerging Role of Alkylphosphocholines as Autophagy Modulators.* Frontiers in Pharmacology, 2020. **11**(547).
253. Parekh, P., et al., *A Cleaning Crew: The Pursuit of Autophagy in Parkinson's Disease.* ACS Chem Neurosci, 2019. **10**(9): p. 3914-3926.
254. Jankovic, J., *Motor fluctuations and dyskinesias in Parkinson's disease: clinical manifestations.* Mov Disord, 2005. **20 Suppl 11**: p. S11-6.
255. Pan, T., et al., *The role of autophagy-lysosome pathway in neurodegeneration associated with Parkinson's disease.* Brain, 2008. **131**(Pt 8): p. 1969-78.
256. Anglade, P., et al., *Apoptosis and autophagy in nigral neurons of patients with Parkinson's disease.* Histol Histopathol, 1997. **12**(1): p. 25-31.
257. Tanji, K., et al., *Alteration of autophagosomal proteins (LC3, GABARAP and GATE-16) in Lewy body disease.* Neurobiol Dis, 2011. **43**(3): p. 690-7.
258. Toulorge, D., A.H. Schapira, and R. Hajj, *Molecular changes in the postmortem parkinsonian brain.* J Neurochem, 2016. **139 Suppl 1**: p. 27-58.
259. Dijkstra, A.A., et al., *Evidence for Immune Response, Axonal Dysfunction and Reduced Endocytosis in the Substantia Nigra in Early Stage Parkinson's Disease.* PLoS One, 2015. **10**(6): p. e0128651.
260. Mutez, E., et al., *Involvement of the immune system, endocytosis and EIF2 signaling in both genetically determined and sporadic forms of Parkinson's disease.* Neurobiol Dis, 2014. **63**: p. 165-70.
261. Heras-Sandoval, D., J.M. Perez-Rojas, and J. Pedraza-Chaverri, *Novel compounds for the modulation of mTOR and autophagy to treat neurodegenerative diseases.* Cell Signal, 2020. **65**: p. 109442.
262. Papadopoli, D., et al., *mTOR as a central regulator of lifespan and aging.* F1000Res, 2019. **8**.
263. Sharp, Z.D. and R. Strong, *The role of mTOR signaling in controlling mammalian life span: what a fungicide teaches us about longevity.* J Gerontol A Biol Sci Med Sci, 2010. **65**(6): p. 580-9.
264. Hands, S.L., C.G. Proud, and A. Wyttenbach, *mTOR's role in ageing: protein synthesis or autophagy?* Aging (Albany NY), 2009. **1**(7): p. 586-97.
265. Norwitz, N.G. and H. Querfurth, *mTOR Mysteries: Nuances and Questions About the Mechanistic Target of Rapamycin in Neurodegeneration.* Front Neurosci, 2020. **14**: p. 775.
266. Kim, J., et al., *AMPK and mTOR regulate autophagy through direct phosphorylation of Ulk1.* Nat Cell Biol, 2011. **13**(2): p. 132-41.
267. Napolitano, G., et al., *mTOR-dependent phosphorylation controls TFEB nuclear export.* Nat Commun, 2018. **9**(1): p. 3312.
268. Colla, E., et al., *Endoplasmic reticulum stress is important for the manifestations of alpha-synucleinopathy in vivo.* J Neurosci, 2012. **32**(10): p. 3306-20.
269. Gertz, H.J., A. Siegers, and J. Kuchinke, *Stability of cell size and nucleolar size in Lewy body containing neurons of substantia nigra in Parkinson's disease.* Brain Res, 1994. **637**(1-2): p. 339-41.
270. Rieker, C., et al., *Nucleolar disruption in dopaminergic neurons leads to oxidative damage and parkinsonism through repression of mammalian target of rapamycin signaling.* J Neurosci, 2011. **31**(2): p. 453-60.
271. Healy-Stoffel, M., et al., *Altered nucleolar morphology in substantia nigra dopamine neurons following 6-hydroxydopamine lesion in rats.* Neurosci Lett, 2013. **546**: p. 26-30.

272. Vilotti, S., et al., *Parkinson's disease DJ-1 L166P alters rRNA biogenesis by exclusion of TTRAP from the nucleolus and sequestration into cytoplasmic aggregates via TRAF6.* PLoS One, 2012. **7**(4): p. e35051.
273. Bockaert, J. and P. Marin, *mTOR in Brain Physiology and Pathologies.* Physiol Rev, 2015. **95**(4): p. 1157-87.
274. Chen, L., et al., *Hydrogen peroxide inhibits mTOR signaling by activation of AMPKα leading to apoptosis of neuronal cells.* Laboratory Investigation, 2010. **90**(5): p. 762-773.
275. Rodriguez-Blanco, J., et al., *Cooperative action of JNK and AKT/mTOR in 1-methyl-4-phenylpyridinium-induced autophagy of neuronal PC12 cells.* J Neurosci Res, 2012. **90**(9): p. 1850-60.
276. Wills, J., et al., *Paraquat, but not maneb, induces synucleinopathy and tauopathy in striata of mice through inhibition of proteasomal and autophagic pathways.* PLoS One, 2012. **7**(1): p. e30745.
277. Nordstroma, U., et al., *Progressive nigrostriatal terminal dysfunction and degeneration in the engrailed1 heterozygous mouse model of Parkinson's disease.* Neurobiol Dis, 2015. **73**: p. 70-82.
278. Decressac, M. and A. Bjorklund, *mTOR inhibition alleviates L-DOPA-induced dyskinesia in parkinsonian rats.* J Parkinsons Dis, 2013. **3**(1): p. 13-7.
279. Pan, T., et al., *Rapamycin protects against rotenone-induced apoptosis through autophagy induction.* Neuroscience, 2009. **164**(2): p. 541-51.
280. Spencer, B., et al., *Beclin 1 gene transfer activates autophagy and ameliorates the neurodegenerative pathology in alpha-synuclein models of Parkinson's and Lewy body diseases.* J Neurosci, 2009. **29**(43): p. 13578-88.
281. Tain, L.S., et al., *Rapamycin activation of 4E-BP prevents parkinsonian dopaminergic neuron loss.* Nat Neurosci, 2009. **12**(9): p. 1129-35.
282. Santini, E., et al., *Inhibition of mTOR signaling in Parkinson's disease prevents L-DOPA-induced dyskinesia.* Sci Signal, 2009. **2**(80): p. ra36.
283. Subramaniam, S., et al., *Rhes, a striatal-enriched small G protein, mediates mTOR signaling and L-DOPA-induced dyskinesia.* Nat Neurosci, 2011. **15**(2): p. 191-3.
284. Stoker, T.B., K.M. Torsney, and R.A. Barker, *Emerging Treatment Approaches for Parkinson's Disease.* Front Neurosci, 2018. **12**: p. 693.
285. Jenner, P., *Dopamine agonists, receptor selectivity and dyskinesia induction in Parkinson's disease.* Curr Opin Neurol, 2003. **16 Suppl 1**: p. S3-7.
286. Bains, M. and J.L. Roberts, *Estrogen protects against dopamine neuron toxicity in primary mesencephalic cultures through an indirect P13K/Akt mediated astrocyte pathway.* Neurosci Lett, 2016. **610**: p. 79-85.
287. Che, Y., et al., *Taurine protects dopaminergic neurons in a mouse Parkinson's disease model through inhibition of microglial M1 polarization.* Cell Death Dis, 2018. **9**(4): p. 435.
288. Manalo, R.V.M. and P.M.B. Medina, *Caffeine Protects Dopaminergic Neurons From Dopamine-Induced Neurodegeneration via Synergistic Adenosine-Dopamine D2-Like Receptor Interactions in Transgenic Caenorhabditis elegans.* Front Neurosci, 2018. **12**: p. 137.
289. Van Kampen, J.M., D. Baranowski, and D.G. Kay, *Progranulin gene delivery protects dopaminergic neurons in a mouse model of Parkinson's disease.* PLoS One, 2014. **9**(5): p. e97032.
290. Zhao, F., et al., *Mfn2 protects dopaminergic neurons exposed to paraquat both in vitro and in vivo: Implications for idiopathic Parkinson's disease.* Biochim Biophys Acta Mol Basis Dis, 2017. **1863**(6): p. 1359-1370.
291. Beal, M.F., et al., *A randomized clinical trial of high-dosage coenzyme Q10 in early Parkinson disease: no evidence of benefit.* JAMA Neurol, 2014. **71**(5): p. 543-52.

292. Bae, W.Y., J.S. Choi, and J.W. Jeong, *The Neuroprotective Effects of Cinnamic Aldehyde in an MPTP Mouse Model of Parkinson's Disease.* Int J Mol Sci, 2018. **19**(2).
293. Thomas, B. and K.P. Mohanakumar, *Melatonin protects against oxidative stress caused by 1-methyl-4-phenyl-1,2,3,6-tetrahydropyridine in the mouse nigrostriatum.* J Pineal Res, 2004. **36**(1): p. 25-32.
294. Wang, Y.L., et al., *Protective Effect of Curcumin Against Oxidative Stress-Induced Injury in Rats with Parkinson's Disease Through the Wnt/ beta-Catenin Signaling Pathway.* Cell Physiol Biochem, 2017. **43**(6): p. 2226-2241.
295. Fernandez-Moriano, C., E. Gonzalez-Burgos, and M.P. Gomez-Serranillos, *Mitochondria-Targeted Protective Compounds in Parkinson's and Alzheimer's Diseases.* Oxid Med Cell Longev, 2015. **2015**: p. 408927.
296. Prasad, E.M. and S.Y. Hung, *Current Therapies in Clinical Trials of Parkinson's Disease: A 2021 Update.* Pharmaceuticals (Basel), 2021. **14**(8).
297. Benn, C.L. and L.A. Dawson, *Clinically Precedented Protein Kinases: Rationale for Their Use in Neurodegenerative Disease.* Front Aging Neurosci, 2020. **12**: p. 242.
298. Hingorani, A.D., et al., *Improving the odds of drug development success through human genomics: modelling study.* Sci Rep, 2019. **9**(1): p. 18911.
299. Takahashi, K., et al., *Induction of pluripotent stem cells from adult human fibroblasts by defined factors.* Cell, 2007. **131**(5): p. 861-72.
300. Yu, J., et al., *Induced pluripotent stem cell lines derived from human somatic cells.* Science, 2007. **318**(5858): p. 1917-20.
301. Sison, S.L., et al., *Using Patient-Derived Induced Pluripotent Stem Cells to Identify Parkinson's Disease-Relevant Phenotypes.* Curr Neurol Neurosci Rep, 2018. **18**(12): p. 84.
302. Kim, T.W., S.Y. Koo, and L. Studer, *Pluripotent Stem Cell Therapies for Parkinson Disease: Present Challenges and Future Opportunities.* Front Cell Dev Biol, 2020. **8**: p. 729.
303. Parmar, M., S. Grealish, and C. Henchcliffe, *The future of stem cell therapies for Parkinson disease.* Nat Rev Neurosci, 2020. **21**(2): p. 103-115.
304. Park, I.H., et al., *Disease-specific induced pluripotent stem cells.* Cell, 2008. **134**(5): p. 877-86.
305. Soldner, F., et al., *Parkinson's disease patient-derived induced pluripotent stem cells free of viral reprogramming factors.* Cell, 2009. **136**(5): p. 964-77.
306. Marotta, N., S. Kim, and D. Krainc, *Organoid and pluripotent stem cells in Parkinson's disease modeling: an expert view on their value to drug discovery.* Expert Opin Drug Discov, 2020. **15**(4): p. 427-441.
307. Weykopf, B., et al., *Induced pluripotent stem cell-based modeling of mutant LRRK2-associated Parkinson's disease.* Eur J Neurosci, 2019. **49**(4): p. 561-589.
308. Petrucci, S., M. Ginevrino, and E.M. Valente, *Phenotypic spectrum of alpha-synuclein mutations: New insights from patients and cellular models.* Parkinsonism Relat Disord, 2016. **22 Suppl 1**: p. S16-20.
309. Simon-Sanchez, J., et al., *Genome-wide association study reveals genetic risk underlying Parkinson's disease.* Nat Genet, 2009. **41**(12): p. 1308-12.
310. Chung, C.Y., et al., *Identification and rescue of alpha-synuclein toxicity in Parkinson patient-derived neurons.* Science, 2013. **342**(6161): p. 983-7.
311. Dettmer, U., et al., *Parkinson-causing alpha-synuclein missense mutations shift native tetramers to monomers as a mechanism for disease initiation.* Nat Commun, 2015. **6**: p. 7314.
312. Kouroupi, G., et al., *Defective synaptic connectivity and axonal neuropathology in a human iPSC-based model of familial Parkinson's disease.* Proc Natl Acad Sci U S A, 2017. **114**(18): p. E3679-E3688.

313. Little, D., et al., *A single cell high content assay detects mitochondrial dysfunction in iPSC-derived neurons with mutations in SNCA.* Sci Rep, 2018. **8**(1): p. 9033.
314. Ryan, S.D., et al., *Isogenic human iPSC Parkinson's model shows nitrosative stress-induced dysfunction in MEF2-PGC1alpha transcription.* Cell, 2013. **155**(6): p. 1351-64.
315. Prots, I., et al., *alpha-Synuclein oligomers induce early axonal dysfunction in human iPSC-based models of synucleinopathies.* Proc Natl Acad Sci U S A, 2018. **115**(30): p. 7813-7818.
316. Byers, B., et al., *SNCA triplication Parkinson's patient's iPSC-derived DA neurons accumulate alpha-synuclein and are susceptible to oxidative stress.* PLoS One, 2011. **6**(11): p. e26159.
317. Devine, M.J., et al., *Parkinson's disease induced pluripotent stem cells with triplication of the alpha-synuclein locus.* Nat Commun, 2011. **2**: p. 440.
318. Flierl, A., et al., *Higher vulnerability and stress sensitivity of neuronal precursor cells carrying an alpha-synuclein gene triplication.* PLoS One, 2014. **9**(11): p. e112413.
319. Heman-Ackah, S.M., et al., *Alpha-synuclein induces the unfolded protein response in Parkinson's disease SNCA triplication iPSC-derived neurons.* Hum Mol Genet, 2017. **26**(22): p. 4441-4450.
320. Ludtmann, M.H.R., et al., *alpha-synuclein oligomers interact with ATP synthase and open the permeability transition pore in Parkinson's disease.* Nat Commun, 2018. **9**(1): p. 2293.
321. Oliveira, L.M., et al., *Elevated alpha-synuclein caused by SNCA gene triplication impairs neuronal differentiation and maturation in Parkinson's patient-derived induced pluripotent stem cells.* Cell Death Dis, 2015. **6**: p. e1994.
322. Chen, C., D.M. Turnbull, and A.K. Reeve, *Mitochondrial Dysfunction in Parkinson's Disease-Cause or Consequence?* Biology (Basel), 2019. **8**(2).
323. Su, Y.C. and X. Qi, *Inhibition of excessive mitochondrial fission reduced aberrant autophagy and neuronal damage caused by LRRK2 G2019S mutation.* Hum Mol Genet, 2013. **22**(22): p. 4545-61.
324. Aboud, A.A., et al., *PARK2 patient neuroprogenitors show increased mitochondrial sensitivity to copper.* Neurobiol Dis, 2015. **73**: p. 204-12.
325. Cartelli, D., et al., *Parkin absence accelerates microtubule aging in dopaminergic neurons.* Neurobiol Aging, 2018. **61**: p. 66-74.
326. Chung, S.Y., et al., *Parkin and PINK1 Patient iPSC-Derived Midbrain Dopamine Neurons Exhibit Mitochondrial Dysfunction and alpha-Synuclein Accumulation.* Stem Cell Reports, 2016. **7**(4): p. 664-677.
327. Imaizumi, Y., et al., *Mitochondrial dysfunction associated with increased oxidative stress and alpha-synuclein accumulation in PARK2 iPSC-derived neurons and postmortem brain tissue.* Mol Brain, 2012. **5**: p. 35.
328. Zanon, A., et al., *SLP-2 interacts with Parkin in mitochondria and prevents mitochondrial dysfunction in Parkin-deficient human iPSC-derived neurons and Drosophila.* Hum Mol Genet, 2017. **26**(13): p. 2412-2425.
329. Azkona, G., et al., *LRRK2 Expression Is Deregulated in Fibroblasts and Neurons from Parkinson Patients with Mutations in PINK1.* Mol Neurobiol, 2018. **55**(1): p. 506-516.
330. Schondorf, D.C., et al., *The NAD+ Precursor Nicotinamide Riboside Rescues Mitochondrial Defects and Neuronal Loss in iPSC and Fly Models of Parkinson's Disease.* Cell Rep, 2018. **23**(10): p. 2976-2988.
331. Iannielli, A., et al., *Pharmacological Inhibition of Necroptosis Protects from Dopaminergic Neuronal Cell Death in Parkinson's Disease Models.* Cell Rep, 2018. **22**(8): p. 2066-2079.
332. Schwab, A.J., et al., *Decreased Sirtuin Deacetylase Activity in LRRK2 G2019S iPSC-Derived Dopaminergic Neurons.* Stem Cell Reports, 2017. **9**(6): p. 1839-1852.
333. Shaltouki, A., et al., *Mitochondrial alterations by PARKIN in dopaminergic neurons using PARK2 patient-specific and PARK2 knockout isogenic iPSC lines.* Stem Cell Reports, 2015. **4**(5): p. 847-59.

334. Ryan, T., et al., *Cardiolipin exposure on the outer mitochondrial membrane modulates alpha-synuclein.* Nat Commun, 2018. **9**(1): p. 817.
335. Cooper, O., et al., *Pharmacological rescue of mitochondrial deficits in iPSC-derived neural cells from patients with familial Parkinson's disease.* Sci Transl Med, 2012. **4**(141): p. 141ra90.
336. Nguyen, H.N., et al., *LRRK2 mutant iPSC-derived DA neurons demonstrate increased susceptibility to oxidative stress.* Cell Stem Cell, 2011. **8**(3): p. 267-80.
337. Ohta, E., et al., *I2020T mutant LRRK2 iPSC-derived neurons in the Sagamihara family exhibit increased Tau phosphorylation through the AKT/GSK-3beta signaling pathway.* Hum Mol Genet, 2015. **24**(17): p. 4879-900.
338. Jiang, H., et al., *Parkin controls dopamine utilization in human midbrain dopaminergic neurons derived from induced pluripotent stem cells.* Nat Commun, 2012. **3**: p. 668.
339. Vera, E., N. Bosco, and L. Studer, *Generating Late-Onset Human iPSC-Based Disease Models by Inducing Neuronal Age-Related Phenotypes through Telomerase Manipulation.* Cell Rep, 2016. **17**(4): p. 1184-1192.
340. Khurana, V., et al., *Genome-Scale Networks Link Neurodegenerative Disease Genes to alpha-Synuclein through Specific Molecular Pathways.* Cell Syst, 2017. **4**(2): p. 157-170 e14.
341. Sanchez-Danes, A., et al., *Disease-specific phenotypes in dopamine neurons from human iPS-based models of genetic and sporadic Parkinson's disease.* EMBO Mol Med, 2012. **4**(5): p. 380-95.
342. Fernandes, H.J., et al., *ER Stress and Autophagic Perturbations Lead to Elevated Extracellular alpha-Synuclein in GBA-N370S Parkinson's iPSC-Derived Dopamine Neurons.* Stem Cell Reports, 2016. **6**(3): p. 342-56.
343. Schondorf, D.C., et al., *iPSC-derived neurons from GBA1-associated Parkinson's disease patients show autophagic defects and impaired calcium homeostasis.* Nat Commun, 2014. **5**: p. 4028.
344. Korecka, J.A., et al., *Neurite Collapse and Altered ER Ca(2+) Control in Human Parkinson Disease Patient iPSC-Derived Neurons with LRRK2 G2019S Mutation.* Stem Cell Reports, 2019. **12**(1): p. 29-41.
345. Lin, L., et al., *Molecular Features Underlying Neurodegeneration Identified through In Vitro Modeling of Genetically Diverse Parkinson's Disease Patients.* Cell Rep, 2016. **15**(11): p. 2411-26.
346. Qing, X., et al., *CRISPR/Cas9 and piggyBac-mediated footprint-free LRRK2-G2019S knock-in reveals neuronal complexity phenotypes and alpha-Synuclein modulation in dopaminergic neurons.* Stem Cell Res, 2017. **24**: p. 44-50.
347. Reinhardt, P., et al., *Genetic correction of a LRRK2 mutation in human iPSCs links parkinsonian neurodegeneration to ERK-dependent changes in gene expression.* Cell Stem Cell, 2013. **12**(3): p. 354-67.
348. Ren, Y., et al., *Parkin mutations reduce the complexity of neuronal processes in iPSC-derived human neurons.* Stem Cells, 2015. **33**(1): p. 68-78.
349. Kouroupi, G., et al., *Patient-Derived Induced Pluripotent Stem Cell-Based Models in Parkinson's Disease for Drug Identification.* International Journal of Molecular Sciences, 2020. **21**(19): p. 7113.
350. Aflaki, E., et al., *A New Glucocerebrosidase Chaperone Reduces alpha-Synuclein and Glycolipid Levels in iPSC-Derived Dopaminergic Neurons from Patients with Gaucher Disease and Parkinsonism.* J Neurosci, 2016. **36**(28): p. 7441-52.
351. Mazzulli, J.R., et al., *Activation of beta-Glucocerebrosidase Reduces Pathological alpha-Synuclein and Restores Lysosomal Function in Parkinson's Patient Midbrain Neurons.* J Neurosci, 2016. **36**(29): p. 7693-706.

352. Burbulla, L.F., et al., *A modulator of wild-type glucocerebrosidase improves pathogenic phenotypes in dopaminergic neuronal models of Parkinson's disease.* Sci Transl Med, 2019. **11**(514).
353. Kim, M.J., et al., *Acid ceramidase inhibition ameliorates alpha-synuclein accumulation upon loss of GBA1 function.* Hum Mol Genet, 2018. **27**(11): p. 1972-1988.
354. Burbulla, L.F., et al., *Dopamine oxidation mediates mitochondrial and lysosomal dysfunction in Parkinson's disease.* Science, 2017. **357**(6357): p. 1255-1261.
355. Plowey, E.D., et al., *Role of autophagy in G2019S-LRRK2-associated neurite shortening in differentiated SH-SY5Y cells.* J Neurochem, 2008. **105**(3): p. 1048-56.
356. Toth, G., et al., *Targeting the intrinsically disordered structural ensemble of alpha-synuclein by small molecules as a potential therapeutic strategy for Parkinson's disease.* PLoS One, 2014. **9**(2): p. e87133.
357. Wrasidlo, W., et al., *A de novo compound targeting alpha-synuclein improves deficits in models of Parkinson's disease.* Brain, 2016. **139**(Pt 12): p. 3217-3236.
358. Simmnacher, K., et al., *Modeling Cell-Cell Interactions in Parkinson's Disease Using Human Stem Cell-Based Models.* Front Cell Neurosci, 2019. **13**: p. 571.
359. Carelli, V., et al., *Syndromic parkinsonism and dementia associated with OPA1 missense mutations.* Ann Neurol, 2015. **78**(1): p. 21-38.
360. Zheng, W., N. Thorne, and J.C. McKew, *Phenotypic screens as a renewed approach for drug discovery.* Drug Discov Today, 2013. **18**(21-22): p. 1067-73.
361. Goodfellow, P.N., *Genomics and drugs. An interview conducted by Holger Breithaupt and Caroline Hadley.* EMBO Rep, 2004. **5**(9): p. 843-6.
362. Burbaum, J.J. and N.H. Sigal, *New technologies for high-throughput screening.* Curr Opin Chem Biol, 1997. **1**(1): p. 72-8.
363. Gitler, A.D., P. Dhillon, and J. Shorter, *Neurodegenerative disease: models, mechanisms, and a new hope.* Dis Model Mech, 2017. **10**(5): p. 499-502.
364. Zhang, M., et al., *Phenotypic screens targeting neurodegenerative diseases.* J Biomol Screen, 2014. **19**(1): p. 1-16.
365. Swinney, D.C. and J. Anthony, *How were new medicines discovered?* Nat Rev Drug Discov, 2011. **10**(7): p. 507-19.
366. Yamaguchi, A., et al., *Identifying Therapeutic Agents for Amelioration of Mitochondrial Clearance Disorder in Neurons of Familial Parkinson Disease.* Stem Cell Reports, 2020. **14**(6): p. 1060-1075.
367. Tabata, Y., et al., *T-type Calcium Channels Determine the Vulnerability of Dopaminergic Neurons to Mitochondrial Stress in Familial Parkinson Disease.* Stem Cell Reports, 2018. **11**(5): p. 1171-1184.
368. Trudler, D., S. Ghatak, and S.A. Lipton, *Emerging hiPSC Models for Drug Discovery in Neurodegenerative Diseases.* Int J Mol Sci, 2021. **22**(15).
369. Fagiani, F., et al., *Targeting dementias through cancer kinases inhibition.* Alzheimers Dement (N Y), 2020. **6**(1): p. e12044.
370. Klaeger, S., et al., *The target landscape of clinical kinase drugs.* Science, 2017. **358**(6367).
371. Wu, P., T.E. Nielsen, and M.H. Clausen, *FDA-approved small-molecule kinase inhibitors.* Trends Pharmacol Sci, 2015. **36**(7): p. 422-39.
372. Ferguson, F.M. and N.S. Gray, *Kinase inhibitors: the road ahead.* Nat Rev Drug Discov, 2018. **17**(5): p. 353-377.
373. Dorval, T., et al., *Contextual automated 3D analysis of subcellular organelles adapted to high-content screening.* J Biomol Screen, 2010. **15**(7): p. 847-57.
374. Hughes, C.S., et al., *Single-pot, solid-phase-enhanced sample preparation for proteomics experiments.* Nat Protoc, 2019. **14**(1): p. 68-85.

375. Tyanova, S., et al., *The Perseus computational platform for comprehensive analysis of (prote)omics data.* Nat Methods, 2016. **13**(9): p. 731-40.
376. Tiscornia, G., O. Singer, and I.M. Verma, *Production and purification of lentiviral vectors.* Nat Protoc, 2006. **1**(1): p. 241-5.
377. Xilouri, M., et al., *Abberant alpha-synuclein confers toxicity to neurons in part through inhibition of chaperone-mediated autophagy.* PLoS One, 2009. **4**(5): p. e5515.
378. Zygogianni, O., et al., *In Vivo Phenotyping of Familial Parkinson's Disease with Human Induced Pluripotent Stem Cells: A Proof-of-Concept Study.* Neurochem Res, 2019. **44**(6): p. 1475-1493.
379. Cohen, P., D. Cross, and P.A. Janne, *Kinase drug discovery 20 years after imatinib: progress and future directions.* Nat Rev Drug Discov, 2021. **20**(7): p. 551-569.
380. Chambers, S.M., et al., *Highly efficient neural conversion of human ES and iPS cells by dual inhibition of SMAD signaling.* Nat Biotechnol, 2009. **27**(3): p. 275-80.
381. Lovestone, S., et al., *A phase II trial of tideglusib in Alzheimer's disease.* J Alzheimers Dis, 2015. **45**(1): p. 75-88.
382. Pagan, F.L., et al., *Pharmacokinetics and pharmacodynamics of a single dose Nilotinib in individuals with Parkinson's disease.* Pharmacol Res Perspect, 2019. **7**(2): p. e00470.
383. Cuny, G.D., *Kinase inhibitors as potential therapeutics for acute and chronic neurodegenerative conditions.* Curr Pharm Des, 2009. **15**(34): p. 3919-39.
384. Yu, T., et al., *The kinase inhibitor BX795 suppresses the inflammatory response via multiple kinases.* Biochem Pharmacol, 2020. **174**: p. 113797.
385. Clark, K., et al., *Use of the pharmacological inhibitor BX795 to study the regulation and physiological roles of TBK1 and IkappaB kinase epsilon: a distinct upstream kinase mediates Ser-172 phosphorylation and activation.* J Biol Chem, 2009. **284**(21): p. 14136-46.
386. Jaishankar, D., et al., *An off-target effect of BX795 blocks herpes simplex virus type 1 infection of the eye.* Sci Transl Med, 2018. **10**(428).
387. Su, A.R., et al., *BX-795 inhibits HSV-1 and HSV-2 replication by blocking the JNK/p38 pathways without interfering with PDK1 activity in host cells.* Acta Pharmacol Sin, 2017. **38**(3): p. 402-414.
388. Walker, D.G., et al., *Changes in properties of serine 129 phosphorylated alpha-synuclein with progression of Lewy-type histopathology in human brains.* Exp Neurol, 2013. **240**: p. 190-204.
389. Bai, L.Y., et al., *BX795, a TBK1 inhibitor, exhibits antitumor activity in human oral squamous cell carcinoma through apoptosis induction and mitotic phase arrest.* Eur J Pharmacol, 2015. **769**: p. 287-96.
390. Cox, J., et al., *Accurate proteome-wide label-free quantification by delayed normalization and maximal peptide ratio extraction, termed MaxLFQ.* Mol Cell Proteomics, 2014. **13**(9): p. 2513-26.
391. Cox, J. and M. Mann, *MaxQuant enables high peptide identification rates, individualized p.p.b.-range mass accuracies and proteome-wide protein quantification.* Nat Biotechnol, 2008. **26**(12): p. 1367-72.
392. Chung, C.Y., et al., *In Situ Peroxidase Labeling and Mass-Spectrometry Connects Alpha-Synuclein Directly to Endocytic Trafficking and mRNA Metabolism in Neurons.* Cell Syst, 2017. **4**(2): p. 242-250 e4.
393. Keren-Shaul, H., G. Lev-Maor, and G. Ast, *Pre-mRNA splicing is a determinant of nucleosome organization.* PLoS One, 2013. **8**(1): p. e53506.
394. Chen, W., L. Luo, and L. Zhang, *The organization of nucleosomes around splice sites.* Nucleic Acids Res, 2010. **38**(9): p. 2788-98.
395. Bowden, H.A. and D. Dormann, *Altered mRNP granule dynamics in FTLD pathogenesis.* J Neurochem, 2016. **138 Suppl 1**: p. 112-33.
396. Park, S.G., P. Schimmel, and S. Kim, *Aminoacyl tRNA synthetases and their connections to disease.* Proc Natl Acad Sci U S A, 2008. **105**(32): p. 11043-9.

397. Kapur, M., C.E. Monaghan, and S.L. Ackerman, *Regulation of mRNA Translation in Neurons-A Matter of Life and Death.* Neuron, 2017. **96**(3): p. 616-637.
398. Carpanini, S.M., et al., *A novel mouse model of Warburg Micro syndrome reveals roles for RAB18 in eye development and organisation of the neuronal cytoskeleton.* Dis Model Mech, 2014. **7**(6): p. 711-22.
399. Feldmann, A., et al., *The RAB GTPase RAB18 modulates macroautophagy and proteostasis.* Biochem Biophys Res Commun, 2017. **486**(3): p. 738-743.
400. Jean, S., et al., *Starvation-induced MTMR13 and RAB21 activity regulates VAMP8 to promote autophagosome-lysosome fusion.* EMBO Rep, 2015. **16**(3): p. 297-311.
401. Rocca, D.L., et al., *The small GTPase Arf1 modulates Arp2/3-mediated actin polymerization via PICK1 to regulate synaptic plasticity.* Neuron, 2013. **79**(2): p. 293-307.
402. Farley, M.M. and T.A. Watkins, *Intrinsic Neuronal Stress Response Pathways in Injury and Disease.* Annu Rev Pathol, 2018. **13**: p. 93-116.
403. Maraganore, D.M., et al., *UCHL1 is a Parkinson's disease susceptibility gene.* Ann Neurol, 2004. **55**(4): p. 512-21.
404. Williams, E.T., X. Chen, and D.J. Moore, *VPS35, the Retromer Complex and Parkinson's Disease.* J Parkinsons Dis, 2017. **7**(2): p. 219-233.
405. Chi, B., et al., *The neurodegenerative diseases ALS and SMA are linked at the molecular level via the ASC-1 complex.* Nucleic Acids Res, 2018. **46**(22): p. 11939-11951.
406. Abramzon, Y.A., et al., *The Overlapping Genetics of Amyotrophic Lateral Sclerosis and Frontotemporal Dementia.* Front Neurosci, 2020. **14**: p. 42.
407. Gonzalez, M.A., et al., *A novel mutation in VCP causes Charcot-Marie-Tooth Type 2 disease.* Brain, 2014. **137**(Pt 11): p. 2897-902.
408. Aminkeng, F., *HINT1 mutations define a novel disease entity - autosomal recessive axonal neuropathy with neuromyotonia.* Clin Genet, 2013. **83**(1): p. 31-2.
409. Haverfield, E.V., et al., *Intragenic deletions and duplications of the LIS1 and DCX genes: a major disease-causing mechanism in lissencephaly and subcortical band heterotopia.* Eur J Hum Genet, 2009. **17**(7): p. 911-8.
410. Bernert, G., M. Fountoulakis, and G. Lubec, *Manifold decreased protein levels of matrin 3, reduced motor protein HMP and hlark in fetal Down's syndrome brain.* Proteomics, 2002. **2**(12): p. 1752-7.
411. Shima, H., et al., *Disruption of the p70(s6k)/p85(s6k) gene reveals a small mouse phenotype and a new functional S6 kinase.* EMBO J, 1998. **17**(22): p. 6649-59.
412. Rabanal-Ruiz, Y., E.G. Otten, and V.I. Korolchuk, *mTORC1 as the main gateway to autophagy.* Essays Biochem, 2017. **61**(6): p. 565-584.
413. Kabeya, Y., et al., *LC3, a mammalian homologue of yeast Apg8p, is localized in autophagosome membranes after processing.* EMBO J, 2000. **19**(21): p. 5720-8.
414. Jiang, P. and N. Mizushima, *LC3- and p62-based biochemical methods for the analysis of autophagy progression in mammalian cells.* Methods, 2015. **75**: p. 13-8.
415. Lopez, A., A. Fleming, and D.C. Rubinsztein, *Seeing is believing: methods to monitor vertebrate autophagy in vivo.* Open Biol, 2018. **8**(10).
416. Pankiv, S., et al., *p62/SQSTM1 binds directly to Atg8/LC3 to facilitate degradation of ubiquitinated protein aggregates by autophagy.* J Biol Chem, 2007. **282**(33): p. 24131-45.
417. Spira, P.J., et al., *Clinical and pathological features of a Parkinsonian syndrome in a family with an Ala53Thr alpha-synuclein mutation.* Ann Neurol, 2001. **49**(3): p. 313-9.
418. Yamaguchi, K., et al., *Abundant neuritic inclusions and microvacuolar changes in a case of diffuse Lewy body disease with the A53T mutation in the alpha-synuclein gene.* Acta Neuropathol, 2005. **110**(3): p. 298-305.

419. Apicco, D.J., et al., *Reducing the RNA binding protein TIA1 protects against tau-mediated neurodegeneration in vivo.* Nat Neurosci, 2018. **21**(1): p. 72-80.
420. Brunello, C.A., X. Yan, and H.J. Huttunen, *Internalized Tau sensitizes cells to stress by promoting formation and stability of stress granules.* Sci Rep, 2016. **6**: p. 30498.
421. De Santis, R., et al., *Mutant FUS and ELAVL4 (HuD) Aberrant Crosstalk in Amyotrophic Lateral Sclerosis.* Cell Rep, 2019. **27**(13): p. 3818-3831 e5.
422. Martinez, F.J., et al., *Protein-RNA Networks Regulated by Normal and ALS-Associated Mutant HNRNPA2B1 in the Nervous System.* Neuron, 2016. **92**(4): p. 780-795.
423. Naftelberg, S., et al., *Regulation of alternative splicing through coupling with transcription and chromatin structure.* Annu Rev Biochem, 2015. **84**: p. 165-98.
424. Milanese, C., et al., *Activation of the DNA damage response in vivo in synucleinopathy models of Parkinson's disease.* Cell Death Dis, 2018. **9**(8): p. 818.
425. Pinho, R., et al., *Nuclear localization and phosphorylation modulate pathological effects of alpha-synuclein.* Hum Mol Genet, 2019. **28**(1): p. 31-50.
426. Schaser, A.J., et al., *Alpha-synuclein is a DNA binding protein that modulates DNA repair with implications for Lewy body disorders.* Sci Rep, 2019. **9**(1): p. 10919.
427. Yeo, G., et al., *Variation in alternative splicing across human tissues.* Genome Biol, 2004. **5**(10): p. R74.
428. Apicco, D.J., et al., *Dysregulation of RNA Splicing in Tauopathies.* Cell Rep, 2019. **29**(13): p. 4377-4388 e4.
429. Johnson, S.C., P.S. Rabinovitch, and M. Kaeberlein, *mTOR is a key modulator of ageing and age-related disease.* Nature, 2013. **493**(7432): p. 338-45.
430. Kim, J. and K.L. Guan, *mTOR as a central hub of nutrient signalling and cell growth.* Nat Cell Biol, 2019. **21**(1): p. 63-71.
431. Xun, Z., et al., *Quantitative proteomics of a presymptomatic A53T alpha-synuclein Drosophila model of Parkinson disease.* Mol Cell Proteomics, 2008. **7**(7): p. 1191-203.
432. Fernandez-Santiago, R., et al., *SNCA and mTOR Pathway Single Nucleotide Polymorphisms Interact to Modulate the Age at Onset of Parkinson's Disease.* Mov Disord, 2019. **34**(9): p. 1333-1344.
433. Arotcarena, M.L., M. Teil, and B. Dehay, *Autophagy in Synucleinopathy: The Overwhelmed and Defective Machinery.* Cells, 2019. **8**(6).
434. Menzies, F.M., et al., *Autophagy and Neurodegeneration: Pathogenic Mechanisms and Therapeutic Opportunities.* Neuron, 2017. **93**(5): p. 1015-1034.
435. Levine, B. and G. Kroemer, *Biological Functions of Autophagy Genes: A Disease Perspective.* Cell, 2019. **176**(1-2): p. 11-42.
436. Pohl, C. and I. Dikic, *Cellular quality control by the ubiquitin-proteasome system and autophagy.* Science, 2019. **366**(6467): p. 818-822.
437. Oakes, J.A., M.C. Davies, and M.O. Collins, *TBK1: a new player in ALS linking autophagy and neuroinflammation.* Mol Brain, 2017. **10**(1): p. 5.
438. Pietri, M., et al., *PDK1 decreases TACE-mediated alpha-secretase activity and promotes disease progression in prion and Alzheimer's diseases.* Nat Med, 2013. **19**(9): p. 1124-31.
439. Bodur, C., et al., *The IKK-related kinase TBK1 activates mTORC1 directly in response to growth factors and innate immune agonists.* 2018. **37**(1): p. 19-38.
440. Centeno, E.G.Z., H. Cimarosti, and A. Bithell, *2D versus 3D human induced pluripotent stem cell-derived cultures for neurodegenerative disease modelling.* Mol Neurodegener, 2018. **13**(1): p. 27.
441. Tekin, H., et al., *Effects of 3D culturing conditions on the transcriptomic profile of stem-cell-derived neurons.* Nat Biomed Eng, 2018. **2**(7): p. 540-554.

442. Baker, M.G. and L. Graham, *The journey: Parkinson's disease.* BMJ, 2004. **329**(7466): p. 611-4.
443. Olanow, C.W. and W.G. Tatton, *Etiology and pathogenesis of Parkinson's disease.* Annu Rev Neurosci, 1999. **22**: p. 123-44.
444. Pfeiffer, R.F., *Non-motor symptoms in Parkinson's disease.* Parkinsonism Relat Disord, 2016. **22 Suppl 1**: p. S119-22.
445. Gibb, W., *Idiopathic Parkinson's disease and the Lewy body disorders.* Neuropathology and applied neurobiology, 1986. **12**(3): p. 223-234.
446. Lewandowsky, M.H., *Handbuch der neurologie: bd. Spezielle Neurologie IV*. Vol. 5. 1914: J. Spring.
447. Baba, M., et al., *Aggregation of alpha-synuclein in Lewy bodies of sporadic Parkinson's disease and dementia with Lewy bodies.* Am J Pathol, 1998. **152**(4): p. 879-84.
448. Breydo, L., J.W. Wu, and V.N. Uversky, *Alpha-synuclein misfolding and Parkinson's disease.* Biochim Biophys Acta, 2012. **1822**(2): p. 261-85.
449. Conway, K.A., et al., *Acceleration of oligomerization, not fibrillization, is a shared property of both alpha-synuclein mutations linked to early-onset Parkinson's disease: implications for pathogenesis and therapy.* Proc Natl Acad Sci U S A, 2000. **97**(2): p. 571-6.
450. Duda, J.E., et al., *Concurrence of alpha-synuclein and tau brain pathology in the Contursi kindred.* Acta Neuropathol, 2002. **104**(1): p. 7-11.
451. Kotzbauer, P.T., et al., *Fibrillization of alpha-synuclein and tau in familial Parkinson's disease caused by the A53T alpha-synuclein mutation.* Exp Neurol, 2004. **187**(2): p. 279-88.
452. Cotzias, G.C., M.H. Van Woert, and L.M. Schiffer, *Aromatic amino acids and modification of parkinsonism.* N Engl J Med, 1967. **276**(7): p. 374-9.
453. Ghosh, D., et al., *alpha-synuclein aggregation and its modulation.* Int J Biol Macromol, 2017. **100**: p. 37-54.
454. Schulz-Schaeffer, W.J., *The synaptic pathology of alpha-synuclein aggregation in dementia with Lewy bodies, Parkinson's disease and Parkinson's disease dementia.* Acta Neuropathol, 2010. **120**(2): p. 131-43.
455. Chen, M., et al., *Common proteomic profiles of induced pluripotent stem cell-derived three-dimensional neurons and brain tissue from Alzheimer patients.* J Proteomics, 2018. **182**: p. 21-33.
456. Yang, Y.M., et al., *A small molecule screen in stem-cell-derived motor neurons identifies a kinase inhibitor as a candidate therapeutic for ALS.* Cell Stem Cell, 2013. **12**(6): p. 713-26.
457. Garcia-Esparcia, P., et al., *Altered machinery of protein synthesis is region- and stage-dependent and is associated with alpha-synuclein oligomers in Parkinson's disease.* Acta Neuropathol Commun, 2015. **3**: p. 76.

# Curriculum Vitae

PERSONAL INFORMATION

**Name:**Athanasia(Nasia)

**Surname**: Antoniou

**Contact Information:**
Tel: +306942205843
Email:nasiaantoniou@gmail.com

EDUCATION/TRAINING

| INSTITUTION AND LOCATION | DEGREE | YEAR(s) | FIELD OF STUDY |
|---|---|---|---|
| National & Kapodistrian University of Athens, Faculty of Biology, Athens, Greece and Division of Basic Neurosciences, Biomedical Research Foundation of the Academy of Athens, Greece (BRFAA) | BSc | 2005-2010 | Biology |
| National & Kapodistrian University of Athens, Faculty of Biology, Athens, Greece and Division of Basic Neurosciences, Biomedical Research Foundation of the Academy of Athens, Greece (BRFAA) | MSc | 2010-2013 | Applications of Biology in Medicine |
| National & Kapodistrian University of Athens, Faculty of Biology, Athens, Greece and Division of Basic Neurosciences, Biomedical Research Foundation of the Academy of Athens, Greece (BRFAA) | Phd | 2014-2022 | Cellular and Molecular Neurobiology |

**A. Research Experience**

2009-2011: BSc thesis in Dr.Stefanis' Lab(Biomedical Research Foundation of the Academy of Athens)
*Mapping the interaction between LRRK2 and FADD that mediates mutant LRRK2 neurodegeneration*

2011-2013: MSc thesis in Dr.Stefanis' Lab(Biomedical Research Foundation of the Academy of Athens)
*a.Identification of a critical region within LRRK2 that mediates the interaction with the cell death adaptor protein FADD*
*b. Caspase-8 dependent cleavage of LRRK2 is required for its oligomerization and induction of neuronal death*

2014- 2022 : Phd in Dr.Matsa's Lab (Hellenic Pasteur Institute)
*Study of the pathogenic mechanisms that lead to Parkinson's disease using neuronal cell models*

2015 September - 2016 January : Training internship in Dr.Grailhe's Lab ( Institute Pasteur Korea)
*Identification of kinase inhibitors that promote dopaminergic differentiation of NPCs using a human induced pluripotent stem cell-based model*

**B.Laboratory techniques and assays**

i.Molecular Genetics, Cellular Biology & Neurobiology

PCR; Cell Culture (Primary cells, Cell lines, iPS cells); Plasmids Construction; Site-Directed Mutagenesis; Transformation; Electroporation; Transfection assays; Cell death assays; Immunocytochemistry; Stereoscopy; Microscopy (Fluorescence, Confocal)

ii.Biochemistry & Chemistry
Extraction Assays (DNA, RNA, Gel); Electrophoresis (Gel Agarose, SDS-PAGE); Western Blotting; Immunoprecipitation assays; Protein cleavage assays; Size-Exclusion Chromatography (SEC)

iii.Electrophysiology

Patch-clamp in cultured neurons

**C. Announcements (selected)**

**Nasia Antoniou**, Kanella Prodromidou, Georgia Kouroupi, EraTaoufik, Regis Grailhe, Martina Samiotaki, George Panayotou, and Rebecca Matsas. High Content Screening in a Human Model of Familial Parkinson's Disease Reveals a Kinase Inhibitor that protects from neurodegeneration. The Hellenic Society for Neuroscience Meeting, October 4-6, 2019, Crete, Athens.

Era Taoufik, Georgia Kouroupi, Konstantinos Tsioras, Ioannis Vlachos, Delphine Bohl, **Nasia Antoniou**, Dafni Chroni , Kostas Vekrellis, Piotr Bregestovski, Leonidas Stefanis , Artemis Hatzigeorgiou and Rebecca

Matsas. *Synaptic dysregulation in human induced pluripotent stem cell-derived neurons carrying the A53T alpha synuclein mutation.* ISSCR 2015 Annual Meeting Stockholm, Sweden, June 24-27 2015

Kouroupi Georgia, Taoufik Era, Tsioras Konstantinos, Bohl Delphine, **Antoniou Nasia**, Chroni Dafni, Politis Panagiotis, Stellas Dimitris, Vekrellis Kostas, Bregestovski Piotr, Stefanis Leonidas, Matsas Rebecca. *Cellular stress responces of A53T alphasynuclein iPS-derived neurons reveal defects in oxidative state, apoptosis and protein degradation.* 12th annual meeting Vancouver, Canada, June 18-21 2014

Rideout HJ, Valkimadi P, **Antoniou N**. *LRRK2 Oligomerization and the recruitment of FADD and caspase -8 to oligomeric cell-death signaling complexes*. 23rd Biennial Meeting of the International Society of Neurochemistry, Athens, August 2011 (**Best Poster Award**)

**N. Antoniou**, P. Valkimadi, H. Rideout. *Identification of a critical region within LRRK2 that mediates the interaction with the cell death adaptor protein FADD*. 15th International Congress of Parkinson's Disease and Movement
Disorders, Toronto, June 2011.

P. Valkimadi, **N. Antoniou**, H. Rideout. *Detection of high molecular weight LRRK2 protein complexes in a cellular model of LRRK2 neurodegeneration.* 15th International Congress of Parkinson's Disease and Movement Disorders,
Toronto, June 2011.

H. Rideout, **N. Antoniou,** P. Valkimadi, W. Dauer. *Mutant LRRK2 and Cell Death-Signaling Complex Formation:*

*Implications for Neurodegeneration in Parkinson's Disease.* 2010 American Academy of Neurology Annual Meeting. Toronto, April 10-17.

**D.Publications**

▪Antoniou, N., Prodromidou, K., Kouroupi, G. et al. High content screening and proteomic analysis identify a kinase inhibitor that rescues pathological phenotypes in a patient-derived model of Parkinson's disease. npj Parkinsons Dis. 8, 15 (2022). https://doi.org/10.1038/s41531-022-00278-y

▪Kouroupi, G.; Antoniou, N.; Prodromidou, K.; Taoufik, E.; Matsas, R. Patient-Derived Induced Pluripotent Stem Cell-Based Models in Parkinson's Disease for Drug Identification. Int. J. Mol. Sci. 2020, 21, 7113. doi.org/10.3390/ijms21197113

▪O. Zygogianni, N. Antoniou, M. Kalomoiri, G. Kouroupi, E. Taoufik, R.Matsas (2019) In vivo phenotyping of familial Parkinson's disease with human induced pluripotent stem cells: a proof-of-concept study Neurochem Res. 2019 Apr 15. doi: 10.1007/s11064-019-02781-w.

▪Antoniou N, Vlachakis D, Memou A, Leandrou E, Valkimadi P, Melachroinou K; Re B. D, Przedborskid S, Dauer W, Stefanis L, Rideout J. H (2017) A motif within the armadillo repeat of Parkinson's-linked LRRK2interacts with FADD to hijack the extrinsic death pathway Scientific Reports, Scientific Reports, 2018. 8(1): p. 3455

▪G. Kouroupi, E. Taoufik, I. S. Vlachos, K. Tsioras, N. Antoniou, F. Papastefanaki, D. Chroni-Tzartou, W. Wrasidlo, D. Bohl, D. Stellas, P. K. Politis, K. Vekrellis, D. Papadimitriou, L. Stefanis, P. Bregestovski, A. G. Hatzigeorgiou, E. Masliah and R. Matsas (2017) Defective synaptic connectivity and axonal neuropathology in a human iPSC-based model of familial Parkinson's disease Proc. Natl. Acad. Sci. USA, Proc Natl Acad Sci U S A, 2017. 114(18): p. E3679-E3688.

▪Aravantinou-Fatorou K, Ortega F, Chroni-Tzartou D, Antoniou N, Poulopoulou C, Politis P, Berninger B, Matsas R, and Thomaidou D (2015) Cend1 and Neurogenin2 reprogram mouse astrocytes and embryonic fibroblasts to induced neural precursors and differentiated neurons Stem Cell Reports5(3):405-18

**E. Awards**

2015-2016: Calmette-Yersin grant: Identification of therapeutic targets for Parkinson’s disease using a humaninduced pluripotent stem cell-based model. Collaborative proposal between IP-Hellenic and IP-Korea.

2016: Grant for participation in the Course: High Content Assay for Target Discovery Using RNAi technology, Institute Pasteur Korea

2017: Grant for participation in the meeting '20 years of alpha- synuclein in Parkinson's Disease & related synucleinopathies: from the bedside to the bench and back to the patient'

2018: FENS and IBRO-PERC stipend to attend Synapses, neuronal circuits and behavior course, 9-20 April 2018, Coimbra, Portugal

2019: Grand for participation in Cell biology course on Proteomics, 27 October- 2 November 2019, Hong Kong

**F. Languages**

Greek (Native speaker)

English (Fluent-Proficiency)

French (Basic)

# APPENDIX

npj | Parkinson's Disease

www.nature.com/npjparkd

ARTICLE OPEN

Check for updates

# High content screening and proteomic analysis identify a kinase inhibitor that rescues pathological phenotypes in a patient-derived model of Parkinson's disease

Nasia Antoniou[1,2], Kanella Prodromidou[1], Georgia Kouroupi[1], Ioanna Boumpoureka[1], Martina Samiotaki[3], George Panayotou[3], Maria Xilouri[4], Ismini Kloukina[4], Leonidas Stefanis[4,5], Regis Grailhe[6], Era Taoufik[1,7] and Rebecca Matsas[1,7]✉

Combining high throughput screening approaches with induced pluripotent stem cell (iPSC)-based disease modeling represents a promising unbiased strategy to identify therapies for neurodegenerative disorders. Here we applied high content imaging on iPSC-derived neurons from patients with familial Parkinson's disease bearing the G209A (p.A53T) α-synuclein (αSyn) mutation and launched a screening campaign on a small kinase inhibitor library. We thus identified the multi-kinase inhibitor BX795 that at a single dose effectively restores disease-associated neurodegenerative phenotypes. Proteomics profiling mapped the molecular pathways underlying the protective effects of BX795, comprising a cohort of 118 protein-mediators of the core biological processes of RNA metabolism, protein synthesis, modification and clearance, and stress response, all linked to the mTORC1 signaling hub. In agreement, expression of human p.A53T-αSyn in neuronal cells affected key components of the mTORC1 pathway resulting in aberrant protein synthesis that was restored in the presence of BX795 with concurrent facilitation of autophagy. Taken together, we have identified a promising small molecule with neuroprotective actions as candidate therapeutic for PD and other protein conformational disorders.

*npj Parkinson's Disease* (2022)8:15 ; https://doi.org/10.1038/s41531-022-00278-y

## INTRODUCTION

Parkinson's disease (PD) is a complex neurodegenerative disorder affecting 2% of the world population over 65 years of age[1]. PD is characterized by motor dysfunction related to the progressive loss of midbrain dopamine neurons[2] while a wide range of non-motor symptoms are also present such as psychiatric manifestations and cognitive impairment[3]. The neuropathological hallmark of PD is the presence of intracytoplasmic inclusions in neuronal cell bodies and neurites, respectively termed Lewy bodies and Lewy neurites[4,5]. These are protein aggregates composed mainly of α-synuclein (αSyn), the major protein linked to sporadic PD[6]. αSyn belongs to a class of intrinsically disordered amyloid proteins that form specific forms of oligomeric and fibrillar aggregates and exert neurotoxicity through various molecular pathways[7]. Several point mutations (A30P, E46K, A53T, G51D) and multiplications of the *SNCA* locus encoding for αSyn cause autosomal dominant forms of PD[8–10]. Among the different variants, the p.A53TαSyn mutation is generally considered to accelerate aggregation[11] resulting in widespread accumulation of insoluble α-syn deposits that have been identified in the post-mortem p.A53T human brain[12,13]. Despite extensive efforts in understanding PD pathogenesis, no disease modifying drugs exist. Currently only symptomatic or palliative treatments are available with none capable to prevent or slow-down disease progression. Dopamine-replacement drugs, such as levodopa, which was identified 53 years ago[14], are used to ameliorate motor symptoms and remain the primary and most effective treatment despite the undesired side-effects and deterioration of efficacy with disease progression. Therefore, the development of disease-modifying drugs is an urgent unmet need. Most present-day efforts in identifying PD therapeutics target the aggregation of misfolded αSyn as the major pathogenic factor that causes cellular toxicity[6,15–17]. Alternative strategies to tackle early steps in neurodegeneration, particularly in an unbiased approach, have lagged behind. Recent advances in patient-derived induced pluripotent stem cell (iPSC)-based models for neurodegenerative diseases permit the detection of early, potentially triggering, pathologic phenotypes and provide amenable systems for drug discovery. In combination with high throughput high content screening technologies, these approaches open new perspectives for identification of disease-modifying compounds[18–21].

We have previously established a model of iPSC-derived neurons from patients with familial PD harboring the p.A53T αSyn mutation (G209A in the *SNCA* gene) that displays disease-relevant phenotypes at basal conditions[22]. In this study, we successfully adapted this cellular system to perform a small molecule screen on human p.A53T-neurons and discovered that the multi-kinase inhibitor BX795 significantly reverts disease-associated phenotypes. A single treatment of patient neurons with BX795 has sustainable effects in supporting neuritic growth, restoring axonal pathology and limiting αSyn protein aggregate formation. Protection from p.A53T-associated pathology was also confirmed in human iPSC-derived neurons in which the mutation was introduced by genome editing, against isogenic wild-type

[1]Laboratory of Cellular and Molecular Neurobiology-Stem Cells, Hellenic Pasteur Institute, 127 Vassilissis Sofias Avenue, 11521 Athens, Greece. [2]Division of Animal and Human Physiology, Department of Biology, National & Kapodistrian University of Athens, Panepistimioupolis, Ilisia, Greece. [3]Institute of Bioinnovation, Biomedical Sciences Research Center "Alexander Fleming", Vari 16672, Greece. [4]Center of Clinical Research, Experimental Surgery and Translational Research, Biomedical Research Foundation of the Academy of Athens (BRFAA), 4 Soranou Efesiou Street, 11527 Athens, Greece. [5]1st Department of Neurology, Eginition Hospital, Medical School, National and Kapodistrian University of Athens, Athens, Greece. [6]Technology Development Platform, Screening Sciences & Novel Assay Technology, Institut Pasteur Korea, Bundang-gu, Seongnam-si, Gyeonggi-do 463-400, Republic of Korea. [7]These authors contributed equally: Era Taoufik, Rebecca Matsas. ✉email: rmatsa@pasteur.gr

Published in partnership with the Parkinson's Foundation

npj nature partner journals

Parkinson's Foundation

controls. Strikingly, proteomics profiling by quantitative mass spectrometry revealed that BX795 treatment results in significant downregulation of a cohort of 118 proteins that are abnormally upregulated in p.A53T-neurons. Enrichment analysis demonstrated that these proteins are associated with mRNA metabolism, mRNA transport and translation, protein metabolism and degradation processes. Using neuronal cells expressing the human p.A53T-αSyn, we demonstrate that BX795 affects the mTORC1 pathway to restrict excessive protein synthesis and facilitate autophagy. Taken together, our data highlight the BX795 kinase inhibitor as a compelling compound and candidate therapeutic that ameliorates p.A53T-related pathology.

## RESULTS

### Assay development for high-content screening of p.A53T-iPSC derived neurons

iPSCs used in this study were previously generated from a PD patient bearing the p.A53T αSyn mutation and thoroughly characterized[22]. For directed differentiation a dual SMAD inhibition protocol was used in the presence of Noggin and TGFβ inhibitor[22–24], which favors the generation and expansion of Pax6+/Nestin+ neural progenitor cells (NPCs; Fig. 1a). NPCs were further differentiated into βIII-tubulin (TUJ1)+ neurons (Fig. 1a) with 15-20% also expressing the dopaminergic marker TH at 21 DIV (Fig. 1a). The expression of dopaminergic lineage markers, such as Nurr1, TH, and aromatic amino acid decarboxylase (AADC) was confirmed by qRT-PCR (Supplementary Fig. 1). As readout for compound screening, we assessed TH immunofluorescence in iPSC-derived neurons adapted in miniature 384-well plates, seeking to identify putative neuroprotective compounds enhancing dopaminergic neuron output. To this end, the fluorescent signal for TH within a well was normalized to the fluorescent signal for the pan-neuronal marker βIII-tubulin (TUJ1) (Fig. 1b), allowing to monitor changes in the TH population in a simple and effective way.

### High content screening of a kinase inhibitor library identifies BX795 as a compound that increases TH immunofluorescence in p.A53T-neurons

Protein kinases represent central molecular hubs that regulate numerous cell processes, thus constituting potentially attractive clinical targets. Indeed, the success of kinase inhibitors in treating cancer has spurred the evaluation of such compounds in phase II/III clinical trials as candidates for treatment of various neurodegenerative diseases[25,26]. Since several kinases have been implicated in PD pathology[27], we screened a collection of 273 small molecule kinase inhibitors (Supplementary Table 1) to identify compounds with prospective neuroprotective properties. p.A53T cells were exposed once (7 DIV) to the library of kinase inhibitors at 1 μM concentration and quantitative image analysis was performed at 21 DIV (Fig. 1a). Hits were defined as compounds that robustly conferred an increase in TH immunofluorescence compared to DMSO-treated p.A53T neurons within a well, normalized to the immunofluorescence of the pan-neuronal marker βIII-tubuin (TUJ1) (Fig. 1b, Supplementary Fig. 2). Toxic compounds were excluded by assessing cellular viability (total nuclei count) of compound-treated as compared to DMSO-treated cells (Supplementary Fig. 3). Four hits were identified in the primary screen (Fig. 1b), which were re-tested for validation in a dose-response assay (Fig. 1d). Of these, only BX795, an aminopyrimidine compound that acts as a multi-kinase inhibitor with pro-survival and/or anti-inflammatory action[28], showed a consistent dose-response effect and significantly increased TH immunofluorescence at 1 μM (Fig. 1c, d). BX-795 was initially developed as an ATP-competitive inhibitor of 3-phosphoinositide-dependent kinase 1 (PDK1), but was later shown to inhibit the IKK-related kinase, TANK-binding kinase 1 (TBK1) and IKKε, as well as to have numerous additional targets[29–31]. Based on the sustained effect of a single dose of BX795 on p.A53T dopaminergic neurons (Fig. 1d), we focused further on this compound to explore its function.

### BX795 rescues neuropathological features of p.A53T neurons

The effects of BX795 on p.A53T-neurons were tested in cells that received a single treatment of the kinase inhibitor (1 μM) at 7 DIV and were analyzed at 21 DIV, in accordance with the protocol applied during the screening procedure. Prior to this, an initial set of experiments was performed using drug concentrations from 0.1-2 μM and repeated drug additions every 3 days, with the selected scheme ensuring optimal efficacy and minimal toxicity. Initially, we asked if the enhancement in TH immunofluorescence could be attributed to an increase in cell survival/proliferation or dopaminergic differentiation in p.A53T-cultures. We could not detect BX795-driven changes in either proliferation, as assessed by the percentage of Ki67+ cells (Supplementary Fig. 1; % Ki67+ cells, DMSO: 43.3 ± 4.4; BX795: 50.3 ± 1.5, $n = 3$), or in differentiation as estimated by the percentage of TH+ cells in the culture (% TH+/TUJ1+ neurons, DMSO: 13.9 ± 3.1; BX795: 18.1.0 ± 3.9, $n = 3$). Moreover, we did not detect any change in total cell viability, as assessed b nuclei count (Supplementary Fig. 1). These observations indicate that the effect of BX795 on dopaminergic neurons is not related to an increase in either survival/proliferation or differentiation.

Next, we investigated if treatment with BX795 could rescue neuropathological features previously identified in p.A53T-neurons, such as compromised neuritic growth, dystrophic or fragmented neurites and the presence of intracellular protein aggregates[22,32]. Overall, disease-associated phenotypes were assessed in iPSC-derived neurons from two p.A53T patients [22] and an iPSC gene-edited line in which the p.A53T mutation was inserted in one allele, against healthy or isogenic controls. Evaluation of total neurite length in TH+ dopaminergic neurons from the first p.A53T patient revealed a significant increase in response to BX795 compatible with the observed increase in TH immunofluorescence (length in μm, ctl: 221.7 ± 16.8, p.A53T:127.2 ± 13.5, p.A53T + BX795: 196.8 ± 21.1, $n = 5$, Fig. 2a). Moreover, examination of the distinct pathological morphology of TUJ1+ p.A53T neurons revealed an almost 50% reduction in axonal degeneration (axon degeneration index: ctl: 2.945 ± 1.325, p.A53T:13.03 ± 1.491, p.A53T + BX795: 7.276 ± 1.017 $n = 3$; Fig. 2b). Finally, exposure to BX795 resulted in a notable 60% decrease in protein aggregate formation in p.A53T cells (number of aggregates per cell, ctl: 2.384 ± 0.89, $n = 30$, p.A53T: 8.431 ± 0.77, $n = 51$, p.A53T+ BX795: 3.242 ± 0.40, $n = 62$; Fig. 2c). This was accompanied by a consistent decline in the levels of (Ser129)-phosphorylated αSyn (Fig. 2d), a modification that renders αSyn prone to self-assembly and is commonly associated with synucleinopathy[33,34]. The neuroprotective effects of BX795 were confirmed in p.A53T-neurons from a second patient[22,32] (Supplementary Fig. 4).

We also assessed the neuroprotective effects of BX795 in a highly enriched culture of mature human midbrain dopaminergic neurons (Fujifilm Cellular Dynamics Inc). These comprised an isogenic pair of wild-type (iCell DOPA) and gene-edited (iCell A53T DOPA) iPSC-derived neurons in which a heterozygous p.A53T mutation was inserted into one allele of the *SNCA* gene. After 14 days, more than 90% of cells were TUJ1+ and more than 80% were TH+ dopaminergic neurons (Fig. 3a). At this time and similarly to patient-derived cells, abundant protein aggregates were detected in the p.A53T iCell neurons compared to their isogenic control, and treatment with BX795 resulted in a significant reduction (number of aggregates per cell, ctl:2.7 ± 0.49, $n = 57$, p.A53T: 9.9 ± 1.1, $n = 76$, p.A53T+ BX795:4.9 ± 0.7, $n = 76$; Fig. 3b, c).

Taken together our results indicate that BX795 exerts prominent and sustainable neuroprotection in p.A53T neurons by improving

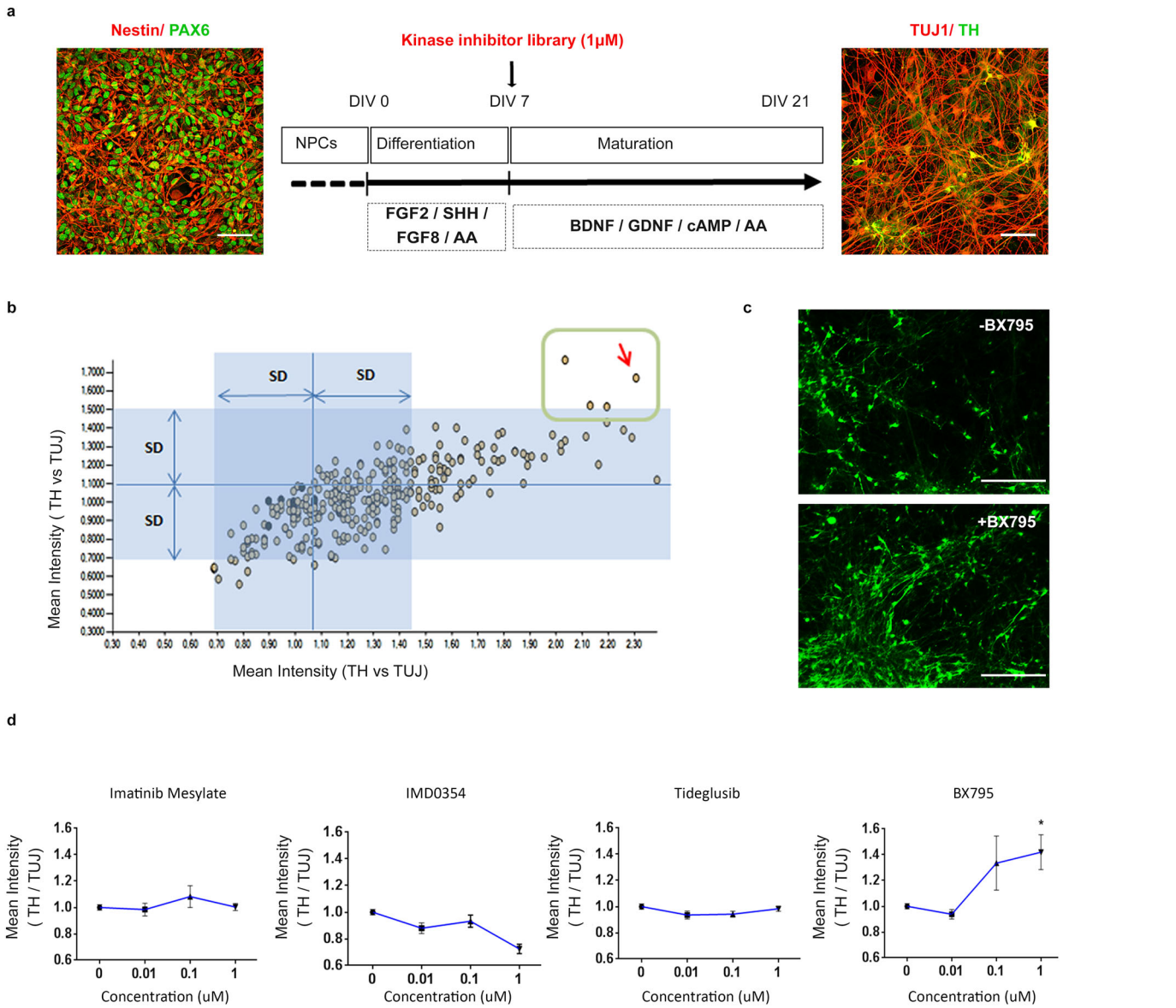


**Fig. 1 Identification of BX795 by high content screening of a kinase inhibitor library. a** Directed differentiation of Pax6+ (green)/Nestin+ (red) neural precursor cells (NPCs; DIV 0, left) into TUJ1+ (red)/ TH+ (green) neurons (DIV 21, right). The differentiation protocol and timeline of analysis are shown in the drawing in the middle. FG2 and FGF8, fibroblast growth factors 2 and 8; SHH Sonic Hedgehog, AA ascorbic acid, Scale bar represents BDNF brain-derived neurotrophic factor, GDNF glial cell-derived neurotrophic factor (GDNF), cAMP cyclic AMP. Scale bars, 50 μm. **b** Scatter plot showing the ratio of TH versus TUJ1 fluorescence intensity in duplicate upon treatment with 273 small molecule kinase inhibitors. The dots inside the green square correspond to the 4 hit compounds showing significant increase of TH versus TUJ1 fluorescence ratio as compared to the DMSO controls (blue dots). The red arrow indicates BX795. **c** Representative images of patient-derived p.A53T-neurons immunolabelled for TH in 384-well plates. Upper micrograph shows control DMSO-treated cells while lower micrograph represents BX795-treated cells. Scale bar represents 150 μm. **d** Tests of the four hit compounds in a dose-response format. Data are presented as mean ± SEM. (one-way ANOVA, $*P < 0.05$, $n = 3$ independent experiments).

neuritic growth, limiting the levels of pathological αSyn and restricting aggregate formation whilst maintaining axonal integrity. The beneficial effects of BX795 were noted whether it was added early during neuronal differentiation (in p.A53T patient-derived neurons) or at later stages of neuronal maturation (in A53T iCell dopaminergic neurons) when disease-associated phenotypes were already established.

## Proteomics analysis identifies cellular pathways targeted by BX795 in p.A53T neurons

Identification of the BX795 affected cellular pathways which vary according to the system investigated[30,31,35], is a challenging task. Therefore, we used an unbiased approach based on comparative proteomics. Similarly to the screening procedure, BX795 was added once at DIV 7 and proteomics analysis was performed at DIV 21 when rescue of neuropathological phenotypes was noted (Fig. 2). A total of 1652 proteins were identified and quantified using the MaxQuant software[36,37], followed by filtering of low quality protein hits with the Perseus software. Initial comparison between p.A53T versus control neurons in the absence of BX795, revealed differential expression of 640 proteins (Supplementary Fig. 5) from which only 67 were down-regulated whilst the rest 573 were up-regulated (Supplementary Fig. 5, Supplementary Table 2). This large increase in protein expression was linked by GO enrichment analysis mainly to the biological processes of transcription, translation, protein synthesis and modification

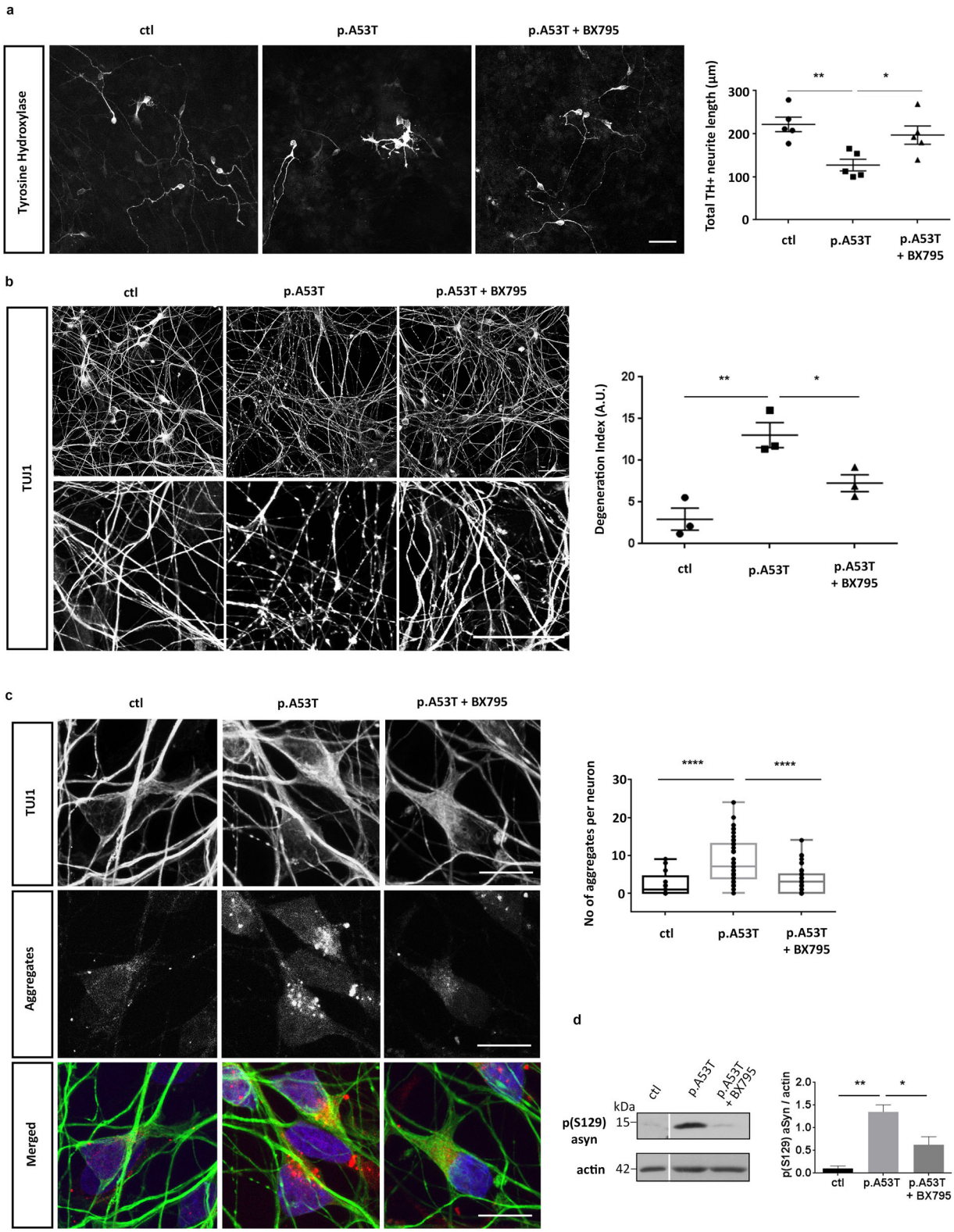


(Supplementary Fig. 5). Remarkably, the levels of a cohort of 118 proteins lying mostly within these biological processes and representing ~20% of the total dysregulated proteins in p.A53T neurons, were restored upon treatment with BX795 ($p < 0.05$) (Fig. 4a, Supplementary Table 3). Most important, this outcome was specific to p.A53T-neurons as BX795 had no significant effect on the proteome of control neurons (Supplementary Fig. 6)

Extensive data mining by GO enrichment analysis for biological processes, molecular function and cellular compartments ($p < 0.01$), complemented by reactome pathway analysis ($p < 0.01$), highlighted the dysregulated core pathways in p.A53T-neurons and, amongst them, those targeted by BX795 to restore neuronal physiology (Fig. 4b). These include proteins associated with RNA metabolism, protein synthesis, protein

**Fig. 2 Rescue of neuropathological features in patient-derived p.A53T neurons by BX795. a** BX795 has a positive effect on neurite length of p.A53T-neurons. Representative confocal images of healthy control (ctl) and p.A53T-neurons immunostained for TH and quantification of total neurite length of TH+ cells. Data represent mean ± SEM. (Comparisons by ANOVA with Tukey correction $^{*}P < 0.05$, $^{**}P < 0.01$, $n = 4$ independent experiments with at least 50 cells analyzed in each experiment). Scale bar, 50 μm. **b** BX795 alleviates axonal neuropathology in p.A53T-neurons. Higher magnification at the right (upper, DMSO-treated cells; lower, BX795-treated cells) shows neurites with swollen varicosities or fragmented processes (arrows). Scale bar, 30 μm. Quantification of axonal degeneration is estimated in the accompanying graph by measuring the ratio of TUJ1+ spots over the total TUJ1+ area in untreated (p.A53T) or BX795-treated p.A53T-neurons. Data represent mean ± SEM.(Comparisons by ANOVA with Tukey correction, $^{*}P < 0.05$, $^{**}P < 0.01$, $n = 20$ randomly selected fields for each condition; data was from three independent experiments). **c** BX795 reduces protein aggregates in p.A53T-neurons. Representative confocal images showing protein aggregates in p.A53T TUJ1+ neurons (Scale bar, 10μm) and quantification in untreated or BX795-treated TUJ1+ cells (Data was from three independent experiments. Mann–Whitney test; $n =$ at least 30 cells per group; $^{****}P < 0.0001$). **d** Detection and quantification of p(Ser129)αSyn by Western blot in control and p.A53T neurons in the absence or presence of BX795, as indicated; Actin shows equal protein loading. Data represent mean ± SEM (*t* test, $^{*}P < 0.05$, $n = 4$ independent experiments).

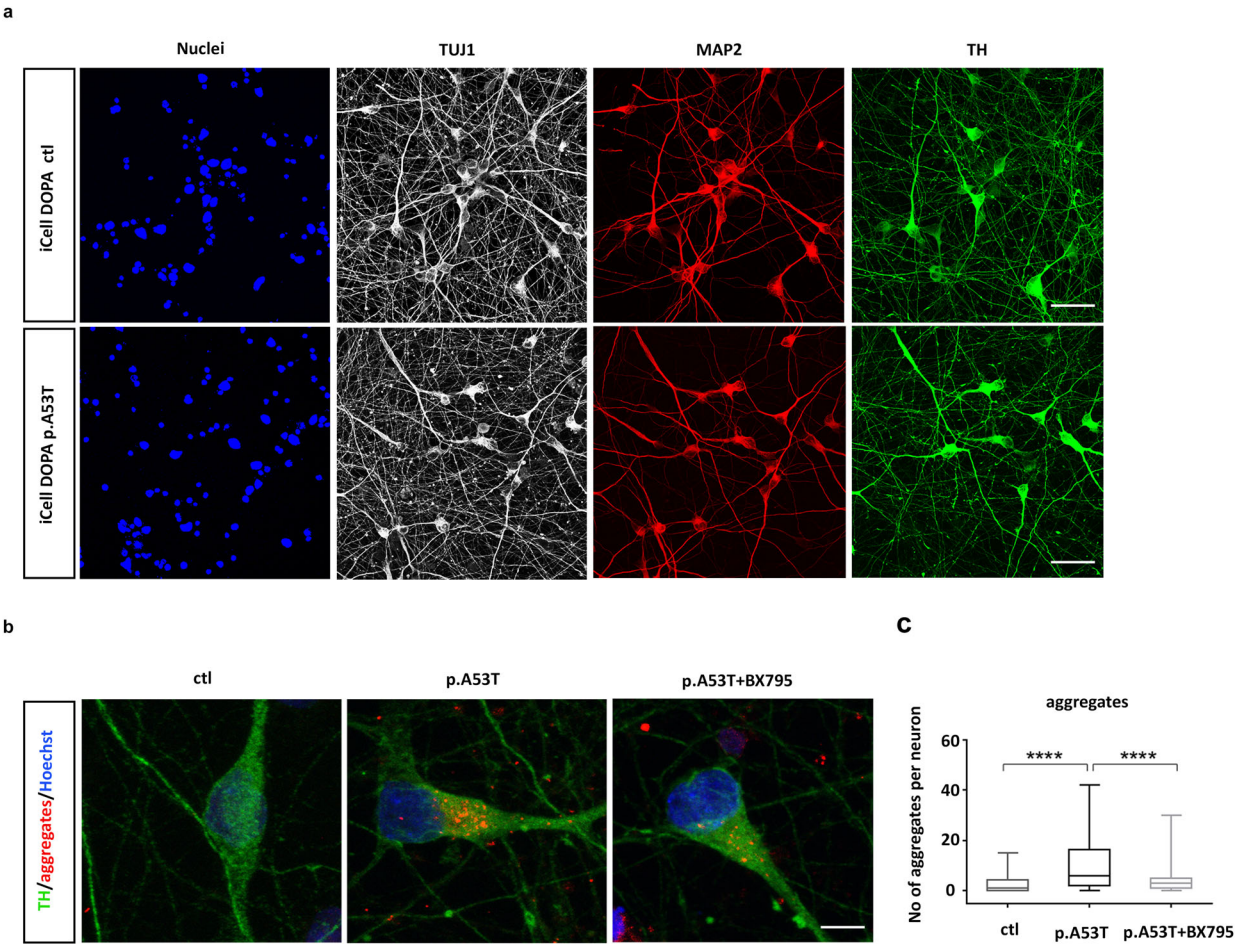


**Fig. 3 BX795 reduces protein aggregates in a gene-edited p.A53T line of mature human iPSC-derived TH neurons. a** Representative confocal images of wild-type (ctl) and isogenic p.A53T iCell Dopa neurons immunolabelled for Nuclei, TUJ1, MAP2 and TH. Scale bar, 30 μm. **b** Representative confocal images of wild-type (ctl) and isogenic p.A53T iCellDopa neurons showing immunostaining for tyrosine hydroxylase (TH green) and protein aggregates (red). p.A53T cells were treated or not with BX795, as indicated. Scale bar, 5 μm. **c** Quantification of aggregates in TH+ neurons. Data represent mean ± SEM. (Comparisons by ANOVA with Tukey correction, $^{****}P < 0.0001$, $n =$ at least 50 randomly selected TH+ cells for each condition).

modification and transport, stress response, and neurodegeneration, as outlined below.

*RNA metabolism*. The p.A53T proteome showed enrichment for proteins in subcellular compartments known to be associated with αSyn[38], including membrane bound organelles (204 proteins), mitochondria (118), ribosomal complexes (29), nucleus (292), and neuron projection/axon cytoplasm (10) (Supplementary Table 4). Processes such as cellular metabolism, translational initiation and regulation, tRNA aminoacetylation and export from nucleus, mRNA stability and export from nucleus, rRNA processing, formation of pre-initiation complex and protein folding were among the top pathways enriched in the p.A53T proteome (Supplementary Fig. 5). A previous study has identified mRNA binding proteins (RBPs) and those involved in protein biosynthesis within the protein network residing in immediate vicinity of αSyn, suggesting that perturbation of these pathways may be directly related to pathology[38]. Herein, we provide evidence that these

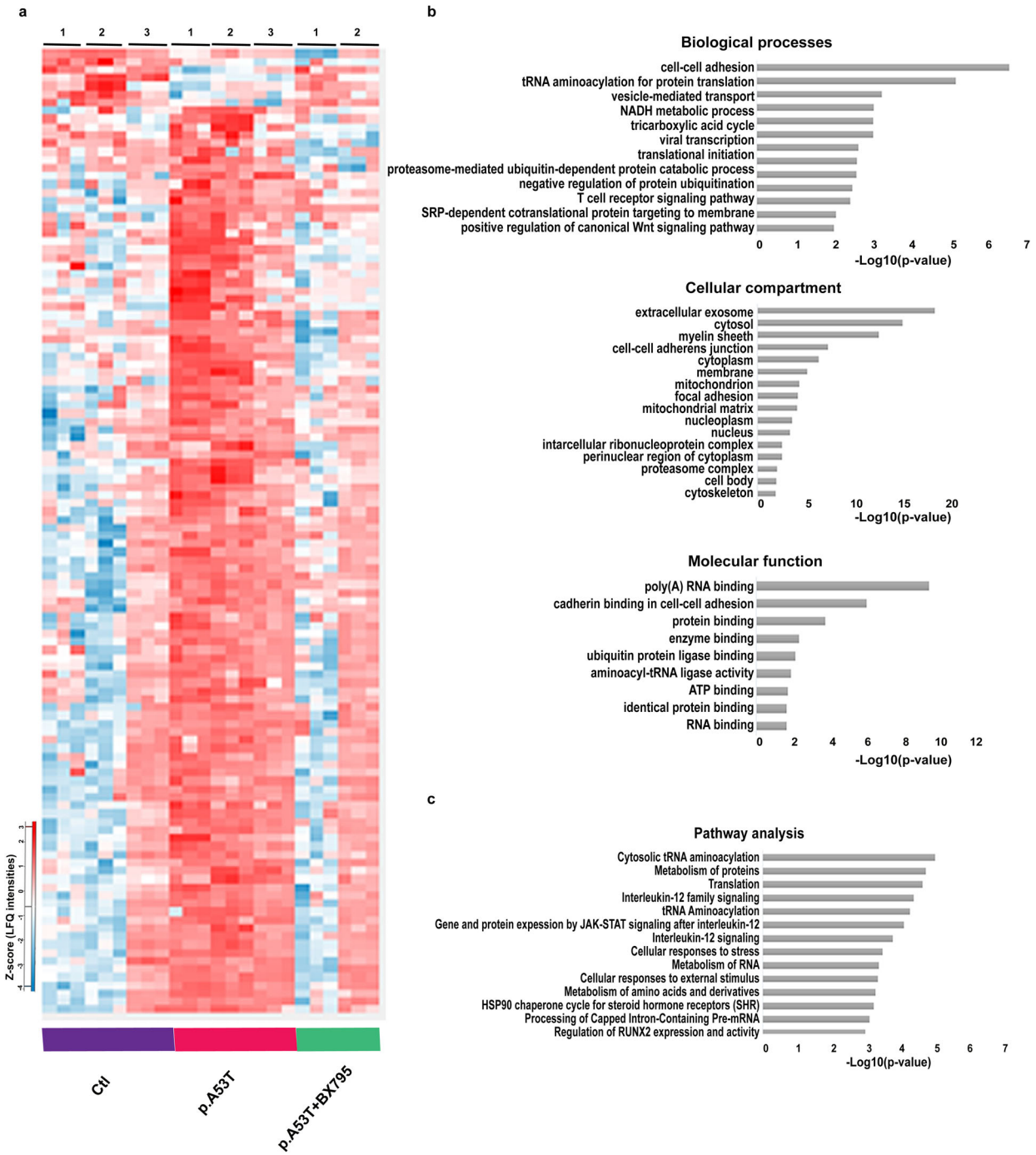


**Fig. 4 Bioinformatics analysis of dysregulated proteins in p.A53T-neurons that are restored by BX795. a** Hierarchical clustering of 118 upregulated proteins in patient-derived p.A53T-neurons that are restored upon treatment with BX795 (one-way ANOVA analysis). Columns in the different groups (control, p.A53T-neurons and p.A53T-neurons treated with BX795) correspond to individual samples tested and rows represent single proteins (blue, low expression; red, high expression; $n = 3$ for control and p.A53T; $n = 2$ for p.A53T + BX795). **b** GO enrichment analysis for biological processes, molecular function and cellular compartments was performed using DAVID software ($p < 0.01$). **c** Pathway analysis using Reactome software ($p < 0.01$).

same pathways are altered when p.A53T is expressed in human neurons (Supplementary Fig. 5). Specifically, a significant number of RBPs (60 proteins) were differentially expressed, including members with known neuronal localization and involvement in neuronal functions, such as ELAV-1, ELAV-3, RBBP7, RNPS1, RNMT, TARDBP, XPO1, XPO5, HNRNPA1, HNRNPA1L2, HNRNPF, HNRNPL, HNRPNPM, HRNNPUL1, PABPC1, PABPC4, PTBP2 and CELF1 (Supplementary Table 2). Since even small changes in RBP expression or activity are amplified due to their broad impact on expression, splicing and translation of numerous RNA substrates, changes in such a large number of these RNA regulators suggest a severe perturbation in RNA homeostasis in p.A53T-neurons. A cluster of RBPs implicated in splicing and adenylation events in the nuclear compartment (DEK, MYEF2, UBTF, SNRPB, PCBP1, ZNF207, HINT1, RAE1, HNRNPUL1) was restored after BX795 treatment (Fig. 5a).

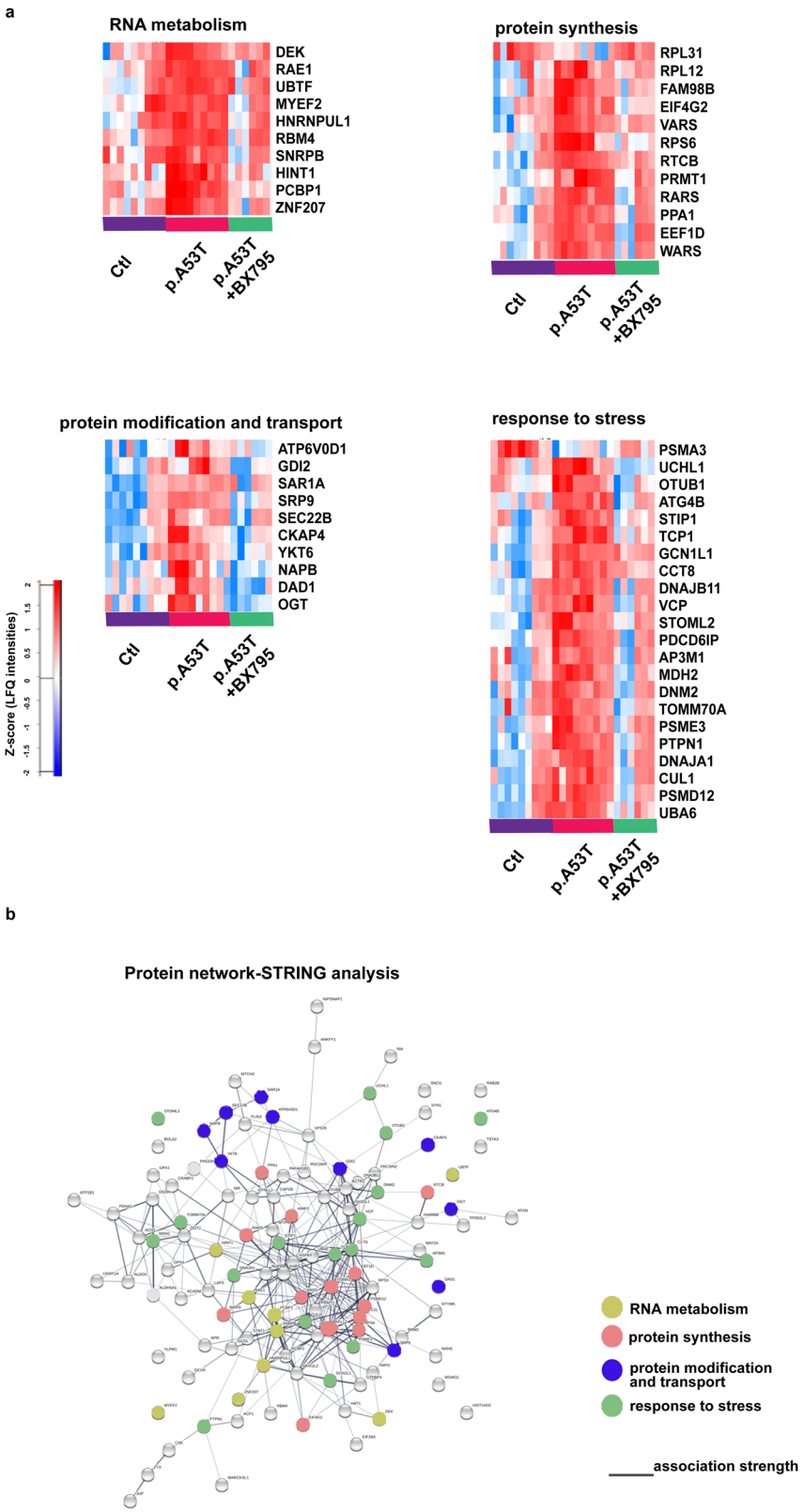


**Fig. 5 Protein network of pathways and processes restored by BX795 treatment. a** Heatmaps illustrating specific proteins upregulated in p.A53T-neurons that are involved in RNA metabolism, protein synthesis, protein modification and transport and response to stress, which are restored after BX795 treatment. High expression is in red and low expression is in blue. **b** STRING-analysis representation of the protein-protein interaction network of the 118 upregulated proteins in p.A53T-neurons that are restored by BX795. Each circular node depicts one protein and the different colors represent the different pathways/processes as indicated. Connecting lines represent protein-protein associations and line intensity represents the confidence score of a functional association.

### Protein synthesis

Disturbances in RBP dosage have detrimental consequences also outside the nucleus, as they control the targeted localization of mRNAs, either proximally in the cell soma or distally in the projecting axon, affecting whether an mRNA will be translated or remain translationally silent and whether it will be stored for local mRNA translation or degraded[39]. Aberrant expression of the translational machinery emerged in the p.A53T proteome with translational initiation and regulation processes being the most affected in mutant neurons (Supplementary Fig. 5, Supplementary Table 2). A total of 18 proteins involved in the formation of the pre-initiation complex were identified and included EIF2, 3, 4 and 5, of which EIF4G2 that functions as a general suppressor of translation by forming translationally inactive stress granules, was affected by BX795 (Fig. 5a). Ribosomal proteins (29 proteins), structural components of ribosome subunits, were upregulated in p.A53T-neurons (Supplementary Table 2) and a significant fraction returned to near-control levels after BX795 treatment (Fig. 5a). These included RPL31 and RPL12, which are involved in 60 S biogenesis, and RPS6, a component of the 40 S subunit and downstream effector of the mTORC1 signaling pathway. tRNA processing represents another important part of the translational cascade that was altered in p.A53T-neurons (Supplementary Table 2), while a significant fraction was restored by BX795, including the aminoacyl-tRNA synthetases RARS (arginyl-tRNA synthase), VARS (valyl-tRNA synthase), and WARS (tryptophanyl-tRNA synthase) together with regulatory or accessory proteins such as PPA1, EEF1D PRMPT1, FAM98B and RTCB. Growing evidence associates changes in tRNA gene biogenesis and processing with neurodegenerative diseases[40]. Our data reveal for the a link between p.A53T-αSyn expression and this molecular process (Fig. 5a, Supplementary Table 2).

### Protein modification and transport

p.A53T-αSyn toxicity has been attributed to problematic modifications at the ER membrane and disturbances in ER-Golgi and early endosomal/vesicle trafficking[33,38,41,42]. In accordance, p.A53T-neurons exhibit altered protein levels in components of these pathways (Supplementary Table 2). Among these, five members of the adaptor protein complexes that function in transport-vesicle mediated transfer between membranous structures are increased by p.A53T-expression (AP1B1, AP2A2, AP3B1, AP3D1 and AP3M1). Another prominent category included members of the largest branch of Ras-like small GTPases involved in membrane trafficking (RAB2A, RAB2B, RAB6B). In addition, proteins participating in ER to Golgi transport and macroautophagy (SEC22B, SEC31A, RAB18, ARF1, ARF3)[43,44], vesicle budding/uncoating in the Golgi apparatus (ARF1,ARF3)[45], SNARE-mediated autophagosome-lysosome fusion (RAB21)[46], retrograde Golgi to ER transport (COPA, COPB, COPG) (Supplementary Table 2) were also differentially expressed in p.A53T neurons.

BX795 had a selective effect on p.A53T-altered membrane transport proteins (SRP9, GDI2, ATP6VOD1, DAD1 subunit of oligosaccahryl transferase complex and OGT, and NAPB) and components of the SNARE complex (SAR1A, SEC22B and YKT6) (Fig. 5a) whilst alterations on molecules of the RAB, adaptor protein complex and coatomer remained largely unaffected.

### Stress response

p.A53T-αSyn protein expression acts as a primary neurotoxin triggering a battery of stress responses in human neurons[47]. The proteomics analysis indicated that p.A53T neurons activate most of these mechanisms. Both the unfolded protein response (UPR), as evidenced by mis-expression of chaperones CCT2, 3, 4, 5, 7 and 8, as well as the heat shock protein response (HSP), with proteins such as DNAJA1, DNAJB11, DNAJC7, HSPA4L, HSP9 and HSPE1, were apparent in the p.A53T-proteome (Supplementary Table 2). These stress response pathways were significantly downregulated in p.A53T neurons treated with BX795, which seems to target many stress response mediators (Fig. 5a). These included TCP-1, a member of the chaperonin TCP1 complex (CCT), PTPN1, a UPR regulator, STIP1, a coordinator of HSP70 and HSP90 function and the chaperone/co-chaperone proteins DNAJB11, GCN1L1, CCT8, and DNAJA1.

Such a dysregulation of the UPR/HSP response systems in p.A53T neurons should result in the production of dangerous protein cargo and the formation of protein aggregates, as indeed identified by immunofluorescence (Fig. 2c). The p.A53T proteome also revealed alterations in protein clearance pathways with mediators of both proteasomal and autophagic systems being affected (Supplementary Table 2). BX795 improved the expression of multiple ubiquitin-associated proteins suggesting partial restoration of proteasome targeting of aberrant protein products, in accordance with the decrease of protein aggregates in BX795-treated p.A53T neurons (Fig. 2c). BX795 restored the expression of components of the proteasome complex and activators of the E2 and E3 ligase binding process (PSMA3, UCHL1, OTUB1, PSME3, CUL1, PSMD12, and UBA6), and VCP, an AAA ATPase that extracts ubiquitinated proteins from large protein complexes for degradation, previously shown to co-localize with protein aggregates in various neurodegenerative diseases (Fig. 5a).

Components of the lysosomal pathway of autophagy targeted by BX795 included vacuole transport components such as ATG4B and proteins required for multivesicular body (MVB) biogenesis and sorting (PDCD6IP, AP3M1 and DNM2) (Fig. 5a). Finally, BX795 also modulated oxidative stress response mechanisms, as the mitochondrial biosynthesis regulators TOMM70A and MDH2 were brought to near control levels. In addition, STOML2, a stimulator of cardiolipin biosynthesis recently shown to be associated with p.A53T neurotoxicity in human dopamine neurons was also positively targeted by BX795[33].

When STRING analysis was used to assess the relatedness level of all 118 proteins affected by BX795, a network with strong functional linkage among the majority of these proteins was revealed (Fig. 5b).

*Proteins associated with neurodegeneration*. An important measure of the biological significance of the proteomic profile of p.A53T neurons comes from comparisons with human genetic studies. Enrichment analysis for PD and other neurodegenerative diseases identified several proteins comprising both known and new converging targets that were modified by BX795 (Fig. 6a). Among those, UCHL1/PARK5 is linked to lower susceptibility for PD, while a point mutation co-segregating with the disease has been identified in one family[48] and VPS35/PARK17-D620N mutated protein causes late-onset autosomal dominant PD[49]. FAM98B has been linked to SMA and ALS[50], VCP mutations can cause FTD, ALS and Charcot-Marie-Tooth diseases[51,52], HINT1 autosomal recessive mutations lead to neuromytotonia and axonal neuropathy[53], PAFAHB1 mutations and gene deletions lead to lissencephaly syndrome[54] and RBM4 is linked to Down's syndrome[55] (Fig. 6a, b). STRING analysis of the BX795-modified protein network to which αSyn was also incorporated, demonstrated a strong association between αSyn and two other neurodegeneration-linked proteins (Fig. 6c).

These findings deepen our understanding of p.A53T-mediated neurotoxicity and reveal key biological processes that are targeted by BX795 to alleviate p.A53T-αSyn-related phenotypes in human neurons.

### BX795 affects the mTORC1 signaling pathway to attenuate protein synthesis and facilitate autophagic flux in p.A53T neurons

The p.A53T proteome clearly indicates aberrant mRNA translation and protein clearance mechanisms, both linked to mammalian aging

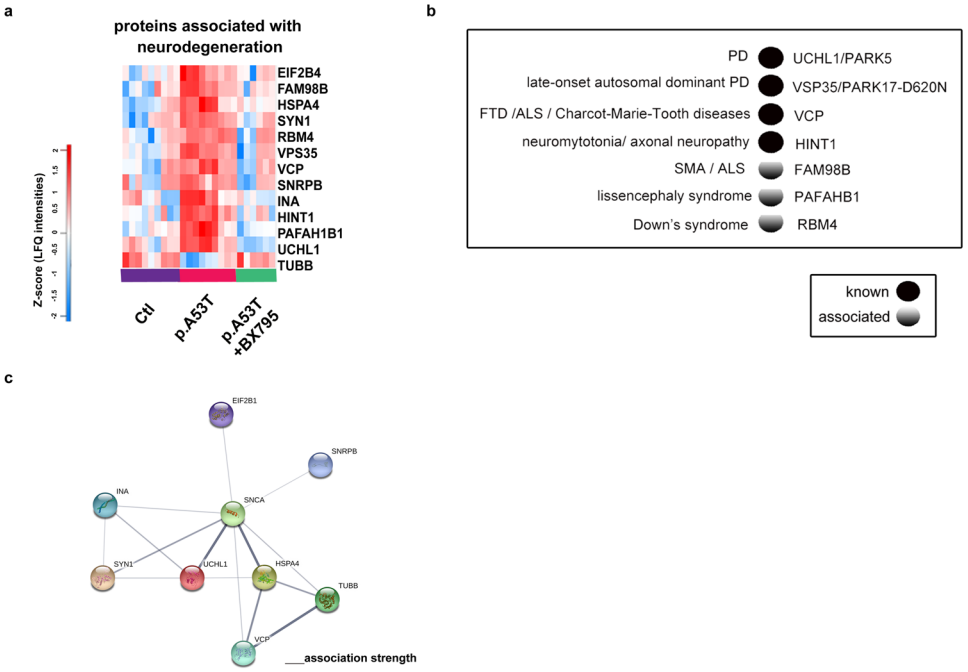


**Fig. 6 Restoration of disease-associated proteins by BX795 in p.A53T-neurons. a** Heatmap of proteins associated with neurodegeneration that are restored after BX795 treatment. High expression is in red and low expression is in blue. **b** Disease-associated proteins that are modified by BX795 are either known or associated genetic risk factors for neurodegenerative diseases as revealed by human genetic studies. **c** STRING network analysis of the neurodegeneration-associated proteins restored by BX795 in p.A53T-neurons and their interaction with αSyn. Each αSyn interactor is shown as a colored circle and connecting lines between proteins represent protein-protein associations. The intensity of lines represents the confidence score of a functional association.

and neurodegenerative diseases that can be effectively restored by BX795. The mammalian target of rapamycin (mTOR) signaling pathway is a central regulator of proteostasis and the p.A53T proteome clearly indicates hyperfunctional overactive biosynthetic processes that could be associated with alterations in mTORC1 activation. Components of this signaling cascade have emerged in the proteomics analysis of p.A53T- neurons, including RPS6, a major downstream effector of mTORC1, together with several RAG GTPases like IQGAP1, required for efficient activation of mTORC1, which were largely restored after BX795 treatment (Supplementary Table 3). To validate the activation of the mTORC1 pathway in p.A53T patient-derived neurons, we examined the levels of phosphorylated RPS6 (pRPS6), which is commonly used as a readout for mTOR signaling. Indeed, we observed significantly higher levels of pRPS6 in p.A53T neurons as compared to control that were efficiently downregulated upon BX795 treatment (Fig. 7a, b).

To confirm that the p.A53T mutation is causally related to dysregulation of protein metabolism and verify that BX795 can restore this effect in mature human neurons, we exploited the isogenic system of iCell DopaNeurons where we measured the levels of the activated form of RPS6, and the total protein synthesis rate. The presence of the p.A53T mutation led to a significant increase in the levels of pRPS6 (Fig. 7c, d) that correlated with a significant increase of global protein synthesis in iCell Dopa p.A53T neurons (Fig. 7c, d). BX795 could lower significantly the levels of pRPS6 and reverse the aberrantly increased protein synthesis rate (Fig. 7c, d). This data suggests that BX795 targets and restores dysregulated mRNA translation and protein synthesis pathways instigated by the p.A53T mutation in neuronal cells.

To examine further the effect of the p.A53T mutation on mTORC1 activity and protein synthesis, we created stably transduced SH-SY5Y neuroblastoma cells co-expressing the human p.A53T-αSyn and the fluorescent protein DsRed or DsRed only as a control (Fig. 8a). Upon neuronal differentiation, SH-SY5Y cells expressing the human p.A53T-αSyn displayed a prominent upregulation in the levels of phosphorylated mTOR and pRPS6 as compared to control cells (Fig. 8b), whilst BX795 had an acute effect in downregulating their levels (Fig. 8c), as determined by Western blot analysis.

Biochemical and genetic studies have identified the upstream p70 S6 kinase as the main in vivo kinase responsible for RPS6 phosphorylation[56]. Since a most prominent observation in all p.A53T-bearing cells tested in our study was an up-regulation of pRPS6 and its downregulation by BX795, we asked if the compound could inhibit the activity of p70 S6 kinase. To this end, we assessed the kinase activity of purified recombinant p70 S6K in the absence or presence of BX795 and found a notable dose-dependent inhibitory effect (Fig. 8d), indicating that BX795 may restore pRPS6 levels and protein synthesis by targeting p70 S6K. Finally, we checked if MHY-1485, a synthetic mTOR activator, could counteract the beneficial effects of BX795 in p.A53T cells. Consistently, upon co-treatment with MHY-1485 and BX795, we could not see a reduction in pathological p129S-αSyn levels in SH-SY5Y cells expressing human p.A53T-αSyn or a decrease in neuronal aggregates in p.A53T iPSC-derived neurons (Fig. 8e, f).

mTORC1 also controls autophagy, the major degradation pathway essential for removing aggregation-prone αSyn[57,58]. To test if BX795 could also affect this clearance pathway, we utilized a previously established inducible SH-SY5Y cell line that expresses the human p.A53T-αSyn upon withdrawal of Doxycycline (-Dox). In this model, expression of mutant p.A53T has been shown to cause perturbation of the autophagy lysosomal pathway resulting in increased steady-state levels of LC3II and p62[59]; (Fig. 9 a, b). p62 is a receptor for ubiquitinated cargo destined to be degraded by autophagy and is associated with LC3-II, the processed form of LC3, within autophagosomes and autolysosomes[60,61]. To visualize LC3-II and quantify GFP-LC3-II+ puncta comprising brightly fluorescent autophagosomes and more weakly labeled autolysosomes (Fig. 9a), we transfected the inducible SH-SY5Y line with a fusion construct containing the green fluorescent protein tagged to LC3 (GFP-LC3)[62].

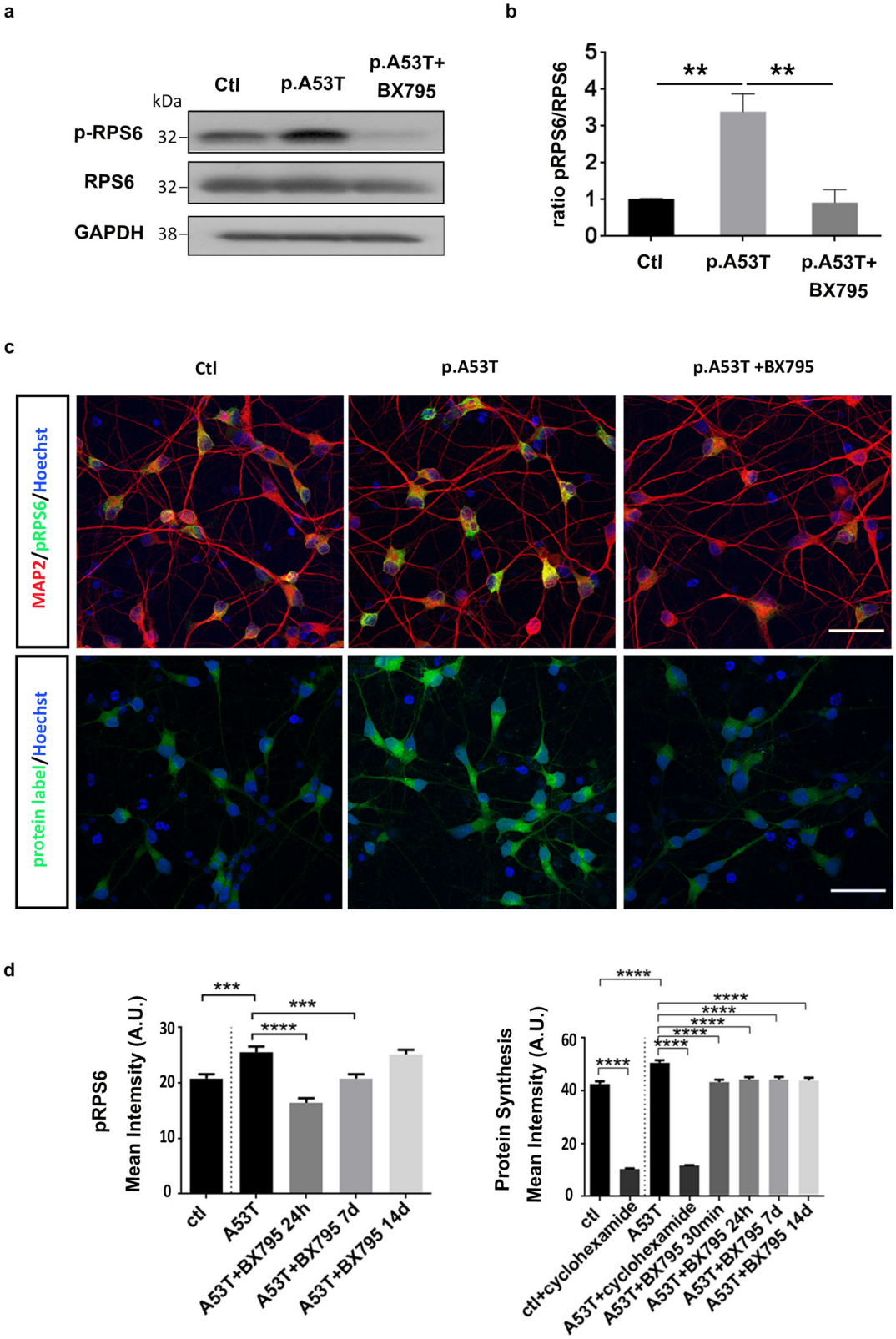


In agreement with the Western blot data, GFP-LC3-II+ puncta were scarce in p.A53T cells treated with DMSO while in the presence of BX795 there was a small, yet not significant increase (Fig. 9c, d). As expected, when DMSO-treated cells were exposed to bafilomycin, a blocker of autophagosome-lysosome fusion that prevents lysosome-mediated protein degradation, GFP-LC3-II+ puncta increased significantly (Fig. 9c, d)., Addition of both bafilomycin and BX795 further increased the number and brightness of GFP-LC3-II+ puncta, suggesting that BX795 acts as an autophagy inducer (Fig. 9c, d).

**Fig. 7 BX795 affects the mTORC1 signaling pathway in p.A53T patient-derived and iCell Dopa neurons to attenuate protein synthesis.** **a** Western blot showing increased levels of p-RPS6 in p.A53T-patient iPSC-derived neurons and a notable reduction in the presence of BX795. GADPH shows equal protein. **b** Quantification of p-RPS6 levels in p.A53T-patient iPS-derived neurons. Data represent mean ± SEM (Comparisons by ANOVA with Bonferroni's multiple comparisons test. $^{**}P < 0.01$, $n = 3$ independent experiments). **c** Representative confocal images of control (ctl) and isogenic gene-edited p.A53T iCellDopa neurons, either non-treated or treated with BX795. Cells were immunolabeled for phosphorylated RPS6 (green) andmicrotubule associated protein 2 (MAP2; red)(upper panel) and labeled for total protein synthesis (protein label, green)(lower panel). Nuclei are seen with Hoechst dye (blue). Scale bar, 30 μm. **d** BX795 reduces phosphorylated RPS6 levels and reduces total protein synthesis in p.A53T-neurons. Quantification of fluorescence intensity in control, untreated p.A53T or BX795-treated p.A53T neurons. Data represent mean ± SEM (Comparisons by ANOVA with Tukey correction, $^{***}P < 0.001$ $^{****}P < 0.0001$, $n = 100$ randomly selected cells for each condition).

To distinguish labeled autophagosomes from autolysosomes and monitor the autophagic flux, we used a dual fluorophore probe consisting of a tandem fluorescent mCherry-GFP-p62 construct[63]. GFP fluorescence is sensitive to low-pH and labels only neutral-pH autophagosomes, while mCherry retains fluorescence in both autophagosomes and low-pH autolysosomes[61] (Fig. 9e). Calculation of the ratio of GFP+ /mCherry+ puncta presents a measure of the autophagic flux, and a reduction in this ratio mirrors an increase in the progress of autophagy. Indeed, quantification of green and red puncta revealed a significantly lower GFP/mCherry ratio in the presence of BX795 as compared to DMSO-treated cells, indicating that BX795 facilitates the the autophagic flux (Fig. 9f, g). In agreement, a decrease in the total levels of p62 was noted upon treatment with BX95 (Fig. 9h).

Last, we examined if BX795 had a similar effect in facilitating autophagic flux in p.A53T patient-derived neurons. Electron microscopy observations revealed that these cells have prominent autophagosomes exemplified by multi-lamellar vacuoles that were never detected in control cells (Fig. 9i). These findings are consistent with an accumulation of autophagosomes resulting from stalled autophagic flux in p.A53T cells. To assess the effect of BX795, we used the Cyto-ID® autophagy detection kit that monitors autophagosomes and autophagic flux using a using a dye that selectively labels accumulated autophagic vacuoles by fluorescence microscopy. As expected, p.A53T neurons showed an accumulation of fluorescent autophagosomes that were effectively decreased upon BX795 treatment, indicative of restoration of autophagic flux (Fig. 9j).

Overall, our results indicate that BX795 can restore proteostasis in p.A53T cells by modulating aberrant protein synthesis and facilitating protein clearance mechanisms.

## DISCUSSION

The generation of human models based on patient-derived iPSCs has opened up new perspectives for investigation of disease mechanisms and discovery of new therapeutics. In this work, we used a well-characterized human model of p.A53T pathology[22] to screen for small molecules with protective function. We identified the multi-kinase inhibitor BX795 as a compound that exerts a consistent and sustainable beneficial effect on patient-derived p.A53T-neurons. Remarkably, we found that a single treatment with BX795 has long-lasting consequences in supporting neuritic growth, limiting αSyn protein aggregate formation and restoring axonal neuropathology, recorded two weeks after its addition in human p.A53T neurons.

This study represents a high-content drug discovery screen performed in human p.A53T iPSC-derived neurons to identify candidate therapeutics for PD. Using an unbiased screening approach in combination with quantitative proteomics profiling, we were able to show that treatment with BX795 restored proteins associated with key cellular processes, most notably RNA metabolism, protein synthesis and degradation processes, as well as stress response, suggesting that restoration of proteostasis is key for rescuing the neuropathological features in p.A53T-neurons. Dissecting further the pathways affected by BX795, we demonstrated that BX795 modulates the mTORC1 pathway to restrict excessive protein synthesis and facilitate autophagy. Taken together, our data highlight the BX795 kinase inhibitor as a promising compound and candidate therapeutic that ameliorates p.A53T-associated pathology. Moreover, our results show that interfering with and restoring proteostasis downstream mTOR signaling can have long-term beneficial consequences in cellular health by instigating constitutive changes.

Considerable progress in understanding the neurotoxic properties of α-Syn has been achieved by exploiting causal mutations resulting in rare familial forms of PD, most notably the p.A53T-αSyn mutation (G209A in the *SNCA* gene)[64,65]. We and others have shown that disease-associated characteristics can be recapitulated in patient-derived p.A53T-neurons, including axonal degeneration and accumulation of protein inclusions resembling Lewy bodies and neurites[22]. These have been linked to multiple molecular defects in mRNA processing and translation, endocytic and retrograde trafficking[38,42], protein misfolding, redox homeostasis[20,33] and the synaptic protein machinery[22]. The p.A53T proteome examined here revealed a profound increase in proteins related to the biological processes of RNA metabolism, protein synthesis, modification and transport, protein clearance and stress response. Notably, the cohort of 118 proteins that was specifically restored in p.A53T-neurons upon treatment with BX795, was associated with these key cellular processes.

The pathways affected by mutant αSyn in our study have a high similarity with the αSyn connectome reported by Chung et al.[38] for mouse neurons, and the predictions of the in silico "humanized" map of αSyn proteotoxicity reported in the accompanying study of Khurana et al.[42]. Our proteomics analysis, accomplished in p.A53T-human neurons, identified perturbations in RNA metabolic processes that started from the nucleus and reached the ribosome. Alternative mRNA processing greatly increases the dimensions of gene expression through splicing, polyadenylation, targeted localization and post-transcriptional silencing. Neurons take advantage of all these strategies as the brain has the highest levels of alternative splicing compared to any other human tissue[66]. This process has recently been shown to be defective in the PS19 Tau model of Alzheimer's disease, where alternative splicing events affected genes particularly involved in synaptic transmission[67]. Similarly, the p.A53T-proteome suggests that this process could be excessively induced in p.A53T-neurons as a number of RBPs known to be linked to αSyn aggregation have emerged, including ELAV1, ELAV3 and CELF, suggesting a possible association with the abnormal expression of synaptic genes and the defective synaptic connectivity we have previously reported in p.A53T neurons-[22].

An excess of mRNAs coming out of the nucleus in p.A53T-neurons could explain the abnormal expression of proteins involved in translation, the next step of mRNA processing. The significant increase of components of the tRNA splicing ligase complex, various aminoacyl-tRNA synthetases, ribosomal subunits and eukaryotic translation initiation factors indicate an enhanced translation of spliced mRNAs. Moreover, in post-mortem PD brains, region and stage-dependent alterations in the machinery of protein synthesis have been reported and have been associated with α-synuclein oligomers in remaining neurons[68].

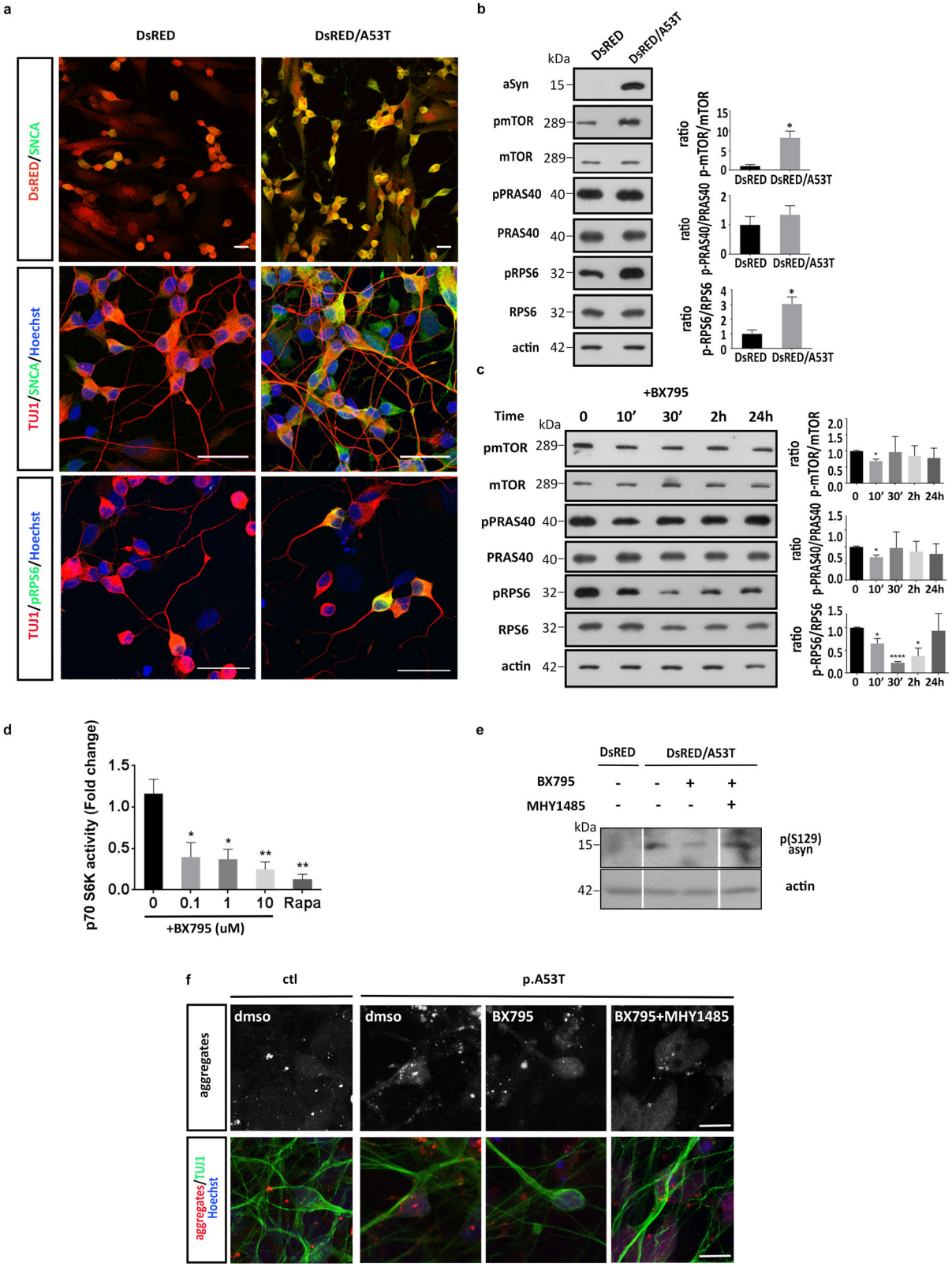


The mTOR kinase is a master regulator of cellular metabolism that functions in two distinct complexes: mTORC1 and mTORC2[69] with the first implicated in protein and lipid biosynthesis through a signaling cascade that includes SK6 and 4E-BP1 proteins[70]. Unlike proliferating cells where this pathway is utilized for growth and division, in neurons it acts as a regulator of healthy metabolism and aging[71] with its restriction being associated with prolonged life span and delay of age-related pathologies. p.A53T neurons have increased RPS6, IQGAP1 and RAG-GTPases, components of mTORC1 pathway and this seems to be associated with

**Fig. 8 BX795 restores neurodegenerative phenotypes via the mTORC1 signaling pathway. a** Representative images of SH-SY5Y cells stably transduced to express DsRed only or DsRed and human pA53T-αSyn. After neuronal differentiation, cells were immunolabled for αSyn (SNCA), TUJ1 and pRPS6. **b** Western blot showing that the presence of mutant SNCA in differentiated p.A53T-transduced SH-SY5Y cells, results in an increase in the levels p-mTOR and p-RPS6. Actin shows equal protein loading. Data represent mean ± SEM (*t* test, $^{*}P < 0.05$, $n = 3$ independent experiments). **c** Western blot showing an acute reduction in the levels of p-mTOR and p-RPS6 in the above stably transduced and differentiated SH-SY5Y cells, in the presence of BX795. Actin shows equal protein loading. Data represent mean ± SEM (Comparisons by ANOVA with Tukey correction, $^{*}P < 0.05$, $^{****}P < 0.0001$, $n = 3$ independent experiments). **d** BX795 inhibits the kinase activity of pure recombinant p70 S6K (25 ng/assay) in a dosedependent manner. Rapamycin (Rapa) was used as a positive control. Data represent mean ± SEM (Comparisons by ANOVA with Tukey correction, $^{*}P < 0.05$, $^{**}P < 0.01$, $n = 3$). **e** Western blot showing the effect of BX795 treatment alone and in combination with mTOR activator MHY-1485 on the p(Ser129)-αSyn levels in SH-SY5Y cells stably transduced to express DsRed only or DsRed and human pA53T-αSyn. **f** Representative confocal images show protein aggregates in control (ctl) and patient p.A53T neurons, either non-treated (DMSO) or treated with BX795 alone or in combination with the mTOR activator MHY-1485.

an increased translation of a subset of mRNAs that are linked to RNA metabolism and the stress response. Similarly, a quantitative proteomics study of a pre-symptomatic p.A53T-αSyn Drosophila model shows significant upregulation of ribosomal proteins in the p.A53T flies[72]. Although the mechanistic link between p.A53T-αSyn and mTORC1 remains to be established, recent evidence shows that genetic variability in the mTOR pathway contributes to SNCA effects in disease pathogenesis[73].

Concomitantly with promoting protein synthesis mTORC1 acts to repress autophagy through ULK1 phosphorylation. Autophagy has a central role in promoting health and longevity while this process is impaired in neurodegenerative diseases and αSyn pathology[74,75]. The p.A53T-proteome shows that neurons are under stress as proteins involved in the UPR or the heat-shock stress response, proteasome assembly and regulation, known to be orchestrated by mTORC1 in neurons, are significantly upregulated[71]. Restoration of numerous components of RNA metabolism and protein translation cascades by BX795 is directly related to the diminished stress response that emerges by the lower levels of UPR and heat-shock-associated proteins also conferred by this molecule. In parallel, a significant number of ubiquitin/proteasome-associated proteins were brought back to near control levels suggesting that BX795 helps misfolded protein clearance by limiting protein synthesis. This is in agreement with its demonstrated ability to decrease protein aggregates in p.A53T-neurons, as shown in this study, along with facilitation of autophagy both in SYSH-5Y cells expressing p.A53T and in patient-derived neurons.

BX795 is a multi-kinase inhibitor that targets numerous pathways, including the kinases TBK1 and PDK1[29–31,35]. Although in our system differences in the total or phosphorylated levels of these two kinases were not observed in the presence of BX795 (data not shown), we cannot exclude that its effects are mediated through these two kinases as both are involved in neurodegeneration, mTOR signaling and autophagy[76,77]. Yet four other PDK1 inhibitors that were included in the Selleck library did not emerge as hits during the screening campaign. Interestingly, we found that BX795 could inhibit purified recombinant p70 S6K, the major kinase that phosphorylates RPS6 in vivo, indicating that the acute effect of the compound on RPS6 in p.A53T-expressing cells could be mediated through inhibition of p70 S6K. It is notable that multiple other inhibitors of mTOR phosphorylation present in the kinase inhibitor library tested (26 in total, including rapamycin), failed to show any protective effects. Considering that BX795 has been proposed to act through distinct mechanisms in different pathologies, future mechanistic studies should reveal its direct targets in p.A53T neurons. Nevertheless, the work presented here uniquely identifies BX795 as a promising compound that may have therapeutic potential for patients with PD and other protein conformational disorders. Further, our collective data along with previous proteomics and systems approaches shed light into the molecular and cellular pathways of αSyn proteotoxicity unveiling new disease targets for the development of combined therapeutics.

## METHODS

### Directed neuronal differentiation

iPSCs used in this study were previously generated and characterized from two Parkinson's disease patients harboring the p.A53T-α-synuclein mutation and a healthy subject (control, wild-type SNCA)[22]. For directed differentiation, iPSCs were allowed to form embryoid bodies and neural induction was initiated by applying a dual SMAD inhibition protocol in the presence of Noggin and TGFβ inhibitor for generation of neural precursor cells (NPCs)[22]. NPCs were expanded in DMEM/F12/B27/N2-medium supplemented with HEPES, Glutamax, non-essential amino acids [NEAA] and 20ug/ml FGF2. For neuronal differentiation, NPCs were dissociated with accutase and seeded onto poly-L-ornithine (20 µg/ml; Sigma-Aldrich)/ laminin (5 µg/ml; Sigma-Aldrich)-coated dishes in DMEM/F12/ B27/N2-medium supplemented with 200 ng/ml human recombinant sonic hedgehog (SHH, R&D Systems) and 100 ng/ml murine recombinant fibroblast growth factor 8b (FGF-8b, R&D Systems) for 7 days in vitro (DIV). Cells were then replated in medium supplemented with 20 ng/ml brain-derived neurotrophic factor (BDNF, R&D Systems), 20 ng/ml glial cell-derived neurotrophic factor (GDNF, R&D Systems), 200 µM ascorbic acid (AA, Sigma-Aldrich) and 0.5 mM cyclic AMP (cAMP, Sigma- Aldrich). The medium was changed every 2 to 3 days for 2 weeks.

### iCell Dopa neurons and isogenic iCell DopaNeurons PD SNCA A53T HZ

Commercially available iCell DopaNeurons 01279, Catalog No C1028, and a heterozygous (HZ) A53T allelic variant isogenic to iCell DopaNeurons, PD SNCA A53T HZ 01279, Catalog No C1113, in which the site-specific p.A53T mutation was introduced into the *SNCA* gene by nuclease-mediated SNP alteration, were purchased from Fujifilm Cellular Dynamics International and were maintained according to the User's Guide protocol for two weeks unless otherwise stated.

### Compound screening and High Content image analysis

iPSC-derived NPCs at 7 DIV were dissociated with accutase, seeded (9,000 cells/well) onto poly-L-ornithine/ laminin-coated 384-well optical bottom plates containing the kinase inhibitors (Greiner Bio-One, Kremsmünster, Austria) and cultured in neuronal differentiation medium for two weeks (Fig. 1a). A collection of 273 small molecule kinase inhibitors from Selleck Chemicals was used. The list of inhibitors and their known targets according to the provider, is shown in Supplementary Table 1. The compounds were dispensed in duplicate in 384-well optical bottom plates at a final concentration of 1 µM, followed by NPC seeding. After 2 weeks of neuronal differentiation, cells were fixed in 4% paraformaldehyde for 20 min followed by immunofluorescence for βIII-tubulin (TUJ1) and Tyrosine hydroxylase (TH) at 4 °C overnight and incubation with appropriate secondary antibodies (Molecular Probes, Thermo Fisher Scientific) conjugated to AlexaFluor 488 (green) or 546 (red), for at least 1 h at room temperature. Nuclei were stained with Hoechst dye. Images were captured by automated confocal microscopy (Opera High-Content Screening System, Perkin Elmer, Hamburg, Germany). A total of 15 images per well were acquired using a 10X magnifying objective. Cell nuclei and fluorescence staining were quantified by segmentation on 15 images per well in a duplicate experimental setup. Parameters were set as follows: primary object detection (cell nuclei) was based on Hoechst staining, captured in channel 1. Detection of neurons was based on TUJ1 immunofluorescence signal, captured in channel 2 and on TH immunofluorescence

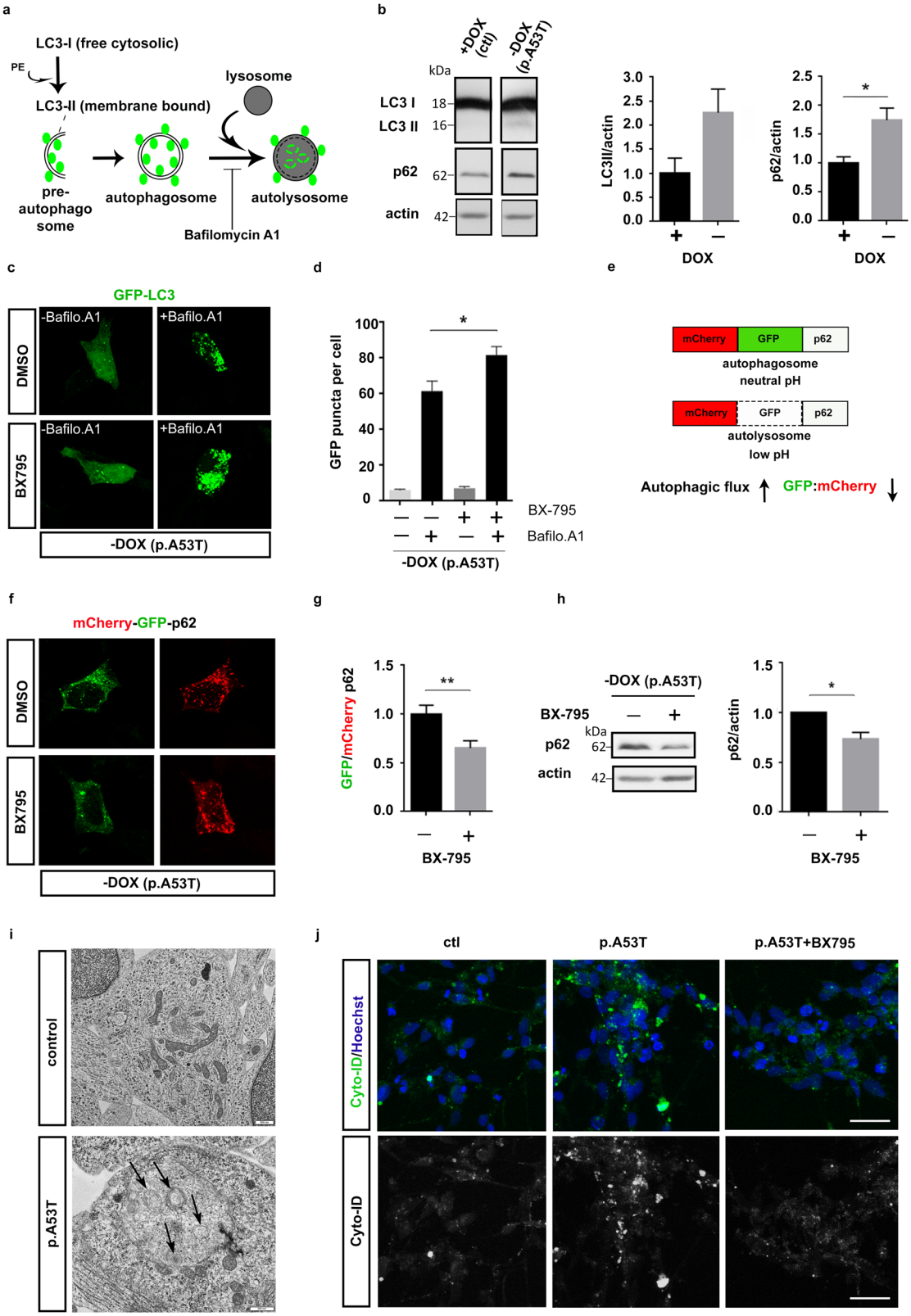


signal, captured in channel 3. For quantification of TUJ1 and TH intensity Image Mining was used, a custom-made image processing and analysis application with an extendable "plug-in" infrastructure[78]. DMSO was used as negative control at the same concentration as in the compound library. Hit compounds were selected using the following criteria: (1) all molecules that decreased the cell number within a well by more than 30% were considered toxic and were discarded; (2) compounds with a mean intensity ratio of TH vs TUJ1 outside two standard deviations of the negative DMSO control were selected as positive.

## RNA isolation, cDNA Synthesis and qRT-PCR

Total RNA was extracted from cell pellets using the TRIzol® Reagent (Life Technologies). Following digestion with DNaseI, 1 µg of total RNA was used

**Fig. 9 BX795 facilitates autophagy in an inducible SH-SY5Y cell line expressing human p.A53T-αSyn. a** Schema illustrating that cytosolic LC3 is cleaved to yield LC3-I, which is subsequently conjugated to phosphatidylethanolamine (PE) to form membrane-bound LC3-II (green circles). Pre-autophagosomal structures engulfing protein cargo and organelles destined for degradation close to form double membrane spherical autophagosomes. These fuse with lysosomes to yield autolysosomes and their contents are degraded. Bafilomycin blocks autophagic flux by inhibiting autophagosome-lysosome fusion, which results in accumulation of LC3-II+ autophagosomes. **b** Representative immunoblot showing steady-state levels of LC3-II and p62 in lysates of inducible SH-SY5Y cells expressing the human p.A53T-αSyn (-Dox) and quantification relative to actin. Data represent mean ± SEM, *t* est, $*P < 0.05$, $n = 3$ independent experiments. **c** Representative confocal images of individual p.A53T SH-SY5Y cells (-Dox) transfected with GFP-LC3 that were treated or not with bafilomycin A1 in the absence or presence of BX795. **d** Quantification of GFP-LC3 puncta per cell. Comparisons by ANOVA with Tukey correction. $*P < 0.05$, $n = 72$ cells (control DMSO), $n = 79$ cells (BX795), $n = 67$ cells (Bafilomycin A1), $n = 68$ cells BX795 + Bafilomycin A1. Data are representative of three independent experiments). **e** Assessment of autophagic flux using mCherry-GFP-LC3 color change between autophagosomes and autolysosomes. Autophagic flux is induced when the GFP:mCherry ratio is reduced. f, g. Representative confocal images of individual cells [inducible SH-SY5Y cell line expressing p.A53T-αSyn (-Dox)] transfected with GFP-mCherry-p62 that were treated with DMSO (control) or BX795 and quantification of the ratio of GFP +/mCherry+ puncta (*t* test, $n = 60$ (control DMSO), $n = 53$ (BX795) $**P < 0.01$ Data are representative of three independent experiments). **h** Representative immunoblot showing steady-state levels of p62 in cells [inducible SH-SY5Y cell line expressing p.A53T-αSyn (-Dox)] treated or not with BX795, and quantification relative to actin. Data represent mean ± SEM, *t* test, $n = 3$ independent experiments. **i** Representative electron micrographs showing control and patient-derived p.A53T cells. Multilamellar autophagic vacuoles (arrows) are depicted in p. A53T cells; in this case they seem to be engulfed by an additional membranous structure. Scale bar 500 nm. **j** Representative confocal images showing autophagosome accumulation (brightly labeled green spheroids) in patient-derived p.A53T neurons as compared to either control (ctl) or p.A53T cells treated with BX795. Scale bar, 30 μm.

for first strand cDNA synthesis with the ImProm-II Reverse Transcription System (Promega) according to the manufacturer's instructions. Quantitative RT-PCR analyses were carried out in a Light Cycler 96 (Roche) real time PCR detection system using KAPA SYBR FAST qPCR Master Mix (KapaBiosystems). All primers used are listed in Supplementary Table 5.

### Immunofluorescence staining

Cells were paraformaldehyde-fixed, blocked with 5% donkey serum in PBS/0.1% Triton X-100 (Sigma-Aldrich) for 30 min and immunofluorescence labeled as above. Coverslips were mounted with ProLong Gold antifade reagent with DAPI (Cell Signaling) and images were acquired using a Leica TCS SP8 confocal microscope (LEICA Microsystems) and analyzed using ImageJ software (NIH). All primary antibodies used are listed in Supplementary Table 6.

### Neurite analysis

Neurite length was estimated manually by tracing the length of all neurites on TH-labeled neurons at 21 DIV using the NeuronJ plugin of ImageJ (NIH). At least 50 single TH+ neurons per sample were analyzed.

### Axon degeneration index

The number of TUJ1+ spots in blebbed or fragmented axons was counted manually (ImageJ) on twenty randomly selected fields and the ratio between the number of spots and the total TUJ1+ staining area (ImageJ) was defined as axon degeneration index [22].

### Protein aggregate quantification

Protein aggregates were detected with the PROTEOSTAT Aggresome Detection Kit (Enzo) followed by immunolabeling for TUJ1 or TH[22,32]. Manual analysis was performed by isolating individual cells from images (ROIs), applying a threshold, and utilizing the 'analyze particles' ImageJ function.

### Proteomic analysis

The same line of patient-derived neurons used for high content screening was used for proteomics analysis vis-à-vis a healthy control. At 21 DIV iPSC-derived neurons were suspended, lysed and the proteins reduced in 4% SDS, 100 mM DTT, 100 mM Tris pH 7.8 through heating for 5 min. Next, the proteins were alkylated by 100 mM iodoacetamide treatment for 30 min in the dark. Samples were further processed according to the Single-Pot Solid-Phase enhanced Sample Preparation (SP3) method of Hughes et al.[79]. Digestion was carried out overnight at 37 °C using Trypsin/LysC mix (Promega) at a protein/enzyme ratio of 50:1 in a ThermoMixer under continuous mixing at 1000 rpm. After digestion, the tubes were placed on a magnetic rack, and the supernatant containing the peptides was collected and dried down in a centrifugal evaporator (Savant SPD 1010, Thermo scientific). The peptide mixtures were reconstituted in a solution of 2% (v/v) ACN/ 0.1% (v/v) formic acid and incubated for 3 min in a sonication water bath. Peptide concentration was determined by nanodrop absorbance measurement at 280 nm.

### Ultra-high pressure nanoLC

2.5 μg peptides were pre-concentrated with a flow of 3 μL/min for 10 min using a C18 trap column (Acclaim PepMap100, 100 μm × 2 cm, Thermo Scientific) and then loaded onto a 50 cm long C18 column (75 μm ID, particle size 2 μm, 100 Å, Acclaim PepMap100 RSLC, Thermo Scientific). The binary pumps of the HPLC (RSLCnano, Thermo Scientific) consisted of Solution A (2% (v/v) ACN in 0.1% (v/v) formic acid) and Solution B (80% (v/v) ACN in 0.1% (v/v) formic acid). The peptides were separated using a linear gradient of 4% B up to 40% B in 340 min with a flow rate of 300 nL/min. The column was placed in an oven at 35 °C.

### LC-MS/MS

Eluted peptides were ionized by a nanospray source and detected by an LTQ Orbitrap XL mass spectrometer (Thermo Fisher Scientific, Waltham, MA, USA) operating in a data dependent mode (DDA). Full scan MS spectra were acquired in the orbitrap (m/z 300–1600) in profile mode with resolution set to 60,000 at m/z 400 and automatic gain control target at 106 ions. The six most intense ions were sequentially isolated for collision-induced (CID) MS/MS fragmentation and detection in the linear ion trap. Dynamic exclusion was set to 1 min and activated for 90 sec. Ions with single charge states were excluded. Lockmass of m/z 445,120025 was used for continuous internal calibration. XCalibur (Thermo Scientific) was used to control the system and acquire the raw files.

### Protein identification and quantification

The raw mass spectral files were processed using MaxQuant software (version 1.6.9.0) with default parameters for protein identification and quantification. Trypsin specificity was set to allow two missed cleavages and minimum peptide length was set to 7 amino acids. Cysteine carbamidomethylation was set as fixed, and methionine oxidation, deamidation of asparagine and glutamine and N-terminal acetylation were set as variable modifications. A maximum of 5 modifications per peptide was set. The false discovery rate both for peptide and protein was set to 1%. For calculation of protein abundances, label-free quantification (LFQ) was performed with both "second peptides" and "match between run" options enabled. The human FASTA files were from UniProt downloaded on 15 October 2019.

### Proteomic data analysis

Statistical analysis was performed using Perseus (1.6.6.0). Proteins identified as contaminants, "reverse" and "only identified by site" were filtered out. The LFQ intensities were transformed to logarithmic values [log2(x)]. The protein groups were filtered to obtain at least 2 valid values in at least one group. The label-free quantified proteins were subjected to statistical analysis with ANOVA test (permutation-based p-value with 0.05 cutoff). LC-MS/MS data after statistical analysis were plotted in a volcano graph based on the

difference between the two samples expressed as log2(x) versus their statistical significance expressed as −Log10(p-value). Hierarchical clustering was carried out on Z-score transformed LFQ values using average linkage of Euclidian distance. For statistical and bioinformatics analysis, as well as for visualization, Perseus, which is part of Maxquant, was used[80]. GO Enrichment analysis for biological processes, molecular function and cellular compartment was performed using DAVID functional annotation tools with official gene symbol as identifiers, the Homo sapiens background and the GOTERM_DIRECT annotation categories. A P value of 0.05 was selected as the cutoff criterion. The enrichment of proteins involved in signaling pathways was performed using the Reactome pathway database. A P value of 0.01 was selected as the cutoff criterion.

### Western blot

Cells were lysed at 4 °C for 15 min in ice cold lysis buffer [150mMNaCl, 50 mM Tris pH 7.5, 1% Triton X-100, 1 mM EDTA, 1 mM EGTA, 0.1% SDS, 0.5% sodium deoxycholate containing PhosSTOP phosphatase inhibitors and a complete protease inhibitor mixture (Roche Life Science)], and centrifuged at 20,000 g. Protein concentration was estimated in the supernatant by Bradford assay (Applichem). Proteins were separated by SDS-polyacrylamide gel electrophoresis and transferred onto nitrocellulose membranes (Maine Manufacturing). For phospho-(Ser129)-αSyn detection, the membrane was heated at 65 °C overnight in PBS. Nonspecific binding sites were blocked in TBS/ 0.1% Tween 20/ 5% skimmed milk for 1 hour at 20 °C followed by overnight incubation with primary antibodies diluted in the same buffer. Incubation with appropriate HRP-conjugated secondary antibodies (Thermo) was for 2 hours at room temperature and protein bands were visualized using the Clarity Western ECL Substrate (BIO-RAD). Densitometric analysis was performed using ImageJ software (NIH). All blots were derived from the same experiment and were processed in parallel. Original unprocessed blots are shown in Supplementary Fig. 7.

### Production of CMV.DsRed and CMV.DsRed.A53T lentiviral vectors

Four plasmids were used for lentivirus generation: the lentiviral transfer vector and three lentiviral packaging vectors (pMDL, pRev and pVSVG; provided by Dr. Fred Gage, the Salk Institute for Biological Studies). The lentiviral transfer vectors for expression of either the red fluorescent protein DsRed under the control of CMV promoter (LV.CMV.DsRed) or for co-expression of the red fluorescent protein DsRed, a T2A bicistronic configuration and human p.A53T-αSyn under the control of CMV promoter (LV.CMV.DsRed.T2A.A53T) were constructed by VectorBuilder. The preparation and purification of the lentiviral vectors were performed as previously described[81].

### Generation of stably transduced SH-SY5Y cells

SH-SY5Y cells were transduced with the control vector LV.CMV.DsRed or LV.CMV.DsRed.T2A.A53T for expression of DsRed or co- expression of DsRed and human p.A53T-αSyn. Transduced cells were maintained in regular RPMI 1640 medium/ 10% FBS (Gibco)/ 1% penicillin/streptomycin (Life Technologies) for 48 h with one change of medium, and were then transferred in selection medium containing 300 µg/ml gentamycin-disulfate G418. After 3 weeks of selection, when 100% of cells expressed the DsRED protein, they were frozen as a polyclonal pool.

### Differentiation of SH-SY5Y cells

Cells were plated on PLL/Laminin coated plates ($2 \times 10^4$ cells/cm$^2$) in regular RPMI 1640 medium/ 5% FBS/ 1% penicillin/streptomycin (DIV 0). The following day, 10 µM Retinoic Acid (RA) was added (DIV1). On DIV3, the medium was changed to Neurobasal supplemented with B27, N2, Glutamax and BDNF (50 ng/ml) with fresh medium added every 2-3 days until DIV9.

### Cell culture and transfection of an inducible SH-SY5Y line expressing human p.A53T-αSyn

The inducible SH-SY5Y cell line, in which expression of p.A53T-αSyn was switched off in the presence of doxycycline (Dox, 2 µg/mL), was previously reported[59]. Transfection with GFP-LC3 or mCherry-GFP-p62 plasmids (provided by Dr Tamotsu Yoshimori, Osaka University, Japan and Dr Terje Johansen, University of Tromso, Norway, respectively) was performed in the absence of Dox using Lipofectamine 2000, according to the manufacturer's protocol (Invitrogen; Thermo Fisher Scientific, Inc.).

### Protein synthesis assay

For detection of total protein synthesis, an assay Kit (ab239725; Abcam) was used that utilizes a cell permeable analog of puromycin, which once inside the cell, stops translation by forming covalent conjugates with nascent polypeptide chains. Truncated polypeptides can be detected based on a click reaction with fluorescent azide. Cells were pre-treated with DMSO vehicle or BX795 for different time points and were incubated for 2 h with fresh aliquots of media containing either Protein Label or Protein Label and BX795. Cyclohexamide that blocks protein synthesis was used as a negative control. Fluorescence images were acquired using a Leica TCS SP8 confocal microscope (LEICA Microsystems) and analyzed using ImageJ software (NIH).

### Autophagy detection assay

For detection of autophagosomes and monitoring autophagic flux, cells were seeded in 48-well plates on coverslips. After 7d incubation, the cells were treated with BX795 (1uM). The Cyto-ID® autophagy detection kit (Enzo Life Sciences, Plymouth Meeting, PA) was used according to the manufacturer's instructions in live cells. Samples were briefly exposed to Cyto-ID Green Dye and Hoechst 33342 at 37 °C for 30 min. The cells were then washed with 1× assay buffer and fixed with 4% parafolmadehyde. Coverslips were mounted with ProLong Gold antifade reagent with DAPI (Cell Signaling) and images were acquired using a Leica TCS SP8 confocal microscope (LEICA Microsystems) and analyzed using ImageJ software (NIH).

### P70 S6K kinase activity

A p70 S6K activity assay kit (ADI-EKS-470 Enzo Life Sciences) was used based on a solid phase enzyme-linked immunoabsorbent assay (ELISA) that utilizes a specific synthetic peptide as substrate for p70 S6K and a polyclonal antibody that recognizes the phosphorylated form of the substrate. The assay was developed according to the manufacturer's instructions. Briefly, purified recombinant kinase provided by the manufacturer was incubated in the absence or presence of the BX795 inhibitor for 30 min prior to initiating the kinase reaction. Rapamycin was used as a positive control. Samples were then transfered in a 96−well plate coated with the p70 S6K substrate, a synthesized peptide containing the S6 consensus sequence (KRRRLASLR) and the reaction was initiated with the addition of ATP. After removal of the reaction mixture and three washes, the plate was incubated with a phosphospecific substrate antibody (1:1000) for 1 h, followed by a secondary antibody conjugated to horseradish peroxidase (HRP) for 20 min. Color was developed using tetramethylbenzidine as substrate (TMB) and the absorbance was measured at 450 nm in a Bio-Rad 680 microplate reader.

### Electron microscopy

For conventional electron microscopy, p.A53T patient-derived and control neurons were seeded on aclar film placed in glass petri dishes. The medium was replaced with pre-warmed fixative (2.5% glutaraldehyde in 0.1 M phosphate buffer) for 1 h. Cells were rinsed in buffer and post-fixed with 1% osmium tetroxide at 4 °C for 1 hour. The samples were dehydrated in a graded series of ethanol, followed by propylene oxide (PO). Cells were further processed for infiltration in a mixture of Epon/Araldite resins diluted in PO and were flat-embedded in fresh epoxy resin mixture. Finally, the specimens were allowed to polymerize at 60 °C for 24 h. Small epoxy pieces were peeled away from the petri dishes, glued on epoxy blocks for sectioning and were allowed to polymerize for additional 24 h. Ultrathin sections were cut with a Diatome diamond knife at a thickness of 65 nm on a Leica EM UC7 ultramicrotome and stained with uranyl acetate and lead citrate. Sections were examined with a Philips 420 transmission electron microscope and photographed with a Megaview G2 CCD camera.

### Statistics

All experiments were replicated at least three times and data from parallel cultures were acquired. Statistical analysis was performed using GraphPad Prism 6 software. Before performing parametric tests, data were assessed for normality with a D'Agostino–Pearson omnibus. Statistical significance was calculated for two groups using Student's *t* tests or the Mann–Whitney test for non-parametric distribution. Group comparisons of data were performed by one-way ANOVA test followed by Tukey post hoc test using PRISM (Graph Pad). *P* values < 0.05 were considered significant; $*p < 0.05$, $**p < 0.01$, $***p < 0.001$, $****p < 0.0001$.

## Reporting summary

Further information on research design is available in the Nature Research Reporting Summary linked to this article.

## DATA AVAILABILITY

The mass spectrometry proteomics data have been deposited to the ProteomeXchange Consortium via the PRIDE partner repository with the dataset identifier PXD019574. All data needed to evaluate the conclusions in the paper are present in the paper and/or the Supplementary Materials. The raw and analyzed datasets generated during the study are available for research purposes from the corresponding author on reasonable request. Additional data related to this paper may be requested from the authors.

Received: 8 April 2021; Accepted: 12 January 2022;
Published online: 11 February 2022

## REFERENCES

1. Baker, M. G. & Graham, L. The journey: Parkinson's disease. *BMJ* **329**, 611–614 (2004).
2. Olanow, C. W. & Tatton, W. G. Etiology and pathogenesis of Parkinson's disease. *Annu. Rev. Neurosci.* **22**, 123–144 (1999).
3. Pfeiffer, R. F. Non-motor symptoms in Parkinson's disease. *Parkinsonism Relat. Disord.* **22**, S119–S122 (2016).
4. Gibb, W. Idiopathic Parkinson's disease and the Lewy body disorders. *Neuropathol. Appl. Neurobiol.* **12**, 223–234 (1986).
5. Lewandowsky, M. H. *Handbuch* der neurologie: bd. Spezielle Neurologie IV, (J. Spring, 1914).
6. Baba, M. et al. Aggregation of alpha-synuclein in Lewy bodies of sporadic Parkinson's disease and dementia with Lewy bodies. *Am. J. Pathol.* **152**, 879–884 (1998).
7. Breydo, L., Wu, J. W. & Uversky, V. N. Alpha-synuclein misfolding and Parkinson's disease. *Biochimica et. biophysica acta* **1822**, 261–285 (2012).
8. Chartier-Harlin, M. C. et al. Alpha-synuclein locus duplication as a cause of familial Parkinson's disease. *Lancet* **364**, 1167–1169 (2004).
9. Petrucci, S., Ginevrino, M. & Valente, E. M. Phenotypic spectrum of alpha-synuclein mutations: New insights from patients and cellular models. *Parkinsonism Relat. Disord.* **22**, S16–S20 (2016).
10. Simon-Sanchez, J. et al. Genome-wide association study reveals genetic risk underlying Parkinson's disease. *Nat. Genet*. **41**, 1308–1312 (2009).
11. Conway, K. A. et al. Acceleration of oligomerization, not fibrillization, is a shared property of both alpha-synuclein mutations linked to early-onset Parkinson's disease: implications for pathogenesis and therapy. *Proc. Natl. Acad. Sci. USA* **97**, 571–576 (2000).
12. Duda, J. E. et al. Concurrence of alpha-synuclein and tau brain pathology in the Contursi kindred. *Acta neuropathologica* **104**, 7–11 (2002).
13. Kotzbauer, P. T. et al. Fibrillization of alpha-synuclein and tau in familial Parkinson's disease caused by the A53T alpha-synuclein mutation. *Exp. Neurol.* **187**, 279–288 (2004).
14. Cotzias, G. C., Van Woert, M. H. & Schiffer, L. M. Aromatic amino acids and modification of parkinsonism. *N. Engl. J. Med* **276**, 374–379 (1967).
15. Ghosh, D., Mehra, S., Sahay, S., Singh, P. K. & Maji, S. K. Alpha-synuclein aggregation and its modulation. *Int. J. Biol. Macromol.* **100**, 37–54 (2017).
16. Ghosh, D. et al. The Parkinson's disease-associated H50Q mutation accelerates alpha-Synuclein aggregation in vitro. *Biochemistry* **52**, 6925–6927 (2013).
17. Schulz-Schaeffer, W. J. The synaptic pathology of alpha-synuclein aggregation in dementia with Lewy bodies, Parkinson's disease and Parkinson's disease dementia. *Acta Neuropathologica* **120**, 131–143 (2010).
18. Chen, M. et al. Common proteomic profiles of induced pluripotent stem cell-derived three-dimensional neurons and brain tissue from Alzheimer patients. *J. Proteom.* **182**, 21–33 (2018).
19. Cooper, O. et al. Pharmacological rescue of mitochondrial deficits in iPSC-derived neural cells from patients with familial Parkinson's disease. *Sci. Transl. Med.* **4**, 141ra190 (2012).
20. Ryan, S. D. et al. Isogenic human iPSC Parkinson's model shows nitrosative stress-induced dysfunction in MEF2-PGC1alpha transcription. *Cell* **155**, 1351–1364 (2013).
21. Yang, Y. M. et al. A small molecule screen in stem-cell-derived motor neurons identifies a kinase inhibitor as a candidate therapeutic for ALS. *Cell Stem Cell* **12**, 713–726 (2013).
22. Kouroupi, G. et al. Defective synaptic connectivity and axonal neuropathology in a human iPSC-based model of familial Parkinson's disease. *Proc. Natl. Acad. Sci. USA* **114**, E3679–E3688 (2017).
23. Chambers, S. M. et al. Highly efficient neural conversion of human ES and iPS cells by dual inhibition of SMAD signaling. *Nat. Biotechnol.* **27**, 275–280 (2009).
24. Soldner, F. et al. Parkinson's disease patient-derived induced pluripotent stem cells free of viral reprogramming factors. *Cell* **136**, 964–977 (2009).
25. Lovestone, S. et al. A phase II trial of tideglusib in Alzheimer's disease. *J. Alzheimers Dis.* **45**, 75–88 (2015).
26. Pagan, F. L. et al. Pharmacokinetics and pharmacodynamics of a single dose Nilotinib in individuals with Parkinson's disease. *Pharm. Res. Perspect.* **7**, e00470 (2019).
27. Cuny, G. D. Kinase inhibitors as potential therapeutics for acute and chronic neurodegenerative conditions. *Curr. Pharm. Des.* **15**, 3919–3939 (2009).
28. Yu, T. et al. The kinase inhibitor BX795 suppresses the inflammatory response via multiple kinases. *Biochemical Pharmacol.* **174**, 113797 (2020).
29. Clark, K., Plater, L., Peggie, M. & Cohen, P. Use of the pharmacological inhibitor BX795 to study the regulation and physiological roles of TBK1 and IkappaB kinase epsilon: a distinct upstream kinase mediates Ser-172 phosphorylation and activation. *J. Biol. Chem.* **284**, 14136–14146 (2009).
30. Jaishankar, D. et al. An off-target effect of BX795 blocks herpes simplex virus type 1 infection of the eye. *Sci. Transl. Med.* **10**, eaan5861 (2018).
31. Su, A. R. et al. BX-795 inhibits HSV-1 and HSV-2 replication by blocking the JNK/p38 pathways without interfering with PDK1 activity in host cells. *Acta Pharm. Sin.* **38**, 402–414 (2017).
32. Zygogianni, O. et al. In vivo phenotyping of familial Parkinson's disease with human induced pluripotent stem cells: a proof-of-concept study. *Neurochem. Res.* **44**, 1475–1493 (2019).
33. Ryan, T. et al. Cardiolipin exposure on the outer mitochondrial membrane modulates alpha-synuclein. *Nat. Commun.* **9**, 817 (2018).
34. Walker, D. G. et al. Changes in properties of serine 129 phosphorylated alpha-synuclein with progression of Lewy-type histopathology in human brains. *Exp. Neurol.* **240**, 190–204 (2013).
35. Bai, L. Y. et al. BX795, a TBK1 inhibitor, exhibits antitumor activity in human oral squamous cell carcinoma through apoptosis induction and mitotic phase arrest. *Eur. J. Pharm.* **769**, 287–296 (2015).
36. Cox, J. et al. Accurate proteome-wide label-free quantification by delayed normalization and maximal peptide ratio extraction, termed MaxLFQ. *Mol. Cell Proteom.* **13**, 2513–2526 (2014).
37. Cox, J. & Mann, M. MaxQuant enables high peptide identification rates, individualized p.p.b.-range mass accuracies and proteome-wide protein quantification. *Nat. Biotechnol.* **26**, 1367–1372 (2008).
38. Chung, C. Y. et al. In situ peroxidase labeling and mass-spectrometry connects alpha-synuclein directly to endocytic trafficking and mRNA metabolism in neurons. *Cell Syst.* **4**, 242–250 (2017). e244.
39. Bowden, H. A. & Dormann, D. Altered mRNP granule dynamics in FTLD pathogenesis. *J. neurochemistry* **138**, 112–133 (2016).
40. Kapur, M., Monaghan, C. E. & Ackerman, S. L. Regulation of mRNA translation in. *Neurons-A Matter Life Death. Neuron* **96**, 616–637 (2017).
41. Chung, C. Y. et al. Identification and rescue of alpha-synuclein toxicity in Parkinson patient-derived neurons. *Science* **342**, 983–987 (2013).
42. Khurana, V. et al. Genome-scale networks link neurodegenerative disease genes to alpha-synuclein through specific molecular pathways. *Cell Syst.* **4**, 157–170 (2017). e114.
43. Carpanini, S. M. et al. A novel mouse model of Warburg Micro syndrome reveals roles for RAB18 in eye development and organisation of the neuronal cytoskeleton. *Dis. Model Mech.* **7**, 711–722 (2014).
44. Feldmann, A. et al. The RAB GTPase RAB18 modulates macroautophagy and proteostasis. *Biochem Biophys. Res. Commun.* **486**, 738–743 (2017).
45. Rocca, D. L. et al. The small GTPase Arf1 modulates Arp2/3-mediated actin polymerization via PICK1 to regulate synaptic plasticity. *Neuron* **79**, 293–307 (2013).
46. Jean, S., Cox, S., Nassari, S. & Kiger, A. A. Starvation-induced MTMR13 and RAB21 activity regulates VAMP8 to promote autophagosome-lysosome fusion. *EMBO Rep.* **16**, 297–311 (2015).
47. Farley, M. M. & Watkins, T. A. Intrinsic neuronal stress response pathways in injury and disease. *Annu Rev. Pathol.* **13**, 93–116 (2018).
48. Maraganore, D. M. et al. UCHL1 is a Parkinson's disease susceptibility gene. *Ann. Neurol.* **55**, 512–521 (2004).
49. Williams, E. T., Chen, X. & Moore, D. J. VPS35, the retromer complex and Parkinson's disease. *J. Parkinsons Dis.* **7**, 219–233 (2017).
50. Chi, B. et al. The neurodegenerative diseases ALS and SMA are linked at the molecular level via the ASC-1 complex. *Nucleic Acids Res.* **46**, 11939–11951 (2018).
51. Abramzon, Y. A., Fratta, P., Traynor, B. J. & Chia, R. The overlapping genetics of amyotrophic lateral sclerosis and frontotemporal dementia. *Front Neurosci.* **14**, 42 (2020).
52. Gonzalez, M. A. et al. A novel mutation in VCP causes Charcot-Marie-Tooth Type 2 disease. *Brain* **137**, 2897–2902 (2014).
53. Aminkeng, F. HINT1 mutations define a novel disease entity - autosomal recessive axonal neuropathy with neuromyotonia. *Clin. Genet* **83**, 31–32 (2013).
54. Haverfield, E. V., Whited, A. J., Petras, K. S., Dobyns, W. B. & Das, S. Intragenic deletions and duplications of the LIS1 and DCX genes: a major disease-causing

mechanism in lissencephaly and subcortical band heterotopia. *Eur. J. Hum. Genet* **17**, 911–918 (2009).
55. Bernert, G., Fountoulakis, M. & Lubec, G. Manifold decreased protein levels of matrin 3, reduced motor protein HMP and hlark in fetal Down's syndrome brain. *Proteomics* **2**, 1752–1757 (2002).
56. Shima, H. et al. Disruption of the p70(s6k)/p85(s6k) gene reveals a small mouse phenotype and a new functional S6 kinase. *EMBO J.* **17**, 6649–6659 (1998).
57. Parekh, P. et al. A cleaning crew: the pursuit of autophagy in Parkinson's disease. *ACS Chem. Neurosci.* **10**, 3914–3926 (2019).
58. Rabanal-Ruiz, Y., Otten, E. G. & Korolchuk, V. I. mTORC1 as the main gateway to autophagy. *Essays Biochem* **61**, 565–584 (2017).
59. Xilouri, M., Vogiatzi, T., Vekrellis, K., Park, D. & Stefanis, L. Abberant alpha-synuclein confers toxicity to neurons in part through inhibition of chaperone-mediated autophagy. *PLoS One* **4**, e5515 (2009).
60. Kabeya, Y. et al. LC3, a mammalian homologue of yeast Apg8p, is localized in autophagosome membranes after processing. *EMBO J.* **19**, 5720–5728 (2000).
61. Jiang, P. & Mizushima, N. LC3- and p62-based biochemical methods for the analysis of autophagy progression in mammalian cells. *Methods* **75**, 13–18 (2015).
62. Lopez, A., Fleming, A. & Rubinsztein, D. C. Seeing is believing: methods to monitor vertebrate autophagy in vivo. *Open Biology* **8**, 180106 (2018).
63. Pankiv, S. et al. p62/SQSTM1 binds directly to Atg8/LC3 to facilitate degradation of ubiquitinated protein aggregates by autophagy. *J. Biol. Chem.* **282**, 24131–24145 (2007).
64. Spira, P. J., Sharpe, D. M., Halliday, G., Cavanagh, J. & Nicholson, G. A. Clinical and pathological features of a Parkinsonian syndrome in a family with an Ala53Thr alpha-synuclein mutation. *Ann. Neurol.* **49**, 313–319 (2001).
65. Yamaguchi, K. et al. Abundant neuritic inclusions and microvacuolar changes in a case of diffuse Lewy body disease with the A53T mutation in the alpha-synuclein gene. *Acta Neuropathologica* **110**, 298–305 (2005).
66. Yeo, G., Holste, D., Kreiman, G. & Burge, C. B. Variation in alternative splicing across human tissues. *Genome Biol.* **5**, R74 (2004).
67. Apicco, D. J. et al. Dysregulation of RNA splicing in tauopathies. *Cell Rep.* **29**, 4377–4388 (2019). e4374.
68. Garcia-Esparcia, P. et al. Altered machinery of protein synthesis is region- and stage-dependent and is associated with alpha-synuclein oligomers in Parkinson's disease. *Acta Neuropathologica Commun.* **3**, 76 (2015).
69. Johnson, S. C., Rabinovitch, P. S. & Kaeberlein, M. mTOR is a key modulator of ageing and age-related disease. *Nature* **493**, 338–345 (2013).
70. Kim, J. & Guan, K. L. mTOR as a central hub of nutrient signalling and cell growth. *Nat. Cell Biol.* **21**, 63–71 (2019).
71. Papadopoli, D. et al. mTOR as a central regulator of lifespan and aging. *F1000Res* **8**, 998 (2019).
72. Xun, Z., Sowell, R. A., Kaufman, T. C. & Clemmer, D. E. Quantitative proteomics of a presymptomatic A53T alpha-synuclein Drosophila model of Parkinson disease. *Mol. Cell Proteom.* **7**, 1191–1203 (2008).
73. Fernandez-Santiago, R. et al. SNCA and mTOR pathway single nucleotide polymorphisms interact to modulate the age at onset of Parkinson's Disease. *Mov. Disord.* **34**, 1333–1344 (2019).
74. Arotcarena, M. L., Teil, M. & Dehay, B. Autophagy in synucleinopathy: the overwhelmed and defective machinery. *Cells* **8**, 565 (2019).
75. Menzies, F. M. et al. Autophagy and neurodegeneration: pathogenic mechanisms and therapeutic opportunities. *Neuron* **93**, 1015–1034 (2017).
76. Oakes, J. A., Davies, M. C. & Collins, M. O. TBK1: a new player in ALS linking autophagy and neuroinflammation. *Mol. Brain* **10**, 5 (2017).
77. Pietri, M. et al. PDK1 decreases TACE-mediated alpha-secretase activity and promotes disease progression in prion and Alzheimer's diseases. *Nat. Med.* **19**, 1124–1131 (2013).
78. Dorval, T. et al. Contextual automated 3D analysis of subcellular organelles adapted to high-content screening. *J. Biomol. Screen.* **15**, 847–857 (2010).
79. Hughes, C. S. et al. Single-pot, solid-phase-enhanced sample preparation for proteomics experiments. *Nat. Protoc.* **14**, 68–85 (2019).
80. Tyanova, S. et al. The perseus computational platform for comprehensive analysis of (prote)omics data. *Nat. Methods* **13**, 731–740 (2016).
81. Tiscornia, G., Singer, O. & Verma, I. M. Production and purification of lentiviral vectors. *Nat. Protoc.* **1**, 241–245 (2006).

## ACKNOWLEDGEMENTS

We thank Drs. Tamotsu Yoshimori and Terje Johansen for providing GFP-LC3 and mCherry-GFP-p62 plasmids, respectively. This work was supported by: a Stavros Niarchos Foundation grant to the Hellenic Pasteur Institute as part of the Foundation's initiative to support the Greek Research Center ecosystem; the Greek General Secretariat for Research and Technology (GSRT) grant BIOIMAGING-GR MIS 5002755 implemented under the Action "Reinforcement of Research and Innovation Infrastructure", and EATRIS-GR OPS5028091, both funded by the Operational Programme "Competitiveness, Entrepreneurship and Innovation" (NSRF 2014-2020) and co-financed by Greece and the European Union (European Regional Development Fund); the GSRT Flagship Action for Neurodegenerative Diseases on the basis of Personalized Medicine; the Hellenic Foundation for Research and Innovation (HFRI) 899-PARKINSynapse grant to G.K and HFRI 1019-DiseasePhenoTarget grant to R.M.; the South Korea Ministry of Science and ICT (MSIT) grant (NRF-2017M3A9G6068257) to RG. N.A. was recipient of a Calmette & Yersin Fellowship for a technology exchange visit to the Institut Pasteur Korea.

## AUTHOR CONTRIBUTIONS

N.A. carried out the experiments analyzed and interpreted the data, generated the figures, participated in the study design and in writing the manuscript. K.P. and E.T. analyzed proteomics data. G.K. generated the patient-derived p.A53T and control iPSCs used in this study and provided training on iPSC culture and differentiation. I.B. participated in some experiments involving cell culture and confocal microscopy, phenotype analysis and quantification. M.S. and G.P. performed the proteomic analysis. M.X. and L.S. provided reagents, analytic tools and guidance for autophagy experiments. I.K. performed electron microscopy and interpretation. N.A. and R.G. performed high-content imaging and drug screening on p.A53T neurons. E.T. and R.M. conceived, designed and supervised the study, analyzed the data and wrote the paper with contribution from all authors.

## COMPETING INTERESTS

The authors declare no competing interests.

## ADDITIONAL INFORMATION

**Supplementary information** The online version contains supplementary material available at https://doi.org/10.1038/s41531-022-00278-y.

**Correspondence** and requests for materials should be addressed to Rebecca Matsas.

**Reprints and permission information** is available at http://www.nature.com/reprints

**Publisher's note** Springer Nature remains neutral with regard to jurisdictional claims in published maps and institutional affiliations.

International Journal of
*Molecular Sciences*

MDPI

*Review*

# Patient-Derived Induced Pluripotent Stem Cell-Based Models in Parkinson's Disease for Drug Identification

**Georgia Kouroupi, Nasia Antoniou, Kanella Prodromidou, Era Taoufik and Rebecca Matsas ***

Laboratory of Cellular and Molecular Neurobiology-Stem Cells, Hellenic Pasteur Institute, 127 Vassilissis Sofias Avenue, 11521 Athens, Greece; gkouroupi@pasteur.gr (G.K.); nantoniou@pasteur.gr (N.A.); kprodromidou@pasteur.gr (K.P.); etaoufik@pasteur.gr (E.T.)
* Correspondence: rmatsa@pasteur.gr

Received: 31 August 2020; Accepted: 25 September 2020; Published: 26 September 2020


**Abstract:** Parkinson's disease (PD) is a common progressive neurodegenerative disorder characterized by loss of striatal-projecting dopaminergic neurons of the ventral forebrain, resulting in motor and cognitive deficits. Despite extensive efforts in understanding PD pathogenesis, no disease-modifying drugs exist. Recent advances in cell reprogramming technologies have facilitated the generation of patient-derived models for sporadic or familial PD and the identification of early, potentially triggering, pathological phenotypes while they provide amenable systems for drug discovery. Emerging developments highlight the enhanced potential of using more sophisticated cellular systems, including neuronal and glial co-cultures as well as three-dimensional systems that better simulate the human pathophysiology. In combination with high-throughput high-content screening technologies, these approaches open new perspectives for the identification of disease-modifying compounds. In this review, we discuss current advances and the challenges ahead in the use of patient-derived induced pluripotent stem cells for drug discovery in PD. We address new concepts implicating non-neuronal cells in disease pathogenesis and highlight the necessity for functional assays, such as calcium imaging and multi-electrode array recordings, to predict drug efficacy. Finally, we argue that artificial intelligence technologies will be pivotal for analysis of the large and complex data sets obtained, becoming game-changers in the process of drug discovery.

**Keywords:** disease phenotypes; high-content screening; chemical libraries; disease-modifying drugs; hiPSC-derived neurons; hiPSC-based co-culture systems; brain organoids

## 1. Introduction

Parkinson's disease (PD) is the second most common neurodegenerative disorder, with an increasing incidence in aged people, while an estimated 4% are diagnosed before the age of 50. Due to the high prevalence of PD and the increase in the proportion of aging population resulting from extended life expectancy, the disease has become a rapidly growing area of concern. PD is characterized by progressive loss of striatal-projecting midbrain dopaminergic neurons of the substantia nigra pars compacta [1], leading to motor symptoms, such as bradykinesia, rigidity and resting tremor, with a wide range of severity [2]. Although considered a classic movement disorder, PD is associated with a broad spectrum of non-motor symptoms, including psychiatric and cognitive manifestations such as depression, dementia and hallucinosis, as well as sleep and sensory disturbances. These persistent symptoms may appear long before motor dysfunction becomes apparent while they remain unaffected by currently available therapeutics, severely impairing patients' quality of life [3].

Most PD cases are sporadic with unknown etiology; however, an approximate 10% represent familial cases (reviewed in [4]). Among the genes linked to heritable monogenic PD, mutations in the α-synuclein gene *SNCA* (*PARK1/4*) [5] and the leucine-rich repeat kinase 2 gene *LRRK2* (*PARK8*) [6] are

accountable for autosomal-dominant PD forms, while mutations in *PINK1* (PTEN-induced putative kinase 1; *PARK6*) [7], *Parkin* (*PARK2*) [8], protein deglycase *DJ-1* (*PARK7*) [9], *ATP13A2* (*PARK9*) [10] and β-glucocerebrosidase (*GBA*) [11] are responsible for an autosomal recessive mode of inheritance.

Currently, only symptomatic or palliative treatments are available with none capable to prevent or slow down PD progression and revert neurological disabilities. Regardless of the divergent pathologies and clinical manifestations, dopamine-replacement drugs such as Levodopa (L-dopa), which was identified 53 years ago, are used as a first-line treatment to address the cardinal motor issues arising from nigrostriatal degeneration [12]. For most patients though, oral dopaminergic medication falls short after a few years and advanced therapies such as deep brain stimulation, continuous intestinal gel levodopa/carbidopa, and subcutaneous apomorphine administration, are considered as alternative options [13]. However, such treatments are administered only in a small subset of patients as they have limited benefit while they are associated with serious side effects, including deterioration of non-motor symptoms [14]. Therefore, although the field of therapies for PD continues to expand, there is still no therapeutic strategy capable to change or reverse the disease course.

Most present-day efforts in identifying novel PD drugs target the aggregation of misfolded α-synuclein (αSyn) as the major pathogenic factor that causes cellular toxicity (reviewed in [15]). αSyn is a presynaptic neuronal protein linked genetically and neuropathologically to PD [16–18]. It accumulates abnormally in the PD brain and is the main component of intracellular neuronal inclusions, termed Lewy bodies or Lewy neurites, which represent the histopathological hallmark of PD. The pioneering discovery that αSyn is the major gene associated with both sporadic and genetic PD [16,19,20] spurred intensive research over the past two decades for understanding the mechanisms of αSyn misfolding, oligomerization and aggregation. These studies resulted in deciphering the molecular pathways involved (reviewed in [21]) and developing drugs aiming to halt or even clear αSyn aggregation. A number of promising compounds have been developed targeting pathological αSyn in animal models of PD (reviewed in [22]), but have largely failed when tested in early phase clinical trials, causing disappointment. Several limitations lie behind these unsuccessful endeavors. Notably, despite the flood of studies that have revealed numerous disease-associated processes, fundamental knowledge gaps still exist in PD pathophysiology. Our understanding of the disease covers processes such as mitochondrial impairment resulting in energy failure and increased oxidative stress; lysosomal deficiency and misfolded protein accumulation in large inclusions impeding axonal transport; distorted synaptic vesicle trafficking affecting neurotransmission and synaptic connections. Yet the spatiotemporal sequence of events leading to PD and, most importantly, the initial disease-triggering factors still remain elusive [2,23]. Strikingly, a recent study in which cutting-edge imaging technologies were applied indicated that αSyn immunopositive Lewy bodies and Lewy neurites consist mainly of lipid vesicle clusters instead of the long-assumed proteinacious core [24], pointing to a paradigm shift with important implications for understanding and treating neurodegeneration in PD.

Another drawback in the course of PD drug development is that assessment of novel therapeutics has been performed in animal models that fail by large to recapitulate the human condition. Last, but not least, the traditionally held conviction that the basal ganglia is the main brain region implicated in PD, has been recently challenged. It is now acknowledged that PD is a system-level disorder that affects overlapping neural circuits comprising the entire basal ganglia-cortico-cerebellar axis, which works in concert to mediate motor and cognitive functions [25]. Embracing such a system-level perspective together with using human cell-based disease models for understanding and treating PD has higher potential for the development of innovative treatments.

In this review, we discuss how revolutionary human cell-derived systems based on induced pluripotent stem cell (hiPSC) technology offer an unprecedented opportunity to study PD in models that exhibit clinically relevant disease phenotypes. Such systems provide powerful platforms for understanding pathology and, in combination with recent cutting-edge drug discovery technologies, open up new perspectives for identification of disease-modifying compounds. Yet, there are still limitations and

hurdles to face ahead before these young technologies come to fruition and fulfill their promise, particularly in reducing the number of drug failures in clinical trials.

## 2. Identification of Disease-Relevant Phenotypes in hiPSC-Derived Models of PD: A Glimpse into Human Pathology

Since the initial discovery of human cell reprogramming technology in 2007 [26], a new exciting era for the field of drug discovery has been ushered. hiPSCs have been widely used to generate "disease-in-a-dish" models for numerous neurodegenerative diseases from which selected cellular systems have been applied in drug evaluation for efficacy and toxicity assessment (Figure 1). Compared to other traditional cellular systems and existing animal models, hiPSC-based platforms offer multiple advantages: human origin in a personalized manner, easy accessibility and expandability, capacity to give rise to many different cell types and avoidance of ethical concerns associated with the use of human embryonic stem cells. Moreover, scalability and manipulation of hiPSC lines for obtaining target cells in large quantities and desirable purity is also possible at GMP grade. In the PD field, intensive efforts have been made to generate high-purity human ventral midbrain dopaminergic neurons for in vitro maturation, but mainly for intracerebral transplantation that has long been an attractive prospect for PD treatment (reviewed in [27,28]). To date, a number of sporadic and familial PD hiPSC-based models have been created displaying a variety of disease-relevant characteristics that could be exploited in either target-based or unbiased phenotypic screens. The percentage of dopamine neurons in these models varies as validated by the expression of markers associated with neuronal type and subtype specificity. However, this may not be a problem, but rather an advantage, in view of the realization that PD is more likely a system-level disorder rather than a dysfunction of the nigrostriatal dopaminergic system.

The first PD-patient specific iPSC lines were generated in 2008 by Park et al. [29] followed by a second group [30]. Both teams provided proof-of-principle that it is feasible to produce hiPSC-derived dopaminergic neurons from patients with sporadic PD, but did not proceed further to identify disease-associated phenotypes. Since then, the majority of hiPSC-based PD models have been developed mostly from patients carrying various genetic mutations (reviewed in [31]). Most studied lines carry the G2019S mutation in the *LRRK2* gene, one of the most prominent monogenetic risk factors for PD linked to both familial and sporadic forms of the disease (reviewed in [32]). hiPSC-derived cultures from patients bearing point mutations in the *SNCA* gene (A53T, A30P and E46K) or *SNCA* multiplications have also been extensively studied, while hiPSC-derived neurons carrying *Parkin* (*PARK2*), *PINK1* or *GBA* mutations have been analyzed to a lesser extent (reviewed in [33]). Overall morphological, biochemical and functional analyses have revealed a battery of disease-associated phenotypes (Table 1), initially after induction of cellular stress and later—upon careful observations—at basal conditions. Some of these phenotypes were previously described in post-mortem PD brains or in relevant animal models, while a number were identified for the first time in hiPSC-based models.

### 2.1. α-Synuclein Accumulation

As discussed, αSyn is the major protein associated with both sporadic and genetic PD [19,20]. It is a small neuronal protein widely distributed in the brain with preferential localization at pre-synaptic terminals and direct association with synaptic vesicles, suggesting possible roles in the regulation of neurotransmitter release, synaptic function and plasticity [21]. Even though the physiological function of αSyn is not well understood [34], its involvement in neurodegeneration is well established [35]. αSyn accumulation and/or aggregation has been shown in hiPSC-derived neurons generated from PD patients carrying disease-associated mutations. In particular, increased αSyn protein levels were detected in hiPSC-derived neurons carrying the A53T (G209A) point mutation [5,36–39] or *SNCA* duplication [40] and triplication [39,41–46]. Accumulation of αSyn has also been described in several other hiPSC models of familial PD, including *LRRK2*, *Parkin*, *PINK1* and hiPSC-derived neurons from *GBA* patients, as well as, in hiPSC models of sporadic PD (reviewed in [33]). Detection of the

pathological species relies largely on the presence of phosphorylated αSyn, particularly at serine 129, but also on the presence of specific oligomeric and fibrillar forms as aggregation proceeds. The presence of cellular protein aggregates has also been observed using fluorescence-based assays. In particular, our team [38] and Ryan et al. [36] have shown discrete αSyn accumulations co-localizing with Tau and ubiquitin in both the soma and axons of hiPSC-derived neurons from patients bearing the A53T mutation.

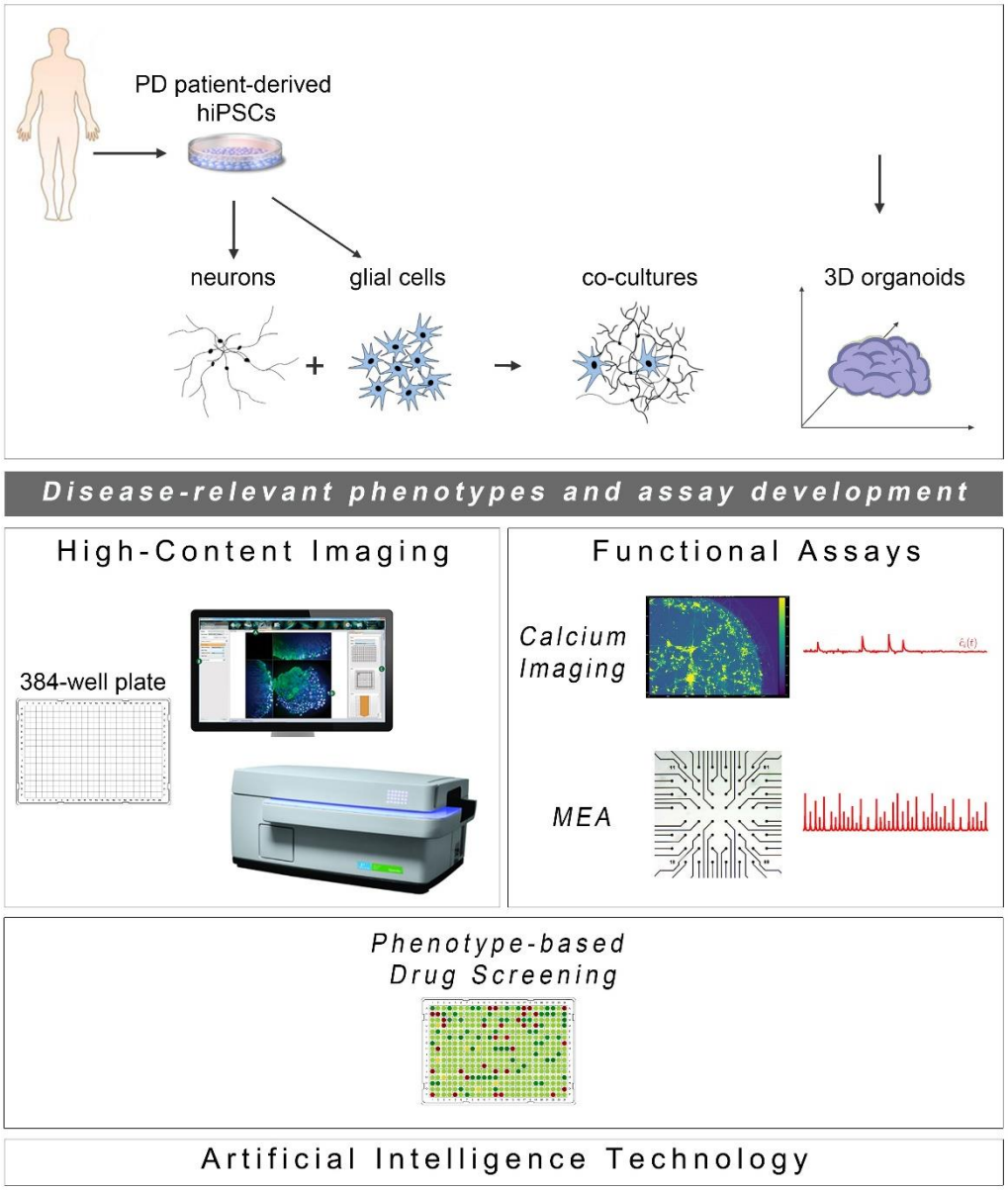


**Figure 1.** Cell reprogramming technologies allowed the generation of Parkinson's disease (PD) patient-derived hiPSCs that are further differentiated into neuronal and glial cell populations (astrocytes (shown), but also oligodendrocytes or microglia (not shown)) studied separately or in co-culture with neurons. hiPSC-derived brain organoids are being created to better simulate the human disease. The PD-relevant phenotypes identified in these cellular systems form the foundations for the development of drug discovery platforms encompassing high-content imaging/chemical library screening as well as functional assays, such as calcium imaging and high-resolution multi-electrode array (MEA) recordings (phenotypic drug screening). The application of artificial intelligence technologies will be critical for analysis of the resulting large and complex data sets.

### 2.2. Mitochondrial Defects

Mitochondrial impairment is thought to be a key factor in PD pathology, with PD-associated mutations in *Parkin*, *PINK1*, *DJ-1*, *GBA*, *LRRK2* and *SNCA* being linked to distortions in mitochondrial function [47]. Studies in hiPSC-derived neurons from PD patients have revealed mitochondrial defects, including morphological and functional alterations (reviewed in [33]). In particular, fragmented mitochondria or mitochondria with abnormal morphology have been observed in hiPSC-derived neurons carrying *LRRK2-G2019S* [48], *Parkin* [49–53], *PINK1* [51,54] or *GBA* mutations [55], but also *SNCA-G209A* or triplication [39]. Others have reported decreased mitochondrial content in patient neurons [56–58]. Altered mitochondrial functionality has also been demonstrated [52,55,57], with decreased ATP production [43,48], reduced membrane potential [59] or dysfunctional mobility [60], affecting multiple cellular processes and altering the redox status of the neuron.

### 2.3. Oxidative Stress

As mitochondrial respiration is the major source of reactive oxygen species (ROS) in the cell, mitochondrial defects should result in an increase in oxidative stress within patient neurons. A number of studies have demonstrated changes in mitochondrial and oxidative stress-related proteins observed in the human parkinsonian brain (reviewed in [61]). Similarly, oxidative stress phenotypes, such as increased ROS and carbonylated proteins or upregulation of proteins involved in dopamine oxidation, have been observed in several hiPSC-based models carrying *LRRK2* [62,63], *Parkin* [49,50,64] and *PINK1* [60,65] mutations as well as in hiPSC-derived neurons with *SNCA*-triplication [41,43,46].

### 2.4. ER Stress and Autophagy-Related Phenotypes

Consistent with protein aggregation and cellular stress, studies in hiPSC models reveal that endoplasmic reticulum (ER) dysregulation and increased ER stress may be involved in PD pathogenesis promoting neuronal cell death [37,45,66]. Additionally, altered function of other cellular organelles, such as lysosomes, together with autophagy impairment, has been observed in *LRRK2* [48,63,67], *SNCA* [44] and *GBA* [68,69] mutant hiPSC-derived neurons, as well as in a hiPSC-based model of sporadic PD [67], resulting in defective clearance of aggregated proteins. Finally, several studies have shown that genetically diverse PD patient-derived neurons exhibit increased susceptibility to various forms of cellular stress, including proteotoxic [38,62,70] or nitrosative stress [36,37], linking specific cellular pathways to disease pathology that have not been previously described in other systems.

### 2.5. Compromised Neuritic Growth, Axonal Degeneration and Decreased Synaptic Connectivity

Interestingly, studies on *LRRK2-G2019S* [67,71–74], on *Parkin*-mutated [75] and on *SNCA*-mutated [38,44] hiPSC-derived neurons have revealed previously unrecognized morphological changes, including compromised neuritic outgrowth, reduced neurite complexity and axonal degeneration, resulting in impaired synaptic connectivity and network function. In particular, *LRRK2-G2019S* mutant neurons displayed shorter and less complex processes, reminiscent of immature neurons. Over time, these cells exhibited clear signs of degeneration, including very short or absent neurites, vacuolated soma, fragmented nucleus and positive staining for cleaved caspase-3. In the case of *SNCA* mutations, αSyn overexpression due to triplication of the gene led to poor formation of the neuronal network that correlated with significantly lower generation of action potentials in response to current injections [44]. In a later study performed by our team, A53T-αSyn neurons had a profound downregulation of mRNAs associated with synaptic formation, maintenance and function. The neuronal network formed was also less complex with neurite number, length and morphology being compromised when compared to control cells [38]. It will be interesting to investigate further whether the impaired synaptic connectivity and aberrant electrophysiological recordings noted in PD neurons represent early events in disease pathogenesis and how they are linked to distorted mitochondrial and/or axonal transport and ER

stress. In any case it is an important finding that should be taken into account when developing new therapeutic or disease-intervening strategies.

**Table 1.** Major phenotypes observed in PD hiPSC-derived neurons. This table summarizes key pathogenic phenotypes associated with PD mutant neurons as described in the cited publications.

| Major PD-Relevant Phenotypes | Patient-Derived iPSC-Based Models in PD | | | | | |
|---|---|---|---|---|---|---|
| | *Gene Mutations* | | | | | |
| | ***SNCA*** | ***LRKK2*** | ***PARKIN*** | ***PINK1*** | ***GBA*** | ***OPA1*** |
| αSyn accumulation and/or aggregation; increased phosphorylated αSyn (Ser 129); presence of oligomeric and fibrillar αSyn forms | G209A [5,36–39] Duplication [40] Triplication [39,41–46] | G2019S [62,67,71–73] | Ex2–4 del and Ex6–7 del [49] Ex3del, R42P, Ex3–4del, 1-BP del 255A, R275W, R42P [56] V324A [51] c.255delA [72] | Q456X [51] | L444P [68] N370S [69] | |
| Mitochondrial defects: fragmented mitochondria or mitochondria with abnormal morphology; decreased mitochondrial content; decreased ATP production; reduced membrane potential; dysfunctional mitochondrial mobility | G209A Triplication [39] | G2019S [48,57] | Ex2–4 del and Ex6–7 del [49] Ex3, 5, and 6 del [50] V324A [51] c.1072delT, p.A324fsX110 [52] Ex2–4 del and Ex6–7 del [53] | Q456X [51] G309D; Ex7/del [54] | N370S, L444P, and RecNcil [55] | p.G488R and p.A495V [58] |
| Oxidative stress: increased ROS and carbonylated proteins; upregulation of proteins involved in dopamine oxidation | Triplication [41,43,46] | G2019S [62] I2020T [63] | Ex2–4 del & Ex6–7 del [49] Ex3, 5, and 6 del [50] Ex3 del/Ex5 del and Ex3 del/Ex 3 del [64] | Q456X [60,65] | | |
| ER dysregulation; increased ER stress; autophagy impairment | G209A [37,66] Triplication [44,45] | G2019S [48,67] I2020T [63] | | | RecNcil, L444P and N370S [68] N370S [69] | |
| Compromised neurite growth & complexity; neurite swellings; axonal degeneration; decreased synaptic connectivity; impaired axonal transport | G209A [38] Triplication [44] | G2019S [67,71–73] | Ex3 del/Ex5 del and Ex3 del/Ex 3 del [75] | | | |

## 3. Rescue of Disease-Related Phenotypes in hiPSC-Derived Models of PD: Setting the Foundations towards Drug Discovery

Contrary to the initial skepticism regarding the potential of hiPSC-based systems to recapitulate age-related diseases such as PD, the identification of a wealth of cellular and molecular phenotypes, either previously known or novel, has prompted the use of such systems for early drug discovery. A number of candidate drugs have been tested for their ability to restore disease-related phenotypes in hiPSC-derived models of PD with promising results (Table 2). These studies have laid the groundwork for future application of hiPSC models in larger drug screening campaigns, assisting in the development of robust assays.

Analyses of hiPSC-derived neurons from patients with different PD-linked mutations have shown that αSyn accumulation presents a common theme regardless of the gene mutated, suggesting that it could serve as a read-out when testing novel therapeutics. Accordingly, in hiPSC-derived dopaminergic neurons from sporadic PD patients, as well as from patients carrying mutations in *GBA*, *LRRK2*, *DJ-1*, *Parkin* and *SNCA* (A53T, triplication) with decreased lysosomal β-glucocerebrosidase (GCase) activity, treatment with small-molecule enhancers of GCase has resulted in reduced αSyn levels and associated toxicity. These observations suggest that non-inhibitory small-molecule chaperones of GCase may prove promising for treatment of PD and related synucleinopathies [76–78]. Additionally, recent data in *GBA*-linked PD patient-derived dopaminergic neurons have implicated increased acid

ceramidase activity in the context of decreased GCase. This led to intracellular accumulation of αSyn, the levels of which were reduced upon inhibition of acid ceramidase by carmofur [79]. In the same lines, Burbulla et al. have applied treatment with mitochondrial antioxidants to smooth out a pathological cascade instigated by mitochondrial oxidant stress causing lysosomal dysfunction and αSyn accumulation in dopaminergic neurons derived from patients with sporadic and familial PD [80].

Alterations in neuronal morphology, neurite outgrowth and complexity as well as axonal degeneration have been used as parameters to evaluate the potential efficacy of compounds in rescuing pathological phenotypes. One study has demonstrated that *LRRK2-G2019S* hiPSC-derived neurons display neurite shortening and fewer neurites compared to wild-type controls [71], a PD-associated phenotype previously linked to ERK signaling [81]. Interestingly, treatment with an inhibitor of ERK phosphorylation or a selective inhibitor of LRRK2 kinase activity increased neurite growth and rescued mutant cultures from degeneration [71]. Similarly, Korecka et al. demonstrated that exposure to a LRRK2 kinase inhibitor or application of a *LRRK2*-specific antisense oligonucleotide (ASO) rescued neurite collapse, also in a model of *LRRK2-G2019S* hiPSC-derived neurons [74].

In the patient-derived *SNCA-G209A* (A53T) hiPSC-based model that we developed, PD neurons exhibited distinct morphological features characterized by extensive neuritic pathology and degeneration [38]. By immunostaining for βIII-tubulin, we observed contorted or fragmented axons with swollen varicosities and spheroid inclusions containing Tau and αSyn. Under morphological examination using a lentiviral vector for expression of the red fluorescent protein DsRed under the control of human synapsin 1 promoter (LV. SYN1.DsRed) to facilitate imaging of single neurons, we also observed a significant reduction in both total neurite length and the number of neurites extending from the soma. Three de novo in silico-designed compounds [82,83] that all interact with and reduce αSyn toxicity by interfering with αSyn oligomer formation could restore neurite length and rescue axonal pathology [38]. Interestingly, a small variation of one of these small molecules, NPT200-11, that was developed by the company Neuropore Therapies in collaboration with UCB Biopharma, is the only αSyn-inhibiting compound that has reached clinical trials successfully completing phase I (https://clinicaltrials.gov/ct2/results?cond=&term=NPT200-11&cntry=&state=&city=&dist=, Study Completion Date: February 2016).

Several studies with hiPSC-derived neurons have revealed dysregulation in the expression of genes involved in numerous cellular processes, rendering cells vulnerable to stressors that activate or modulate these pathways. Oxidative stress, mitochondrial impairment and proteasome inhibition are key factors that cause increased susceptibility and cell death of patient-derived neurons (reviewed in [33,84]). The first study recapitulating PD-associated phenotypes has revealed that dopaminergic neurons derived from *LRRK2-G2019S* hiPSCs displayed increased expression of key oxidative stress-response genes. Moreover, these cells were highly sensitive to cell death caused by exposure to hydrogen peroxide, the proteosomal inhibitor MG-132 or the neurotoxin 6-hydroxydopamine (6-OHDA) [62]. In a similar manner, Reinhardt et al. have confirmed that *LRRK2-G2019S* hiPSC-derived dopaminergic neurons are susceptible to oxidative stress induced by the mitochondrial complex 1 inhibitor rotenone or the neurotoxin 6-OHDA resulting in increased apoptosis, preferentially of dopaminergic neurons [71]. The incurred cytotoxicity was rescued in the presence of the small molecule inhibitor of LRRK2 kinase, LRRK2-IN1, which increased the survival of dopaminergic neurons.

An association between PD and exposure to mitochondrial toxins, including rotenone, has also been reported in *SNCA-G209A* (A53T) mutant neurons [36]. Microarray analysis of *SNCA-G209A* hiPSC-derived dopaminergic neurons has highlighted a pathway where toxin-induced nitrosative/oxidative stress results in S-nitrosylation of the transcription factor MEF2C. High-throughput screening of a chemical library for small molecules capable of targeting the MEF2C-PGC1α pathway pinpointed isoxazole as a potential therapeutic, protecting *SNCA-G209A* neurons from apoptosis induced by mitochondrial toxins [36].

When exposing the A53T-αSyn hiPSC-based model that we generated to epoxomicin or MG132, both of which interfere with αSyn clearance via the proteasome, we observed a significant increase in cleaved caspase-3 immunoreactivity consistent with the levels of LDH release in mutant neurons. This was accompanied by a pronounced disruption of the MAP2+ neuronal network, confirming once

again their susceptibility to proteotoxic stress [38]. The observed stress-induced vulnerability could also be reversed by the three small molecules targeting αSyn [82,83], resulting in restoration of the MAP2+ network [38].

**Table 2.** Summary of hiPSC-based models of PD that have been used for drug testing. This table briefly describes the rescue of disease-related phenotypes in PD hiPSC-derived neurons by selected compounds.

| Gene | Phenotypes Described | Compound Testing | Phenotype Restored | Reference |
|---|---|---|---|---|
| *GBA* mutations | increased levels of αSyn; reduced lysosomal GCase levels, reduced lysosomal GCase activity | small-molecule noninhibitory chaperone of GCase NCGC607 | reduced αSyn levels and associated toxicity | [76] |
| *GBA* (N370S/c.84dupG), *SNCA*- triplication | presence of amyloidogenic αSyn within cell bodies and neurites; accumulation of insoluble αSyn; reduced neuronal viability; reduced lysosomal activity of GCase | small-molecule GCase modulator 758 | improved GCase activity; reduced αSyn levels | [77] |
| *GBA* (c.84dupG frameshift mutation) *LRRK2* and *Parkin* mutations | reduced amounts of GCase; decreased GCase enzymatic activity; accumulation of oxidized dopamine | small-molecule GCase modulator S-181 | increased amounts of lysosomal GCase; enhanced GCase enzymatic activity; decreased dopamine oxidation | [78] |
| *GBA* (c.84dupG frameshift mutation) | increased acid ceramidase activity in the context of decreased GCase, leading to intracellular accumulation of αSyn | carmofur, acid ceramidase inhibitor | reduced αSyn levels | [79] |
| *DJ-1* mutations | mitochondrial oxidant stress causing lysosomal dysfunction and αSyn accumulation | mitochondrial antioxidants | diminished accumulation of oxidized dopamine; improved lysosomal GCase activity and proteolysis | [80] |
| *LRRK2* (G2019S) | reduced neurite outgrowth; increased sensitivity to oxidative stress | ERK phosphorylation inhibitor PD0325901 or LRRK2 kinase inhibitor LRRK2-IN1 | increased neurite growth; reduced cytotoxicity | [71] |
| *LRRK2* (G2019S) | neurite collapse; altered ER calcium homeostasis | LRRK2 kinase inhibitor Mli-2 or *LRRK2*-ASO | rescued neurite collapse | [74] |
| *SNCA* (G209A) | αSyn aggregation; mitochondrial dysfunction; increased susceptibility to mitochondrial toxins | small molecule targeting MEF2C-PGC1α (isoxazole) | reduced apoptosis | [36] |
| *SNCA* (G209A) | αSyn aggregation; compromised neurite outgrowth and axonal neuropathology; defective synaptic connectivity | small molecules targeting αSyn (NPT100-18A, NPT100-14A or ELN484228) | improved neurite outgrowth; rescue of axonal pathology and morphological restoration of the neuronal network | [38] |
| *OPA1* mutation | mitochondrial dysfunction; impaired oxidative phosphorylation and high oxidative stress levels leading to neuronal cell loss | necrostatin-1, specific necroptosis inhibitor | increased survival | [58] |

Finally, a recent study has revealed that increased oxidative stress and inflammation are associated with induction of the necroptotic pathway in hiPSC-derived neural cells from patients with a mutation in the *OPA1* gene encoding a key player in mitochondrial fusion and structure [58] that has been associated with an inherited form of PD and dementia [85]. Mutant cultures exhibited severe mitochondrial dysfunctions, impaired oxidative phosphorylation, and high oxidative stress levels, leading to neuronal

cell loss. Pharmacological treatment of necroptosis with the specific inhibitor necrostatin-1 protected neurons from cell death [58].

The above paradigms provide evidence that, despite the initial concerns in using human iPSC-based models for modeling age-related neurodegenerative pathologies, such systems show multiple disease-associated phenotypes with high relevance to PD pathogenesis and progression and can be of great value in drug discovery.

## 4. Phenotypic Screens using hiPSC-Derived Models of PD: Empowering Drug Discovery

### 4.1. Target-Based Versus Phenotype-Based Drug Screening

The two main high-throughput screening approaches for discovering new disease-modifying therapeutics are either target-based or phenotype-based. Historically, phenotypic-based screening strategies shaped the foundations of pharmaceutical drug discovery long before molecular target-based approaches were applied [86]. However, in the past 25 years, molecular target-based drug screening has become the main route to drug discovery in both the academia and the pharmaceutical industry. This change was mainly due to an accelerated progress in molecular biology and genomics that resulted in efficient mining of genes associated with various diseases [87]. The starting point in this approach is a well-defined molecular target with a predicted role in disease allowing the hypothesis that modulation of its activity would have beneficial effects. Screening of chemical libraries of small molecules is then used to identify lead compounds that interact with high affinity and specificity with the target [88]. Hits from such screens are then used for pharmacological target validation and lead compound optimization. The main advantage of the target-based approach is that the mechanism of action is known right from the start, which can accelerate preclinical assessment. Other advantages include the ability to facilitate optimization of the lead compound as there is a clear structure–activity relationship enabling improvement of its physicochemical properties, and the potential to predict target-associated safety liabilities and toxicity. However, knowledge of the molecular targets has not translated into identification of disease-modifying agents for PD or other neurodegenerative diseases [89]. One reason could be that the underlying mechanism is not clear for PD, as for most neurodegenerative diseases, resulting in a universal lack of well-defined targets. Besides, neurodegenerative diseases, including PD, are highly complex disorders and manipulating a single target may not be sufficient to restore the dysfunctional cellular network.

In phenotypic screens, on the other hand, disease-driving phenotypes can be used to determine compounds that change the outcome of multiple biological pathways without prior knowledge of the molecular mechanisms of the disease. Such screens are unbiased and may identify compounds targeting completely unexpected proteins or pathways. Consequently, phenotypic screens hold promise for the identification of previously unrecognized disease pathways and the discovery of new therapeutic targets [90]. It is notable that, during the past 20 years, phenotypic screening has contributed to most of the first-in-class small-molecule drugs approved by the FDA. Among all the new molecular entities approved from 1999 to 2008, 28 were identified through phenotypic screens, whereas target-based approaches contributed to the discovery of 17 compounds [91]. In particular, in the central nervous system field, phenotypic screening has yielded seven out of nine first-in-class drugs. Consequently, there is renewed interest in reinventing phenotypic screens as a means of drug discovery.

### 4.2. Phenotypic-Based Drug Screening in hiPSC-Derived Models of PD

Although the first PD patient-derived hiPSCs were generated in 2009 [30], surprisingly only two phenotypic screens have been reported so far in hiPSC-derived PD neurons. To identify disease-modifying agents, Yamaguchi et al. established an imaging-based, semi-automatic, high-throughput assay for quantitative detection of mitochondrial clearance and cell viability in dopaminergic neurons from patients with familial PD having *Parkin* or *PINK1* mutations. After screening 320 pharmacologically active inhibitor compounds, the researchers identified four hits, MRS1220, tranylcypromine, flunarizine

and bromocriptine, that improved the pathological clearance of mitochondria possibly by promoting mitochondrial degradation through the lysosomal system, without further investigating the underlying mechanism [92]. In another study, Tabata et al. [93] performed a phenotypic screen in *Parkin* (*PARK2*) patient-derived dopaminergic neurons displaying increased susceptibility to rotenone-induced mitochondrial stress, to identify neuroprotective compounds. From phenotypic screening of an FDA-approved drug library, one voltage-gated calcium channel antagonist, benidipine, was found to suppress rotenone-induced apoptosis [93]. The selective vulnerability of dopaminergic neurons was further attributed in this study to the dysregulation of intracellular calcium homeostasis via T-type calcium channels, revealing a previously unidentified pathway in PD and offering a potential treatment opportunity. More recently, using A53T-αSyn patient-derived neurons, we performed a small-scale phenotypic screen to identify neuroprotective compounds and identified the multikinase inhibitor BX795 as a candidate therapeutic that rescued the pathological features of PD neurons [94].

## 5. Looking into the Future: Optimization of hiPSC-Based Models for Understanding and Treating PD

The development of phenotypic screens in PD hiPSC-based neuronal cultures is still underway with the field awaiting the identification of novel disease targets for therapeutic interventions. In the meantime, new scientific discoveries and technical advances underscore the limitations of using two-dimensional (2D) neuronal platforms lacking a more physiological environment, such as extracellular matrix and the presence of glial cells. Emerging developments highlight the enhanced potential of using neuronal and glial co-cultures as well as three-dimensional (3D) systems of various kinds, including brain organoids that simulate more closely the human pathophysiology. Current progress in these approaches complemented by advances in microfluidics, state-of-the-art imaging methodologies and electrophysiological analyses to evaluate the functionality of neuronal networks, is discussed below (Figure 1).

### *5.1. Glial Cell Involvement in PD Pathogenesis: Mimicking the CNS Microenvironment in hiPSC-Based Co-Culture Systems*

As for most neurodegenerative diseases, the majority of PD studies have been performed in neuronal cultures, preferably consisting of midbrain dopaminergic neurons in various degrees of purity, and assessing neuronal degeneration signs after exposure, or not, to different types of stress. However, neuronal death may also be induced by a microenvironment that does not sufficiently support neuronal survival and/or function, while newer concepts suggest that other neural cell types, such as astrocytes [95] and microglia [96], may contribute to PD pathogenesis and progression.

Studies in post-mortem human brains and in animal models of PD, including Parkinsonian macaques [97–101], have demonstrated astroglial activation, suggesting that astrogliosis in combination with the secretion of pro-inflammatory cytokines may contribute to PD progression [102–104]. Moreover, abnormal αSyn accumulation has been observed in post-mortem astrocytes indicative of pathological alterations [101]. One explanation that has been provided is that neurons transfer pathological αSyn to astrocytes, which in turn could have an active role in its clearance [105]. It is therefore possible that astrocytes could have either a detrimental or a beneficial role, or both depending on the disease stage. It is plausible to assume that, at early stages of PD, astrocytes act to protect neurons from an overload of pathological protein cargo, while, at later stages, they become dysfunctional and contribute to the deterioration of neuronal health.

As evidenced by positron emission tomography (PET), microgliosis is an early and sustained response in PD [106,107], while reactive microglia have also been detected in toxin-induced or transgenic mouse models of PD [108–111]. Interestingly, various studies support that microglia-mediated inflammation can have both beneficial and detrimental effects [112–117]. For example, the interaction of pathogenic αSyn with different microglial receptors promotes microglial clearance of αSyn and phagocytosis of apoptotic neurons, which may be beneficial in controlling pathology [118–121]. On the other hand, it has

been shown that neurotoxic microglia can induce the generation of A1-type astrocytes exhibiting a neurotoxic phenotype, thus revealing a deleterious effect of microglial activation [122]. Interestingly, blocking the microglial-induced A1 astrocyte conversion has been found to be neuroprotective in models of PD offering new therapeutic prospects [123].

Oligodendrocytes appear to be the least affected cell type in PD, although they too present αSyn depositions [101] and show intrinsic formation of pathological αSyn assemblies [124]. Intriguingly, a reduction in the myelination of neuron projections seen in the earliest stages of the disease provides a possible association between oligodendrocyte function and PD pathogenesis [125].

Human cell-derived in vitro models can provide more specific information on the positive and/or negative involvement of glial cells in PD pathogenesis and progression. So far, only a few studies have been reported that explore hiPSC-derived systems for investigating the astrocytic involvement in PD. Human midbrain astrocytes generated from PD patients carrying the *LRRK2-G2019S* mutation showed transcriptomic dysregulation associated with compromised ability to degrade αSyn [126]. A more distinctive involvement of hiPSC-derived astrocytes transpired when they were co-cultured with dopaminergic neurons. In particular, when co-cultured with *LRRK2-G2019S* astrocytes, control hiPSC-derived dopaminergic neurons acquired morphological signs of neurodegeneration and abnormal, astrocyte-derived αSyn accumulation. Conversely, control astrocytes partially prevented the appearance of disease-related phenotypes in PD neurons [127]. In a recent study, astrocytes derived from patients with *GBA*-associated Parkinsonism displayed a cytokine and chemokine profile indicative of an inflammatory response [128]. Moreover, when these cells were co-cultured with dopaminergic neurons generated from the same hiPSC lines, excessive αSyn released from neurons was endocytosed by the *GBA*-derived astrocytes, translocating into lysosomes. It therefore seems that in *GBA*-associated Parkinsonism, astrocytes play a role in αSyn accumulation and processing, contributing to neuroinflammation. Similarly, Sonninen et al. have just published that *LRRK2-G2019S* hiPSC-derived astrocytes exhibit pathological hallmarks of the disease, including increased αSyn expression, which results in altered metabolism, disturbed Ca2+ homeostasis and increased release of cytokines upon inflammatory stimulation [129]. These findings are in line with the manifestation of αSyn inclusions in activated astrocytes in the post-mortem human PD brain as well as in animal models and suggest that pathogenic astrocytes may contribute to non-cell autonomous build-up of toxic αSyn species and the initiation of neuronal deterioration.

Recent developments in more efficient methodologies have allowed for the generation of hiPSC-derived macrophages that can be induced towards a microglial phenotype by co-culture with neurons [130]. These derived microglial cells acquired a highly dynamic ramified morphology and exhibited neuronal surveillance activity mimicking the in vivo situation. Building on this advancement, a subsequent study demonstrated that *LRRK2* expression in macrophages and microglia plays an important role in phagosome maturation and in the regulation of recycling pathways, implying that *LRRK2* mutations in PD patients may disrupt microglial clearance mechanisms [131]. Additionally, it has been shown that the *LRRK2-G2019S* mutation influences fate decision in hiPSC-derived human monocytes, further endorsing the involvement of the immune system in the development of PD [132].

Overall, the limited research performed so far on more complex human experimental set-ups has emphasized that considering bilateral or non-cell autonomous interactions between neurons, astrocytes and microglia is critical for elucidating the pathogenic processes occurring in PD and uncovering the molecular mechanisms triggering disease appearance and progression. Furthermore, the few studies performed indicated the need for using more complex systems as physiologically relevant disease models for drug discovery.

### *5.2. Emergence of Three-Dimensional (3D) hiPSC- Based Platforms for PD*

The appearance of 3D systems of increasing complexity mimicking the brain microenvironment meets the requirement for more efficient modeling of disease phenotypes not only towards elucidating context-dependent human pathologies, but also for the development of novel platforms for high-throughput

drug screening. Yet, there are still serious hurdles to overcome, including the reduced long-term viability of such systems due to lack of sufficient oxygenation within the 3D core and the large variability observed [133]. In a first attempt within the PD field, the culture of patient neurons derived from hiPSCs carrying the *LRRK2-G2019S* mutation was optimized in 3D microfluidics [134]. Automated high-content imaging revealed decreased dopaminergic differentiation and branching complexity, altered mitochondrial morphology, and increased cell death in the absence of external stressors. In two subsequent efforts, midbrain-like organoids were produced from sporadic or familial PD patients carrying the *LRRK2-G2019S* mutation that, respectively, displayed αSyn accumulation and dopaminergic neuron degeneration [135,136].

Clearly, further optimization and analysis are needed for the production of advanced patient-specific platforms that can be useful in modelling and treating PD. In this respect, research is progressing fast to generate more complex 3D cultures yielding organoids or spheroids that incorporate neurons and different glial cell types [137–141] offering promising tools to simulate PD pathology with higher fidelity to the in vivo scenario. Enriched 3D systems can be more informative on the cellular and molecular basis of neuron-glia cross-talk, monitoring glial activation and inflammation, also in correlation with toxic αSyn accumulation and neuronal decline. Of relevance, an optimized protocol was devised recently for the generation of midbrain-like organoids containing mature midbrain dopaminergic and GABAergic neurons, functional astrocytes and oligodendrocytes, exhibiting electrophysiological activity and producing dopamine and neuromelanin-like granules [142]. A PD-mimicking neurotoxin-based protocol was then applied to assess cell-to-cell interactions in neurodegeneration, demonstrating glia-mediated massive cell death of dopaminergic neurons. Interestingly, Ormel et al. showed that microglia can also develop innately within cerebral organoids and display their characteristic ramified morphology [141]. This was an unexpected finding since the consensus was that cerebral organoids consist of cells derived from the neuroectodermal lineage and should therefore lack mesodermal-derived microglia. Yet, this study exemplified a model where the interplay between microglia, macroglia and neurons can be studied in human brain development and disease.

Even though 3D organoids have not been used yet for high-throughput drug screening in PD, the technology for adaptation is developing and has been used successfully in other neurodegenerative diseases, indicating the feasibility of such strategies [143]. Developments include a number of microtissue and nanoculture products to support 3D architecture in 96- or 384-well format, introduction of enriched extracellular matrix (ECM) products and inducers of endogenous ECM proteins and specialized synthetic biomaterials [144]. Nevertheless, the high cost of such products, the disruption of viscosity and temperature during automated handling, the sample processing for high-content analysis and the poor penetration of tested compounds present serious limitations for performing preclinical testing in a large scale and within a reasonable timescale. New approaches that target the issues of high-throughput scale and cost while offering amenable systems with a high level of biological complexity and clinical relevance, such as formulation and optimization of engineered microenvironments, are in great demand. Such brain-on-a-chip platforms comprising miniaturized microfluidic perfusion systems that permit long-term growth in a format that is financially viable and has the potential of scaling up for launching high-throughput discovery campaigns, might pave the way for future fundamental discoveries and the development of more effective drugs [145]. Microfluidic devices have already been used to study the interaction of microglia and neurons in PD and to demonstrate neuronal internalization of αSyn fibrils before their propagation along the axons [146–148]. However, today, the most relevant formats are restricted to low-throughput applications awaiting their adaptation for automated screening on a large scale.

## 6. Functional Assays for PD Studies and Drug Screening in hiPSC-Derived Systems

As the ultimate success of drug discovery depends on the functional recovery it can produce, a pipeline based solely on assessment of morphological rescue of human PD neurons will have a high chance of failing. PD is characterized by severe changes in neuronal connectivity and data derived from electrophysiological analyses of patient-derived neurons highlight the importance of recording

changes in synaptogenesis, network formation and neurotransmitter balance when new drugs are tested or during unbiased phenotypic screens. Two functional assays may be used in drug screening based on their potential for adaptation and scalability: calcium imaging and the multi-electrode array system (Figure 1).

### 6.1. Calcium Imaging

Calcium homeostasis is fundamental to neuronal survival and function and, when deregulated, can lead to neurodegeneration via complex and diverse mechanisms resulting in selective neuronal impairment and death. Fluorescent calcium imaging is a well-established method, which enables the visualization of free intracellular Ca2+ in populations of cells. Calcium indicators are sensitive to calcium changes and can be loaded in a non-invasive manner to neuronal cells, although prolonged exposure to the dye is toxic. Fluorescent dyes can either be single or multiple wavelengths. Calcium imaging allows to explore calcium-mediated processes happening over different time scales. For example, calcium-mediated neurotransmitter release occurs much more rapidly than calcium-mediated gene expression in the nucleus [149]. The development of genetically encoded calcium indicators offers a better alternative to the use of fluorescent dyes, since they are non-invasive and can be targeted to specific neurons and/or astrocytes, allowing for a longer duration of imaging without the risk of phototoxicity [150]. Additionally, other issues observed with fluorescent dyes such as background fluorescence and non-specific dye loading can be overcome with genetic indicators [150].

In relation to PD, increasing evidence suggests that defective calcium signaling plays an important role in disease pathogenesis. Schwab and Ebert showed that *LRRK2-G2019S* hiPSC-derived sensory neurons display altered calcium dynamics and treatment with LRRK2 kinase inhibitors resulted in significant rescue [151]. Moreover, Tabata et al. demonstrated that there is a dysregulation of calcium homeostasis in *Parkin* and *PINK1* hiPSC-derived dopamine neurons which is prevented by T-type calcium channel knockdown or antagonists [93]. We have also demonstrated aberrant Ca+ fluxes in A53T-αSyn neurons [152] that could be linked to the decreased spontaneous synaptic activity recorded by patch-clamp electrophysiology [38]. Currently, high-content imaging or drug screening based on recording Ca+ dynamics has not yet been performed in PD hiPSC-derived systems.

### 6.2. Multi-Electrode Arrays (MEAs)

High-resolution MEA systems enable one to assess novel electrophysiological parameters of hiPSC-derived neurons, which can be potentially used as biomarkers for phenotype screening and drug testing. MEAs comprise a platform for monitoring prolonged, non-destructive recordings of spontaneously firing neurons in vitro with applications in neurodegenerative diseases. A MEA system combines a cell culture plate with an embedded array of high- or low-impedance electrodes allowing for parallel detection of local field potentials generated by spontaneous or evoked firing of neurons [153–155]. The generation of synchronously active neuronal networks depends on sequential developmental processes. Neuronal network formation starts with excitable and spontaneously active neurons that are asynchronously active due to lack of functional connectivity between neurons. With the formation of functional synapses, two or more neurons become functionally interconnected and capable to generate synchronous bursting. In a population of neurons, the connectivity between neurons is increasing over time and finally results in synchronous bursting activity of hundreds or thousands of interconnected cells. So, calcium imaging and MEA recordings could reveal the inability of pathological cells to make the physiological transition of asynchronously active neurons into few synchronous bursting neurons and finally into a population of neurons that are highly synchronously active. One characteristic example is described by Woodard et al., in which hiPSC-derived dopamine neurons were examined from monozygotic male twins of Ashkenazi Jewish background that were discordant for PD [156]. The investigators noticed that neurons from the unaffected twin developed robust synchronous bursting patterns indicative of maturing neuronal networks in contrast to neurons from the affected twin that did not produce synchronous bursting patterns with their spontaneous activity also being significantly lower [156]. In another study, however,

on hiPSC-derived dopaminergic neurons from patients with young-onset PD, MEA recordings did not show differences between disease and control cultures [157].

Nonetheless, the value of MEA recordings in uncovering disease-related phenotypes in an in vitro setting is highlighted in primary cultures derived from animal models of neurodegenerative diseases. Amin et al. applied MEA recordings to characterize the early activity-dependent changes induced by toxic Aβ-oligomers in neuronal networks using a simple in vitro model based on a rat hippocampal cell culture system. It is interesting to note that, in this study, a clinically applied N-methyl D-aspartate antagonist used for Alzheimer's disease treatment, could reverse Aβ-neurotoxicity and rescue network-wide firing [158]. The importance of monitoring coordinated neuronal activity and its disruption in the development of neurodegeneration has also been emphasized by Iaccarino et al. in a mouse model of Alzheimer's disease [159].

Regarding the adaptation of the methodology for use in high-throughput screening, Durens et al. have described a method for multiplexing MEA recordings and Ca2+ imaging to examine local microcircuits in 3D brain organoids and assess inter-experimental consistency, necessary for drug screening [160]. Examination of such circuit-based mechanisms in hiPSC-derived systems would be of great interest and importance for the development of new and more efficient drugs. However, while it seems a very attractive readout for the development of high-throughput drug screening platforms, one should be careful with the interpretation of MEA and calcium imaging results as chemically induced effects on neuronal network activity, such as spontaneous firing and bursting behavior, depend on the ratio of inhibitory to excitatory neurons that are present in the culture system and may vary either due to the differentiation and enrichment protocols applied or to intrinsic defects of the lines used. Therefore, hiPSC-derived neuronal models must be carefully characterized prior to large-scale functional applications in drug screening.

## 7. Artificial Intelligence Technologies

Concurrent with advances in imaging technologies and the morphological, biochemical or functional analyses of neuronal populations has been the increase in volume and complexity of data sets generated. To exploit the ever-growing amount of data that become available, computational techniques are constantly evolving. As a result, artificial intelligence technologies such as deep learning and machine learning methods have emerged to identify meaningful patterns and cellular features that may be interpreted into novel biological insights. Still, these approaches have yet to be developed and adapted for high-throughput analyses in the medical and biological sciences. The creation of automated platforms that can perform phenotypic screens, process raw data and analyze them using deep neural network algorithms will increase both the capacity of the screens as well as the quality and size of the data collected. Several groups are trying to develop new methods that would have the potential to be used in large-scale phenotypic screens of hiPSC-based models. For example, Schwartz et al. developed a 3D model of hiPSC-derived neural tissue constructs comprising diverse neuronal and glial populations, interconnected vascular networks, and ramified microglia by seeding neural precursor cells on synthetic hydrogels [161]. Machine learning was used to build a predictive model from the changes occurring in global gene expression resulting from exposure to toxic and nontoxic training chemicals. This combined strategy reveals the value of human cell-based assays for predictive toxicology. Similarly, Monzel et al. developed a pipeline for a machine learning method, allowing for detailed image-based cell profiling and toxicity prediction in brain organoids treated with the neurotoxic compound 6-hydroxydopamine (6-OHDA) [162].

The analysis of large biological data sets derived from high-throughput screens assessing simultaneously multiple morphological and functional parameters in hiPSC-based platforms is time-consuming and will certainly benefit from artificial intelligence methodologies. Machine learning has the potential to shrink drug discovery timelines, helping researchers accelerate drug discovery and ultimately patients obtain disease-modifying therapies. Because these methodologies are expected to make the quest for new pharmaceuticals not only quicker, but also cheaper and more effective, leading biopharmaceutical

companies to begin to embrace artificial intelligence platforms in their pursuit for new therapies. However, in the short term, these technologies have a number of challenges to overcome, especially when combined with automation.

## 8. Concluding Remarks

Many hiPSC lines have been generated from patients with familial or sporadic PD uncovering known or previously unrecognized disease-relevant phenotypes that, in many cases, could be effectively restored using small molecules. These investigations have laid the foreground for developing bioassays for screening small or larger chemical libraries in the search of lead compounds that may evolve into PD disease-modifying therapeutics. However, robust assays still need to be established before hiPSC-based systems become amenable to high-throughput technologies. In the meantime, more advanced co-culture systems encompassing neurons and glial cells or 3D brain organoids mimicking more closely the in vivo human situation are being developed to assist in PD studies and drug discovery. The necessity for functional assays to predict drug efficacy is also being recognized while technological advancements render complicated screens more feasible. Last but not least, the emergence of artificial intelligence over the past few years may prove to be a game-changing technology in drug discovery. Nevertheless, opportunities and challenges still remain ahead before these young technologies come to fruition and fulfill their promise for understanding and treating neurodegeneration in PD.

**Author Contributions:** All authors wrote and corrected the paper. All authors have read and agreed to the published version of the manuscript.

**Funding:** This work was supported by the Hellenic Foundation for Research and Innovation 899-PARKINSynapse grant to G.K.; a Stavros Niarchos Foundation grant to the Hellenic Pasteur Institute as part of the Foundation's initiative to support the Greek Research Center ecosystem; the Greek General Secretariat for Research and Technology grant BIOIMAGING-GR MIS 5002755 implemented under the Action "Reinforcement of Research and Innovation Infrastructure", funded by the Operational Programme "Competitiveness, Entrepreneurship and Innovation" (NSRF 2014–2020) and co-financed by Greece and the European Union (European Regional Development Fund).

**Conflicts of Interest:** The authors declare no conflict of interest. The funders had no role in the design of the study; in the collection, analyses, or interpretation of data; in the writing of the manuscript, or in the decision to publish the results.

## Abbreviations

| | |
|---|---|
| PD | Parkinson's disease |
| *SNCA (PARK1/4)* | α-synuclein gene |
| *LRRK2 (PARK8)* | leucine-rich repeat kinase 2 gene |
| *PINK1 (PARK6)* | PTEN-induced putative kinase 1 |
| *DJ-1 (PARK7)* | protein deglycase |
| *ATP13A2 (PARK9)* | endo-/lysosomal-associated P5 type transport ATPase |
| *GBA* | β-glucocerebrosidase gene |
| αSyn | α-synuclein protein |
| hiPSC | human induced pluripotent stem cell |
| GMP | good manufacturing practices |
| ROS | reactive oxygen species |
| ER | endoplasmic reticulum |
| GCase | β-glucocerebrosidase |
| ASO | antisense oligonucleotide |
| 6-OHDA | 6-hydroxydopamine |
| LDH | lactate dehydrogenase |
| OPA1 | mitochondrial dynamin-like GTPase |
| PET | positron emission tomography |
| ECM | extracellular matrix |
| MEA | multi-electrode array |

## References


1. Lees, A.J.; Hardy, J.; Revesz, T. Parkinson's disease. *Lancet* **2009**, *373*, 2055–2066. [CrossRef]
2. Kalia, L.V.; Lang, A.E. Parkinson's disease. *Lancet* **2015**, *386*, 896–912. [CrossRef]
3. Pfeiffer, R.F. Non-motor symptoms in Parkinson's disease. *Parkinsonism Relat. Disord.* **2016**, *22* (Suppl. 1), S119–S122. [CrossRef] [PubMed]
4. Klein, C.; Westenberger, A. Genetics of Parkinson's disease. *Cold Spring Harb. Perspect. Med.* **2012**, *2*, a008888. [CrossRef] [PubMed]
5. Dettmer, U.; Newman, A.J.; Soldner, F.; Luth, E.S.; Kim, N.C.; von Saucken, V.E.; Sanderson, J.B.; Jaenisch, R.; Bartels, T.; Selkoe, D. Parkinson-causing alpha-synuclein missense mutations shift native tetramers to monomers as a mechanism for disease initiation. *Nat. Commun.* **2015**, *6*, 7314. [CrossRef]
6. Zimprich, A.; Biskup, S.; Leitner, P.; Lichtner, P.; Farrer, M.; Lincoln, S.; Kachergus, J.; Hulihan, M.; Uitti, R.J.; Calne, D.B.; et al. Mutations in LRRK2 cause autosomal-dominant parkinsonism with pleomorphic pathology. *Neuron* **2004**, *44*, 601–607. [CrossRef]
7. Valente, E.M.; Abou-Sleiman, P.M.; Caputo, V.; Muqit, M.M.; Harvey, K.; Gispert, S.; Ali, Z.; Del Turco, D.; Bentivoglio, A.R.; Healy, D.G.; et al. Hereditary early-onset Parkinson's disease caused by mutations in PINK1. *Science* **2004**, *304*, 1158–1160. [CrossRef]
8. Kitada, T.; Asakawa, S.; Hattori, N.; Matsumine, H.; Yamamura, Y.; Minoshima, S.; Yokochi, M.; Mizuno, Y.; Shimizu, N. Mutations in the parkin gene cause autosomal recessive juvenile parkinsonism. *Nature* **1998**, *392*, 605–608. [CrossRef]
9. Bonifati, V.; Rizzu, P.; van Baren, M.J.; Schaap, O.; Breedveld, G.J.; Krieger, E.; Dekker, M.C.; Squitieri, F.; Ibanez, P.; Joosse, M.; et al. Mutations in the DJ-1 gene associated with autosomal recessive early-onset parkinsonism. *Science* **2003**, *299*, 256–259. [CrossRef]
10. Ramirez, A.; Heimbach, A.; Grundemann, J.; Stiller, B.; Hampshire, D.; Cid, L.P.; Goebel, I.; Mubaidin, A.F.; Wriekat, A.L.; Roeper, J.; et al. Hereditary parkinsonism with dementia is caused by mutations in ATP13A2, encoding a lysosomal type 5 P-type ATPase. *Nat. Genet.* **2006**, *38*, 1184–1191. [CrossRef]
11. Goker-Alpan, O.; Schiffmann, R.; LaMarca, M.E.; Nussbaum, R.L.; McInerney-Leo, A.; Sidransky, E. Parkinsonism among Gaucher disease carriers. *J. Med. Genet.* **2004**, *41*, 937–940. [CrossRef] [PubMed]
12. Kim, H.J.; Jeon, B.S.; Jenner, P. Hallmarks of Treatment Aspects: Parkinson's Disease Throughout Centuries Including l-Dopa. *Int. Rev. Neurobiol.* **2017**, *132*, 295–343. [CrossRef] [PubMed]
13. Kulisevsky, J.; Oliveira, L.; Fox, S.H. Update in therapeutic strategies for Parkinson's disease. *Curr. Opin. Neurol.* **2018**, *31*, 439–447. [CrossRef] [PubMed]
14. Dijk, J.M.; Espay, A.J.; Katzenschlager, R.; de Bie, R.M.A. The Choice Between Advanced Therapies for Parkinson's Disease Patients: Why, What, and When? *J. Parkinsons Dis.* **2020**. [CrossRef] [PubMed]
15. Fields, C.R.; Bengoa-Vergniory, N.; Wade-Martins, R. Targeting Alpha-Synuclein as a Therapy for Parkinson's Disease. *Front. Mol. Neurosci.* **2019**, *12*, 299. [CrossRef] [PubMed]
16. Polymeropoulos, M.H.; Lavedan, C.; Leroy, E.; Ide, S.E.; Dehejia, A.; Dutra, A.; Pike, B.; Root, H.; Rubenstein, J.; Boyer, R.; et al. Mutation in the alpha-synuclein gene identified in families with Parkinson's disease. *Science* **1997**, *276*, 2045–2047. [CrossRef]
17. Spillantini, M.G.; Schmidt, M.L.; Lee, V.M.; Trojanowski, J.Q.; Jakes, R.; Goedert, M. Alpha-synuclein in Lewy bodies. *Nature* **1997**, *388*, 839–840. [CrossRef]
18. Goedert, M.; Jakes, R.; Spillantini, M.G. The Synucleinopathies: Twenty Years On. *J. Parkinsons Dis.* **2017**, *7*, S51–S69. [CrossRef]
19. Simon-Sanchez, J.; Schulte, C.; Bras, J.M.; Sharma, M.; Gibbs, J.R.; Berg, D.; Paisan-Ruiz, C.; Lichtner, P.; Scholz, S.W.; Hernandez, D.G.; et al. Genome-wide association study reveals genetic risk underlying Parkinson's disease. *Nat. Genet.* **2009**, *41*, 1308–1312. [CrossRef]
20. Petrucci, S.; Ginevrino, M.; Valente, E.M. Phenotypic spectrum of alpha-synuclein mutations: New insights from patients and cellular models. *Parkinsonism Relat. Disord.* **2016**, *22* (Suppl. 1), S16–S20. [CrossRef]
21. Lashuel, H.A.; Overk, C.R.; Oueslati, A.; Masliah, E. The many faces of alpha-synuclein: From structure and toxicity to therapeutic target. *Nat. Rev. Neurosci.* **2013**, *14*, 38–48. [CrossRef] [PubMed]
22. Savitt, D.; Jankovic, J. Targeting alpha-Synuclein in Parkinson's Disease: Progress Towards the Development of Disease-Modifying Therapeutics. *Drugs* **2019**, *79*, 797–810. [CrossRef] [PubMed]

23. Nguyen, M.; Wong, Y.C.; Ysselstein, D.; Severino, A.; Krainc, D. Synaptic, Mitochondrial, and Lysosomal Dysfunction in Parkinson's Disease. *Trends Neurosci* **2019**, *42*, 140–149. [CrossRef] [PubMed]
24. Shahmoradian, S.H.; Lewis, A.J.; Genoud, C.; Hench, J.; Moors, T.E.; Navarro, P.P.; Castano-Diez, D.; Schweighauser, G.; Graff-Meyer, A.; Goldie, K.N.; et al. Lewy pathology in Parkinson's disease consists of crowded organelles and lipid membranes. *Nat. Neurosci.* **2019**, *22*, 1099–1109. [CrossRef] [PubMed]
25. Caligiore, D.; Helmich, R.C.; Hallett, M.; Moustafa, A.A.; Timmermann, L.; Toni, I.; Baldassarre, G. Parkinson's disease as a system-level disorder. *NPJ Parkinsons Dis.* **2016**, *2*, 16025. [CrossRef] [PubMed]
26. Takahashi, K.; Tanabe, K.; Ohnuki, M.; Narita, M.; Ichisaka, T.; Tomoda, K.; Yamanaka, S. Induction of pluripotent stem cells from adult human fibroblasts by defined factors. *Cell* **2007**, *131*, 861–872. [CrossRef]
27. Parmar, M.; Grealish, S.; Henchcliffe, C. The future of stem cell therapies for Parkinson disease. *Nat. Rev. Neurosci.* **2020**, *21*, 103–115. [CrossRef]
28. Kim, T.W.; Koo, S.Y.; Studer, L. Pluripotent Stem Cell Therapies for Parkinson Disease: Present Challenges and Future Opportunities. *Front. Cell Dev. Biol.* **2020**, *8*, 729. [CrossRef]
29. Park, I.H.; Arora, N.; Huo, H.; Maherali, N.; Ahfeldt, T.; Shimamura, A.; Lensch, M.W.; Cowan, C.; Hochedlinger, K.; Daley, G.Q. Disease-specific induced pluripotent stem cells. *Cell* **2008**, *134*, 877–886. [CrossRef]
30. Soldner, F.; Hockemeyer, D.; Beard, C.; Gao, Q.; Bell, G.W.; Cook, E.G.; Hargus, G.; Blak, A.; Cooper, O.; Mitalipova, M.; et al. Parkinson's disease patient-derived induced pluripotent stem cells free of viral reprogramming factors. *Cell* **2009**, *136*, 964–977. [CrossRef]
31. Marotta, N.; Kim, S.; Krainc, D. Organoid and pluripotent stem cells in Parkinson's disease modeling: An expert view on their value to drug discovery. *Expert Opin. Drug Discov.* **2020**, *15*, 427–441. [CrossRef] [PubMed]
32. Weykopf, B.; Haupt, S.; Jungverdorben, J.; Flitsch, L.J.; Hebisch, M.; Liu, G.H.; Suzuki, K.; Belmonte, J.C.I.; Peitz, M.; Blaess, S.; et al. Induced pluripotent stem cell-based modeling of mutant LRRK2-associated Parkinson's disease. *Eur. J. Neurosci.* **2019**, *49*, 561–589. [CrossRef] [PubMed]
33. Sison, S.L.; Vermilyea, S.C.; Emborg, M.E.; Ebert, A.D. Using Patient-Derived Induced Pluripotent Stem Cells to Identify Parkinson's Disease-Relevant Phenotypes. *Curr. Neurol. Neurosci. Rep.* **2018**, *18*, 84. [CrossRef] [PubMed]
34. Bendor, J.T.; Logan, T.P.; Edwards, R.H. The function of alpha-synuclein. *Neuron* **2013**, *79*, 1044–1066. [CrossRef] [PubMed]
35. Wong, Y.C.; Krainc, D. alpha-synuclein toxicity in neurodegeneration: Mechanism and therapeutic strategies. *Nat. Med.* **2017**, *23*, 1–13. [CrossRef] [PubMed]
36. Ryan, S.D.; Dolatabadi, N.; Chan, S.F.; Zhang, X.; Akhtar, M.W.; Parker, J.; Soldner, F.; Sunico, C.R.; Nagar, S.; Talantova, M.; et al. Isogenic human iPSC Parkinson's model shows nitrosative stress-induced dysfunction in MEF2-PGC1alpha transcription. *Cell* **2013**, *155*, 1351–1364. [CrossRef] [PubMed]
37. Chung, C.Y.; Khurana, V.; Auluck, P.K.; Tardiff, D.F.; Mazzulli, J.R.; Soldner, F.; Baru, V.; Lou, Y.; Freyzon, Y.; Cho, S.; et al. Identification and rescue of alpha-synuclein toxicity in Parkinson patient-derived neurons. *Science* **2013**, *342*, 983–987. [CrossRef]
38. Kouroupi, G.; Taoufik, E.; Vlachos, I.S.; Tsioras, K.; Antoniou, N.; Papastefanaki, F.; Chroni-Tzartou, D.; Wrasidlo, W.; Bohl, D.; Stellas, D.; et al. Defective synaptic connectivity and axonal neuropathology in a human iPSC-based model of familial Parkinson's disease. *Proc. Natl. Acad. Sci. USA* **2017**, *114*, E3679–E3688. [CrossRef]
39. Little, D.; Luft, C.; Mosaku, O.; Lorvellec, M.; Yao, Z.; Paillusson, S.; Kriston-Vizi, J.; Gandhi, S.; Abramov, A.Y.; Ketteler, R.; et al. A single cell high content assay detects mitochondrial dysfunction in iPSC-derived neurons with mutations in SNCA. *Sci. Rep.* **2018**, *8*, 9033. [CrossRef]
40. Prots, I.; Grosch, J.; Brazdis, R.M.; Simmnacher, K.; Veber, V.; Havlicek, S.; Hannappel, C.; Krach, F.; Krumbiegel, M.; Schutz, O.; et al. alpha-Synuclein oligomers induce early axonal dysfunction in human iPSC-based models of synucleinopathies. *Proc. Natl. Acad. Sci. USA* **2018**, *115*, 7813–7818. [CrossRef]
41. Byers, B.; Cord, B.; Nguyen, H.N.; Schule, B.; Fenno, L.; Lee, P.C.; Deisseroth, K.; Langston, J.W.; Pera, R.R.; Palmer, T.D. SNCA triplication Parkinson's patient's iPSC-derived DA neurons accumulate alpha-synuclein and are susceptible to oxidative stress. *PLoS ONE* **2011**, *6*, e26159. [CrossRef] [PubMed]

42. Devine, M.J.; Ryten, M.; Vodicka, P.; Thomson, A.J.; Burdon, T.; Houlden, H.; Cavaleri, F.; Nagano, M.; Drummond, N.J.; Taanman, J.W.; et al. Parkinson's disease induced pluripotent stem cells with triplication of the alpha-synuclein locus. *Nat. Commun.* **2011**, *2*, 440. [CrossRef] [PubMed]
43. Flierl, A.; Oliveira, L.M.; Falomir-Lockhart, L.J.; Mak, S.K.; Hesley, J.; Soldner, F.; Arndt-Jovin, D.J.; Jaenisch, R.; Langston, J.W.; Jovin, T.M.; et al. Higher vulnerability and stress sensitivity of neuronal precursor cells carrying an alpha-synuclein gene triplication. *PLoS ONE* **2014**, *9*, e112413. [CrossRef] [PubMed]
44. Oliveira, L.M.; Falomir-Lockhart, L.J.; Botelho, M.G.; Lin, K.H.; Wales, P.; Koch, J.C.; Gerhardt, E.; Taschenberger, H.; Outeiro, T.F.; Lingor, P.; et al. Elevated alpha-synuclein caused by SNCA gene triplication impairs neuronal differentiation and maturation in Parkinson's patient-derived induced pluripotent stem cells. *Cell Death Dis.* **2015**, *6*, e1994. [CrossRef] [PubMed]
45. Heman-Ackah, S.M.; Manzano, R.; Hoozemans, J.J.M.; Scheper, W.; Flynn, R.; Haerty, W.; Cowley, S.A.; Bassett, A.R.; Wood, M.J.A. Alpha-synuclein induces the unfolded protein response in Parkinson's disease SNCA triplication iPSC-derived neurons. *Hum. Mol. Genet.* **2017**, *26*, 4441–4450. [CrossRef]
46. Ludtmann, M.H.R.; Angelova, P.R.; Horrocks, M.H.; Choi, M.L.; Rodrigues, M.; Baev, A.Y.; Berezhnov, A.V.; Yao, Z.; Little, D.; Banushi, B.; et al. alpha-synuclein oligomers interact with ATP synthase and open the permeability transition pore in Parkinson's disease. *Nat. Commun.* **2018**, *9*, 2293. [CrossRef]
47. Chen, C.; Turnbull, D.M.; Reeve, A.K. Mitochondrial Dysfunction in Parkinson's Disease-Cause or Consequence? *Biology (Basel)* **2019**, *8*, 38. [CrossRef]
48. Su, Y.C.; Qi, X. Inhibition of excessive mitochondrial fission reduced aberrant autophagy and neuronal damage caused by LRRK2 G2019S mutation. *Hum. Mol. Genet.* **2013**, *22*, 4545–4561. [CrossRef]
49. Imaizumi, Y.; Okada, Y.; Akamatsu, W.; Koike, M.; Kuzumaki, N.; Hayakawa, H.; Nihira, T.; Kobayashi, T.; Ohyama, M.; Sato, S.; et al. Mitochondrial dysfunction associated with increased oxidative stress and alpha-synuclein accumulation in PARK2 iPSC-derived neurons and postmortem brain tissue. *Mol. Brain* **2012**, *5*, 35. [CrossRef]
50. Aboud, A.A.; Tidball, A.M.; Kumar, K.K.; Neely, M.D.; Han, B.; Ess, K.C.; Hong, C.C.; Erikson, K.M.; Hedera, P.; Bowman, A.B. PARK2 patient neuroprogenitors show increased mitochondrial sensitivity to copper. *Neurobiol. Dis.* **2015**, *73*, 204–212. [CrossRef]
51. Chung, S.Y.; Kishinevsky, S.; Mazzulli, J.R.; Graziotto, J.; Mrejeru, A.; Mosharov, E.V.; Puspita, L.; Valiulahi, P.; Sulzer, D.; Milner, T.A.; et al. Parkin and PINK1 Patient iPSC-Derived Midbrain Dopamine Neurons Exhibit Mitochondrial Dysfunction and alpha-Synuclein Accumulation. *Stem Cell Rep.* **2016**, *7*, 664–677. [CrossRef] [PubMed]
52. Zanon, A.; Kalvakuri, S.; Rakovic, A.; Foco, L.; Guida, M.; Schwienbacher, C.; Serafin, A.; Rudolph, F.; Trilck, M.; Grunewald, A.; et al. SLP-2 interacts with Parkin in mitochondria and prevents mitochondrial dysfunction in Parkin-deficient human iPSC-derived neurons and Drosophila. *Hum. Mol. Genet.* **2017**, *26*, 2412–2425. [CrossRef] [PubMed]
53. Cartelli, D.; Amadeo, A.; Calogero, A.M.; Casagrande, F.V.M.; De Gregorio, C.; Gioria, M.; Kuzumaki, N.; Costa, I.; Sassone, J.; Ciammola, A.; et al. Parkin absence accelerates microtubule aging in dopaminergic neurons. *Neurobiol. Aging* **2018**, *61*, 66–74. [CrossRef] [PubMed]
54. Azkona, G.; Lopez de Maturana, R.; Del Rio, P.; Sousa, A.; Vazquez, N.; Zubiarrain, A.; Jimenez-Blasco, D.; Bolanos, J.P.; Morales, B.; Auburger, G.; et al. LRRK2 Expression Is Deregulated in Fibroblasts and Neurons from Parkinson Patients with Mutations in PINK1. *Mol. Neurobiol.* **2018**, *55*, 506–516. [CrossRef]
55. Schondorf, D.C.; Ivanyuk, D.; Baden, P.; Sanchez-Martinez, A.; De Cicco, S.; Yu, C.; Giunta, I.; Schwarz, L.K.; Di Napoli, G.; Panagiotakopoulou, V.; et al. The NAD+ Precursor Nicotinamide Riboside Rescues Mitochondrial Defects and Neuronal Loss in iPSC and Fly Models of Parkinson's Disease. *Cell Rep.* **2018**, *23*, 2976–2988. [CrossRef]
56. Shaltouki, A.; Sivapatham, R.; Pei, Y.; Gerencser, A.A.; Momcilovic, O.; Rao, M.S.; Zeng, X. Mitochondrial alterations by PARKIN in dopaminergic neurons using PARK2 patient-specific and PARK2 knockout isogenic iPSC lines. *Stem Cell Rep.* **2015**, *4*, 847–859. [CrossRef]
57. Schwab, A.J.; Sison, S.L.; Meade, M.R.; Broniowska, K.A.; Corbett, J.A.; Ebert, A.D. Decreased Sirtuin Deacetylase Activity in LRRK2 G2019S iPSC-Derived Dopaminergic Neurons. *Stem Cell Rep.* **2017**, *9*, 1839–1852. [CrossRef]

58. Iannielli, A.; Bido, S.; Folladori, L.; Segnali, A.; Cancellieri, C.; Maresca, A.; Massimino, L.; Rubio, A.; Morabito, G.; Caporali, L.; et al. Pharmacological Inhibition of Necroptosis Protects from Dopaminergic Neuronal Cell Death in Parkinson's Disease Models. *Cell Rep.* **2018**, *22*, 2066–2079. [CrossRef]
59. Ryan, T.; Bamm, V.V.; Stykel, M.G.; Coackley, C.L.; Humphries, K.M.; Jamieson-Williams, R.; Ambasudhan, R.; Mosser, D.D.; Lipton, S.A.; Harauz, G.; et al. Cardiolipin exposure on the outer mitochondrial membrane modulates alpha-synuclein. *Nat. Commun.* **2018**, *9*, 817. [CrossRef]
60. Cooper, O.; Seo, H.; Andrabi, S.; Guardia-Laguarta, C.; Graziotto, J.; Sundberg, M.; McLean, J.R.; Carrillo-Reid, L.; Xie, Z.; Osborn, T.; et al. Pharmacological rescue of mitochondrial deficits in iPSC-derived neural cells from patients with familial Parkinson's disease. *Sci. Transl. Med.* **2012**, *4*, 141ra190. [CrossRef]
61. Toulorge, D.; Schapira, A.H.; Hajj, R. Molecular changes in the postmortem parkinsonian brain. *J. Neurochem.* **2016**, *139* (Suppl. 1), 27–58. [CrossRef] [PubMed]
62. Nguyen, H.N.; Byers, B.; Cord, B.; Shcheglovitov, A.; Byrne, J.; Gujar, P.; Kee, K.; Schule, B.; Dolmetsch, R.E.; Langston, W.; et al. LRRK2 mutant iPSC-derived DA neurons demonstrate increased susceptibility to oxidative stress. *Cell Stem Cell* **2011**, *8*, 267–280. [CrossRef] [PubMed]
63. Ohta, E.; Nihira, T.; Uchino, A.; Imaizumi, Y.; Okada, Y.; Akamatsu, W.; Takahashi, K.; Hayakawa, H.; Nagai, M.; Ohyama, M.; et al. I2020T mutant LRRK2 iPSC-derived neurons in the Sagamihara family exhibit increased Tau phosphorylation through the AKT/GSK-3beta signaling pathway. *Hum. Mol. Genet.* **2015**, *24*, 4879–4900. [CrossRef]
64. Jiang, H.; Ren, Y.; Yuen, E.Y.; Zhong, P.; Ghaedi, M.; Hu, Z.; Azabdaftari, G.; Nakaso, K.; Yan, Z.; Feng, J. Parkin controls dopamine utilization in human midbrain dopaminergic neurons derived from induced pluripotent stem cells. *Nat. Commun.* **2012**, *3*, 668. [CrossRef]
65. Vera, E.; Bosco, N.; Studer, L. Generating Late-Onset Human iPSC-Based Disease Models by Inducing Neuronal Age-Related Phenotypes through Telomerase Manipulation. *Cell Rep.* **2016**, *17*, 1184–1192. [CrossRef]
66. Khurana, V.; Peng, J.; Chung, C.Y.; Auluck, P.K.; Fanning, S.; Tardiff, D.F.; Bartels, T.; Koeva, M.; Eichhorn, S.W.; Benyamini, H.; et al. Genome-Scale Networks Link Neurodegenerative Disease Genes to alpha-Synuclein through Specific Molecular Pathways. *Cell Syst.* **2017**, *4*, 157–170 e114. [CrossRef] [PubMed]
67. Sanchez-Danes, A.; Richaud-Patin, Y.; Carballo-Carbajal, I.; Jimenez-Delgado, S.; Caig, C.; Mora, S.; Di Guglielmo, C.; Ezquerra, M.; Patel, B.; Giralt, A.; et al. Disease-specific phenotypes in dopamine neurons from human iPS-based models of genetic and sporadic Parkinson's disease. *EMBO Mol. Med.* **2012**, *4*, 380–395. [CrossRef] [PubMed]
68. Schondorf, D.C.; Aureli, M.; McAllister, F.E.; Hindley, C.J.; Mayer, F.; Schmid, B.; Sardi, S.P.; Valsecchi, M.; Hoffmann, S.; Schwarz, L.K.; et al. iPSC-derived neurons from GBA1-associated Parkinson's disease patients show autophagic defects and impaired calcium homeostasis. *Nat. Commun.* **2014**, *5*, 4028. [CrossRef] [PubMed]
69. Fernandes, H.J.; Hartfield, E.M.; Christian, H.C.; Emmanoulidou, E.; Zheng, Y.; Booth, H.; Bogetofte, H.; Lang, C.; Ryan, B.J.; Sardi, S.P.; et al. ER Stress and Autophagic Perturbations Lead to Elevated Extracellular alpha-Synuclein in GBA-N370S Parkinson's iPSC-Derived Dopamine Neurons. *Stem Cell Rep.* **2016**, *6*, 342–356. [CrossRef]
70. Liu, G.H.; Qu, J.; Suzuki, K.; Nivet, E.; Li, M.; Montserrat, N.; Yi, F.; Xu, X.; Ruiz, S.; Zhang, W.; et al. Progressive degeneration of human neural stem cells caused by pathogenic LRRK2. *Nature* **2012**, *491*, 603–607. [CrossRef]
71. Reinhardt, P.; Schmid, B.; Burbulla, L.F.; Schondorf, D.C.; Wagner, L.; Glatza, M.; Hoing, S.; Hargus, G.; Heck, S.A.; Dhingra, A.; et al. Genetic correction of a LRRK2 mutation in human iPSCs links parkinsonian neurodegeneration to ERK-dependent changes in gene expression. *Cell Stem Cell* **2013**, *12*, 354–367. [CrossRef] [PubMed]
72. Lin, L.; Goke, J.; Cukuroglu, E.; Dranias, M.R.; VanDongen, A.M.; Stanton, L.W. Molecular Features Underlying Neurodegeneration Identified through In Vitro Modeling of Genetically Diverse Parkinson's Disease Patients. *Cell Rep.* **2016**, *15*, 2411–2426. [CrossRef] [PubMed]
73. Qing, X.; Walter, J.; Jarazo, J.; Arias-Fuenzalida, J.; Hillje, A.L.; Schwamborn, J.C. CRISPR/Cas9 and piggyBac-mediated footprint-free LRRK2-G2019S knock-in reveals neuronal complexity phenotypes and alpha-Synuclein modulation in dopaminergic neurons. *Stem Cell Res.* **2017**, *24*, 44–50. [CrossRef] [PubMed]

74. Korecka, J.A.; Talbot, S.; Osborn, T.M.; de Leeuw, S.M.; Levy, S.A.; Ferrari, E.J.; Moskites, A.; Atkinson, E.; Jodelka, F.M.; Hinrich, A.J.; et al. Neurite Collapse and Altered ER Ca(2+) Control in Human Parkinson Disease Patient iPSC-Derived Neurons with LRRK2 G2019S Mutation. *Stem Cell Rep.* **2019**, *12*, 29–41. [CrossRef] [PubMed]
75. Ren, Y.; Jiang, H.; Hu, Z.; Fan, K.; Wang, J.; Janoschka, S.; Wang, X.; Ge, S.; Feng, J. Parkin mutations reduce the complexity of neuronal processes in iPSC-derived human neurons. *Stem Cells* **2015**, *33*, 68–78. [CrossRef] [PubMed]
76. Aflaki, E.; Borger, D.K.; Moaven, N.; Stubblefield, B.K.; Rogers, S.A.; Patnaik, S.; Schoenen, F.J.; Westbroek, W.; Zheng, W.; Sullivan, P.; et al. A New Glucocerebrosidase Chaperone Reduces alpha-Synuclein and Glycolipid Levels in iPSC-Derived Dopaminergic Neurons from Patients with Gaucher Disease and Parkinsonism. *J. Neurosci.* **2016**, *36*, 7441–7452. [CrossRef] [PubMed]
77. Mazzulli, J.R.; Zunke, F.; Tsunemi, T.; Toker, N.J.; Jeon, S.; Burbulla, L.F.; Patnaik, S.; Sidransky, E.; Marugan, J.J.; Sue, C.M.; et al. Activation of beta-Glucocerebrosidase Reduces Pathological alpha-Synuclein and Restores Lysosomal Function in Parkinson's Patient Midbrain Neurons. *J. Neurosci.* **2016**, *36*, 7693–7706. [CrossRef]
78. Burbulla, L.F.; Jeon, S.; Zheng, J.; Song, P.; Silverman, R.B.; Krainc, D. A modulator of wild-type glucocerebrosidase improves pathogenic phenotypes in dopaminergic neuronal models of Parkinson's disease. *Sci. Transl. Med.* **2019**, *11*. [CrossRef]
79. Kim, M.J.; Jeon, S.; Burbulla, L.F.; Krainc, D. Acid ceramidase inhibition ameliorates alpha-synuclein accumulation upon loss of GBA1 function. *Hum. Mol. Genet.* **2018**, *27*, 1972–1988. [CrossRef]
80. Burbulla, L.F.; Song, P.; Mazzulli, J.R.; Zampese, E.; Wong, Y.C.; Jeon, S.; Santos, D.P.; Blanz, J.; Obermaier, C.D.; Strojny, C.; et al. Dopamine oxidation mediates mitochondrial and lysosomal dysfunction in Parkinson's disease. *Science* **2017**, *357*, 1255–1261. [CrossRef]
81. Plowey, E.D.; Cherra, S.J., 3rd; Liu, Y.J.; Chu, C.T. Role of autophagy in G2019S-LRRK2-associated neurite shortening in differentiated SH-SY5Y cells. *J. Neurochem.* **2008**, *105*, 1048–1056. [CrossRef] [PubMed]
82. Toth, G.; Gardai, S.J.; Zago, W.; Bertoncini, C.W.; Cremades, N.; Roy, S.L.; Tambe, M.A.; Rochet, J.C.; Galvagnion, C.; Skibinski, G.; et al. Targeting the intrinsically disordered structural ensemble of alpha-synuclein by small molecules as a potential therapeutic strategy for Parkinson's disease. *PLoS ONE* **2014**, *9*, e87133. [CrossRef] [PubMed]
83. Wrasidlo, W.; Tsigelny, I.F.; Price, D.L.; Dutta, G.; Rockenstein, E.; Schwarz, T.C.; Ledolter, K.; Bonhaus, D.; Paulino, A.; Eleuteri, S.; et al. A de novo compound targeting alpha-synuclein improves deficits in models of Parkinson's disease. *Brain* **2016**, *139*, 3217–3236. [CrossRef] [PubMed]
84. Simmnacher, K.; Lanfer, J.; Rizo, T.; Kaindl, J.; Winner, B. Modeling Cell-Cell Interactions in Parkinson's Disease Using Human Stem Cell-Based Models. *Front. Cell. Neurosci.* **2019**, *13*, 571. [CrossRef] [PubMed]
85. Carelli, V.; Musumeci, O.; Caporali, L.; Zanna, C.; La Morgia, C.; Del Dotto, V.; Porcelli, A.M.; Rugolo, M.; Valentino, M.L.; Iommarini, L.; et al. Syndromic parkinsonism and dementia associated with OPA1 missense mutations. *Ann. Neurol.* **2015**, *78*, 21–38. [CrossRef]
86. Zheng, W.; Thorne, N.; McKew, J.C. Phenotypic screens as a renewed approach for drug discovery. *Drug Discov. Today* **2013**, *18*, 1067–1073. [CrossRef]
87. Goodfellow, P.N. Genomics and drugs. An interview conducted by Holger Breithaupt and Caroline Hadley. *EMBO Rep.* **2004**, *5*, 843–846. [CrossRef]
88. Burbaum, J.J.; Sigal, N.H. New technologies for high-throughput screening. *Curr. Opin. Chem. Biol.* **1997**, *1*, 72–78. [CrossRef]
89. Gitler, A.D.; Dhillon, P.; Shorter, J. Neurodegenerative disease: Models, mechanisms, and a new hope. *Dis. Model. Mech.* **2017**, *10*, 499–502. [CrossRef]
90. Zhang, M.; Luo, G.; Zhou, Y.; Wang, S.; Zhong, Z. Phenotypic screens targeting neurodegenerative diseases. *J. Biomol. Screen.* **2014**, *19*, 1–16. [CrossRef]
91. Swinney, D.C.; Anthony, J. How were new medicines discovered? *Nat. Rev. Drug Discov.* **2011**, *10*, 507–519. [CrossRef] [PubMed]
92. Yamaguchi, A.; Ishikawa, K.I.; Inoshita, T.; Shiba-Fukushima, K.; Saiki, S.; Hatano, T.; Mori, A.; Oji, Y.; Okuzumi, A.; Li, Y.; et al. Identifying Therapeutic Agents for Amelioration of Mitochondrial Clearance Disorder in Neurons of Familial Parkinson Disease. *Stem Cell Rep.* **2020**, *14*, 1060–1075. [CrossRef] [PubMed]

93. Tabata, Y.; Imaizumi, Y.; Sugawara, M.; Andoh-Noda, T.; Banno, S.; Chai, M.; Sone, T.; Yamazaki, K.; Ito, M.; Tsukahara, K.; et al. T-type Calcium Channels Determine the Vulnerability of Dopaminergic Neurons to Mitochondrial Stress in Familial Parkinson Disease. *Stem Cell Rep.* **2018**, *11*, 1171–1184. [CrossRef]
94. Antoniou, N.; Prodromidou, K.; Kouroupi, G.; Samiotaki, M.; Panayotou, G.; Xilouri, M.; Stefanis, L.; Grailhe, R.; Taoufik, E.; Matsas, R. High Content Screening and Proteomic Analysis Identify the Kinase Inhibitor BX795 as a Potent Neuroprotective Compound in a Patient-Derived Model of Parkinson's Disease. *BioRxiv* **2020**. [CrossRef]
95. Oksanen, M.; Lehtonen, S.; Jaronen, M.; Goldsteins, G.; Hamalainen, R.H.; Koistinaho, J. Astrocyte alterations in neurodegenerative pathologies and their modeling in human induced pluripotent stem cell platforms. *Cell Mol. Life Sci.* **2019**, *76*, 2739–2760. [CrossRef]
96. Heneka, M.T. Microglia take centre stage in neurodegenerative disease. *Nat. Rev. Immunol.* **2019**, *19*, 79–80. [CrossRef]
97. Braak, H.; Sastre, M.; Del Tredici, K. Development of alpha-synuclein immunoreactive astrocytes in the forebrain parallels stages of intraneuronal pathology in sporadic Parkinson's disease. *Acta Neuropathol.* **2007**, *114*, 231–241. [CrossRef]
98. Kovacs, G.G.; Wagner, U.; Dumont, B.; Pikkarainen, M.; Osman, A.A.; Streichenberger, N.; Leisser, I.; Verchere, J.; Baron, T.; Alafuzoff, I.; et al. An antibody with high reactivity for disease-associated alpha-synuclein reveals extensive brain pathology. *Acta Neuropathol.* **2012**, *124*, 37–50. [CrossRef]
99. Takeda, A.; Hashimoto, M.; Mallory, M.; Sundsumo, M.; Hansen, L.; Masliah, E. C-terminal alpha-synuclein immunoreactivity in structures other than Lewy bodies in neurodegenerative disorders. *Acta Neuropathol.* **2000**, *99*, 296–304. [CrossRef]
100. Terada, S.; Ishizu, H.; Yokota, O.; Tsuchiya, K.; Nakashima, H.; Ishihara, T.; Fujita, D.; Ueda, K.; Ikeda, K.; Kuroda, S. Glial involvement in diffuse Lewy body disease. *Acta Neuropathol.* **2003**, *105*, 163–169. [CrossRef]
101. Wakabayashi, K.; Hayashi, S.; Yoshimoto, M.; Kudo, H.; Takahashi, H. NACP/alpha-synuclein-positive filamentous inclusions in astrocytes and oligodendrocytes of Parkinson's disease brains. *Acta Neuropathol.* **2000**, *99*, 14–20. [CrossRef] [PubMed]
102. Barcia, C.; Ros, C.M.; Annese, V.; Gomez, A.; Ros-Bernal, F.; Aguado-Yera, D.; Martinez-Pagan, M.E.; de Pablos, V.; Fernandez-Villalba, E.; Herrero, M.T. IFN-gamma signaling, with the synergistic contribution of TNF-alpha, mediates cell specific microglial and astroglial activation in experimental models of Parkinson's disease. *Cell Death Dis.* **2011**, *2*, e142. [CrossRef] [PubMed]
103. Gu, X.L.; Long, C.X.; Sun, L.; Xie, C.; Lin, X.; Cai, H. Astrocytic expression of Parkinson's disease-related A53T alpha-synuclein causes neurodegeneration in mice. *Mol. Brain* **2010**, *3*, 12. [CrossRef]
104. Halliday, G.M.; Stevens, C.H. Glia: Initiators and progressors of pathology in Parkinson's disease. *Mov. Disord.* **2011**, *26*, 6–17. [CrossRef] [PubMed]
105. Loria, F.; Vargas, J.Y.; Bousset, L.; Syan, S.; Salles, A.; Melki, R.; Zurzolo, C. alpha-Synuclein transfer between neurons and astrocytes indicates that astrocytes play a role in degradation rather than in spreading. *Acta Neuropathol.* **2017**, *134*, 789–808. [CrossRef] [PubMed]
106. Bartels, A.L.; Willemsen, A.T.; Doorduin, J.; de Vries, E.F.; Dierckx, R.A.; Leenders, K.L. [11C]-PK11195 PET: Quantification of neuroinflammation and a monitor of anti-inflammatory treatment in Parkinson's disease? *Parkinsonism Relat. Disord.* **2010**, *16*, 57–59. [CrossRef]
107. Gerhard, A.; Pavese, N.; Hotton, G.; Turkheimer, F.; Es, M.; Hammers, A.; Eggert, K.; Oertel, W.; Banati, R.B.; Brooks, D.J. In vivo imaging of microglial activation with [11C](R)-PK11195 PET in idiopathic Parkinson's disease. *Neurobiol. Dis.* **2006**, *21*, 404–412. [CrossRef]
108. Sanchez-Guajardo, V.; Febbraro, F.; Kirik, D.; Romero-Ramos, M. Microglia acquire distinct activation profiles depending on the degree of alpha-synuclein neuropathology in a rAAV based model of Parkinson's disease. *PLoS ONE* **2010**, *5*, e8784. [CrossRef]
109. McGeer, P.L.; McGeer, E.G.; Kawamata, T.; Yamada, T.; Akiyama, H. Reactions of the immune system in chronic degenerative neurological diseases. *Can. J. Neurol. Sci.* **1991**, *18*, 376–379. [CrossRef]
110. Hoenen, C.; Gustin, A.; Birck, C.; Kirchmeyer, M.; Beaume, N.; Felten, P.; Grandbarbe, L.; Heuschling, P.; Heurtaux, T. Alpha-Synuclein Proteins Promote Pro-Inflammatory Cascades in Microglia: Stronger Effects of the A53T Mutant. *PLoS ONE* **2016**, *11*, e0162717. [CrossRef]

111. Czlonkowska, A.; Kohutnicka, M.; Kurkowska-Jastrzebska, I.; Czlonkowski, A. Microglial reaction in MPTP (1-methyl-4-phenyl-1,2,3,6-tetrahydropyridine) induced Parkinson's disease mice model. *Neurodegeneration* **1996**, *5*, 137–143. [CrossRef] [PubMed]
112. Ransohoff, R.M. A polarizing question: Do M1 and M2 microglia exist? *Nat. Neurosci.* **2016**, *19*, 987–991. [CrossRef] [PubMed]
113. Wyss-Coray, T.; Mucke, L. Inflammation in neurodegenerative disease—A double-edged sword. *Neuron* **2002**, *35*, 419–432. [CrossRef]
114. Wu, D.C.; Jackson-Lewis, V.; Vila, M.; Tieu, K.; Teismann, P.; Vadseth, C.; Choi, D.K.; Ischiropoulos, H.; Przedborski, S. Blockade of microglial activation is neuroprotective in the 1-methyl-4-phenyl-1,2,3,6-tetrahydropyridine mouse model of Parkinson disease. *J. Neurosci.* **2002**, *22*, 1763–1771. [CrossRef]
115. Manocha, G.D.; Floden, A.M.; Puig, K.L.; Nagamoto-Combs, K.; Scherzer, C.R.; Combs, C.K. Defining the contribution of neuroinflammation to Parkinson's disease in humanized immune system mice. *Mol. Neurodegener.* **2017**, *12*, 17. [CrossRef]
116. Marinova-Mutafchieva, L.; Sadeghian, M.; Broom, L.; Davis, J.B.; Medhurst, A.D.; Dexter, D.T. Relationship between microglial activation and dopaminergic neuronal loss in the substantia nigra: A time course study in a 6-hydroxydopamine model of Parkinson's disease. *J. Neurochem.* **2009**, *110*, 966–975. [CrossRef]
117. Walsh, S.; Finn, D.P.; Dowd, E. Time-course of nigrostriatal neurodegeneration and neuroinflammation in the 6-hydroxydopamine-induced axonal and terminal lesion models of Parkinson's disease in the rat. *Neuroscience* **2011**, *175*, 251–261. [CrossRef]
118. Stefanova, N.; Fellner, L.; Reindl, M.; Masliah, E.; Poewe, W.; Wenning, G.K. Toll-like receptor 4 promotes alpha-synuclein clearance and survival of nigral dopaminergic neurons. *Am. J. Pathol.* **2011**, *179*, 954–963. [CrossRef]
119. Lee, H.J.; Suk, J.E.; Bae, E.J.; Lee, S.J. Clearance and deposition of extracellular alpha-synuclein aggregates in microglia. *Biochem. Biophys. Res. Commun.* **2008**, *372*, 423–428. [CrossRef]
120. Fellner, L.; Irschick, R.; Schanda, K.; Reindl, M.; Klimaschewski, L.; Poewe, W.; Wenning, G.K.; Stefanova, N. Toll-like receptor 4 is required for alpha-synuclein dependent activation of microglia and astroglia. *Glia* **2013**, *61*, 349–360. [CrossRef]
121. Kim, C.; Ho, D.H.; Suk, J.E.; You, S.; Michael, S.; Kang, J.; Joong Lee, S.; Masliah, E.; Hwang, D.; Lee, H.J.; et al. Neuron-released oligomeric alpha-synuclein is an endogenous agonist of TLR2 for paracrine activation of microglia. *Nat. Commun.* **2013**, *4*, 1562. [CrossRef] [PubMed]
122. Liddelow, S.A.; Guttenplan, K.A.; Clarke, L.E.; Bennett, F.C.; Bohlen, C.J.; Schirmer, L.; Bennett, M.L.; Munch, A.E.; Chung, W.S.; Peterson, T.C.; et al. Neurotoxic reactive astrocytes are induced by activated microglia. *Nature* **2017**, *541*, 481–487. [CrossRef] [PubMed]
123. Yun, S.P.; Kam, T.I.; Panicker, N.; Kim, S.; Oh, Y.; Park, J.S.; Kwon, S.H.; Park, Y.J.; Karuppagounder, S.S.; Park, H.; et al. Block of A1 astrocyte conversion by microglia is neuroprotective in models of Parkinson's disease. *Nat. Med.* **2018**, *24*, 931–938. [CrossRef] [PubMed]
124. Mavroeidi, P.; Arvanitaki, F.; Karakitsou, A.K.; Vetsi, M.; Kloukina, I.; Zweckstetter, M.; Giller, K.; Becker, S.; Sorrentino, Z.A.; Giasson, B.I.; et al. Endogenous oligodendroglial alpha-synuclein and TPPP/p25alpha orchestrate alpha-synuclein pathology in experimental multiple system atrophy models. *Acta Neuropathol.* **2019**, *138*, 415–441. [CrossRef]
125. Alieva, A.K.; Zyrin, V.S.; Rudenok, M.M.; Kolacheva, A.A.; Shulskaya, M.V.; Ugryumov, M.V.; Slominsky, P.A.; Shadrina, M.I. Whole-Transcriptome Analysis of Mouse Models with MPTP-Induced Early Stages of Parkinson's Disease Reveals Stage-Specific Response of Transcriptome and a Possible Role of Myelin-Linked Genes in Neurodegeneration. *Mol. Neurobiol.* **2018**, *55*, 7229–7241. [CrossRef]
126. Booth, H.D.E.; Wessely, F.; Connor-Robson, N.; Rinaldi, F.; Vowles, J.; Browne, C.; Evetts, S.G.; Hu, M.T.; Cowley, S.A.; Webber, C.; et al. RNA sequencing reveals MMP2 and TGFB1 downregulation in LRRK2 G2019S Parkinson's iPSC-derived astrocytes. *Neurobiol.Dis.* **2019**, *129*, 56–66. [CrossRef]
127. di Domenico, A.; Carola, G.; Calatayud, C.; Pons-Espinal, M.; Munoz, J.P.; Richaud-Patin, Y.; Fernandez-Carasa, I.; Gut, M.; Faella, A.; Parameswaran, J.; et al. Patient-Specific iPSC-Derived Astrocytes Contribute to Non-Cell-Autonomous Neurodegeneration in Parkinson's Disease. *Stem Cell Rep.* **2019**, *12*, 213–229. [CrossRef]
128. Aflaki, E.; Stubblefield, B.K.; McGlinchey, R.P.; McMahon, B.; Ory, D.S.; Sidransky, E. A characterization of Gaucher iPS-derived astrocytes: Potential implications for Parkinson's disease. *Neurobiol. Dis.* **2020**, *134*, 104647. [CrossRef]

129. Sonninen, T.M.; Hamalainen, R.H.; Koskuvi, M.; Oksanen, M.; Shakirzyanova, A.; Wojciechowski, S.; Puttonen, K.; Naumenko, N.; Goldsteins, G.; Laham-Karam, N.; et al. Metabolic alterations in Parkinson's disease astrocytes. *Sci. Rep.* **2020**, *10*, 14474. [CrossRef]
130. Haenseler, W.; Zambon, F.; Lee, H.; Vowles, J.; Rinaldi, F.; Duggal, G.; Houlden, H.; Gwinn, K.; Wray, S.; Luk, K.C.; et al. Excess alpha-synuclein compromises phagocytosis in iPSC-derived macrophages. *Sci. Rep.* **2017**, *7*, 9003. [CrossRef]
131. Lee, H.; Flynn, R.; Sharma, I.; Haberman, E.; Carling, P.J.; Nicholls, F.J.; Stegmann, M.; Vowles, J.; Haenseler, W.; Wade-Martins, R.; et al. LRRK2 Is Recruited to Phagosomes and Co-recruits RAB8 and RAB10 in Human Pluripotent Stem Cell-Derived Macrophages. *Stem Cell Rep.* **2020**, *14*, 940–955. [CrossRef] [PubMed]
132. Speidel, A.; Felk, S.; Reinhardt, P.; Sterneckert, J.; Gillardon, F. Leucine-Rich Repeat Kinase 2 Influences Fate Decision of Human Monocytes Differentiated from Induced Pluripotent Stem Cells. *PLoS ONE* **2016**, *11*, e0165949. [CrossRef] [PubMed]
133. Qian, X.; Song, H.; Ming, G.L. Brain organoids: Advances, applications and challenges. *Development* **2019**, *146*. [CrossRef] [PubMed]
134. Bolognin, S.; Fossepre, M.; Qing, X.; Jarazo, J.; Scancar, J.; Moreno, E.L.; Nickels, S.L.; Wasner, K.; Ouzren, N.; Walter, J.; et al. 3D Cultures of Parkinson's Disease-Specific Dopaminergic Neurons for High Content Phenotyping and Drug Testing. *Adv. Sci.* **2019**, *6*, 1800927. [CrossRef]
135. Kim, H.; Park, H.J.; Choi, H.; Chang, Y.; Park, H.; Shin, J.; Kim, J.; Lengner, C.J.; Lee, Y.K. Modeling G2019S-LRRK2 Sporadic Parkinson's Disease in 3D Midbrain Organoids. *Stem Cell Rep.* **2019**, *12*, 518–531. [CrossRef]
136. Smits, L.M.; Reinhardt, L.; Reinhardt, P.; Glatza, M.; Monzel, A.S.; Stanslowsky, N.; Rosato-Siri, M.D.; Zanon, A.; Antony, P.M.; Bellmann, J.; et al. Modeling Parkinson's disease in midbrain-like organoids. *NPJ Parkinsons Dis.* **2019**, *5*, 5. [CrossRef]
137. Brull, M.; Spreng, A.S.; Gutbier, S.; Loser, D.; Krebs, A.; Reich, M.; Kraushaar, U.; Britschgi, M.; Patsch, C.; Leist, M. Incorporation of stem cell-derived astrocytes into neuronal organoids to allow neuro-glial interactions in toxicological studies. *ALTEX* **2020**, *37*, 409–428. [CrossRef]
138. Qian, X.; Su, Y.; Adam, C.D.; Deutschmann, A.U.; Pather, S.R.; Goldberg, E.M.; Su, K.; Li, S.; Lu, L.; Jacob, F.; et al. Sliced Human Cortical Organoids for Modeling Distinct Cortical Layer Formation. *Cell Stem Cell* **2020**, *26*, 766–781 e769. [CrossRef]
139. Marton, R.M.; Miura, Y.; Sloan, S.A.; Li, Q.; Revah, O.; Levy, R.J.; Huguenard, J.R.; Pasca, S.P. Differentiation and maturation of oligodendrocytes in human three-dimensional neural cultures. *Nat. Neurosci.* **2019**, *22*, 484–491. [CrossRef]
140. Madhavan, M.; Nevin, Z.S.; Shick, H.E.; Garrison, E.; Clarkson-Paredes, C.; Karl, M.; Clayton, B.L.L.; Factor, D.C.; Allan, K.C.; Barbar, L.; et al. Induction of myelinating oligodendrocytes in human cortical spheroids. *Nat. Methods* **2018**, *15*, 700–706. [CrossRef]
141. Ormel, P.R.; Vieira de Sa, R.; van Bodegraven, E.J.; Karst, H.; Harschnitz, O.; Sneeboer, M.A.M.; Johansen, L.E.; van Dijk, R.E.; Scheefhals, N.; Berdenis van Berlekom, A.; et al. Microglia innately develop within cerebral organoids. *Nat. Commun.* **2018**, *9*, 4167. [CrossRef]
142. Kwak, T.H.; Kang, J.H.; Hali, S.; Kim, J.; Kim, K.P.; Park, C.; Lee, J.H.; Ryu, H.K.; Na, J.E.; Jo, J.; et al. Generation of homogeneous midbrain organoids with in vivo-like cellular composition facilitates neurotoxin-based Parkinson's disease modeling. *Stem Cells* **2020**, *38*, 727–740. [CrossRef] [PubMed]
143. Yadav, A.; Seth, B.; Chaturvedi, R.K. Brain Organoids: Tiny Mirrors of Human Neurodevelopment and Neurological Disorders. *Neuroscientist* **2020**, 1073858420943192. [CrossRef] [PubMed]
144. Liu, H.; Wang, Y.; Cui, K.; Guo, Y.; Zhang, X.; Qin, J. Advances in Hydrogels in Organoids and Organs-on-a-Chip. *Adv. Mater.* **2019**, *31*, e1902042. [CrossRef] [PubMed]
145. Miccoli, B.; Braeken, D.; Li, Y.E. Brain-on-a-chip Devices for Drug Screening and Disease Modeling Applications. *Curr. Pharm. Des.* **2018**, *24*, 5419–5436. [CrossRef]
146. Fernandes, J.T.; Chutna, O.; Chu, V.; Conde, J.P.; Outeiro, T.F. A Novel Microfluidic Cell Co-culture Platform for the Study of the Molecular Mechanisms of Parkinson's Disease and Other Synucleinopathies. *Front. Neurosci.* **2016**, *10*, 511. [CrossRef]
147. Seidi, A.; Kaji, H.; Annabi, N.; Ostrovidov, S.; Ramalingam, M.; Khademhosseini, A. A microfluidic-based neurotoxin concentration gradient for the generation of an in vitro model of Parkinson's disease. *Biomicrofluidics* **2011**, *5*, 22214. [CrossRef]

148. Freundt, E.C.; Maynard, N.; Clancy, E.K.; Roy, S.; Bousset, L.; Sourigues, Y.; Covert, M.; Melki, R.; Kirkegaard, K.; Brahic, M. Neuron-to-neuron transmission of alpha-synuclein fibrils through axonal transport. *Ann. Neurol.* **2012**, *72*, 517–524. [CrossRef]
149. Grienberger, C.; Konnerth, A. Imaging calcium in neurons. *Neuron* **2012**, *73*, 862–885. [CrossRef]
150. Mank, M.; Griesbeck, O. Genetically encoded calcium indicators. *Chem. Rev.* **2008**, *108*, 1550–1564. [CrossRef]
151. Schwab, A.J.; Ebert, A.D. Neurite Aggregation and Calcium Dysfunction in iPSC-Derived Sensory Neurons with Parkinson's Disease-Related LRRK2 G2019S Mutation. *Stem Cell Rep.* **2015**, *5*, 1039–1052. [CrossRef] [PubMed]
152. Zygogianni, O.; Antoniou, N.; Kalomoiri, M.; Kouroupi, G.; Taoufik, E.; Matsas, R. In Vivo Phenotyping of Familial Parkinson's Disease with Human Induced Pluripotent Stem Cells: A Proof-of-Concept Study. *Neurochem. Res.* **2019**, *44*, 1475–1493. [CrossRef] [PubMed]
153. Negri, J.; Menon, V.; Young-Pearse, T.L. Assessment of Spontaneous Neuronal Activity In Vitro Using Multi-Well Multi-Electrode Arrays: Implications for Assay Development. *ENeuro* **2020**, *7*. [CrossRef]
154. Spira, M.E.; Hai, A. Multi-electrode array technologies for neuroscience and cardiology. *Nat. Nanotechnol.* **2013**, *8*, 83–94. [CrossRef]
155. Obien, M.E.; Deligkaris, K.; Bullmann, T.; Bakkum, D.J.; Frey, U. Revealing neuronal function through microelectrode array recordings. *Front. Neurosci.* **2014**, *8*, 423. [CrossRef] [PubMed]
156. Woodard, C.M.; Campos, B.A.; Kuo, S.H.; Nirenberg, M.J.; Nestor, M.W.; Zimmer, M.; Mosharov, E.V.; Sulzer, D.; Zhou, H.; Paull, D.; et al. iPSC-derived dopamine neurons reveal differences between monozygotic twins discordant for Parkinson's disease. *Cell Rep.* **2014**, *9*, 1173–1182. [CrossRef] [PubMed]
157. Laperle, A.H.; Sances, S.; Yucer, N.; Dardov, V.J.; Garcia, V.J.; Ho, R.; Fulton, A.N.; Jones, M.R.; Roxas, K.M.; Avalos, P.; et al. iPSC modeling of young-onset Parkinson's disease reveals a molecular signature of disease and novel therapeutic candidates. *Nat. Med.* **2020**, *26*, 289–299. [CrossRef] [PubMed]
158. Amin, H.; Nieus, T.; Lonardoni, D.; Maccione, A.; Berdondini, L. High-resolution bioelectrical imaging of Abeta-induced network dysfunction on CMOS-MEAs for neurotoxicity and rescue studies. *Sci. Rep.* **2017**, *7*, 2460. [CrossRef]
159. Iaccarino, H.F.; Singer, A.C.; Martorell, A.J.; Rudenko, A.; Gao, F.; Gillingham, T.Z.; Mathys, H.; Seo, J.; Kritskiy, O.; Abdurrob, F.; et al. Gamma frequency entrainment attenuates amyloid load and modifies microglia. *Nature* **2016**, *540*, 230–235. [CrossRef]
160. Durens, M.; Nestor, J.; Williams, M.; Herold, K.; Niescier, R.F.; Lunden, J.W.; Phillips, A.W.; Lin, Y.C.; Dykxhoorn, D.M.; Nestor, M.W. High-throughput screening of human induced pluripotent stem cell-derived brain organoids. *J. Neurosci. Methods* **2020**, *335*, 108627. [CrossRef]
161. Schwartz, M.P.; Hou, Z.; Propson, N.E.; Zhang, J.; Engstrom, C.J.; Santos Costa, V.; Jiang, P.; Nguyen, B.K.; Bolin, J.M.; Daly, W.; et al. Human pluripotent stem cell-derived neural constructs for predicting neural toxicity. *Proc. Natl. Acad. Sci. USA* **2015**, *112*, 12516–12521. [CrossRef] [PubMed]
162. Monzel, A.S.; Hemmer, K.; Kaoma, T.; Smits, L.M.; Bolognin, S.; Lucarelli, P.; Rosety, I.; Zagare, A.; Antony, P.; Nickels, S.L.; et al. Machine learning-assisted neurotoxicity prediction in human midbrain organoids. *Parkinsonism Relat. Disord.* **2020**, *75*, 105–109. [CrossRef] [PubMed]